The neodymium composition of Atlantic Ocean water masses: implications for the past and present

Alison E. Hartman

Submitted in partial fulfillment of the
requirements for the degree of
Doctor of Philosophy
in the Graduate School of Arts and Sciences

COLUMBIA UNIVERSITY
2015

ABSTRACT

The Nd-composition of Atlantic Ocean water masses: implications for the past and present

Alison E. Hartman

Ocean circulation plays an integral part in a multitude of Earth's processes including the transfer of heat and nutrients across the globe. Additionally, its role in initiating and/or responding to global climate change is thought to be significant though poorly constrained. One tool used to further understand the influence of changes in ocean circulation during climate transitions is paleocirculation records developed from deep sea cores. These records paint a picture of how ocean circulation changed throughout time and are composed of an array of elements and isotopes extracted from different sediment archives. Neodymium (Nd) isotopes have been applied to paleocirculation because of the geographic variability of these isotopes in seawater and their ability to be preserved in deep sea sediments. Nd isotope records have been extracted from Fe-Mn crusts, leachates of sediment coatings, fish debris and foraminifera dissolutions to investigate changes in circulation at both deep and shallow ocean depths. Several of these records have been developed to investigate changes in the amount of northern vs. southern sourced waters in the South Atlantic Ocean. The advancement of northern sourced waters into the South Atlantic and Southern Ocean is an important branch of the global ocean circulation system known as Atlantic Meridional Overturning Circulation (AMOC). In order to further investigate changes of AMOC in the South Atlantic, we have developed a Nd isotope record from Cape Basin core TN057-6 for the last ~400 kyr. In agreement with the literature, the developed Nd record shows a decrease in AMOC during the Last Glacial Maximum and for previous glacial stages. Interglacial or warm periods defined by increased AMOC of comparable

magnitude to modern circulation. These findings are summarized in the first two chapters of this thesis.

The potential for Nd isotopes (ε_{Nd}) as a water mass tracer is dependent on a thorough understanding of Nd cycling within the water column. The use of Nd isotopes in the modern ocean is also a valuable tool for investigating biogeochemical cycles and environmental perturbations such as dust or freshwater inputs. The distribution of ε_{Nd} within the oceans suggests quasi-conservative behavior, traces water masses and shows correlations with both salinity and silicate. However, one observation known as the "Nd-paradox" suggests there are some poorly constrained sources and sinks of Nd in the ocean. The "Nd-paradox" refers to an apparent decoupling of Nd isotopes and Nd concentration ([Nd]) within the water column. In order to explain such features and the Nd cycle as a whole, it is essential to expand the database of Nd seawater data. As part of the GEOTRACES initiative, there have been a growing number of studies to measure seawater Nd-composition. The last two chapters of this thesis focus on the Nd-composition of seawater samples collected along GEOTRACES cruise transect GA03 from Lisbon, Portugal to Cape Verde Islands to Woods Hole, USA. The major water masses sampled as part of this cruise are Mediterranean Outflow Water, Antarctic Intermediate Water, North Atlantic Deep Water and Antarctic Bottom Water. Additional features sampled are near shore and open ocean stations, the Saharan dust plume, an expansive oxygen minimum zone, nepheloid layers and a Mid-Atlantic Ocean Ridge hydrothermal site. For each sample we calculate a predicted Nd-composition based on water mass mixing. By comparing the predicted and measured Nd-composition, we are able to investigate how Nd deviates from conservative behavior. Results from this work show that ε_{Nd} is predominately conservative at deep depths at open ocean stations and is sensitive to small changes in water mass end-member Nd-

compositions. This finding has important implications for the way end-members are defined in paleoceanographic Nd studies. Hydrothermal inputs are shown to have no influence on the isotopic composition of nearby water mass ε_{Nd} compositions. However, an expansive nepheloid layer in the deep western North Atlantic does influence seawater ε_{Nd}. [Nd] does not show conservative behavior but rather follows the "Nd-Paradox" such that concentrations increase with depth across the basin and exceed predicted [Nd] values.

Table of Contents

Tables

Figures

Acknowledgements

The completion of this PhD is easily the hardest thing I have yet had to do and I have learned as much about myself as I have learned about Nd isotopes. Luckily this was not a solo journey and there are many people to recognize for their help. My advisor, Steve Goldstein was tirelessly dedicated to editing this piece of work and guiding me along the way to becoming an independent scientist. His dedication to science has been contagious and has further motivated me to pursue answers to the Earth's mysteries.

My other committee members Sidney Hemming and Bob Anderson were both outstanding support during the completion of this degree. I am grateful for Sidney's open ear when seeking her advice both on and off campus and continue to feel inspired by her. Bob's particular dedication to scientific collaboration and exchange of ideas has been a great lesson and truly influenced my approach to these hurdles. I feel truly honored to have worked with these three brilliant scientists and I look forward to future collaborations.

There are several other great scientists that influenced me during this process. Katharina Pahnke has been a great mentor along this journey and helped me from day one in the lab all the way to providing feedback on chapters of this very thesis. Leo Pena was also invaluable during this process and always provided an open door and advice for all matters of science and life. Torben Stichel's contribution to this work was vital and I am excited to continue our collaboration. I am also excited to continue working with Howie Scher and Brian Duggan as we continue to develop and discuss the dataset introduced in this thesis.

This work could not have come about without the support of all the Lamont Isotope Geochemistry lab members. In particular, I feel great gratitude for Merry Cai, Louise Bolge, Jason Jweda and Rachel Lupien whose contributions to this experience went far beyond the lab. I have made many great friends during this time, which is arguably the best part of obtaining this degree. Both Elizabeth Pierce and Meg Reitz provided some of the strongest support I have ever experienced and I am lucky to have found them.

Last but not least, my family has without a doubt been the most important support I had during this process. My mother and father, Donna and Robert Hartman, provided unconditional encouragement and love during this entire journey and I couldn't have done it without them. I am truly blessed by the people who surrounded me during this time and could not have done it without their professional guidance, encouragement and friendship.

Dedication

This work is dedicated to Mom-mom and Pop-pop. I miss you both very much and I know you would be proud.

Chapter 1: Use of Nd isotopes as a water mass and an ocean paleocirculation tracer

1.1 Introduction

Ocean circulation plays an important role in the distribution of heat and nutrients across the globe and is subject to reorganizations during global climatic change. Shifts in the ocean 'conveyor belt' (e.g. Broecker and Peng, 1983; Broecker and Denton, 1989) are used to explain glacial-interglacial transitions and the connections between southern and northern hemisphere climate events. The connection between circulation changes and climate shifts have been studied across the globe in different environments. This chapter discusses paleo-circulation proxies used to study changes in deep-sea circulation during glacial-interglacial shifts of the late Quaternary in the South Atlantic. The South Atlantic is a key region to study changes in ocean circulation because the water masses present in the basin are susceptible to changes in Atlantic Meridional Overturning Circulation (***AMOC; acronyms used in this chapter are listed in Table 1.1***), which is a critical branch of the ocean circulation system. The changes observed during glacial-interglacial shifts involve the flux of the southward export of North Atlantic Deep Water (***NADW***) and the northward export of southern sourced waters such as Antarctic Intermediate Water (***AAIW***) and Antarctic Bottom Water (***AABW***). Proxies that have been used to study changes of AMOC in the South Atlantic and are discussed here are kaolonite/chlorite ratios, Cd/Ca, $\delta^{13}C$ and Neodymium (***Nd***) isotopes.

Nd isotopes as a water mass tracer are reviewed in this chapter and are applied as a paleo-circulation proxy in the second chapter of this thesis. The last three chapters of this thesis focus on the modern day distribution of Nd in the North Atlantic Ocean. Early studies of Nd in the oceans revealed that the Nd isotopic composition (ε_{Nd}) of the oceans is derived from continental

erosion and recorded in Fe-Mn nodules and sediments on the seafloor (O'Nions et al., 1978; Piepgras and Wasserburg, 1979; Goldstein and O'Nions, 1981). These studies, along with the first direct studies of Nd in seawater revealed unique ε_{Nd} compositions in each ocean basin (e.g. Piepgras and Wasserburg, 1980, 1982, 1983, 1985, 1987; Stordal and Wasserburg, 1986), moreover they documented high variability within the water column. The geographical variability of ε_{Nd} in seawater in combination with the preservation of the Nd signal in Fe-Mn deposits, provided the ground work for its potential use as a paleo-water mass tracer. Early applications of Nd isotopes demonstrated that changes in seawater Nd reflected both changes in water mass mixing and continental inputs and could be monitored with both the Fe-Mn coatings of foraminifera (reflects bottom water) and reductively cleaned planktonic foraminifera (reflects seawater depths in which foraminifera grow) (e.g. Palmer and Elderfield, 1985, 1986; Vance and Burton, 1999; Burton and Vance 2000). The first Nd isotope record of AMOC changes on sub-glacial time-scales was derived from Fe-Mn oxyhydroxide sediment coatings, by Rutberg *et al.* (2000), in core RC11-83 in the southeast Atlantic. The record was developed for the last ~70 kyr and revealed differences in the ε_{Nd} composition of bottom waters during the different Marine Isotope Stages (***MIS***) as well as shifts at the times of the transitions, all consistent with shifts in AMOC. Records of bottom water ε_{Nd} continue to be developed for the South Atlantic and elsewhere and have expanded to include foraminifera dissolutions, fish debris and foraminiferal calcite (Thomas et al., 2003; Thomas, 2004; Scher and Martin, 2004, 2008; Piotrowski et al., 2004, 2005, 2008, 2012; Martin and Scher, 2006; Gutjahr et al., 2008; 2010; Gourlan et al., 2008; Klevenz et al., 2008; Pahnke et al., 2008; Basak et al., 2010; Roberts et al., 2010, 2012; Gutjahr and Lippold, 2011; Wilson et al., 2012; Kraft et al., 2013; Pena et al., 2013; Pena and Goldstein, 2014). In an effort to expand on this work we have developed a record of authigenic

ε_{Nd} in Cape Basin core TN057-6 for the last ~400 kyr. This record monitors changes in the mixing contributions of northern and southern component waters in the South Atlantic and is the first study to use Nd isotopes to monitor changes in AMOC between 100 and 400 kyr as further discussed in the second chapter of this thesis.

1.2 Hydrographic setting

1.2.1 Circulation of surface waters in the South Atlantic

The present day circulation of the South Atlantic provides context for the paleoceanographic records used to investigate changes in AMOC. Peterson and Stramma (1991) and Stramma and England (1999) have completed an extensive review of the deep and surface hydrology in this region. They show that the subtropical gyre dominates surface water circulation (Figure 1.1). North of the subtropical gyre, there are several equatorial currents and countercurrents that shift on seasonal scales, four of which make up the South Equatorial Current (***SEC***) as it travels from southern Africa to the coast of Brazil (Figure 1.2). The southern SEC, central SEC, equatorial SEC and the northern SEC combine to make up the northern limb of the gyre. At approximately 10°S, surface flow of the SEC forks into the North Brazil Current ***(NBC)*** and the Brazil Current (Figure 1.2). The SEC is responsible for transporting 16 x 10^6 m^3/s (16 Sv) of water across 30°W in the upper 500m. It has been observed that only 4 Sv turn into the Brazil Current while the remainder (12 Sv) turns north into the North Brazil Current (Peterson and Stramma, 1991). Stramma and England (1999) determined that the location of the northern limb of the South Atlantic Gyre is depth dependent. At the central water layer (500 m) the splitting of the SEC occurs closer to 20°S, contributing to the Brazil and North Brazil Currents. This results in an overall southern shift of the northern limb of the gyre with increasing depth.

Because of the loss of water to the north, the Brazil Current is a surprisingly weak western boundary current. It flows southward along the western rim of the South Atlantic Basin (Figure 1.2) and is relatively shallow flowing along the coast, mostly on the continental shelf. Until ~24°S, the Brazil Current remains shallow and weak with the bulk of the transport occurring at the 200 m isobath and consisting of about 11 Sv. After this latitude, the transport increases at about 5% per 100km (Peterson and Stramma, 1991). Contributing to the flow of the Brazil Current is a recirculation cell re-entering the Brazil Current flow path south of 30°S. The recirculation current is responsible for the transport of 12 Sv in the upper 1400m and contributes to an overall transport of 19-22 Sv in the Brazil Current by 38°S (Peterson and Stramma, 1991). The current eventually deviates from the western boundary and joins with the Falkland Current on its path southward.

The southern component of the South Atlantic Gyre is the South Atlantic Current, which is bounded to the south by a sharp discontinuity in sea surface temperature and salinity known as the Subtropical Front (Figure 1.1). This current is fed by the Brazil Current and travels eastward at about 43°S to the southern extent of Africa. In the Argentine Basin at 1000m depth, the South Atlantic Current is responsible for a transport of 30 to 37 Sv. So far an unexplainable feature, both the volume transport and surface velocity decrease by a half by the time the current reaches the Cape Basin in the east (Peterson and Stramma, 1991). The South Atlantic Current splits at around 0° longitude feeding the Benguela Current to the north and continuing its eastern route to the Indian Ocean. The Benguela Current moves northward up the coast of Africa and closes the South Atlantic Gyre. Along with being fed by the South Atlantic Current, the Benguela Current receives water from the Indian Ocean through the Agulhas Leakage. This leakage occurs at the Agulhas Retroflection and consists of 3-14 Sv transport to the South Atlantic to 1500m depth

(Peterson and Stramma, 1991). The Agulhas leakage has been associated with an influx of Indian Ocean sourced AAIW (e.g. Gordon et al., 1992; Roman and Lutjeharms 2010). As the Benguela Current moves up the eastern boundary of the South Atlantic, it is responsible for a transport of about 21 Sv. Of importance in this region is the coastal upwelling that occurs from about 18°S to 34°S as a result of offshore winds. The majority of the Benguela Current moves offshore to the west at approximately 30°S to become part of the South Equatorial Current system but remains of the current follow the coast to the north and flow into the Angola Basin. Within the Angola Basin, the Angola Gyre is separated from the Benguela Current by the Angola-Benguela Front at ~ 20°S to depths of ~ 200m.

1.2.2 Circulation of deep waters in the South Atlantic

The deep-water circulation of the South Atlantic (summarized in Figure 1.3) differs from the surface water hydrology. The deep and intermediate water masses of the South Atlantic are Antarctic Intermediate Water (***AAIW***), NADW, Circumpolar Deep Water (***CDW***) and Antarctic Bottom Water (***AABW***) (T-S properties are shown in Figure 1.4 and listed in Table 1.2). NADW enters the South Atlantic primarily through a western route within the Deep Western Boundary Current and is dictated by the topography of the ocean basin. As NADW moves southward, the thickness decreases as the water mass mixes with AAIW, CDW and AABW. As southern sourced water masses move to the north, they mix with NADW and are less prevalent north of the equator. South of the subtropical gyre, a combination of polar fronts and circumpolar currents cross the Southern Ocean and are important locations for the formation of deep waters (Figures 1.1, 1.2, 1.3). The Subtropical Front (***STF***), the Subantarctic Front (***SAF***), and the Antarctic Polar Front (***APF***) represent discontinuities of sea surface properties. Between these fronts,

frontal zones represent regions where deep and intermediate waters sink and flow north (Figure 1.5). Subantarctic Mode Water forms within the Subantarctic Zone and contributes to both mode waters in the subtropical gyre and also in the formation AAIW (Stramma and England, 1999). The most important region for AAIW formation is within the Polar Frontal Zone (Figure 1.1) although there are also contributions from the Agulhas Leakage. AAIW is identified by a salinity minimum and oxygen maximum that can be traced north to about 20°S in the central and eastern Atlantic. Moreover, a salinity minimum characteristic of AAIW has been detected to 24°N in the western Atlantic with limited traces found as far north as the Nordic Seas (Reid, 1994; Schmitz, 1996; Stramma and England, 1999). AABW forms just off the coast of Antarctica and has a flow path that is strongly influenced by bottom topography. AABW makes its way across the equator along the western boundary, passes through the Romanche Fracture Zone and fills the deep Angola Basin from the north (Stramma and England, 1999). Additionally, AABW enters the Cape Basin from the south and flows clockwise to the Walvis Ridge before flowing south toward the Agulhas region near the African continent (dashed lines, Figure 1.3). South of the SAF, CDW is present at depth and joins with the southern extent of NADW to flow east as part of the Antarctic Circumpolar Current (***ACC***). Volume transport of the ACC has a wide range of estimates (87 to 148 Sv) and can vary up to 40 Sv annually (Whitworth and Peterson, 1985; Peterson 1988). An average value of ~100 Sv transport is assigned to the ACC (Peterson and Stramma, 1991; Orsi et al., 1995; Stramma, 2001).

1.3 Early applications of paleo-water mass tracers in the South Atlantic

1.3.1 Kaolinite/Chlorite Ratios

Provenance tracers can be used to determine the source regions of sediment to a specific core site. An extensive study of sea floor sediments within the South Atlantic reveals the diversity of sediments in the basin and also highlights regional patterns of clay mineral deposition (Figure 1.6; e.g. Biscaye, 1965; Petschick et al., 1996; Diekmann et al., 2004). The distribution of clay minerals in the South Atlantic is a result of weathering of the surrounding continents and transport by glacial, atmospheric, and hydrographic processes (e.g. Biscaye, 1965; Petschick et al., 1996). Kaolinite is a clay mineral that is derived from intense chemical weathering of feldspars in the tropical latitudes. It is found in old, acidic soils and is sourced from low latitudes. Conversely, chlorite is derived from high latitudes in the South Atlantic, where it is sourced from the Patagonian Andes and Antarctic Peninsula, and where weathering favors the formation of chlorite from low-grade metamorphic rocks (e.g. Diekman et al., 1999; Krueger et al., 2008). Both minerals are distributed across the South Atlantic via deep-water currents. Since kaolinite and chlorite are sourced from the north and south regions of the South Atlantic respectively, they can be used to monitor the northward or southward extent of corresponding water masses. Kaolinite is used as a proxy for NADW and chlorite is used as a proxy for southern sourced water masses and consequently kaolinite/chlorite (***K/C***) can been used to reconstruct changes in bottom water circulation from down-core records in the South Atlantic (e.g. Diekmann et al., 1999; Diekmann and Kuhn, 2002; Diekmann et al., 2003; Krueger et al., 2008). The conclusions of these studies support a shoaling and northward retreat of NADW in the South Atlantic during glacial periods based on a K/C greater than 0.5 as evidence for NADW presence (Figure 1.7).

1.3.2 Nutrient Proxies

Other water mass tracers applied to paleo-circulation studies in the South Atlantic are nutrient proxies. These proxies effectively tag water masses based on the amount of nutrient utilization that occurred in that water mass during its formation. The two nutrient proxies discussed here are $\delta^{13}C$ and Cd/Ca. The modern day distribution of $\delta^{13}C$ can distinguish NADW from water masses formed in the Southern Ocean and reveals NADW being "sandwiched" by Antarctic sourced water bodies (Figure 1.8). The northern or southern extent of these water masses during glacial times can be reconstructed by determining the $\delta^{13}C$ of benthic foraminifera preserved in deep-sea cores. $\delta^{13}C$ is defined as:

$$\delta^{13}C = [(({}^{13}C/{}^{12}C)_{samp}/({}^{13}C/{}^{12}C)_{std}) - 1] * 1000.$$

The average value of $\delta^{13}C$ for dissolved inorganic carbon (DIC) within the ocean is controlled by the balance between the ocean, atmosphere and terrestrial biosphere (reviewed in Ravelo and Hillaire-Marcel, 2007). For example, the terrestrial biosphere grows and becomes a reservoir for ^{13}C-depleted carbon because photosynthesis favors light carbon (^{12}C). In response the atmosphere and the ocean balances ^{13}C rich carbon. This drives $\delta^{13}C$ to higher values within the ocean. Also the $\delta^{13}C_{DIC}$ at any one location in the surface ocean is influenced by the amount of respiration and photosynthesis occurring, with greater photosynthesis increasing local $\delta^{13}C_{DIC}$. Lastly, local $\delta^{13}C_{DIC}$ is also influenced by changes in water mass mixing. The $\delta^{13}C$ of foraminiferal calcite can be used to reconstruct the $\delta^{13}C_{DIC}$ of the waters in which the foraminifera lived. In the South Atlantic, benthic foraminifera are used to reconstruct the $\delta^{13}C_{DIC}$ of past bottom waters and are used to produce records of changes in bottom water chemistry (e.g.

Curry and Lohmann, 1982; Duplessy et al., 1988; Mackensen et al., 2001; Hodell et al., 2003; Martínez-Méndez et al., 2009).

The presence of NADW in the South Atlantic is evidenced by anomalously high $\delta^{13}C_{DIC}$ and low nutrient concentration because NADW forms from sinking of nutrient depleted surface waters. This is contrasted against Southern Ocean sourced water masses such as AABW, which is rich in nutrients and low in $^{13}C/^{12}C$ as a result of an accumulation of respired ^{12}C during its extended deep-water residence time (Lynch-Stieglitz, et al., 2007). The deep North Pacific is defined by $\delta^{13}C$ values lower than that of the deep Southern Ocean and representative of the oldest deep waters (Figure 1.9). Studies using stable carbon isotopes of benthic foraminifera to determine bottom water $\delta^{13}C$ during the LGM suggest that the South Atlantic experienced more negative values during glacial periods (Figure 1.8). This shift of benthic $\delta^{13}C$ is indicative of an increased presence of southern sourced waters and less northern sourced waters and is seen across the basin for this time period (e.g. Oppo and Fairbanks, 1987; Charles and Fairbanks, 1992; Mackensen et al., 2001; Ninnemann and Charles, 2002; Hodell et al., 2003; Curry and Oppo, 2005; Martínez-Méndez et al., 2009). Of particular interest to this study is the similarity of the $\delta^{13}C$ records produced at core sites RC11-83 (40°36' S, 9°48' E, 4718m) and TN057-21 (41°08' S, 7°49' E, 4981m) (Figure 1.10*;* Ninnemann and Charles, 2002). These two sites are close to one another and at similar depths in the Cape Basin. The excellent agreement of the benthic $\delta^{13}C$ records demonstrates that these two sites were exposed to the same water masses during both the Holocene and LGM and also recorded the change in AMOC at the period. The reproducibility of these two sites is utilized to compare and splice together individual measurements from each core to create one dataset for Nd isotopes as discussed further below.

Despite the similarities of changes in seawater $\delta^{13}C$ seen in records from across the globe, $\delta^{13}C$ has some important limitations as a paleo-circulation tracer. As discussed above, local $\delta^{13}C_{DIC}$ (from which benthic calcite $\delta^{13}C$ is derived) can be influenced by factors other than water mass mixing. For example, sinking C_{org}, which varies with productivity, can influence $\delta^{13}C_{DIC}$ (e.g. Diz et al., 2007; Mackensen et al., 1993, 2001). Additionally, the low $\delta^{13}C$ values recorded during the LGM in core RC11-83 and TN057-21 are more negative than the $\delta^{13}C$ of the deep Pacific. This suggests that the $\delta^{13}C$ of the deep Cape Basin is influenced not only by water mass mixing but also local productivity, pore-water and air-sea exchange effects (e.g. Mackensen et al., 1993; Lynch-Stieglitz et al., 1995; Ninnemann and Charles, 2002; Piotrowski et al., 2005). The best approach for understanding the validity of paleoceanographic records that may be influenced by factors other than water mass mixing is by combining them with other circulation proxies. One additional proxy used in the South Atlantic to compare with benthic $\delta^{13}C$ is Cd/Ca.

Cd is taken up by organisms at the sea surface and released at depth during respiration, so high Cd/Ca is associated with nutrient rich waters with low $\delta^{13}C$. Cd/Ca is preserved in benthic foraminiferal calcite, similar to $\delta^{13}C$, and can be used to reconstruct changes in AMOC. Some records of Cd content of deep waters during the LGM suggest no change in the flux of NADW (low Cd concentrations) to the deep South Atlantic (e.g. Boyle et al., 1992; Rosenthal et al., 1997). However, other Cd/Ca records indicate increased flux of southern sourced waters into the deep South Atlantic and show better agreement with $\delta^{13}C$ records (Marchitto and Broecker, 2006). Resolving the conflicts between these records depends on understanding of the controls on Cd/Ca and benthic $\delta^{13}C$. For instance, surface productivity can significantly influence $\delta^{13}C$ (e.g. Mackensen and Licari, 2004). One tool for examining how productivity has changed in the

South Atlantic and Southern Ocean is to study how the flux of organic material has changed through time. However, only a very small amount of organic material is buried (<0.5%) so paleoceanographers must rely on other proxies buried in deep-sea cores. Authigenic uranium precipitates in reducing conditions, areas with high organic rain rate reduce pore water U(VI) to insoluble U(IV) and therefore high productivity regions are identified by high uranium concentrations preserved down core (Chase and Anderson, 2001). High authigenic uranium and therefore productivity was greater during glacial times and associated with high sea-surface temperatures in the Cape Basin (Sachs and Anderson, 2003, 2005). In addition to high productivity during glacials, anomalously cold intervals caused by Heinrich Events, associated with large-scale releases of icebergs into the North Atlantic, were times of high productivity in the South Atlantic (Figure 1.11; Sachs and Anderson, 2005). The combination of these findings reveals that during colder periods such as the LGM and Heinrich Events, the Cape Basin experienced a reduced flux of northern sourced waters, as revealed by $\delta^{13}C$ and K/C ratios. Additionally the anomalously cold periods were associated with increased productivity, as revealed by increased authigenic U, which would play a role in bottom water chemistry recorded by nutrient paleo-circulation proxies. The use of a paleoceanographic tracer that is independent of nutrient cycling and insusceptible to changes in regional productivity is essential to understanding water mass mixing changes in the South Atlantic. Nd isotopes are not influenced by changes in nutrient cycling and faithfully record changes in bottom water chemistry as a result of changes in water mass mixing (e.g. Goldstein and Hemming, 2003). The application of this paleoproxy in the Atlantic Ocean is further discussed below.

1.4 Development of Nd isotopes as a water mass tracer

Long-lived radioactive decay systems such as Sm-Nd are fundamental tools in earth science studies. In this case, as a result of the differing behavior of parent and daughter elements during partial melting of the mantle, Nd is favored over Sm in the liquid phase during partial melting and therefore the melt has a lower Sm/Nd than the melt-residue. A consequence is that the continental crust has a lower Sm/Nd than the "bulk Earth", and the mantle has a higher Sm/Nd. As ^{147}Sm decays to ^{143}Nd ($t_{1/2}$ = 1.06x10^{11} yr), the ^{143}Nd/^{144}Nd ratio of the continental crust reflects the enrichment of Nd over Sm and has a lower ^{143}Nd/^{144}Nd than the mantle. Also older continental material has a lower ^{143}Nd/^{144}Nd than rocks recently sourced from the mantle such as mid-ocean ridge and ocean island basalts. The resulting distribution of ^{143}Nd/^{144}Nd across the continents is heterogeneous, reflecting the age of the continent at any location, providing the basis for the use of Nd-isotopes as a geologic tracer. In order to compare Nd isotope ratios we report values as ε_{Nd} which is defined as the sample's ^{143}Nd/^{144}Nd value as a fractional deviation from the "bulk earth" (or chondritic uniform reservoir - CHUR) value, where (^{143}Nd/^{144}Nd)$_{CHUR}$ = 0.512638 (Jacobsen and Wasserburg, 1980).

$$\varepsilon_{Nd} = \left[\frac{(^{143}Nd/^{144}Nd)_R - (^{143}Nd/^{144}Nd)_{CHUR}}{(^{143}Nd/^{144}Nd)_{CHUR}} \right] * 10000$$

The ^{143}Nd/^{144}Nd ratio of eroded continent is preserved during the erosion process and the Nd isotope ratios of terrigenous sediments mirror those of the source regions. Material weathered from the continents is the dominant source of Nd to the oceans and ocean basins reflect the ε_{Nd} of surrounding continents (e.g. O'Nions et al., 1978, Piepgras et al., 1979; Goldstein and O'Nions, 1981). The North Atlantic Ocean is fed by runoff from very old continental crust and therefore

the dissolved Nd, and that of terrigenous sediments and authigenic precipitates, reflect old rock with low ε_{Nd}, while the North Pacific Ocean is defined by more positive ε_{Nd} values as a result of greater contributions from more radiogenic volcanic sources (e.g. Piepgras and Wasserburg, 1980, 1987; Goldstein and Hemming, 2003). Because the residence time of Nd is comparable to the mixing time of the ocean, ε_{Nd} in seawater reflects the geographic variability seen in the ε_{Nd} composition of the continents and can be used as a tracer for the mixing of water masses (e.g. Tachikawa et al., 1999; Jeandel et al., 1995; Frank, 2002; Goldstein and Hemming, 2003). The North Atlantic Ocean is characterized by ε_{Nd} values between -26 and -8, the Pacific Ocean is characterized by higher values (-4 to 0), and the Southern Ocean is defined by intermediate values (-9 to -7) reflecting contributions from both the Atlantic and the Pacific (e.g. Piepgras and Wasserburg, 1980, 1982, 1987; Piepgras and Jacobsen, 1988; Bertram and Elderfield, 1993; Shimizu et al., 1994). Nd isotopes correlate with salinity throughout the world's oceans and have been shown to vary in water column profiles; moreover they vary coherently with water mass mixing (Figure 1.12; von Blanckenburg, 1999; Goldstein and Hemming, 2003). The ε_{Nd} signatures of water near the seafloor reflect the water masses present, and are preserved in deep-sea archives such as authigenic Fe-Mn deposits (e.g. Piepgras et al., 1979; Rutberg et al., 2000). Down core samples of these types of deposits, provide great potential for the development of records of changes in bottom water ε_{Nd} and therefore changes in the water masses present through time. A growing number of studies make use of Nd isotopes and have been particularly successful in investigating AMOC in the Atlantic Ocean, as further discussed below (e.g. Rutberg et al., 2000; Bayon et al., 2002; Piotrowski et al., 2004, 2005, 2008; Gutjahr et al., 2008, 2010; Pahnke et al., 2008; Roberts et al., 2010, 2012; Gutjahr and Lippold, 2011; Xie et al., 2012).

1.5 Paleoceanographic studies using Nd isotopes in the Atlantic Ocean

Early studies of Nd isotopes in Fe-Mn nodules and core-top Fe-Mn coatings of sediments showed that these archives reflected the distribution of ε_{Nd} in bottom waters (O'Nions et al., 1978; Piepgras et al., 1979; Goldstein and O'Nions, 1981). Rutberg *et al.* (2000) developed the first ε_{Nd} record of Fe-Mn sediment leachates at subglacial timescales at Cape Basin site RC11-83, which was followed by additional studies in the Cape Basin (e.g. Bayon et al., 2002; Piotrowski et al., 2004, 2005, 2008). While a reliable recorder of bottom water ε_{Nd} in many cases, leachates of bulk sediment coatings could be contaminated by easily leachable materials in the sample such as fine clays or volcanic materials (e.g. Roberts et al., 2010, 2012; Piotrowski et al., 2012; Wilson et al., 2013). As a result, records derived from bulk or fine fraction sediment leachates are sometimes paired with data derived from the dissolutions of foraminiferal calcite and fossil fish debris which are devoid of terrigenous materials that may influence the seawater signal (e.g. Roberts et al., 2010, 2012; Elmore et al., 2011; Piotrowski et al., 2012). Agreement between these methods has been taken as evidence that the data reflect the ε_{Nd} of past bottom waters.

Nd isotopes applied in the Cape Basin, South Atlantic indicate changes in bottom waters with distinctly different ε_{Nd} values, making it possible to characterize the water masses present at the core site during a specific time interval. One Nd isotope record from sediment leachates, foraminiferal leachates and fish debris was developed by splicing records from cores RC11-83 (40°36' S, 9°48' E, 4718m) and TN057-21 (41°08' S, 7°49' E, 4981m) spanned the last ~90 kyr (Rutberg et al., 2000; Piotrowski et al., 2004; 2005; 2008; 2012). During present day, deep water at this core site is mainly composed of CDW and has a core top ε_{Nd} value of ~ -9.3 ± 0.16. There

is a positive shift of ~ 3 ε_{Nd} units during the LGM (~25 ka). More positive or radiogenic ε_{Nd} compositions of bottom waters during the LGM indicates more southern sourced waters at this depth. High ε_{Nd} values are also recorded during Marine Isotope Stage (***MIS***) 4 indicating that deep-water circulation during this glacial period resembled that of the LGM. During late interglacial MIS 5 (where these cores end), ε_{Nd} resembles more NADW like values. The record also shows shifts in ε_{Nd} on shorter time scales that coincide with abrupt climatic events in the Northern Hemisphere. For example, the ε_{Nd} indicates higher NADW export to the South Atlantic during warmer periods in the North Atlantic during the last ice age, and lower NADW export during colder periods (Piotrowski et al., 2004, 2005, 2012). A ε_{Nd} record from the northern Cape Basin (MD96-2086; 25°48.8', 12°7.7'; 3606 m), reports Holocene values of -12, which is indicative of more NADW influence in comparison to RC11-83-TNO57-21, likely reflecting its more northerly location and shallower depth (Bayon et al., 2002). This record shows a shift in ε_{Nd} from ~ -8 to ~ -12 from 14 ka BP to 6 ka BP, indicating that ε_{Nd} of bottom waters that were more Pacific-like at the site before the Holocene. These South Atlantic Nd isotope records record changes in bottom water composition that indicates a reduction in the influence of NADW during colder climate periods. These findings are in agreement with $\delta^{13}C$ records from the Cape Basin and support a weakening of AMOC during colder climate intervals.

Other Atlantic Basin ε_{Nd} records support the fluctuations of AMOC seen in the Cape Basin. A study from central South Atlantic core MD07-3076 shows an increase in ε_{Nd} associated with less northern sourced waters reaching the site during the LGM and suggests that reorganizations in AMOC are also recorded at this site (Skinner et al., 2013). In the North Atlantic, Nd studies reveal changes in bottom water chemistry associated with changes in the contributions of southern-sourced waters to both the deep and intermediate waters of the North

Atlantic. Roberts et al. (2010) show an increase in the influence of southern sourced waters to the deep northwest Atlantic during the LGM and Younger Dryas (***YD***). ε_{Nd} of deep waters along the Bermuda Rise shifted from ~ -10.5 to ~ -16 during the most recent deglaciation and reveals that waters at this site were composed of a mixture of both northern and southern sourced waters during the LGM (Figure 1.13; Roberts et al., 2010). In the eastern North Atlantic, the influence of southern sourced waters is apparent during the LGM but to a greater extent than the Bermuda Rise record (Figure 1.13; Piotrowski et al., 2012). In the eastern North Atlantic, Holocene ε_{Nd} values were similar to those at the Bermuda Rise but LGM ε_{Nd} values resembled those of Cape Basin glacial levels suggesting the greatest influence of southern sourced waters in the eastern North Atlantic during the LGM (Figure 1.13; Piotrowski et al., 2012). Changes in the presence of shallower southern sourced water masses like AAIW in the North Atlantic have also be monitored using Nd isotopes though the conclusions of these studies suggest both a greater influence during the LGM and during times associated with reduced NADW production (Pahnke et al., 2008) and a reduced presence of AAIW during the LGM (Xie et al., 2011). The general agreement of ε_{Nd} records in indicating changes in the water masses during the late Quaternary, and similarities to the changes in AMOC predicted by benthic $\delta^{13}C$, demonstrates the value of using Nd isotopes and affirms the value of benthic $\delta^{13}C$, to investigate reorganizations of ocean circulation.

1.6 Conclusions and goals

The South Atlantic Ocean is an important region for the study of sudden changes in NADW export to the Southern Ocean and AMOC reorganizations. By using deep-sea sediment archives such as clay mineral assemblages, stable carbon isotopes and Cd/Ca ratios of benthic

foraminifera, and long-lived isotope ratios, changes in bottom water chemistry can be reconstructed. These proxies show agreement in terms of the implications for the behavior of NADW circulation during warm and cold climate intervals on short millennial to long glacial-interglacial time scales. The Last Glacial Maximum is a period of reduced northern sourced water and increased southern sourced water in the deep South Atlantic. Applying several proxies in one region offers significant promise in determining accurate records of paleoceanographic changes in the South Atlantic Ocean. The following chapter of this thesis utilizes the Nd paleoproxy to investigate changes in AMOC and presents the first ε_{Nd} data collected in the Cape Basin for 100 – 400 ka. The Nd-composition of seawater in the modern North Atlantic is evaluated in the second half of this thesis and sheds light on the Nd-composition of water mass signatures and transport. The aim of this thesis is to further understand the Nd cycle of the oceans, its influence on water mass compositions and the application of Nd isotopes in distinguishing changes of water mass mixing in modern oceans and of changes in the AMOC in ancient oceans.

1.7 References

Antonov, J. I., et al. World Ocean Atlas 2009 Volume 2: Salinity. S. Levitus, Ed., NOAA Atlas NESDIS 69, U.S. Government Printing Office, Washington, D.C., 184 pp. (2010).

Basak, C., et al. "Southern Ocean source of 14C-depleted carbon in the North Pacific Ocean during the last deglaciation." Nature Geoscience 3.11 (2010): 770-773.

Bayon, G., et al. "An improved method for extracting marine sediment fractions and its application to Sr and Nd isotopic analysis." Chemical Geology 187.3 (2002): 179-199.

Bertram, C. J., and H. Elderfield. "The geochemical balance of the rare earth elements and neodymium isotopes in the oceans." Geochimica et Cosmochimica Acta 57.9 (1993): 1957-1986.

Biscaye, P. E. "Mineralogy and sedimentation of recent deep-sea clay in the Atlantic Ocean and adjacent seas and oceans." Geological Society of America Bulletin 76.7 (1965): 803-832.

Burton, K. W., and D. Vance. "Glacial–interglacial variations in the neodymium isotope composition of seawater in the Bay of Bengal recorded by planktonic foraminifera." *Earth and Planetary Science Letters* 176.3 (2000): 425-441.

Boyle, E.A. (1992). “Cadmium and d13C paleochemical ocean distributions during the stage 2 glacial maximum.” Annu. Rev. Earth Planet. Sci. 20: 245-87.

Charles, C. D; Fairbanks, R.G. (1992). "Evidence from Southern Ocean sediments for the effect of North Atlantic deep-water flux on climate." Nature 355: 416-419.

Chase, Z; and R. F. Anderson, (2001). "Evidence from authigenic uranium for increased productivity of the glacial Subantarctic Ocean." Paleoceanography 16(5): 468-478.

Curry, W. B., and G. P. Lohmann. "Carbon isotopic changes in benthic foraminifera from the western South Atlantic: Reconstruction of glacial abyssal circulation patterns." Quaternary Research 18.2 (1982): 218-235.

Curry, W. B., and D. W. Oppo. "Glacial water mass geometry and the distribution of δ13C of ΣCO2 in the western Atlantic Ocean." *Paleoceanography* 20.1 (2005).

Diekmann, B., and G. Kuhn. "Sedimentary record of the mid-Pleistocene climate transition in the southeastern South Atlantic (ODP Site 1090)." Palaeogeography, Palaeoclimatology, Palaeoecology 182.3 (2002): 241-258.

Diekmann, B., et al. "Kaolinite and chlorite as tracers of modern and late Quaternary deep water circulation in the South Atlantic and the adjoining Southern Ocean." Use of Proxies in Paleoceanography. Springer Berlin Heidelberg, 1999. 285-313.

Diekmann, B., et al. "Terrigenous sediment supply in the polar to temperate South Atlantic: Land-ocean links of environmental changes during the late Quaternary." The South Atlantic in the Late Quaternary. Springer Berlin Heidelberg, 2004. 375-399.

Diekmann, B., et al. "Environmental history of the south‐eastern South Atlantic since the Middle Miocene: Evidence from the sedimentological records of ODP Sites 1088 and 1092." Sedimentology 50.3 (2003): 511-529.

Diz, P, et al. "Paleoceanography of the southern Agulhas Plateau during the last 150 ka: Inferences from benthic foraminiferal assemblages and multispecies epifaunal carbon isotopes." Paleoceanography 22. (2007).

Duplessy, J. C., et al. "Deepwater source variations during the last climatic cycle and their impact on the global deepwater circulation." Paleoceanography 3.3 (1988): 343-360.

Emery, W. J., “Water types and water masses.” Encyclopedia of Atmospheric Sciences., pp 3179–3187 (2001)

Elmore, A. C., et al. "Testing the extraction of past seawater Nd isotopic composition from North Atlantic deep sea sediments and foraminifera." Geochemistry, Geophysics, Geosystems 12.9 (2011)

Frank, M. "Radiogenic isotopes: Tracers of past ocean circulation and erosional input." Reviews of Geophysics. 40. (2002)

Goldstein, S. L and S. R. Hemming. "Long-lived Isotopic tracers in Oceanography, Paleococeanography and Ice-sheet dynamics". Treatise on Geochemistry. E. H. Elderfield, Elsevier, Oxford. 6: 453-489. (2003).

Goldstein, S. L and R. K. O'Nions. "Nd and Sr isotopic relationships in pelagic clays and ferromanganese deposits." Nature. 292: 324-327. (1981)

Gordon, A. L., et al. "Thermocline and intermediate water communication between the South Atlantic and Indian Oceans." Journal of Geophysical Research: Oceans (1978–2012) 97.C5 (1992): 7223-7240.

Gutjahr, M., and J. Lippold. "Early arrival of Southern Source Water in the deep North Atlantic prior to Heinrich event 2." Paleoceanography 26.2 (2011).

Gutjahr, M., et al. "Changes in North Atlantic Deep Water strength and bottom water masses during Marine Isotope Stage 3 (45–35kaBP)." Quaternary Science Reviews 29.19 (2010): 2451-2461.

Gutjahr, M., et al. "Tracing the Nd isotope evolution of North Atlantic deep and intermediate waters in the Western North Atlantic since the Last Glacial Maximum from Blake Ridge sediments." Earth and Planetary Science Letters 266.1 (2008): 61-77.

Hodell, D. A., et al. "Pleistocene vertical carbon isotope and carbonate gradients in the South Atlantic sector of the Southern Ocean." Geochemistry, Geophysics, Geosystems 4.1 (2003): 1-19.

Jacobsen, S. B., and G. J. Wasserburg. "Sm-Nd isotopic evolution of chondrites." Earth and Planetary Science Letters 50.1 (1980): 139-155.

Jeandel, C., J. K. Bishop, and A. Zindler. "Exchange of neodymium and its isotopes between seawater and small and large particles in the Sargasso Sea." Geochimica et Cosmochimica Acta 59.3 (1995): 535-547.

Klevenz, V., et al. "Neodymium isotopes in benthic foraminifera: core-top systematics and a down-core record from the Neogene south Atlantic." Earth and Planetary Science Letters 265.3 (2008): 571-587.

Kraft, S., et al. "Assessment of seawater Nd isotope signatures extracted from foraminiferal shells and authigenic phases of Gulf of Guinea sediments." Geochimica et Cosmochimica Acta 121 (2013): 414-435.

Krueger, S., et al. "Ocean circulation patterns and dust supply into the South Atlantic during the last glacial cycle revealed by statistical analysis of kaolinite/chlorite ratios." Marine Geology 253.3 (2008): 82-91.

Locarnini, R. A., et al., World Ocean Atlas 2009, Volume 1: Temperature. S. Levitus, Ed., NOAA Atlas NESDIS 68, U.S. Government Printing Office, Washington, D.C., 184 pp. (2010).

Lynch-Stieglitz, J., et al. "The influence of air-sea exchange on the isotopic composition of oceanic carbon: Observations and modeling." *Global Biogeochemical Cycles* 9.4 (1995): 653-665.

Lynch-Stieglitz, J., et al. "Atlantic meridional overturning circulation during the last glacial maximum." Science 316: 66-69 (2007).

Mackensen, A., and L. Licari. "Carbon isotopes of live benthic foraminifera from the South Atlantic: sensitivity to bottom water carbonate saturation state and organic matter rain rates." The South Atlantic in the Late Quaternary. Springer Berlin Heidelberg, 2004. 623-644.

Mackensen, A., et al. "The δ13C in benthic foraminiferal tests of *Fontbotia wuellerstorfi* (Schwager) relative to the δ13C of dissolved inorganic carbon in southern ocean deep water: implications for glacial ocean circulation models." Paleoceanography 8.5 (1993): 587-610.

Mackensen, A., et al. "Late Pleistocene deep-water circulation in the subantarctic eastern Atlantic." Global and Planetary Change 30.3 (2001): 197-229.

Marchitto, T. M., and W. S. Broecker. "Deep water mass geometry in the glacial Atlantic Ocean: A review of constraints from the paleonutrient proxy Cd/Ca." Geochemistry, Geophysics, Geosystems 7.12 (2006).

Martin, E. E., and H. D. Scher. "Preservation of seawater Sr and Nd isotopes in fossil fish teeth: bad news and good news." Earth and Planetary Science Letters 220.1 (2004): 25-39.

Martínez-Méndez, G., et al. "Variable water column structure of the South Atlantic on glacial–interglacial time scales." Quaternary Science Reviews 28.27 (2009): 3379-3387.

Ninneman, U. S and C. D. Charles. "Changes in the mode of Southern Ocean circulation over the last glacial cycle revealed by foraminiferal stable isotopic variability." Earth and Planetary Science Letters 201: 383-396. (2002).

O'Nions, R. K., et al. "Pb, Nd and Sr isotopes in oceanic ferromanganese deposits and ocean floor basalts." Nature 273 (1978): 435-438.

Oppo, D. W; and R. G. Fairbanks. "Variability in the deep and intermediate water circulation of the Atlantic Ocean during the past 25,000 years: Northern Hemisphere modulation of the Southern Ocean." Earth and Planetary Science Letters 86. (1987).

Orsi, A. H., et al. "On the meridional extent and fronts of the Antarctic Circumpolar Current." Deep Sea Research Part I: Oceanographic Research Papers 42.5 (1995): 641-673.

Pahnke, K., et al. "Abrupt changes in Antarctic Intermediate Water circulation over the past 25,000 years." Nature Geoscience 1.12 (2008): 870-874.

Palmer, M. R., and H. Elderfield. "Variations in the Nd isotopic composition of foraminifera from Atlantic Ocean sediments." *Earth and planetary science letters* 73.2 (1985): 299-305.

Palmer, M. R., and H. Elderfield. "Rare earth elements and neodymium isotopes in ferromanganese oxide coatings of Cenozoic foraminifera from the Atlantic Ocean." *Geochimica et Cosmochimica Acta* 50.3 (1986): 409-417.

Pena, L. and S. L. Goldstein, "Thermohaline circulation crisis and impacts during the mid-Pleistocene transition." Science 345 (2014): 318-322.

Pena, L. D., et al. "Rapid changes in meridional advection of Southern Ocean intermediate waters to the tropical Pacific during the last 30kyr." Earth and Planetary Science Letters 368 (2013): 20-32.

Peterson, R. G and L. Stramma. "Upper-level circulation in the South Atlantic Ocean." Prog. Oceanog 26: 1-73. (1991).

Peterson, R. G. "On the transport of the Antarctic Circumpolar Current through Drake Passage and its relation to wind." Journal of Geophysical Research: Oceans (1978–2012) 93.C11 (1988): 13993-14004.

Petschick, R; Kuhn, G; Gingele, F. "Clay mineral distribution in the surface sediments of the South Atlantic: sources, transport, and relation to oceanography". Marine Geology. 130: 203-229. (1996).

Piepgras, D. J. and G. J. Wasserburg. "Influence of the Mediterranean outflow on the isotopic composition of neodymium in waters of the North Atlantic." Journal of Geophysical Research: Oceans (1978–2012) 88.C10 (1983): 5997-6006.

Piepgras, D. J. and G. J. Wasserburg. "Isotopic composition of neodymium in waters from the Drake Passage." Science 217.4556 (1982): 207-214.

Piepgras, D. J. and G. J. Wasserburg. "Strontium and neodymium isotopes in hot springs on the East Pacific Rise and Guaymas Basin." Earth and planetary science letters 72.4 (1985): 341-356.

Piepgras, D. J. and G. J. Wasserburg. “Rare Earth Element Transport in the Western North Atlantic Inferred from Nd Isotopic Observations.” Geochimica et Cosmochimica Acta 51, no. 5 (1987): 1257–71.

Piepgras, D. J. et al. "The isotopic composition of Nd in different ocean masses." Earth and Planetary Science Letters 45.2 (1979): 223-236.

Piepgras, D. J., and G. J. Wasserburg. "Neodymium isotopic variations in seawater." Earth and Planetary Science Letters 50.1 (1980): 128-138.

Piepgras, D. J., and S. B. Jacobsen. "The isotopic composition of neodymium in the North Pacific." Geochimica et Cosmochimica Acta 52.6 (1988): 1373-1381.

Piotrowski, A. M; et al. "Oscillating glacial northern and southern deep water formation from combined neodymium and carbon isotopes." Earth and Planetary Science Letters 272: 394-405. (2008).

Piotrowski, A. M; et al. "Intensification and variability of ocean thermohaline circulation through the last deglaciation." Earth and Planetary Science Letters 225: 205-220. (2004).

Piotrowski, A. M, et al. "Temporal Relationships of Carbon Cycling and ocean circulation at glacial boundaries." Science 307: 1933-1938.

Piotrowski, A. M., et al. "Reconstructing deglacial North and South Atlantic deep water sourcing using foraminiferal Nd isotopes." Earth and Planetary Science Letters 357 (2012): 289-297.

Ravelo, A. C. and C. Hillaire-Marcel. "The Use of oxygen and carbon isotopes of foraminifera in paleoceanography." Developments in Marine Geology v.1. Chapter 18. (2007).

Reid, J. L. "On the total geostrophic circulation of the North Atlantic Ocean: Flow patterns, tracers, and transports." Progress in Oceanography 33.1 (1994): 1-92.

Roberts, N. L., et al. “Synchronous Deglacial Overturning and Water Mass Source Changes.” Science 327, no. 5961 (January 1, 2010): 75–78.

Roberts, N. L., et al. "Rare earth element association with foraminifera." Geochimica et Cosmochimica Acta 94 (2012): 57-71.

Roman, R. E., and J. R. E. Lutjeharms. "Antarctic intermediate water at the Agulhas Current retroflection region." Journal of Marine Systems 81.4 (2010): 273-285.

Rosenthal, Y., et al. "Last glacial maximum paleochemistry and deepwater circulation in the Southern Ocean: Evidence from foraminiferal cadmium." Paleoceanography 12.6 (1997): 787-796.

Rutberg, R. H., et al. "Reduced North Atlantic Deep Water flux to the glacial Southern Ocean inferred from neodymium isotope ratios." Nature 405. (2000)

Sachs, J. A., and R. F. Anderson. "Fidelity of alkenone paleotemperatures in southern Cape Basin sediment drifts." Paleoceanography 18(4). (2003).

Sachs, J. A., and R. F. Anderson "Increased productivity in the subantarctic ocean during Heinrich events." Nature 434: 1118-1121. (2005).

Sarmiento, J. L., et al. "Response of ocean ecosystems to climate warming." Global Biogeochemical Cycles 18.3 (2004).

Scher, H. D., and E. E. Martin. "Oligocene deep water export from the North Atlantic and the development of the Antarctic Circumpolar Current examined with neodymium isotopes." Paleoceanography 23.1 (2008).

Scher, H. D., and E. E. Martin. "Timing and climatic consequences of the opening of Drake Passage." Science 312.5772 (2006): 428-430.

Schmitz Jr, W. J. On the World Ocean Circulation. Volume 1. Some Global Features/North Atlantic Circulation. No. WHOI-96-03-VOL-1. WOODS HOLE OCEANOGRAPHIC INSTITUTION MA, 1996.

Shimizu, H., et al. "Cerium and neodymium isotope ratios and REE patterns in seawater from the North Pacific Ocean." Geochimica et cosmochimica acta 58.1 (1994): 323-333.

Skinner, L. C., et al. "North Atlantic versus Southern Ocean contributions to a deglacial surge in deep ocean ventilation." Geology 41.6 (2013): 667-670.

Stordal, M. C., and G. J. Wasserburg. "Neodymium isotopic study of Baffin Bay water: sources of REE from very old terranes." Earth and Planetary Science Letters 77.3 (1986): 259-272.

Stramma, L. “Current Systems in the Atlantic Ocean.” 1st edition of Encyclopedia of Ocean Sciences, volume 1, pp 589–598 (2001)

Stramma, L., and M. England. "On the water masses and mean circulation of the South Atlantic Ocean." Journal of Geophysical Research 104(C9): 20863-20883. (1999).

Tachikawa, K., et al. "Neodymium budget in the modern ocean and paleo‐oceanographic implications." Journal of Geophysical Research: Oceans (1978–2012) 108.C8 (2003).

Thomas, D. J. "Evidence for deep-water production in the North Pacific Ocean during the early Cenozoic warm interval." Nature 430.6995 (2004): 65-68.

Thomas, D. J., et al. "Neodymium isotopic reconstruction of late Paleocene–early Eocene thermohaline circulation." Earth and Planetary Science Letters 209.3 (2003): 309-322.

Vance, D., and K. Burton. "Neodymium isotopes in planktonic foraminifera: a record of the response of continental weathering and ocean circulation rates to climate change." *Earth and Planetary Science Letters* 173.4 (1999): 365-379.

von Blanckenburg, F. "Tracing past ocean circulation?." Science 286.5446 (1999): 1862-1863.

Whitworth III, T., and R. G. Peterson. "Volume transport of the Antarctic Circumpolar Current from bottom pressure measurements." Journal of Physical Oceanography 15.6 (1985): 810-816.

Wilson, D. J., et al. "A boundary exchange influence on deglacial neodymium isotope records from the deep western Indian Ocean." Earth and Planetary Science Letters 341 (2012): 35-47.

Wilson, D. J., et al. "Reactivity of neodymium carriers in deep sea sediments: Implications for boundary exchange and paleoceanography." *Geochimica et Cosmochimica Acta* 109 (2013): 197-221.

Xie, R. C., et al. "Deglacial variability of Antarctic Intermediate Water penetration into the North Atlantic from authigenic neodymium isotope ratios." Paleoceanography 27.3 (2012).

Table 1.1: Acronyms used in the chapter

AABW	Antarctic Bottom Water
AAIW	Antarctic Intermediate Water
ACC	Antarctic Circumpolar Current
AMOC	Atlantic Meridional Overturning Circulation
APF	Antarctic Polar Front
CDW	Circumpolar Deep Water
NADW	North Atlantic Deep Water
NBC	North Brazil Current
SAF	Subantarctic Front
SEC	South Equatorial Current
STF	Subtropical Front

Table 1.2: T-S properties of deep and intermediate water masses in the South Atlantic

	T (°C)	S
AABW	-0.9 - 1.7	34.64 - 34.72
AAIW	2.0 – 6.0	33.80 - 34.80
CDW	1.0 – 2.0	34.62 - 34.73
NADW	1.5 – 4.0	34.80 - 35.00

1.8 Figures

Figure 1.1. Shallow and upper-level currents and fronts in the South Atlantic demonstrate the dominance of the subtropical gyre circulation. Within the Cape Basin, surface waters are sourced from both the western basin and from the Agulhas Current carrying Indian Ocean waters to the Atlantic. Surface waters leave the Cape Basin to the north in the Benguela Current (Peterson and Stramma 1991).

Figure 1.2. Additional diagram of upper-level (<100m) currents in the South Atlantic showing increased detail of equatorial currents (Stramma and England, 1999). Shown are Falkland Current (FC); the Brazil Current; the South Equatorial Current (SEC), with the northern (NSEC), equatorial (ESEC), central (CSEC), and southern (SSEC) branches; the South Equatorial Countercurrent (SECC); the South Equatorial Undercurrent (SEUC); the Angola Gyre; the Equatorial Undercurrent (EUC); the North Brazil Current (NBC); the North Equatorial Countercurrent (NECC); and the Guinea Current (GC).

Figure 1.3. Representation of deep water mass transport (Stramma and England, 1999). North Atlantic Deep Water (NADW) flow is shown as gray arrows. Antarctic Bottom Water (AABW) flow paths are shown as black dashed lines. NADW enters the Cape Basin from the north and the west. AABW enters the study region from the south.

Figure 1.4. Temperature and salinity properties of the intermediate and deep Cape Basin from WOA09 (Antonov et al., 2009; Locarnini et al., 2009). T-S properties highlight the water masses present in the basin. The water masses listed are Antarctic Intermediate Water (AAIW), North Atlantic Deep Water (NADW), Circumpolar Deep Water (CDW) and Antarctic Bottom Water (AABW).

Figure 1.5. a) Southern Ocean sea surface temperature (WOA09; Antonov et al., 2009). Drastic changes of sea surface temperature are indicative of polar fronts in this region. b) Schematic modified from Sarmiento et al., 2004 demonstrating the relationship between polar fronts and deep water formation in the Southern Ocean. Acronyms are as follows: Circumpolar Deep Water (CDW), Antarctic Intermediate Water (AAIW), Subantarctic Mode Water (SAMW), Antarctic Polar Front (APF), Polar Frontal Zone (PFZ), Subantarctic Front (SAF), Subantarctic Zone (SAZ), Subtropical Front (STF).

Figure 1.6. Clay mineral distribution, provenances and pathways in the South Atlantic. (Petschick et al., 1996). Kaolinite is sourced from low latitudes and shows strongest transport into the Cape Basin via deep water currents. As a result, kaolinite is linked to North Atlantic Deep Water transport. Chlorite is sourced to the study region from high latitudes and is a proxy for southern sourced deep water currents.

Figure 1.7. Kaolinite/chlorite changes in the South Atlantic for the last 800 kyr (modified from Diekmann et al., 2003). Kaolinite is a northern sourced clay mineral while chlorite is southern sourced. During interglacial periods, Kao/Chl is higher indicating the presence of North Atlantic Deep Water. During glacial periods, Kao/Chl decreases to <0.5 indicative of a reduced influx of North Atlantic Deep Water.

Figure 1.8. The $\delta^{13}C$ distribution in the Atlantic Ocean during modern and LGM times (Curry and Oppo, 2005; Ravelo and Hillaire-Marcel, 2007). In the modern Atlantic Ocean, North Atlantic Deep Water is characterized by a high $\delta^{13}C$ and reaches depths ~3000 m in the South Atlantic. During the LGM, the South Atlantic is filled with lower $\delta^{13}C$ waters and North Atlantic Deep Water reaches a shallower depth.

Figure 1.9. Modern $\delta^{13}C$ distribution throughout the western Atlantic and Pacific Oceans (Curry and Oppo, 2005; Ravelo and Hillaire-Marcel, 2007). Asterisks mark ODP cores. North Atlantic Deep Water is characterized by high $\delta^{13}C$ values similar to the shallow waters from which it has formed. The deep Pacific is characterized by very low values as a result of being composed of older ^{12}C rich waters.

Figure 1.10. Benthic foraminifera $\delta^{13}C$ records of South Atlantic cores RC11-83 and TNO57-21 (Ninnemann and Charles, 2002). The two core sites are in close proximity and show good agreement for the last 70 kyr. This record is used as an intercalibration test in order to develop a spliced record of RC11-83 and TNO57-21.

Figure 1.11. Productivity changes in the South Atlantic for the last ~70 kyr (modified from Sachs and Anderson, 2005). a) Alkenone concentration (green) and ^{230}Th-normalized alkenone flux (blue) in TNO57-21. b) Authigenic uranium concentrations in TNO57-21. c) $\delta^{18}O$ variations in Byrd, Antarctica ice core. Climate events such as the Younger Dryas (YD), Heinrich events (H) and Antarctic Cold Reversals (ACR) are labeled. Compiling these records demonstrates an increase in productivity in the Cape Basin not only during the Last Glacial Maximum but also during abrupt events.

Figure 1.12. Salinity distribution in the Atlantic Ocean shown with ε_{Nd} seawater profiles. (von Blanckenburg, 1999). Nd-isotope ratios vary in the water column with salinity demonstrating the behavior of ε_{Nd} as a water mass tracer.

Figure 1.13. ε_{Nd} records from the Atlantic Ocean during Termination I (Piotrowski et al., 2012). Records show more radiogenic values during the LGM consistent with a weakening of AMOC. North Atlantic sites exhibit more NADW like values during the Holocene than the Cape Basin record but during the LGM the northeastern Atlantic site has values comparable to the Cape Basin suggesting southern sourced waters dominated mixing during the LGM. The Bermuda Rise record however shows lower values during the LGM indicating that southern sourced waters did not occupy the western Atlantic to the same extent as in the eastern basin. Figure is from Piotrowski et al., 2012.

Figure 1.1: Upper-level currents and fronts in the South Atlantic

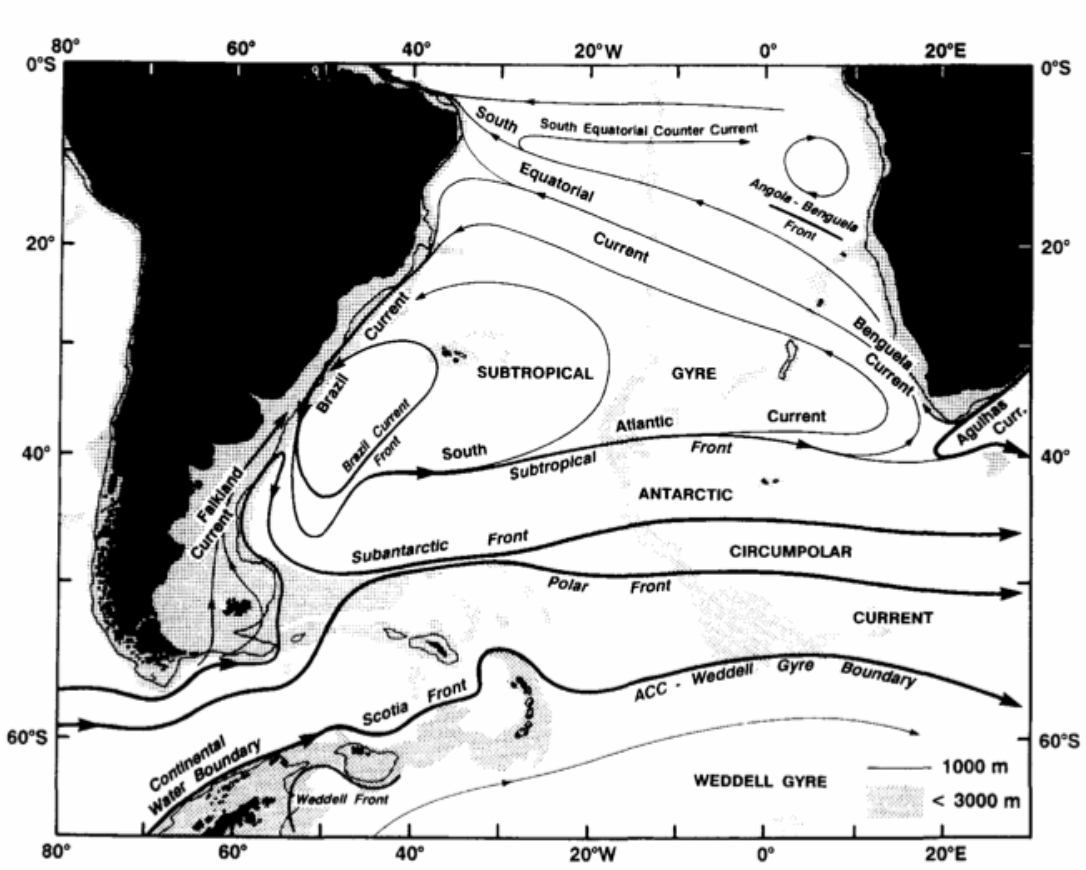

Figure 1.2: Upper-level currents in the Equatorial South Atlantic

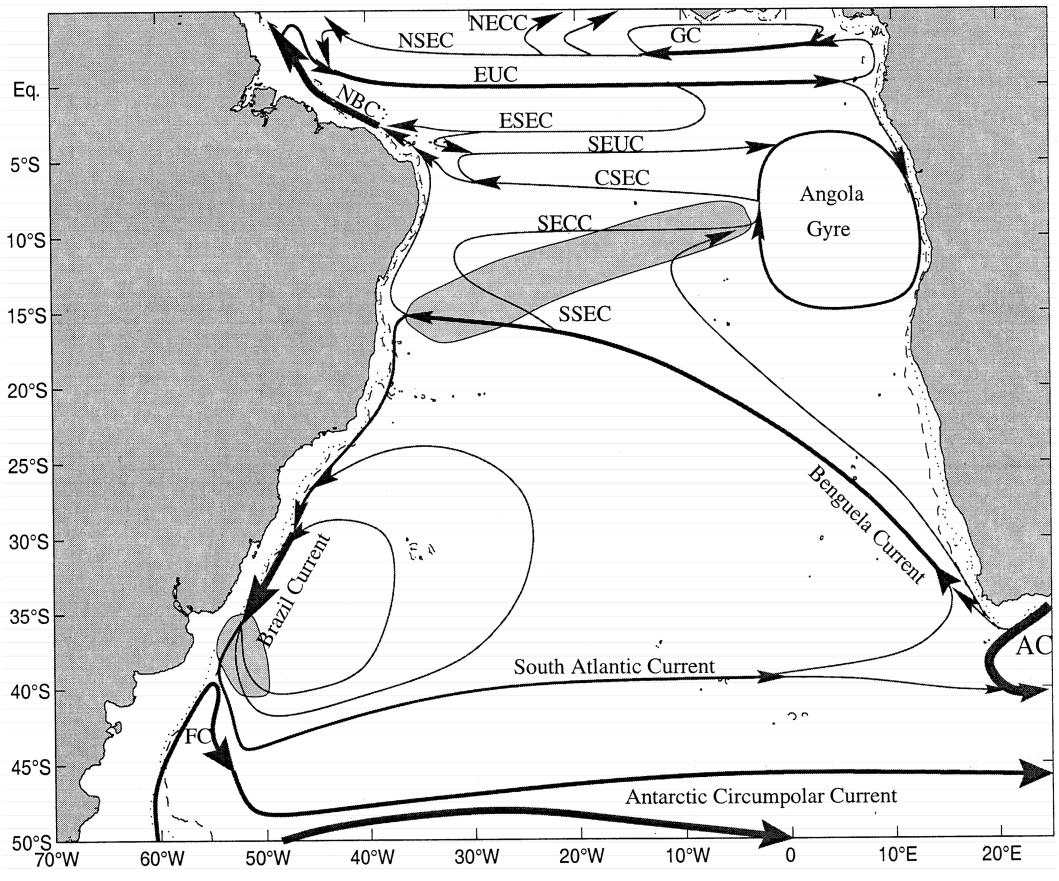

Figure 1.3: Deep water circulation in the South Atlantic

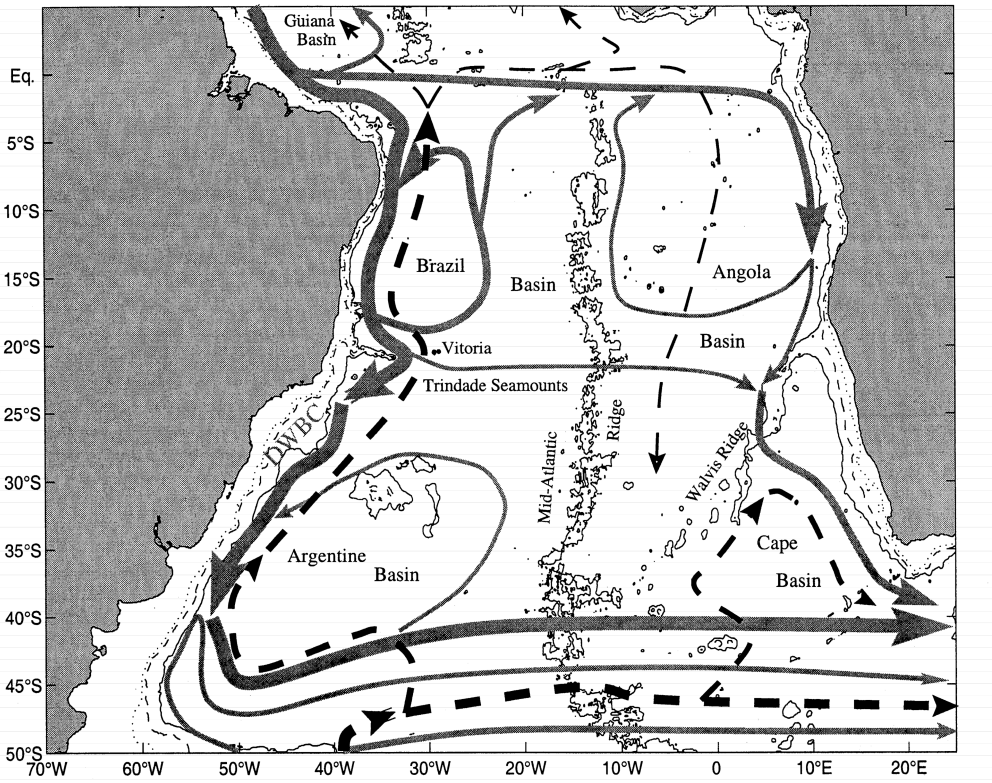

Figure 1.4: T-S properties of waters in the Cape Basin from WOA09

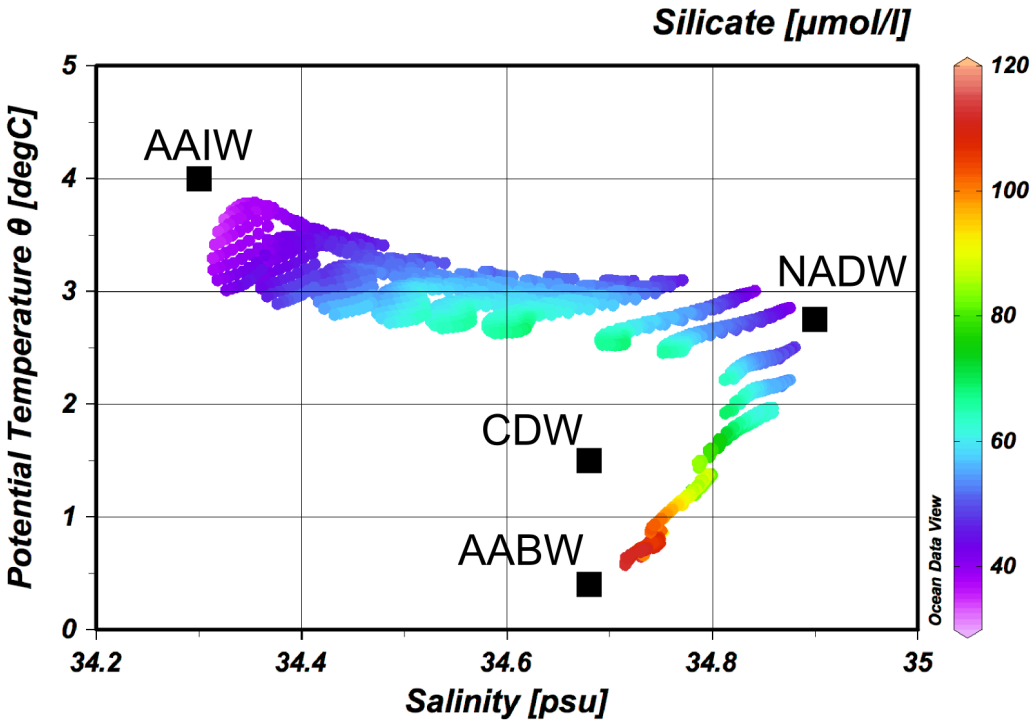

Figure 1.5: Southern Ocean sea surface temperature and deep water formation diagram

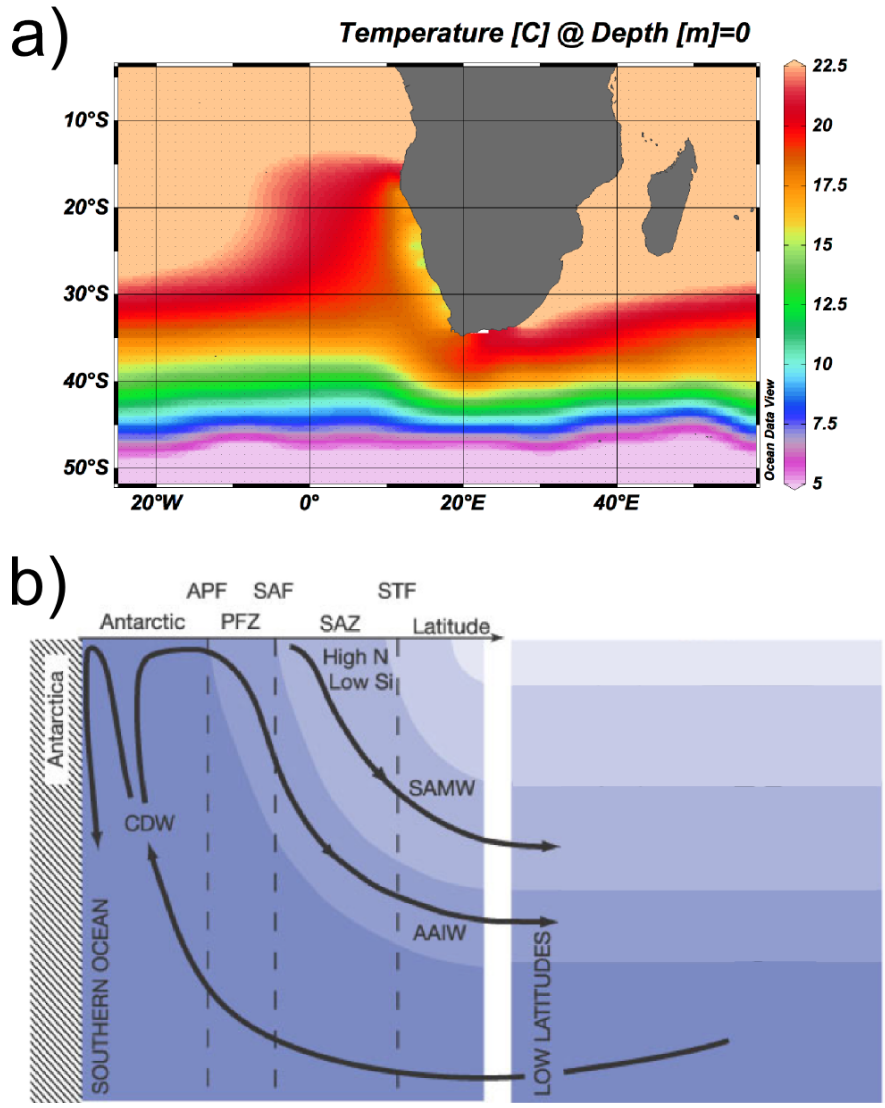

Figure 1.6: Clay mineral distributions in the South Atlantic

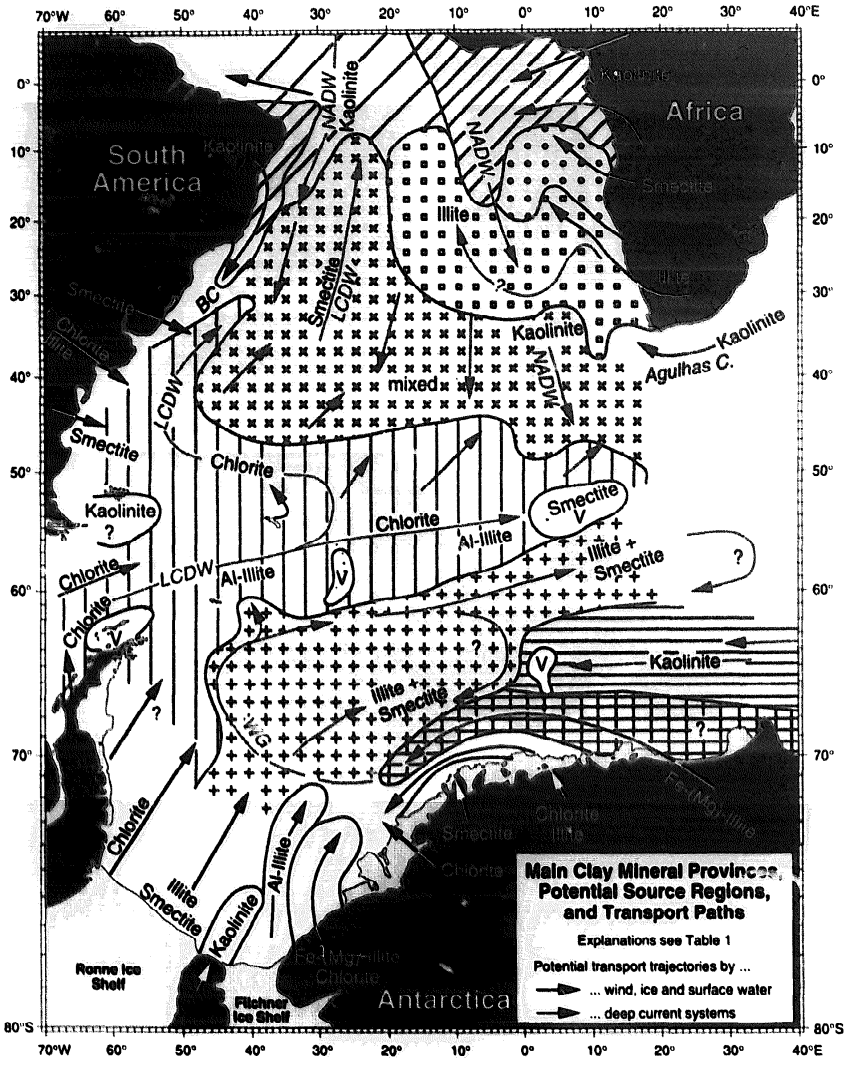

Figure 1.7: Kaolonite/Chlorite changes in the South Atlantic during the last 800 kyr

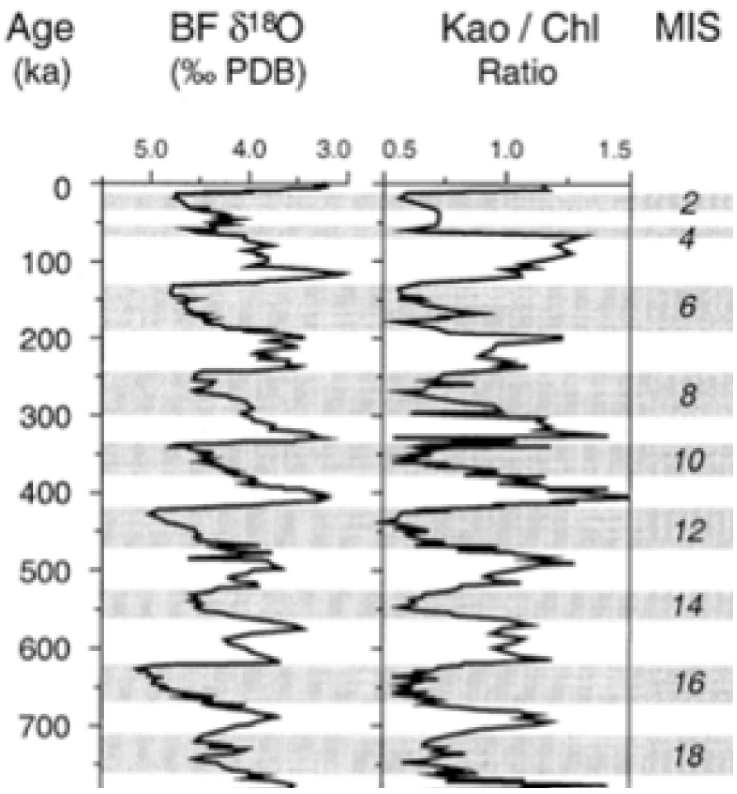

Figure 1.8: $\delta^{13}C$ distribution in the modern and LGM Atlantic Ocean

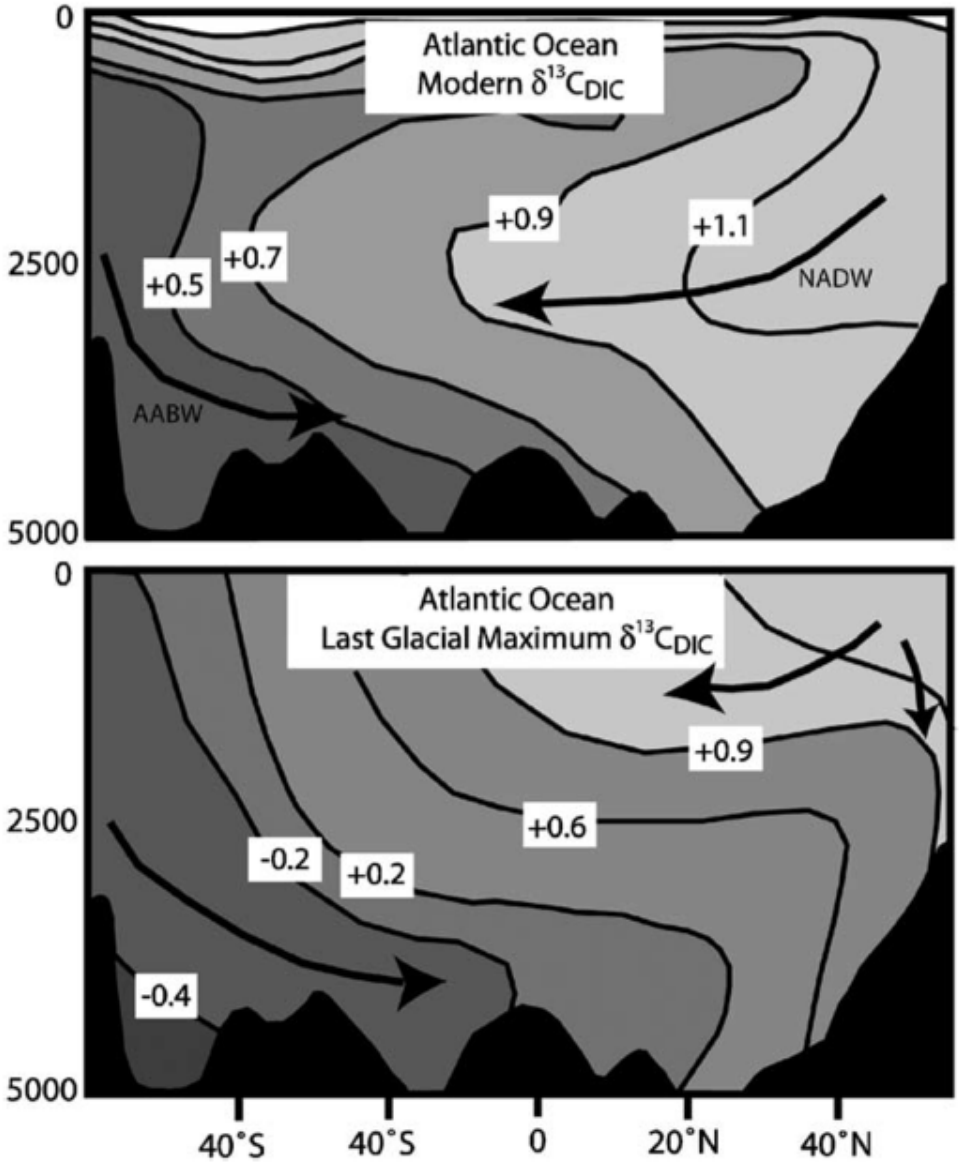

Figure 1.9: $\delta^{13}C$ distribution in the modern western Atlantic and Pacific Oceans

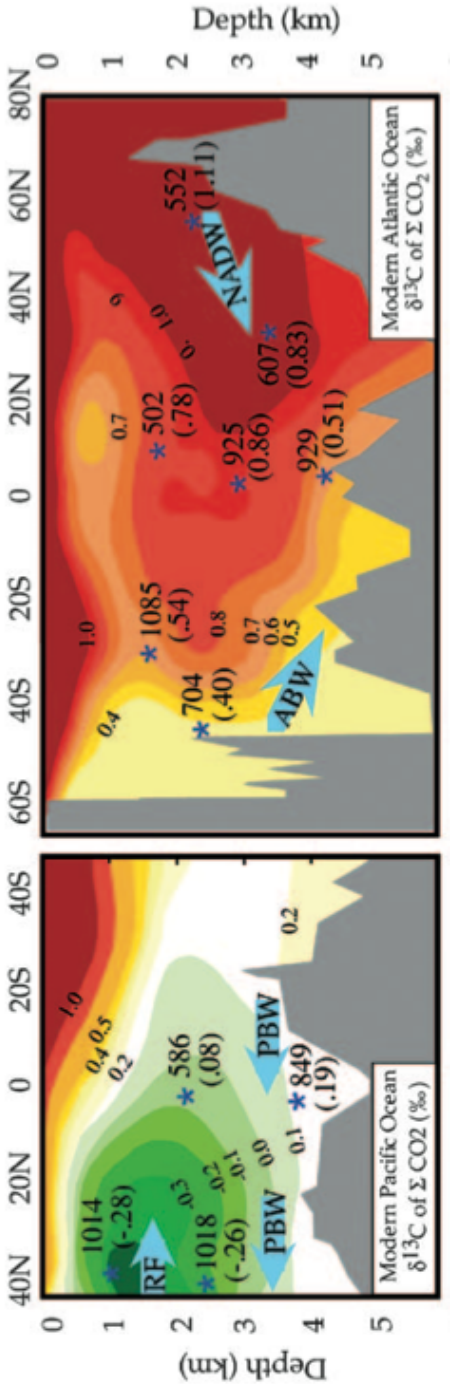

Figure 1.10: $\delta^{13}C$ of benthic foraminifera for two South Atlantic cores

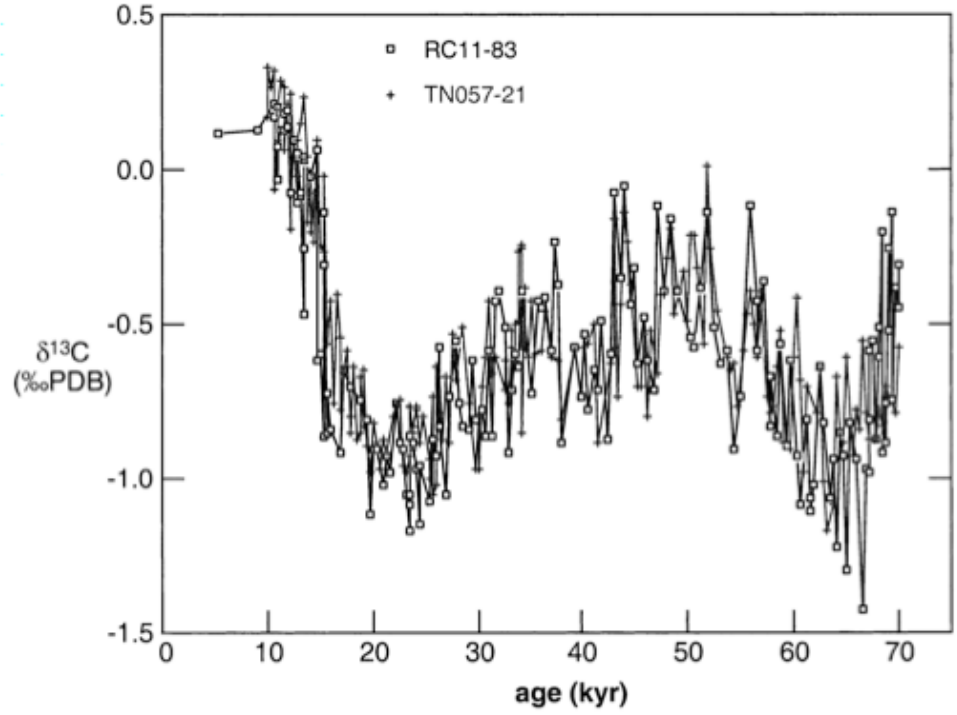

Figure 1.11: Productivity changes in the Cape Basin during the last ~70 kyr

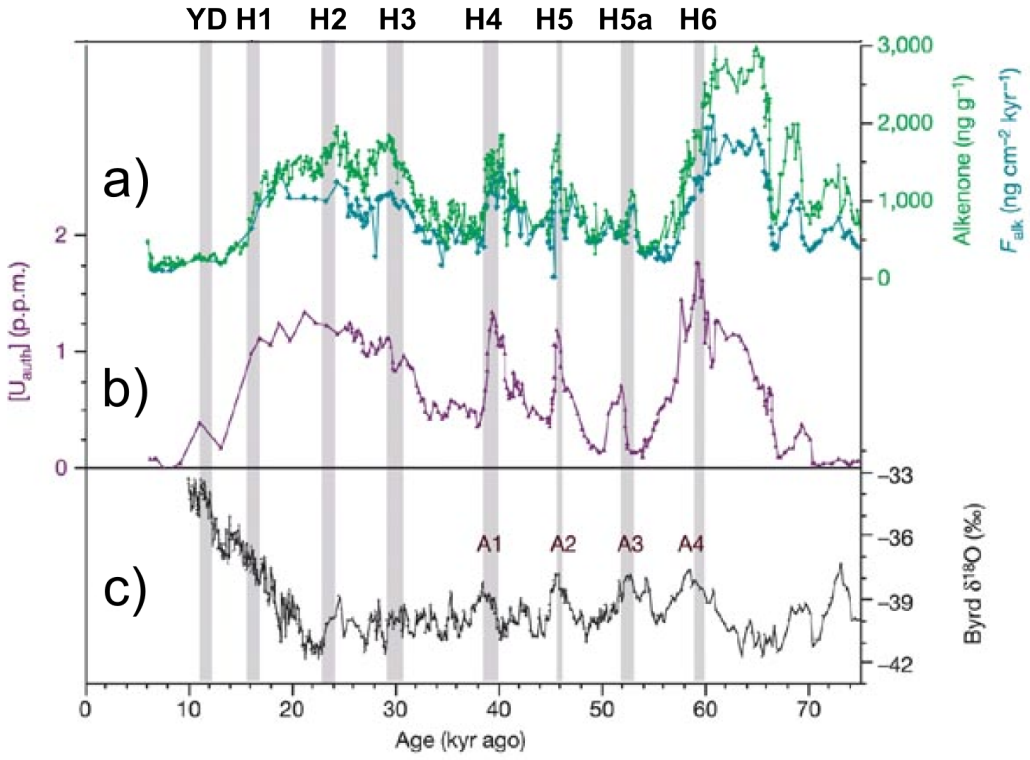

Figure 1.12: Salinity distribution of the Atlantic Basin with ε_{Nd} seawater profiles

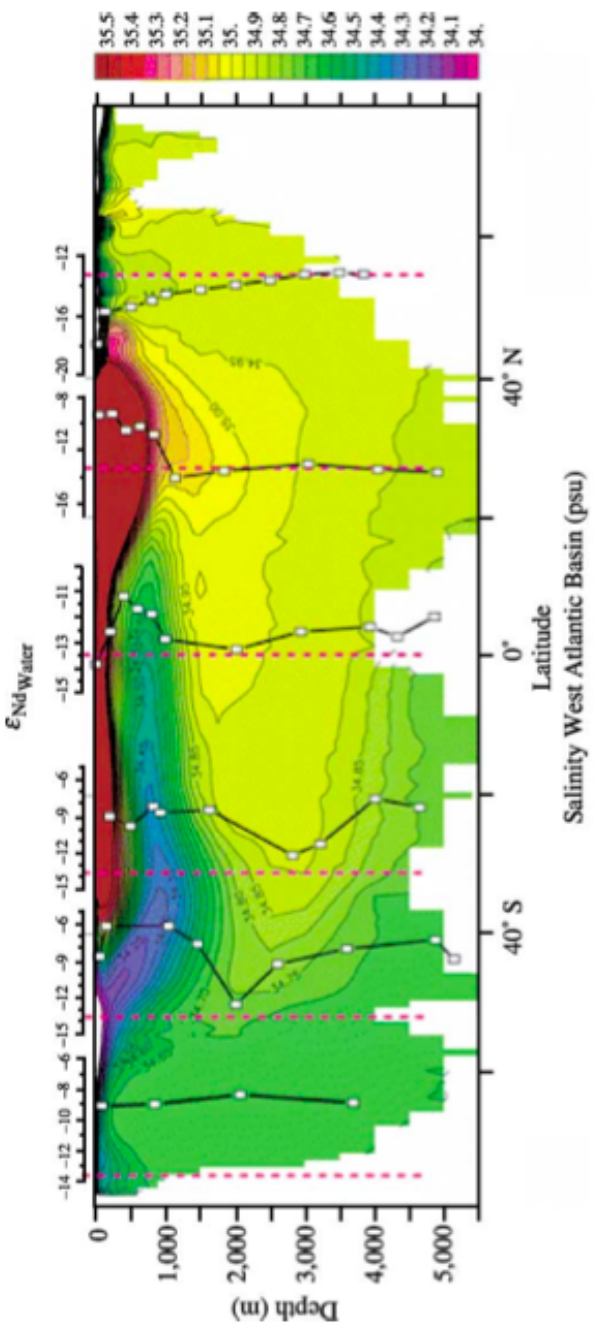

Figure 1.13: ε_{Nd} records from the Atlantic Basin during Termination I

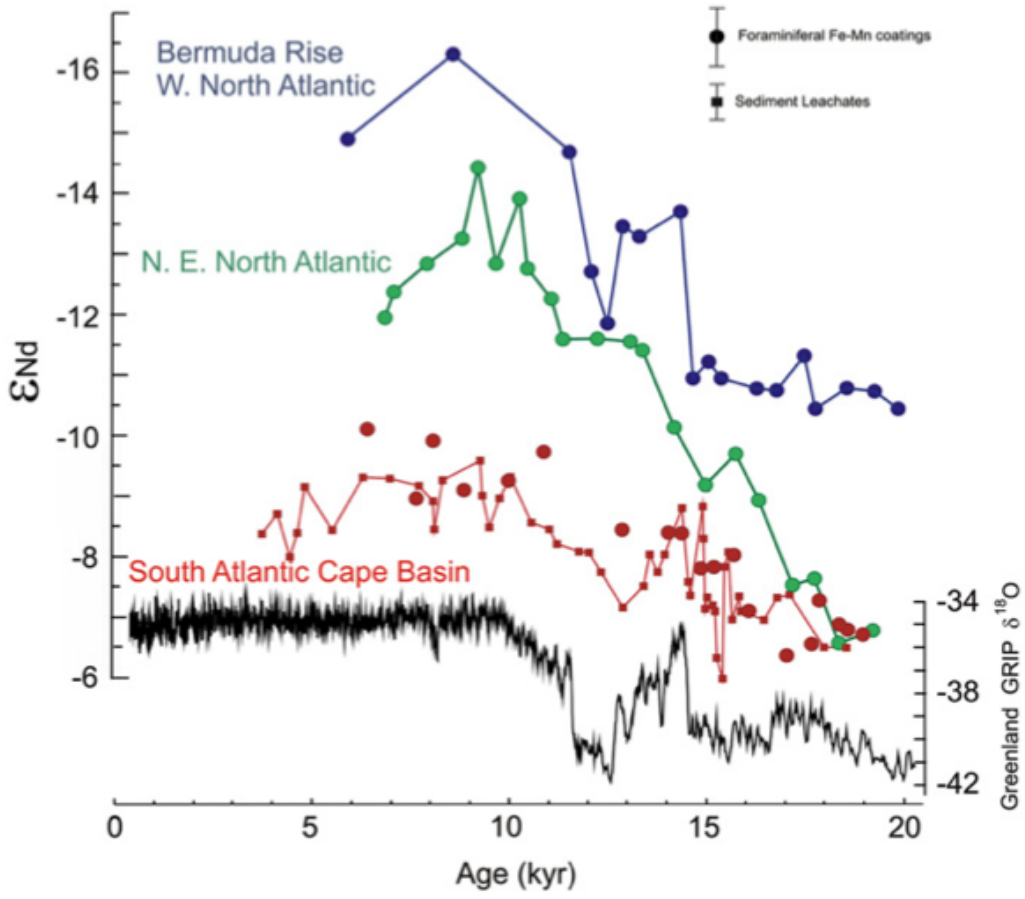

Chapter 2. Atlantic Meridional Overturning Circulation variability through Marine Isotope Stage 11 from Nd isotopes

Abstract

The changing intensity of the Atlantic Meridional Overturning Circulation ***(AMOC)*** is a primary trigger or a major feedback for the Earth's glacial-interglacial cycles. Here we use neodymium ***(Nd)*** isotopes as a water mass tracer to study changes in the presence of North Atlantic Deep Water (***NADW***) in the South Atlantic, which is a dominant branch of AMOC and an important indicator of its strength, during glacial-interglacial cycles over the last ~400 ka, since Marine Isotope Stage ***(MIS)*** 11. Most of the data focus on glacial-interglacial maxima and indicate that glacial cycles since MIS 11 show similar reductions in AMOC and are comparable to the last glacial maximum ***(LGM)***, and the enhanced AMOC during interglacial times mirrors the conditions in the modern South Atlantic. A high resolution Holocene through LGM time series confirms the same magnitude of AMOC weakening during the LGM as previous studies in deeper water, along with a more homogeneous glacial water column dominated by southern-sourced water masses, and a coeval deglacial transition to stronger AMOC. These agreements add additional credence to these previous records. A high resolution time series across the MIS 9/8 transition shows that the timing of the reduction in AMOC coincides with the shift of benthic foraminiferal $\delta^{13}C$ to less northern-sourced water values and lags the shift in $\delta^{18}O$. This comparison shows that both ε_{Nd} and $\delta^{13}C$ are reliably recording changes in AMOC at the core site in the Cape Basin, and suggests that global ice sheet growth and/or cooling predates the reduction in AMOC during this transition. Comparison with published ε_{Nd} records in the South

Atlantic over the last glacial cycle reaffirms that not only does the AMOC weaken during glacial periods but also ε_{Nd} can be utilized as a reliable proxy to follow these changes.

2.1 Introduction

The global ocean circulation system is a major means of transporting heat and distributing nutrients around the Earth, and has been proposed to play an essential role in the onset of glacial-interglacial cycles [e.g. Crowley, 1992; Broecker, 1998; Rahmstorf, 2002; Stocker and Johnsen, 2003; Barker et al., 2009]. In the present-day ocean, a key component of the global circulation system is the formation of North Atlantic Deep Water (***NADW;*** acronyms used in this chapter are listed in Table 2.1) and its transport southward to the Southern Ocean, which is compensated by northward transport of Antarctic Bottom Water and Antarctic Intermediate Water (***AABW*** and ***AAIW***, respectively). Although there is strong evidence from paleocirculation proxies and modeling studies indicating that this Atlantic Meridional Overturning Circulation (***AMOC***) system underwent reorganization during The Last Glacial Maximum (***LGM***) and preceding glacial-interglacial cycles, the magnitude and timing of these changes are not well-known, particularly for the older cycles [e.g. Boyle and Keigwin 1982; Stieglitz et al., 2007; Lippold et al., 2012; Ritz et al., 2013]. The South Atlantic is a key region for the study of these changes because its location at the interface with the Southern Ocean makes it sensitive to variations in the southward flux of NADW.

Studies focusing on nutrient based proxies have revealed complications in the investigation of how the AMOC differed during the last glacial cycle. The variability of $\delta^{13}C$ in benthic foraminifera in the South Atlantic reflects a number of different processes, including the partitioning of carbon between the terrestrial and ocean carbon reservoirs, the environmental and

biological conditions of the foraminifera under study, changes in productivity in the water column, air-sea exchange, changes in the vigor of the AMOC [e.g. Boyle, 1992; Charles and Fairbanks, 1992; Mackensen et al., 2001; Marchitto and Broecker, 2006; Mackensen 2008; Martínez-Méndez et al., 2009]. In addition, benthic $\delta^{13}C$ records disagree with Cd/Ca, another nutrient-based paleo-circulation proxy, in predicting changes in nutrient concentrations of southern ocean waters during glaciations as a result of AMOC changes [e.g. Boyle, 1992]. These complications have motivated the pairing of such records with those derived from proxies independent of nutrient cycling, such as neodymium (***Nd***) isotopes, to investigate changes in AMOC reorganizations over glacial-interglacial cycles.

An important application of Nd isotopes makes use of the differences in values in southern and northern sourced deep waters that reach the South Atlantic, reflecting changes in the strength of NADW export [e.g. Rutberg et al., 2000; Bayon et al., 2002; Piotrowski et al., 2004, 2005, 2008, 2012]. These studies used ε_{Nd} of authigenic phases in deep-sea sediments to investigate the presence of northern-sourced waters in the South Atlantic Ocean. They have shown changes in water ε_{Nd}-values indicative of more southern sourced waters bathing the sediments during the last glacial cycle compared to the Holocene and the last interglacial, and conclude that this reflects reduced NADW production during glacial times [Rutberg et al., 2000; Piotrowski et al., 2004, 2005, 2008, 2012]. Records of Nd isotopes in the North Atlantic support these findings and suggest increased presence of southern sourced waters during glacial times [e.g. Pahnke et al., 2008; Roberts et al., 2010; Piotrowski et al., 2012].

In this study we expand the time-scale of South Atlantic Nd isotope records as a tool to investigate AMOC changes during the last ~400 ka, through Marine Isotope Stage (***MIS***) 11, based on Nd isotopic analyses of foraminifera and fish debris. We focus our attention on core

TN057-6 (42°54.8'S, 8°54'E, 3751m), located at the interface of Circumpolar Deep Water (***CDW***) and NADW. We report analyses from the core top through the LGM at this critical depth for comparison to published deeper records from RC11-83 (40°36' S, 9°48' E, 4718m) and TN057-21 (41°08' S, 7°49' E, 4981m), which are limited to the last glacial cycle [Rutberg et al., 2000; Piotrowski et al., 2004, 2005, 2008, 2012]. Also, in order to investigate the relationship between AMOC reorganizations and climate transitions, we present ε_{Nd} data during the MIS 9/8 glaciation. Finally, we also focus on long-term changes in the AMOC, based on analyses during glacial and interglacial maxima over the length of the core.

2.2 Nd isotopes and ocean circulation

Nd isotopes were shown as far back as the late 1970s to trace water-masses from seawater and Fe-Mn-nodule and crust studies, and a paleocirculation proxy in Fe-Mn crust studies [e.g. O'Nions et al., 1978; Piepgras et al., 1979; Elderfield et al., 1981; Goldstein and O'Nions, 1981; Aplin et al., 1986; Futa et al., 1988; Albarède and Goldstein, 1992]. In deep-sea cores, Palmer and Elderfield [1985, 1986] showed that Nd isotopes in Fe-Mn encrusted core-top foraminifera samples reflect the deep-sea water near the core sites. Rutberg et al., [2000] was the first to use Nd isotope ratios of dispersed Fe-Mn oxide precipitates within sediments to develop a record of changing AMOC intensity on sub-orbital time-scales, and since then this approach has been extensively applied to address late Quaternary ocean circulation based on analyses of Fe-Mn oxides and fish debris [e.g. Goldstein and Hemming, 2003; Piotrowski et al., 2004, 2005, 2012; Gutjahr et al., 2007, 2010; Klevenz et al., 2008; Pahnke et al., 2008; Martin et al., 2010; Roberts et al., 2010, 2012; Gutjahr and Lippold, 2011; Wilson et al., 2012; Xie, et al., 2012; Skinner et al., 2013; Pena and Goldstein, 2014]. In addition, the Nd isotopic composition of

clean planktonic foraminiferal calcite has been shown to mirror the Nd signature of the shallow ocean sites that these foraminifera grow in and has been used to investigate changes in ocean circulation within the upper water column [e.g. Vance and Burton, 1999; Burton and Vance, 2000, Klevenz et al., 2008; Pena et al., 2013].

As a result of the decay of ^{147}Sm to ^{143}Nd ($t_{1/2}$= 106 Ga), the $^{143}Nd/^{144}Nd$ isotope ratios vary in the continental crust depending on the crustal age (here $^{143}Nd/^{144}Nd$ will be referred to as ε_{Nd}, the deviation in parts per 10^4 from the average solar system value of 0.512638 based on chondritic meteorites [Jacobson and Wasserburg, 1980]). Due to the short marine residence time of Nd (500-1000 years), similar to the time of ocean mixing [e.g. Goldstein and O'Nions, 1981; Jeandel et al., 1995; Tachikawa et al., 1999], ε_{Nd} is variable in the oceans. The north Atlantic is surrounded by old continent going back to the Archean with low ε_{Nd}-values, and the north Pacific is surrounded by young volcanoes erupting rocks with high ε_{Nd}-values. This is reflected in low ε_{Nd} = ~ -13.5 in NADW, and ~ -4 in deep Pacific waters (***DPW***). The Circum-Antarctic and the Indian Ocean shows intermediate values as a result of mixing of these end-members ($\varepsilon_{Nd}\approx$ -8 to -9) [Piepgras and Wasserburg, 1982; Piepgras and Wasserburg, 1987; Albarède and Goldstein 1992, von Blankenburg and Nagler, 2001, Goldstein and Hemming, 2003]. Additionally, ε_{Nd} displays no biological or environmental fractionation, which has been shown to have an influence on other water mass tracers. Moreover, Nd behaves quasi-conservatively within the oceans which means that water masses tend to preserve their ε_{Nd} over long transport paths; this is reflected in Atlantic intermediate and deep water masses, which have ε_{Nd}-values that reflect mixing of North Atlantic- and Southern Ocean-derived water masses [e.g. Goldstein and Hemming, 2003]. Interpreting changes in the ε_{Nd} of the bottom waters in the South Atlantic over long time intervals is dependent on an understanding of the compositions of the North

Atlantic and North Pacific water mass end-members. Fe-Mn crust studies have been used to establish the stability of North Atlantic and North Pacific deep-water ε_{Nd} composition and demonstrate that the deep-water masses in these regions are uniform for the time period relevant to this study (last ~400 kyr) [e.g. Abouchami et al., 1997; Burton et al., 1999; Foster et al., 2007].

2.3 Material and Methods

2.3.1 Site Location

TN057-6 was recovered from the Agulhas Ridge, north of the modern day Subantarctic Front and south of the Subtropical Convergence (Figure 2.1a). Its stratigraphy is based on the stable isotope record of Hodell et al. [2000], which shows an approximate sedimentation rate of 3 cm/kyr. We sampled TN057-6 for mixed species planktonic foraminifera every ~3.5 cm from the core top to ~23 ka, resulting in a temporal resolution of approximately a sample every 1 kyr, and found fish debris with a resolution of a sample every 8 kyr. Sample pairs of foraminifera and fish debris samples were taken from glacial and interglacial maxima for the rest of the core through MIS 11 at ~ 400 ka. The MIS 9/8 transition includes a sample every 2 kyr between ~256 ka and ~324 ka. All ages reported in the text are ka cal-BP.

2.3.2 Methods

We applied different methods to size fractions of core material, foraminifera, and fish debris to compare the effects of different leaching procedures on the ε_{Nd} signal of authigenic substrates. These included the fine fraction (<63μm), for which we tried two leaching procedures, and in addition we leached bulk samples, and foraminifera separates. For the fine fraction, ~300 mg were used, carbonates were dissolved with buffered acetic acid, then rinsed

with distilled water three times and treated with a 0.02 M hydroxylamine hydrochloride ***(HH)*** for ~2hr to remove Fe-Mn coatings [Chester and Hughes, 1967; Rutberg et al., 2000; Piotrowski et al., 2004]. A less abrasive leaching protocol was also applied to replicate fine fractions (<63 um) as well as bulk samples, using an HH-EDTA mixed solution for no more than 1hr [Gutjahr et al., 2007]. In addition, mixed species planktonic foraminifera were picked from the >125μm size fraction and processed following a method similar to Roberts et al. [2010]. For the foraminifera, approximately 30mg of material was gently crushed to open chambers and sonicated in water to disaggregate clays. This process was repeated until all clays were removed and any remaining lithogenic material was removed under microscope. The samples were sonicated and dissolved in a weak nitric acid solution (~0.1N) then centrifuged and transferred to a teflon vial. Previous studies have shown that fish debris and authigenic leachates of foraminiferal calcite and sediment agree well without a reductive cleaning protocol [e.g. Martin et al., 2010]. Where available, 30μg of fish debris was positively identified using electronic microscopy and dissolved in 3N nitric acid, centrifuged and transferred to a clean teflon vial [modified from Martin et al., 2010]. In all samples, rare earth elements ***(REE)*** were separated using Tru-spec™ column chemistry. Nd was separated from the other REEs using 0.15M alpha-hydroxy-isobuteric acid (α-HIBA) on AG50W-X4, 200-400 mesh columns. Nd isotope ratios were measured using a Micromass Sector 54-30 thermal ionization mass spectrometer at Lamont-Doherty Earth Observatory. The separated Nd was loaded onto a rhenium filament and $^{143}Nd/^{144}Nd$ ratios were measured as NdO+. $^{146}Nd/^{144}Nd$ ratios were normalized to a value of 0.7219 with a typical ^{144}Nd beam intensity of $0.5x10^{-11}$ amps and adjusted to a JNdi-1 value of $^{143}Nd/^{144}Nd = 0.512115$ (Tanaka et al., 2000). External reproducibility from routine runs of JNdi-1 standards was

$^{143}Nd/^{144}Nd$ = 0.512101±5 (2σ, n = 8) and $^{143}Nd/^{144}Nd$ = 0.512081±14 (2σ, n = 37) during two different measurement sessions.

2.4 Results

2.4.1 Nd isotopes from different authigenic substrates and integrity of the marine signal

Results are listed in Table 2.2. Recent studies have debated whether sediment leachates accurately reflect the near bottom seawater ε_{Nd} [Roberts et al., 2010; Elmore et al., 2011; Piotrowski et al., 2012; Kraft et al., 2013]. In this study, we investigate the validity of published sediment leachate data at core site TN057-6 (42°54.8'S, 8°54'E, 3751m) located in the Cape Basin (Figure 2.1). Previous work has reported Nd isotope measurements of bulk sediment leachates during the LGM and the Holocene [Rutberg et al., 2000; Piotrowski et al., 2004]. Rutberg et al. [2000] reported ε_{Nd} = -8.11±0.35 and -4.02±0.21 for 4.1 ka and 16.6 ka, respectively. Measurements of a Holocene-LGM pair by Piotrowski et al., [2004] showed ε_{Nd} values of -7.69±0.21 and -5.55±0.21 for 5.8 ka and 19.4 ka respectively. These data were interpreted to represent either a reduction of northern-sourced waters reaching the South Atlantic during the LGM, or shoaling of those waters. In comparison to the ε_{Nd} record of nearby but deeper cores RC11-83-TN057-21 (Figure 2.1), Holocene values showed good agreement indicating that these two sites were bathed in similar bottom waters, while during the LGM the TN057-6 ε_{Nd}-values are more positive compared to -6.4±0.22 for RC11-83-TN057-21 (RC11-83 (40°36' S, 9°48' E, 4718m) and TN057-21 (41°08' S, 7°49' E, 4981m)). This was interpreted to indicate that TN057-6 was exposed to more southern-sourced waters, reflecting its location being more to the south (Figure 2.2a) [Rutberg et al., 2000; Piotrowski et al., 2004]. Partly in order to

pursue these differences between TN057-6 and RC11-83-TN057-21, we processed sediment leachates, fish teeth and foraminiferal calcite for Nd isotopes.

In TN057-6 the foraminifera dissolutions show excellent agreement with fish debris but both give consistently more negative ε_{Nd}-values than the sediment leachates (Figure 2.2b). The Holocene sediment leachates reported in this study (gray circles at ~3.5 ka and ~9 ka, Figure 2.2b) show good agreement with the previously published Holocene data for TN057-6 but show up to a 2 ε_{Nd}-unit offset towards more negative values during the LGM. Fine fraction (<63 um) sediment leachates were measured from the same glacial depths as those previously reported and confirmed that the data could not be reproduced using the established protocols of Rutberg et al. [2000] and Piotrowski et al. [2004] (gray circles, Figure 2.2b). This test revealed that despite treating different cuts of the same fine fraction sample with the same leaching protocol that had been used on RC11-83-TN057-21, as confirmed by Piotrowski et al. (2012), on the TN057-6 samples we were not obtaining reproducible bottom water Nd signatures, and the leaching procedure appears to be partly sampling an easily leachable non-authigenic fraction within the sediment. To test for the influence of 'contaminant' material in the sediment, we analyzed four types of substrates for Nd isotope ratios at three different depths (9.4 ka 15.9 ka and 23.8 ka). These are bulk sediment leachates, fine fraction (<63um) leachates, and dissolutions of foraminiferal calcite and fish debris. The bulk and fine fraction sediment leachates show variable agreement with each other and previously reported sediment leachates (teal squares and blue circles; Figure 2.2b), consistent with the findings of other studies [e.g. Roberts et al., 2010; Elmore et al. 2011; Piotrowski et al., 2012; Wilson et al., 2013], who showed when using even gentle leaching methods for brief exposure times, the marine integrity of the Nd isotope ratios in bulk and fine fraction sediment leachates at some core sites are jeopardized by the leaching of

detrital material in the core. On the other hand, in agreement with these previous studies, the ε_{Nd}-values we derived from dissolutions of foraminiferal calcite and fish debris are nearly identical (red diamonds and yellow triangles; Figure 2.2b).

A recent study reports seawater Nd data for the South Atlantic [Stichel et al., 2012] including station PS71/101, which is ~1 degree northeast of TN057-6 (Figure 2.1a) and therefore the ε_{Nd} of present-day nearby seawater can be compared with our core-top measurements. The analyses at 3000 m and 4400 m depth [Stichel et al. 2012], with water properties (S = 34.83 and 34.73, T_{pot}= 1.88 and 0.72, respectively) are comparable to those of bottom waters at site TN057-6 (from a depth in-between at 3751m, S = 34.719, T_{pot} = 1.05; Hodell et al., 2003). Modern seawater analysis yields ε_{Nd}-values of –10.9±0.39 and -9.7±0.39, which matches with core-top planktonic foraminifera dissolutions and fish debris values of ε_{Nd} = -10.0 ±0.28 and -10.12 ±0.28 (Figure 2.3a). The previously published Holocene values for TN057-6 are -7.69 ±0.21 and -8.11 ±0.35 [Rutberg et al., 2000; Piotrowski et al., 2004], which are offset from the modern seawater and again indicates that the ε_{Nd} of these samples do not reflect the bottom seawater. Taking into account the agreement between the foraminifera dissolutions and fish debris, together with the agreement between our new measurements and the recent seawater analyses, we concur with recent studies [e.g. Roberts et al., 2010, 2012; Elmore et al. 2011; Piotrowski et al., 2012] that foraminifera dissolutions are likely to give robust near bottom water signals, and we are confident that the Fe-Mn coatings of the mixed-species planktonic forams and fish debris accurately reflect modern deep-water ε_{Nd}-values.

2.5 Discussion

2.5.1 The South Atlantic overturning circulation during the Holocene and LGM

Extensive work has investigated changes in AMOC utilizing deep-sea cores from the Cape Basin using carbon isotope ratios in benthic foraminifera [e.g. Charles et al., 1996; Hodell et al., 2000, 2003; Ninnemann and Charles, 2002; Venz and Hodell, 2002]. Seawater carbon isotopic composition ($\delta^{13}C_{DIC}$) can be used as a water mass tracer in the South Atlantic but is susceptible to changes in factors other than water mass mixing including the partitioning of carbon between the terrestrial and ocean carbon reservoirs, the environmental and biological conditions of the foraminifera under study, changes in productivity in the water column and air-sea exchange [reviewed in Ravelo and Hillaire-Marcel, 2007]. As benthic foraminifera grow at the water-seafloor interface, the $\delta^{13}C$ of the foraminifera reflects the $\delta^{13}C$ of the ambient bottom water with a small offset as a result of kinetic fractionation and biological vital effects [e.g. Romanek et al., 1992; Mackensen 2008]. Because northern component waters (NADW) posses a relatively high $\delta^{13}C$ that is unique to nutrient depleted surface waters and therefore distinguishable from southern sourced waters, changes in the mixing of these two components in the Atlantic can be recorded down core within the benthic foraminifera shells [e.g. Oppo and Fairbanks, 1987; Zahn et al., 1997; Martínez-Méndez et al., 2008]. Records of $\delta^{13}C$ at site TN057-21 and RC11-83 agree well and demonstrate an abrupt >1.0 ‰ shift during the last deglaciation (Figure 2.4). The records preserve both large and fine scale features and have been used with other South Atlantic cores to demonstrate consistently low $\delta^{13}C$ values in the deep (> 2.4 km) South Atlantic during the LGM [e.g. Ninnemann and Charles, 2002; Charles et al., 2010]. These low values exceed those of the glacial deep Pacific and therefore water mass mixing alone cannot be used to explain these fluctuations. Nevertheless, pairing these records

with Nd isotopes from the same core strongly indicates that the $\delta^{13}C$ pattern changes along with the AMOC [Piotrowski et al., 2005, 2008]. The record of benthic $\delta^{13}C$ for TN057-6 is variable between foraminiferal species and shows that $\delta^{13}C$ values of *Cibicidoides wuellerstorfi* were as much as 0.6‰ heavier than *Cibicidoides kullenbergi* during glacials, although the presence of *C. kullenbergi* is rare during these periods [Hodell et al., 2003]. The shift in benthic $\delta^{13}C$ between LGM and Holocene is ~1‰ derived from *C. wuellerstorfi* and 1.5‰ using *C. kullenbergi*. This shift is consistent with those in RC11-83-TN057-21 and further indicates the presence of a nutrient-rich water mass in the deep Cape Basin during the LGM (Figure 2.4). The *C. kullenbergi* record of TN057-6 shows similarities in timing and magnitude of changes with the *C. wuellerstorfi* record of RC11-83-TN057-21 and suggests that both sites experienced similar bottom water conditions during the LGM.

Our highest resolution record of Nd isotopes at site TN057-6, between 0 to ~24 ka (Figure 2.5), shows the most North Atlantic-like ε_{Nd}-values during the Holocene and more Pacific-like values during the LGM, with the shift to more North Atlantic-like ε_{Nd}-values occurring between 16 and 11 ka, during the Termination. This trend, and the magnitude of the shift, agrees well with the published record of sediment leachates of nearby cores RC11-83-TN057-21 [Piotrowski et al. 2004, 2005], which over this time period is primarily RC11-83 (until 20 ka) and foraminifera dissolutions from TN057-21 [Piotrowski et al., 2012]. However, the ε_{Nd}-values of TN057-6 are slightly more negative in the Holocene (-10.0 ±0.28 vs. -9.34 ±0.16), which may reflect its location at a shallower depth closer to the core of NADW (Figure 2.1b). In this context, Figure 2.3 shows that the closest measured seawater profile for dissolved ε_{Nd} from Stichel et al. (2012) has NADW like values closer to TN057-6 while deeper RC11-83-TN057-51 is bathed in more southern-sourced waters with higher ε_{Nd}. Because TN057-6 sits at a

shallower depth, a high resolution record of AMOC changes at this site will differentiate between a retreat or shoaling of NADW in the Cape Basin during the LGM. In TN057-6, abrupt events during the deglaciation such as Heinrich Event 1, the Bølling-Allerød, and the Younger Dryas do not show up as clearly as in RC11-83 [Piotrowski et al. 2004, 2005], which may reflect the lower sedimentation rate (3 cm/kyr vs. >20 cm/kyr, respectively) as well as the lower sampling resolution (~1000 yr vs ~300 yr).

The Nd isotope record of cores RC11-83-TN057-21 through the last glacial termination was interpreted to represent the transition from more southern-sourced waters in the South Atlantic during the LGM to more northern-sourced waters during the Holocene [Rutberg et al., 2000; Piotrowski et al., 2004, 2005, 2012], and the TN057-6 record supports these findings. The similarity of ε_{Nd}-values between RC11-83-TN057-21 and TN057-6 during the LGM suggests these core sites experienced the same mixture of water masses during this time and unlike today, the water column was uniform in ε_{Nd} between ~3700 m and 4800 m in the Cape Basin. The presence of more southern sourced waters during the LGM in the South Atlantic is consistent with other studies around the Atlantic basin using Nd isotopes to describe the variability of deep water circulation during climate cycles [e.g. Rutberg et al., 2000; Bayon et al., 2002; Piotrowski et al., 2004, 2005, 2008, 2012; Gutjahr et al., 2008; Pahnke et al., 2008; Roberts et al., 2010; Stumpf et al., 2010, Skinner et al., 2013]. These studies all indicate a reduction of NADW export to the South Atlantic paired with increases of southern-sourced waters entering the North Atlantic during the last glacial period.

2.5.2 AMOC changes within the Cape Basin through MIS11.

Given the evidence that site TN057-6 shows the same pattern of deep ocean circulation changes as site RC11-83-TN057-21 during the last glacial cycle, while covering a much longer

time period, we sought to investigate how the AMOC varied during previous glacial-interglacial cycles, over the duration of the core through MIS11 at ~400 ka. Carbon isotope records derived from benthic foraminifera indicate changes in deep-water chemistry over glacial-interglacial cycles, representing changes in deep-water circulation along with additional effects such as the influence of the terrestrial biosphere and regional biological productivity [Hodell et al., 2000, 2003; Venz and Hodell, 2002; Hodell and Venz, 2003]. The record shows lighter $\delta^{13}C$ values during glacial stages, indicating that less NADW reaches the core site. Comparison with intermediate depth cores in the same area shows strong offsets to lighter deep water $\delta^{13}C$ during glacials in TN057-6, indicating more poorly ventilated deep water and greater stratification compared to interglacials [Hodell et al., 2003].

Over the entire 400 ka interval the $\delta^{13}C$ records from benthic foraminifera show shifts of up to ~2.3‰ between interglacials and glacials (Figure 2.6a), and they are variable depending on the interval. For example, the shift of ~2.3‰ between MIS11/10 for *C. wuellerstorfi* is much larger than the shift of only ~1‰ between MIS 2/1. Moreover, the $\delta^{13}C$ values are different during different interglacials and glacials, for example, with *C. wuellerstorfi* approaching 1‰ during MIS 11 but only ~0.3‰ during MIS 9, and -1.6‰ during MIS 8 vs -0.6‰ during MIS 2.

The question arises, to what degree do these variable peak glacial and interglacial $\delta^{13}C$-values (Figure 2.6a) reflect differences in AMOC intensity during different glacials and interglacials over the last 400 ka as opposed to other processes that impact $\delta^{13}C$. The extent that they represent differences in the vigor of the AMOC during different glacials and interglacials should also be reflected in the ε_{Nd}-values. For example, if the AMOC was particularly strong during a super-interglacial such as MIS 11, when $\delta^{13}C$-values are particularly heavy, then this would be manifested by particularly negative ε_{Nd}-values reflecting a particularly strong North Atlantic

component in the South Atlantic. Moreover, glacials when $\delta^{13}C$-values are particularly light (e.g. MIS 8) might be complemented by more positive ε_{Nd}. In order to address the question of the variability of the AMOC in the Cape Basin over the accessible time period, we have analyzed pairs of samples at each of the glacial and interglacial maxima over the last 400 kyr.

Unlike the $\delta^{13}C$ values, the ε_{Nd}-values of the bottom waters at the glacial and interglacial maxima (Figure 2.6a) show shifts between nearly Holocene-like values (-10.0 ±0.28) and LGM-like values (-6.6 ±0.28) through the record, indicating that the amplitude of glacial-interglacial AMOC cyclicity remained similar over the entire 400 ka time interval. That is, there was a similar balance between northern sourced waters and Pacific sourced waters reaching the core site during every interglacial period since MIS 11, and similar fractions during every glacial period. We apply a simple mass balance equation to this dataset in order to determine the fraction of northern sourced waters reaching the study site during glacial and interglacial time periods. We consider the ε_{Nd}-value of bottom waters in this region to be a result of two-component mixing between North Atlantic Sourced Waters (***NASW***) and North Pacific Sourced Water (***NPSW***) [e.g. Piotrowski et al. 2004, Pena and Goldstein, 2014]. There is a unique mixture of NASW and NAPW that will result in the ε_{Nd}-value of bottom waters seen at a site in the Cape Basin at any particular time. Down core changes in ε_{Nd} can be used to evaluate changes in the mixing ratio of NASW and NPSW. During the Holocene, bottom water at TN057-6 is composed of a 75:25 mixture of NASW and NPSW, which is in agreement with additional studies [e.g. Piotrowski et al., 2004, 2005; Pena and Goldstein, 2014]. Preceding interglacials are composed of ~70% NASW in the Cape Basin which is similar to the percentage during the Holocene. The ~3 ε_{Nd} unit shift during the LGM is associated a lower percentage of NASW reaching the study region and represents the most NASW-poor conditions over the time period

(~30%). The bottom water ε_{Nd}-value of earlier glacial periods suggests there was on average 40-45% NASW in the Cape Basin. The compiled record may suggest that the Holocene and LGM represent extreme modes of AMOC during the last 400 ka, but the limited number of data points at most glacial and interglacial peaks means that glacial-interglacial AMOC peaks might not be sampled. Nevertheless, the stability of the ε_{Nd}-values during the peak glacials and peak interglacials are independent of whether there are two samples (MIS 5,6,7,10,11) or several samples (MIS 1,2,8,9). The data support studies that concluded that these climate cycles were associated with reorganizations of deep ocean circulation within the South Atlantic [Hodell et al., 2003; Martínez-Méndez et al., 2008; Riveiros et al., 2010]. Thus despite major instability in the AMOC and the greater climate system, such that major changes occurred over time intervals as short as decades [e.g. Broecker and Hemming, 2001; Alley et al., 2003, 2005; Bentson et al., 2004; McManus et al., 2004], there has been a remarkable stability in that after these shifts occurred the system reached similar glacial and the interglacial AMOC modes.

2.5.3 The timing of AMOC changes during the MIS 9/8 transition

While the Nd isotope data support reorganization of AMOC during glacial-interglacial cycles over the last 400 ka, of particular importance is the timing and mechanisms of these reorganizations during glacial-interglacial transitions. This study reports a higher-resolution record of one sample every 2 kyr during one of the transitions, from MIS 9 to MIS 8, which shows intermediate ε_{Nd} values compared to the interglacial and glacial values. The record shows a positive shift of ~1 ε_{Nd} unit between ~325 and ~275 ka and a more rapid one of ~2 ε_{Nd} units between ~255 ka and ~275 ka (Figure 2.7). The change indicates a decrease in the percentage of NASW in the South Atlantic from ~70% to 40% and is comparable to other glaciations. The ε_{Nd} record during this transition resembles the rate of change of $\delta^{13}C$ and shows good agreement in

terms of the timing of changes during the glaciation. Although $\delta^{18}O$ also demonstrates a 'two-step' shift during the glaciation, the timing of changes occur earlier, estimated to be ~10,000 years prior to changes in $\delta^{13}C$ and ε_{Nd}. Additional measurements would lead to a more robust constraint on the timing of these changes as currently only three stable isotope measurements are reported during this transition.

The relative timing of changes is essential to understanding the processes that drive climate change and those that react to and cause intensification of the changes. In this case the leads and lags reflect relationships between climate change, ocean circulation reorganization and ice sheet growth. A previous ε_{Nd} study in the Cape Basin [Piotrowski et al., 2005] concluded that during the MIS 5/4 transition, ice sheet growth preceded changes in the global biosphere which was followed by the AMOC reorganization, reflected by successive changes in benthic $\delta^{18}O$, benthic $\delta^{13}C$, and ε_{Nd}. The MIS 9/8 record in this study suggests synchronous changes of bottom water $\delta^{13}C$ and ε_{Nd} and suggests $\delta^{13}C$ is a reliable indicator of the timing of AMOC reorganization during this time period. In comparison with $\delta^{18}O$, these records suggest that increased ice sheet volume preceded the AMOC response during MIS 9/8, as during the MIS 5a/4 transition, indicating that AMOC weakening lags the beginning of ice sheet growth during the initiation of glacials.

2.6 Conclusions

This study for the first time presents a record of the ε_{Nd} of deep waters in the South Atlantic during glacial and interglacial cycles through MIS 11, based on measurements of foraminiferal dissolutions and fish debris measurements. This record shows clear shifts in association with changes in the global climate. These changes indicate ~30% less northern

sourced waters reaching the South Atlantic during glacial periods compared to interglacials, reflecting the weakening of AMOC during these glacials. A high resolution Holocene through LGM time series confirms the same magnitude of AMOC weakening during the LGM as previous studies in deeper water, and a coeval deglacial transition to stronger AMOC, thus adding credence to the previous records. The timing of AMOC changes during MIS 9/8 transition indicates that the main change in ocean circulation occurred after a period of ice sheet growth, the same time relationship reported previously [Piotrowski et al., 2005] for a nearby and deeper core site during the MIS 5a/4 transition, suggesting that ice sheet growth prior to ocean circulation changes may be a characteristic of glaciations.

2.7 References

Abouchami, W., et al. "Secular changes of lead and neodymium in central Pacific seawater recorded by a Fe-Mn crust." *Geochimica et Cosmochimica Acta* 61.18 (1997): 3957-3974.

Albarède, F., and S. L. Goldstein. "World map of Nd isotopes in sea-floor ferromanganese deposits." *Geology* 20.8 (1992): 761-763.

Alley, R. B., et al. "Abrupt climate change." *science* 299.5615 (2003): 2005-2010.

Alley, R.B., and A. Ágústsdóttir. "The 8k event: cause and consequences of a major Holocene abrupt climate change." *Quaternary Science Reviews* 24.10 (2005): 1123-1149.

Antonov, J. I., et al. World Ocean Atlas 2009 Volume 2: Salinity. S. Levitus, Ed., NOAA Atlas NESDIS 69, U.S. Government Printing Office, Washington, D.C., 184 pp. (2010).

Aplin, A., et al. "$^{143}Nd/^{144}Nd$ in Pacific ferromanganese encrustations and nodules." *Earth and planetary science letters* 81.1 (1986): 7-14.

Barker, S., et al. "Interhemispheric Atlantic seesaw response during the last deglaciation." *Nature* 457.7233 (2009): 1097-1102.

Bayon, G., et al. "An improved method for extracting marine sediment fractions and its application to Sr and Nd isotopic analysis." *Chemical Geology* 187.3 (2002): 179-199.

Bentsen, M., et al. "Simulated variability of the Atlantic meridional overturning circulation." *Climate Dynamics* 22.6-7 (2004): 701-720.

Blanckenburg, F., and T. F. Nägler. "Weathering versus circulation-controlled changes in radiogenic isotope tracer composition of the Labrador Sea and North Atlantic Deep Water." *Paleoceanography* 16.4 (2001): 424-434.

Boyle, E. A., and L. D. Keigwin. "Deep circulation of the North Atlantic over the last 200,000 years: Geochemical evidence." *Science* 218.4574 (1982): 784-787.

Boyle, E.A. (1992). "Cadmium and d13C paleochemical ocean distributions during the stage 2 glacial maximum." Annu. Rev. Earth Planet. Sci. 20: 245-87.

Broecker, W. S. "Paleocean circulation during the last deglaciation: a bipolar seesaw?." *Paleoceanography* 13.2 (1998): 119-121.

Broecker, W. S., and S. Hemming. "Climate swings come into focus." *Science* 294.5550 (2001): 2308-9.

Burton, K. W., and D. Vance. "Glacial–interglacial variations in the neodymium isotope composition of seawater in the Bay of Bengal recorded by planktonic foraminifera." *Earth and Planetary Science Letters* 176.3 (2000): 425-441.

Burton, K. W., et al. "Actual timing of neodymium isotopic variations recorded by FeMn crusts in the western North Atlantic." *Earth and Planetary Science Letters* 171.1 (1999): 149-156.

Charles, C. D; Fairbanks, R.G. (1992). "Evidence from Southern Ocean sediments for the effect of North Atlantic deep-water flux on climate." *Nature* 355: 416-419.

Charles, C. D., et al. "Climate connections between the hemisphere revealed by deep sea sediment core/ice core correlations." *Earth and Planetary Science Letters* 142.1 (1996): 19-27.

Chester, R., and M. J. Hughes. "A chemical technique for the separation of ferro-manganese minerals, carbonate minerals and adsorbed trace elements from pelagic sediments." *Chemical geology* 2 (1967): 249-262.

Crowley, T. J. "North Atlantic deep water cools the southern hemisphere." *Paleoceanography* 7.4 (1992): 489-497.

Elderfield, H., et al. "Rare earth element geochemistry of oceanic ferromanganese nodules and associated sediments." *Geochimica et Cosmochimica Acta* 45.4 (1981): 513-528.

Elmore, A. C., et al. "Testing the extraction of past seawater Nd isotopic composition from North Atlantic deep sea sediments and foraminifera." *Geochemistry, Geophysics, Geosystems* 12.9 (2011)

Foster, G. L., et al. "No change in the neodymium isotope composition of deep water exported from the North Atlantic on glacial-interglacial time scales." *Geology* 35.1 (2007): 37-40.

Futa, K., et al. "Sr and Nd isotopic variations in ferromanganese crusts from the Central Pacific: Implications for age and source provenance." *Geochimica et Cosmochimica Acta* 52.9 (1988): 2229-2233.

Goldstein, S. L and R. K. O'Nions. "Nd and Sr isotopic relationships in pelagic clays and ferromanganese deposits." *Nature* 292: 324-327. (1981)

Goldstein, S. L and S. R. Hemming. "Long-lived Isotopic tracers in Oceanography, Paleococeanography and Ice-sheet dynamics". *Treatise on Geochemistry*. E. H. Elderfield, Elsevier, Oxford. 6: 453-489. (2003).

Gutjahr, M., and J. Lippold. "Early arrival of Southern Source Water in the deep North Atlantic prior to Heinrich event 2." *Paleoceanography* 26.2 (2011).

Gutjahr, M., et al. "Changes in North Atlantic Deep Water strength and bottom water masses during Marine Isotope Stage 3 (45–35kaBP)." *Quaternary Science Reviews* 29.19 (2010): 2451-2461.

Gutjahr, M., et al. "Reliable extraction of a deepwater trace metal isotope signal from Fe–Mn oxyhydroxide coatings of marine sediments." *Chemical Geology* 242.3 (2007): 351-370.

Gutjahr, M., et al. "Tracing the Nd isotope evolution of North Atlantic deep and intermediate waters in the Western North Atlantic since the Last Glacial Maximum from Blake Ridge sediments." *Earth and Planetary Science Letters* 266.1 (2008): 61-77.

Hodell, D. A., et al. "Comparison of interglacial stages in the South Atlantic sector of the southern ocean for the past 450 kyr: implifications for Marine Isotope Stage (MIS) 11." *Global and Planetary Change* 24.1 (2000): 7-26.

Hodell, D. A., et al. "Pleistocene vertical carbon isotope and carbonate gradients in the South Atlantic sector of the Southern Ocean." *Geochemistry, Geophysics, Geosystems* 4.1 (2003): 1-19.

Jacobsen, S. B., and G. J. Wasserburg. "Sm-Nd isotopic evolution of chondrites." *Earth and Planetary Science Letters* 50.1 (1980): 139-155.

Jeandel, C., et al. "Exchange of neodymium and its isotopes between seawater and small and large particles in the Sargasso Sea." *Geochimica et Cosmochimica Acta* 59.3 (1995): 535-547.

Jeandel, C., J. K. Bishop, and A. Zindler. "Exchange of neodymium and its isotopes between seawater and small and large particles in the Sargasso Sea." *Geochimica et Cosmochimica Acta* 59.3 (1995): 535-547.

Klevenz, V., et al. "Neodymium isotopes in benthic foraminifera: core-top systematics and a down-core record from the Neogene south Atlantic." *Earth and Planetary Science Letters* 265.3 (2008): 571-587.

Kraft, S., et al. "Assessment of seawater Nd isotope signatures extracted from foraminiferal shells and authigenic phases of Gulf of Guinea sediments." *Geochimica et Cosmochimica Act*a 121 (2013): 414-435.

Lippold, J., et al. "Strength and geometry of the glacial Atlantic Meridional Overturning Circulation." *Nature Geoscience* 5.11 (2012): 813-816.

Lynch-Stieglitz, J., et al. "Atlantic Meridonal overturning circulation during the last glacial maximum." *Science* 316: 66-69 (2007).

Mackensen, A. "On the use of benthic foraminiferal δ13C in palaeoceanography: constraints from primary proxy relationships." *Geological Society, London, Special Publications* 303.1 (2008): 121-133.

Mackensen, A., et al. "Late Pleistocene deep-water circulation in the subantarctic eastern Atlantic." *Global and Planetary Change* 30.3 (2001): 197-229.

Marchitto, T. M., and W. S. Broecker. "Deep water mass geometry in the glacial Atlantic Ocean: A review of constraints from the paleonutrient proxy Cd/Ca." *Geochemistry, Geophysics, Geosystems* 7.12 (2006).

Martin, E. E., et al. "Extraction of Nd isotopes from bulk deep sea sediments for paleoceanographic studies on Cenozoic time scales." *Chemical Geology* 269.3 (2010): 414-431.

Martínez-Méndez, G., et al. "Variable water column structure of the South Atlantic on glacial–interglacial time scales." *Quaternary Science Reviews* 28.27 (2009): 3379-3387.

McManus, J. F., et al. "Collapse and rapid resumption of Atlantic meridional circulation linked to deglacial climate changes." *Nature* 428.6985 (2004): 834-837.

Ninneman, U. S and C. D. Charles. "Changes in the mode of Southern Ocean circulation over the last glacial cycle revealed by foraminiferal stable isotopic variability." *Earth and Planetary Science Letters* 201: 383-396. (2002).

O'Nions, R. K., et al. "Pb, Nd and Sr isotopes in oceanic ferromanganese deposits and ocean floor basalts." *Nature* 273 (1978): 435-438.

Oppo, D. W; and R. G. Fairbanks. "Variability in the deep and intermediate water circulation of the Atlantic Ocean during the past 25,000 years: Northern Hemisphere modulation of the Southern Ocean." *Earth and Planetary Science Letters* 86. (1987).

Pahnke, K., et al. "Abrupt changes in Antarctic Intermediate Water circulation over the past 25,000 years." *Nature Geoscience* 1.12 (2008): 870-874.

Palmer, M. R., and H. Elderfield. "Rare earth elements and neodymium isotopes in ferromanganese oxide coatings of Cenozoic foraminifera from the Atlantic Ocean." *Geochimica et Cosmochimica Acta* 50.3 (1986): 409-417.

Palmer, M. R., and H. Elderfield. "Variations in the Nd isotopic composition of foraminifera from Atlantic Ocean sediments." *Earth and planetary science letters* 73.2 (1985): 299-305.

Pena, L. and S. L. Goldstein, "Thermohaline circulation crisis and impacts during the mid-Pleistocene transition." *Science* 345 (2014): 318-322.

Pena, L. D., et al. "Rapid changes in meridional advection of Southern Ocean intermediate waters to the tropical Pacific during the last 30kyr." *Earth and Planetary Science Letters* 368 (2013): 20-32.

Piepgras, D. J. and G. J. Wasserburg. "Isotopic composition of neodymium in waters from the Drake Passage." *Science* 217.4556 (1982): 207-214.

Piepgras, D. J. and G. J. Wasserburg. "Rare Earth Element Transport in the Western North Atlantic Inferred from Nd Isotopic Observations." *Geochimica et Cosmochimica Acta* 51, no. 5 (1987): 1257–71.

Piepgras, D. J. et al. "The isotopic composition of Nd in different ocean masses." *Earth and Planetary Science Letters* 45.2 (1979): 223-236.

Piotrowski, A. M, et al. "Temporal Relationships of Carbon Cycling and ocean circulation at glacial boundaries." *Science* 307 (2005): 1933-1938.

Piotrowski, A. M; et al. "Intensification and variability of ocean thermohaline circulation through the last deglaciation." *Earth and Planetary Science Letters* 225 (2004): 205-220.

Piotrowski, A. M; et al. "Oscillating glacial northern and southern deep water formation from combined neodymium and carbon isotopes." *Earth and Planetary Science Letters* 272 (2008): 394-405.

Piotrowski, A. M., et al. "Reconstructing deglacial North and South Atlantic deep water sourcing using foraminiferal Nd isotopes." *Earth and Planetary Science Letters* 357 (2012): 289-297.

Rahmstorf, S. "Ocean circulation and climate during the past 120,000 years." *Nature* 419.6903 (2002): 207-214.

Ravelo, A. C. and C. Hillaire-Marcel. "The Use of oxygen and carbon isotopes of foraminifera in paleoceanography." *Developments in Marine Geology* v.1. Chapter 18. (2007).

Ritz, S. P., et al. "Estimated strength of the Atlantic overturning circulation during the last deglaciation." *Nature Geoscience* 6.3 (2013): 208-212.

Roberts, N. L., et al. "Rare earth element association with foraminifera." *Geochimica et Cosmochimica Acta* 94 (2012): 57-71.

Roberts, N. L., et al. "Synchronous Deglacial Overturning and Water Mass Source Changes." *Science* 327, no. 5961 (January 1, 2010): 75–78.

Romanek, C. S., et al. "Carbon isotopic fractionation in synthetic aragonite and calcite: effects of temperature and precipitation rate." *Geochimica et Cosmochimica Acta* 56.1 (1992): 419-430.

Rutberg, R. H., et al. "Reduced North Atlantic Deep Water flux to the glacial Southern Ocean inferred from neodymium isotope ratios." *Nature* 405. (2000)

Skinner, L. C., et al. "North Atlantic versus Southern Ocean contributions to a deglacial surge in deep ocean ventilation." Geology 41.6 (2013): 667-670.

Stichel, T., et al. "The hafnium and neodymium isotope composition of seawater in the Atlantic sector of the Southern Ocean." *Earth and Planetary Science Letters* 317 (2012): 282-294.

Stocker, T. F., and S. J. Johnsen. "A minimum thermodynamic model for the bipolar seesaw." *Paleoceanography* 18.4 (2003).

Stumpf, R., et al. "Late Quaternary variability of Mediterranean outflow water from radiogenic Nd and Pb isotopes." *Quaternary Science Reviews* 29.19 (2010): 2462-2472.

Tachikawa, K., et al. "Neodymium budget in the modern ocean and paleo‐oceanographic implications." *Journal of Geophysical Research: Oceans* (1978–2012) 108.C8 (2003).

Tanaka, Tsuyoshi, et al. "JNdi-1: a neodymium isotopic reference in consistency with LaJolla neodymium." *Chemical Geology* 168.3 (2000): 279-281.

Vance, D., and K. Burton. "Neodymium isotopes in planktonic foraminifera: a record of the response of continental weathering and ocean circulation rates to climate change." *Earth and Planetary Science Letters* 173.4 (1999): 365-379.

Vázquez Riveiros, N., et al. "Response of South Atlantic deep waters to deglacial warming during Terminations V and I." *Earth and Planetary Science Letters* 298.3 (2010): 323-333.

Venz, K. A., and D. A. Hodell. "New evidence for changes in Plio–Pleistocene deep water circulation from Southern Ocean ODP Leg 177 Site 1090." *Palaeogeography, Palaeoclimatology, Palaeoecology* 182.3 (2002): 197-220.

Venz, K. A., and D.A. Hodell. "New evidence for changes in Plio–Pleistocene deep water circulation from Southern Ocean ODP Leg 177 Site 1090." *Palaeogeography, Palaeoclimatology, Palaeoecology* 182.3 (2002): 197-220.

von Blanckenburg, F. "Tracing past ocean circulation?." Science 286.5446 (1999): 1862-1863.

Wilson, D. J., et al. "A boundary exchange influence on deglacial neodymium isotope records from the deep western Indian Ocean." *Earth and Planetary Science Letters* 341 (2012): 35-47.

Wilson, D. J., et al. "Reactivity of neodymium carriers in deep sea sediments: Implications for boundary exchange and paleoceanography." *Geochimica et Cosmochimica Acta* 109 (2013): 197-221.

Xie, R. C., et al. "Deglacial variability of Antarctic Intermediate Water penetration into the North Atlantic from authigenic neodymium isotope ratios." *Paleoceanography* 27.3 (2012).

Zahn, R., et al. "Thermohaline instability in the North Atlantic during meltwater events: Stable isotope and ice‐rafted detritus records from Core SO75‐26KL, Portuguese Margin." *Paleoceanography* 12.5 (1997): 696-710.

2.8 Tables

Table 2.1: Acronyms used in this chapter

AABW	Antarctic Bottom Water
AAIW	Antarctic Intermediate Water
AMOC	Atlantic Meridional Overturning Circulation
CDW	Circumpolar Deep Water
DPW	Deep Pacific Waters
HH	Hydroxylamine Hydrochloride
LGM	Last Glacial Maximum
MIS	Marine Isotope Stage
NADW	North Atlantic Deep Water
NASW	North Atlantic Sourced Waters
NPSW	North Pacific Sourced Waters
REEs	Rare Earth Elements

Table 2.2: Nd isotope compositions of TN057-6 samples

Depth in core (cm)	Age (ka-BP)	$^{143}Nd/^{144}Nd$			ε_{Nd}		
Fine fraction sediment leachates							
11.5	3.1	0.512202	±	08	-8.51	±	0.16
33.5	9.3	0.512225	±	11	-8.06	±	0.22
33.5	9.2	0.512154	±	07	-9.43	±	0.14
57.5	15.9	0.512282	±	07	-6.95	±	0.14
58.5	16.2	0.512308	±	08	-6.44	±	0.16
61.5	16.6	0.512329	±	08	-6.03	±	0.16
64.5	18.7	0.512319	±	09	-6.23	±	0.18
68.5	19.0	0.512294	±	09	-6.71	±	0.16
85.5	23.8	0.512321	±	08	-6.18	±	0.16
85.5	23.8	0.512390	±	08	-4.84	±	0.16
85.5	23.8	0.512303	±	08	-6.54	±	0.16
97.5	27.1	0.512378	±	08	-5.06	±	0.16
Bulk sediment leachates							
33.5	9.2	0.512163	±	07	-9.27	±	0.14
57.5	15.9	0.512323	±	08	-6.15	±	0.16
85.5	23.8	0.512402	±	07	-4.60	±	0.14
Fish Debris							
1.5	0.2	0.512119	±	09	-10.12	±	0.18
6.5	1.6	0.512116	±	12	-10.18	±	0.24
21.5	5.9	0.512115	±	11	-10.21	±	0.22
33.5	9.3	0.512140	±	11	-9.72	±	0.22
37.5	10.3	0.512133	±	08	-9.85	±	0.16
57.5	15.9	0.512292	±	08	-6.75	±	0.16
75.5	21.0	0.512288	±	10	-6.82	±	0.20
83.5	23.2	0.512309	±	08	-6.41	±	0.16
85.5	23.8	0.512277	±	10	-7.05	±	0.20
656.5	183.8	0.512158	±	09	-9.36	±	0.18
894.5	332.4	0.512150	±	09	-9.52	±	0.18
1171.5	407.6	0.512151	±	09	-9.49	±	0.18
1174.5	408.4	0.512151	±	09	-9.51	±	0.18
Planktonic foraminifera							
1.5	0.2	0.512125	±	07	-10.00	±	0.14
6.5	1.6	0.512124	±	09	-10.03	±	0.18
11.5	3.0	0.512146	±	08	-9.60	±	0.16
21.5	5.9	0.512139	±	08	-9.74	±	0.16
25.5	7.0	0.512151	±	09	-9.51	±	0.19

31.5	8.7	0.512139	±	08	-9.73	±	0.16
33.5	9.2	0.512122	±	07	-10.08	±	0.14
37.5	10.3	0.512134	±	08	-9.84	±	0.16
43.5	12.0	0.512171	±	08	-9.12	±	0.16
45.5	12.6	0.512205	±	09	-8.45	±	0.18
48.5	13.4	0.512202	±	09	-8.51	±	0.18
50.5	14.0	0.512228	±	09	-8.01	±	0.18
53.5	14.8	0.512252	±	09	-7.53	±	0.18
55.5	15.4	0.512285	±	09	-6.89	±	0.18
57.5	15.9	0.512293	±	07	-6.74	±	0.14
58.5	16.2	0.512290	±	09	-6.79	±	0.18
60	16.6	0.512291	±	08	-6.76	±	0.16
61.5	17.1	0.512316	±	09	-6.29	±	0.18
64.5	17.9	0.512312	±	09	-6.37	±	0.18
67.5	18.7	0.512291	±	07	-6.77	±	0.14
72.5	20.2	0.512296	±	09	-6.67	±	0.18
75.5	21.0	0.512312	±	08	-6.36	±	0.16
77.5	21.6	0.512297	±	09	-6.65	±	0.18
83.5	23.2	0.512301	±	09	-6.58	±	0.18
85.5	23.8	0.512300	±	08	-6.60	±	0.16
435.5	121.9	0.512166	±	09	-9.20	±	0.18
438.5	122.7	0.512171	±	08	-9.10	±	0.16
477.5	133.7	0.512286	±	08	-6.87	±	0.16
481.5	134.8	0.512278	±	09	-7.03	±	0.18
656.5	183.8	0.512140	±	08	-9.72	±	0.16
660.5	185.0	0.512143	±	09	-9.65	±	0.18
768.5	256.2	0.512276	±	09	-7.06	±	0.18
770.5	256.7	0.512291	±	09	-6.77	±	0.18
775.5	258.1	0.512288	±	12	-6.83	±	0.24
780.5	259.9	0.512283	±	09	-6.93	±	0.18
782.5	261.2	0.512298	±	14	-6.64	±	0.28
785.5	263.1	0.512269	±	09	-7.20	±	0.18
788.5	265.0	0.512258	±	09	-7.42	±	0.18
792.5	267.6	0.512223	±	09	-8.09	±	0.18
794.5	268.8	0.512205	±	08	-8.44	±	0.16
796	269.8	0.512243	±	05	-7.71	±	0.10
800	272.3	0.512226	±	09	-8.03	±	0.18
860.5	310.8	0.512170	±	09	-9.13	±	0.18
815	281.8	0.512183	±	04	-8.88	±	0.08
830	291.4	0.512208	±	06	-8.39	±	0.12
839	297.1	0.512172	±	05	-9.10	±	0.10
882.5	324.7	0.512145	±	09	-9.61	±	0.18
894.5	332.4	0.512170	±	08	-9.14	±	0.16
900.5	336.2	0.512217	±	11	-8.20	±	0.22
948.5	350.4	0.512247	±	10	-7.63	±	0.20
954.5	351.9	0.512267	±	09	-7.24	±	0.18
1171.5	407.6	0.512144	±	09	-9.64	±	0.18

2.9 Figures

Figure 2.1. a) Map of South Atlantic ε_{Nd} study regions, seawater profiles PS71/101 and PS71/102 [Stichel et al., 2012] and core sites TN057-6 (this study) and RC11-82-TN057-21 [Rutberg et al., 2000; Piotrowski et al., 2004, 2005, 2008, 2012]. (b) N-S transect (see inset for section path) within the Atlantic basin of salinity from WOA09 [Antonov et al., 2009] showing important water masses and core sites of interest. Water masses shown are North Atlantic Deep Water (NADW), Antarctic Intermediate Water (AAIW) and Antarctic Bottom Water (AABW).

Figure 2.2. a) Previously published sediment leachate derived ε_{Nd} records in the Cape Basin (Rutberg et al., 2000; Piotrowski et al., 2004; 2005). (b) Comparison of different results for TN057-6. Previously published data are in black. A comparison test was completed for different substrates at three depths (blue bars). The data plotted in this study are fine fraction leachates (EDTA-leach (gray circles) and HH leach (blue circles)), bulk fraction leachates (teal squares), foraminiferal carbonate dissolutions (red) and fish debris (yellow). A comparison test was completed for different substrates at three depths, and foraminifera dissolutions show excellent agreement with fish debris. There is direct overlap of the foraminifera dissolution and fish debris at 16 ka. Vertical error bars represent average total ($\pm 2\sigma$) error for ε_{Nd} records.

Figure 2.3. a) Comparison of ε_{Nd} seawater data with previously published core top leachate measurements and core top results from this study. Seawater data is presented in dark blue circles (Station PS71/101; 42° 20.60' S, 8° 59.20' E) [Stichel et al., 2012]. Bulk sediment leachates for core TN057-6 are shown in black symbols and for core RC11-83 is shown as the green triangle [Rutberg et al., 2000; Piotrowski et al., 2004]. From this study, fish debris is shown as a yellow triangle and foraminiferal calcite dissolutions are shown as red diamonds. b) ε_{Nd} plotted against neutral density for comparison with depth. c) ε_{Nd} vs. salinity with PS71/101 seawater data at depths >2000 m [blue circles, Stichel et al., 2012b] and core top measurements (representing bottom water composition) at RC11-83 (green triangle; Piotrowski et al., 2004) and TN057-6 (red diamond). Black line represents two component mixing between Southern Component Water (SCW) and Northern Component Water (NCW) with "mixing envelope" shaded in gray[Goldstein and Hemming, 2003].

Figure 2.4. Carbon isotope records in the Cape Basin. $\delta^{13}C$ record of *C. wuellerstorfi* at site RC11-83-TN057-21 (black squares, [Ninnemann and Charles, 2002]). $\delta^{13}C$ records at TN057-6 on both *C. wuellerstorfi* (blue squares) and *C. kullenbergi* (red squares) [Hodell et al., 2003]. *C. wuellerstorfi* record at TN057-6 shows more positive values during both the Holocene and LGM suggesting the shallower site TN057-6 is being bathed by more northern sourced waters during this time in comparison to RC11-83-TN057-21. However, the alternate species *C. kullenbergi* shows greater similarities to the RC11-83-TN057-21 record, suggesting both sites were bathed in similar waters during the Holocene and LGM.

Figure 2.5. Nd isotope records of the Cape Basin. RC11-83-TN057-21 is shown as a continuous black line (spliced at ~20 ka; [Piotrowski et al., 2004; 2005]). Colored symbols demonstrate TN057-6 measurements (this study). Foraminiferal dissolutions are shown as red triangles and fish debris are shown as yellow diamonds. Vertical bar represents average ($\pm 2\sigma$) error. Records show good agreement during the LGM (gray horizontal bar) but more radiogenic Holocene

values at seen at core site TN057-6 signifying more North Atlantic Sourced Water (NASW) at this time.

Figure 2.6. a) Combined records of TN057-6. $\delta^{13}C$ data for *C. kuellenbergi* (green) and *C. wuellerstorfi* (blue) [Hodell et al., 2003] is shown with ε_{Nd} data of foraminifera dissolutions (red) and fish debris (yellow). Vertical bars represent typical errors ($\pm 2\sigma$) on Nd isotope ratios. Gray horizontal bars represent average Holocene values and LGM values. b) $\delta^{13}C$ records as shown as in Figure 6b. Dark red line now represents %NASW reaching the Cape Basin based on changes in ε_{Nd}. Both ε_{Nd} and % NACW are scaled for comparison with glacial-interglacial cycles in $\delta^{13}C$ record.

Figure 2.7. TN057-6 benthic stable isotope and ε_{Nd} records plotted with LR04 for the last 400 kyr. The two green records represent the benthic $\delta^{13}C$ as measured in both C. kullenbergi and C. wuellerstorfi. Red circles represent measured ε_{Nd} of planktonic formanifera dissolutions. The blue record is benthic $\delta^{18}O$ of species C. wuellerstorfi. Black record is LR04 or an average of benthic $\delta^{18}O$ records derived from globally distributed sediment cores [Lisiecki and Raymo, 2005]. The inset of this plot highlights the changes and timing of bottom water characteristics during the MIS9/8 transition. The blue arrow highlights the glacial value of benthic $\delta^{18}O$ and indicates that this value is reached before the glacial transition seen in $\delta^{13}C$ (green arrow). The ε_{Nd} transition to glacial like values coincides with the timing of the $\delta^{13}C$ transition and therefore suggests that both of these proxies respond during the glaciation at a similar pace and predict a minimum in %NASW at ~260 ka.

Figure 2.1: South Atlantic core sites and deep water circulation

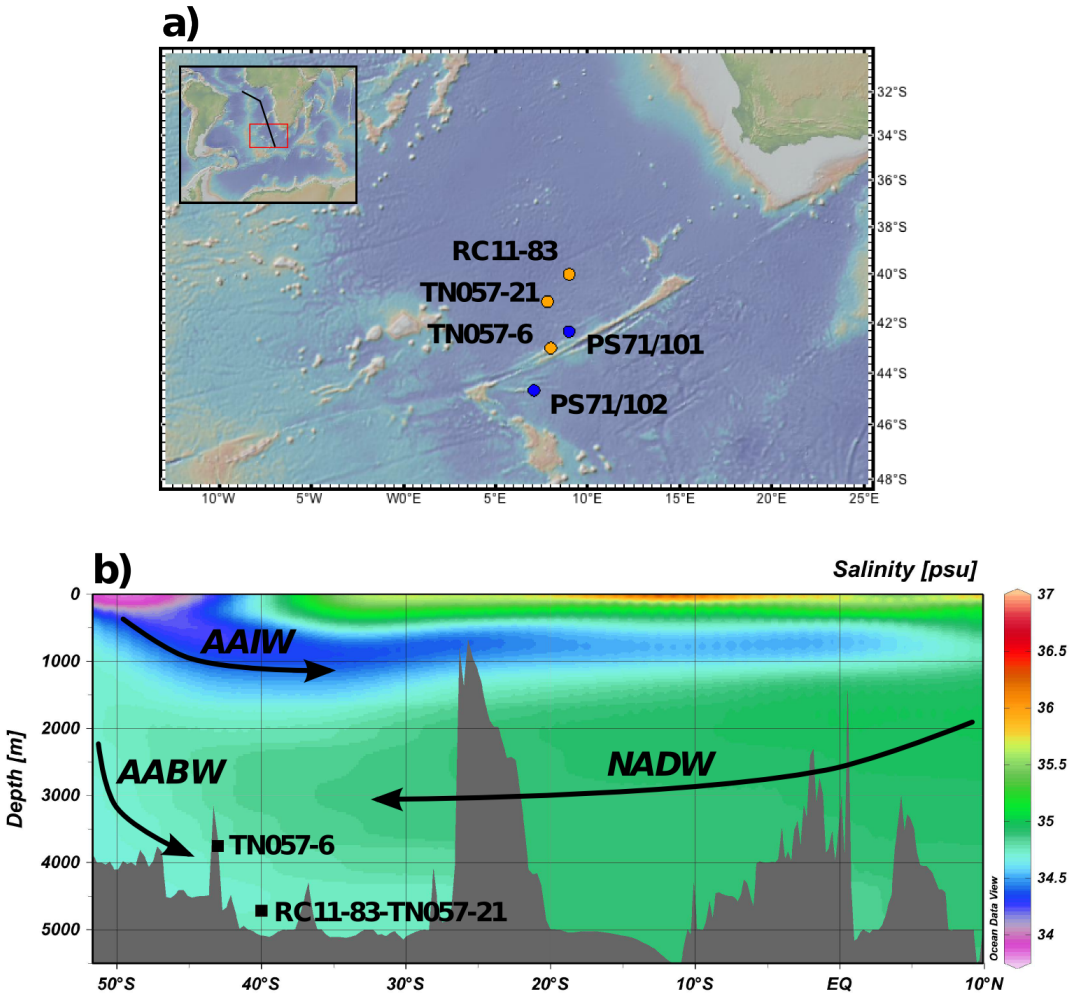

Figure 2.2: Previous South Atlantic ε_{Nd} records with those produced from this study

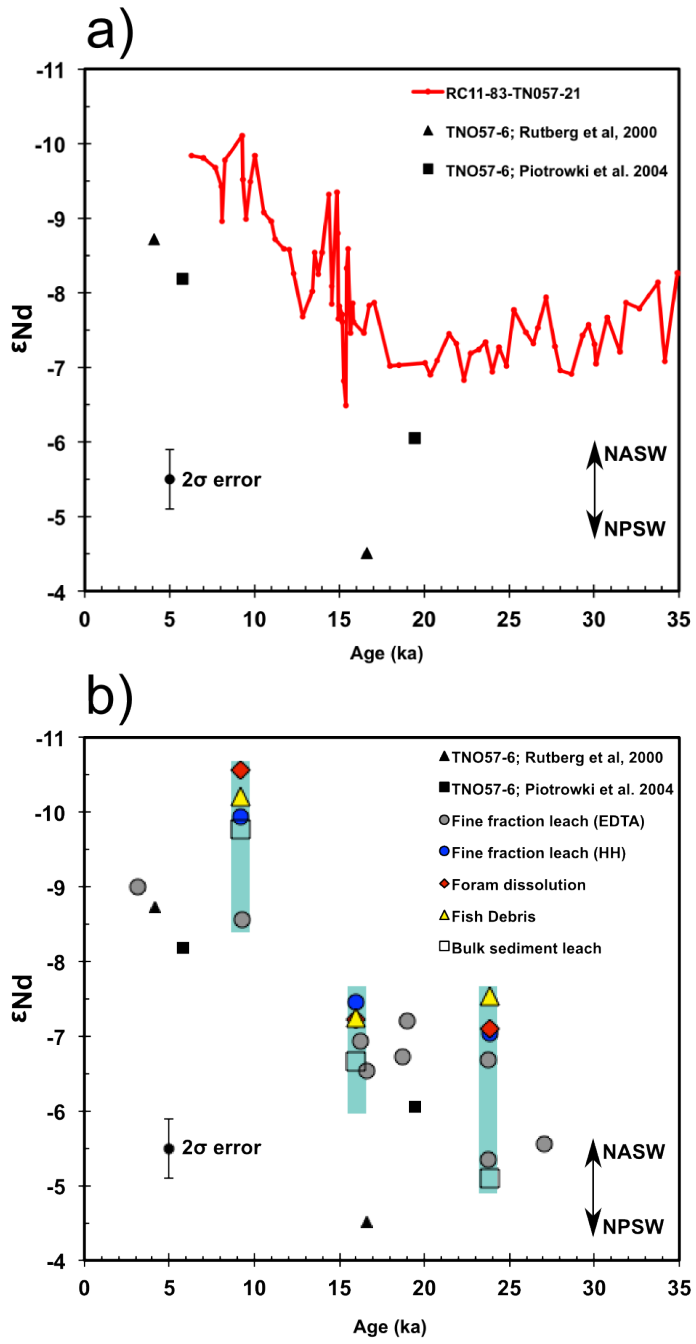

Figure 2.3: South Atlantic ε_{Nd} seawater and core-top leachate data

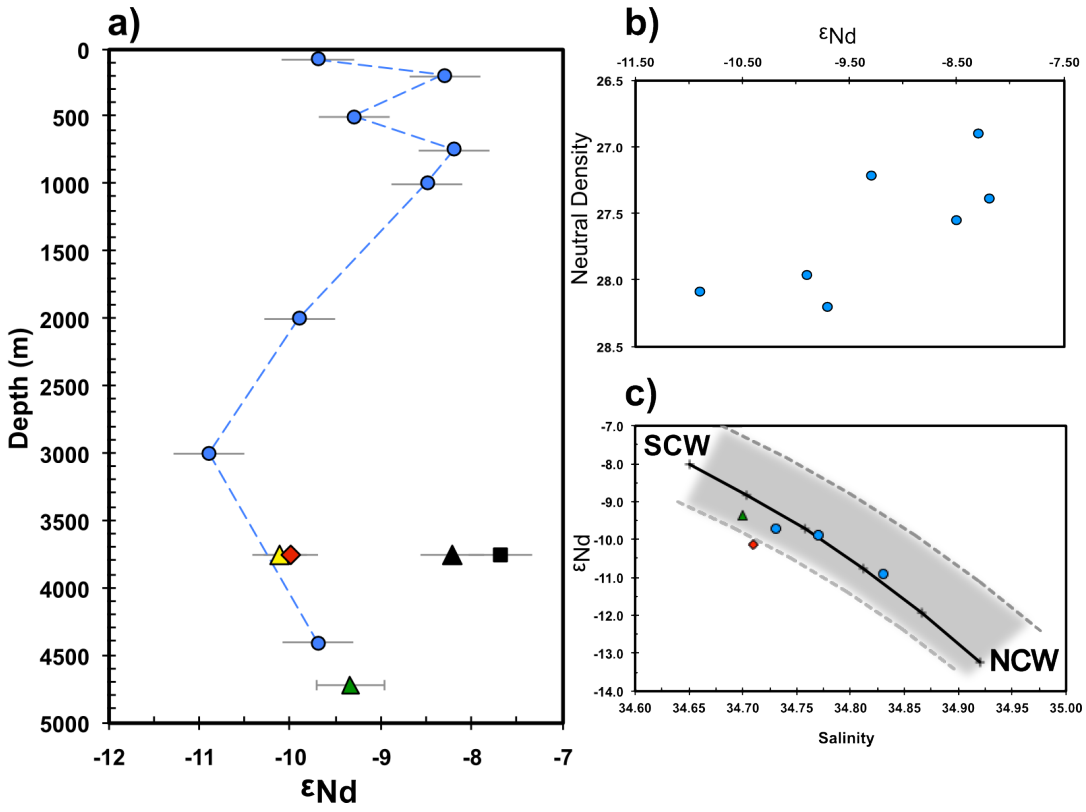

Figure 2.4: South Atlantic stable carbon isotope records

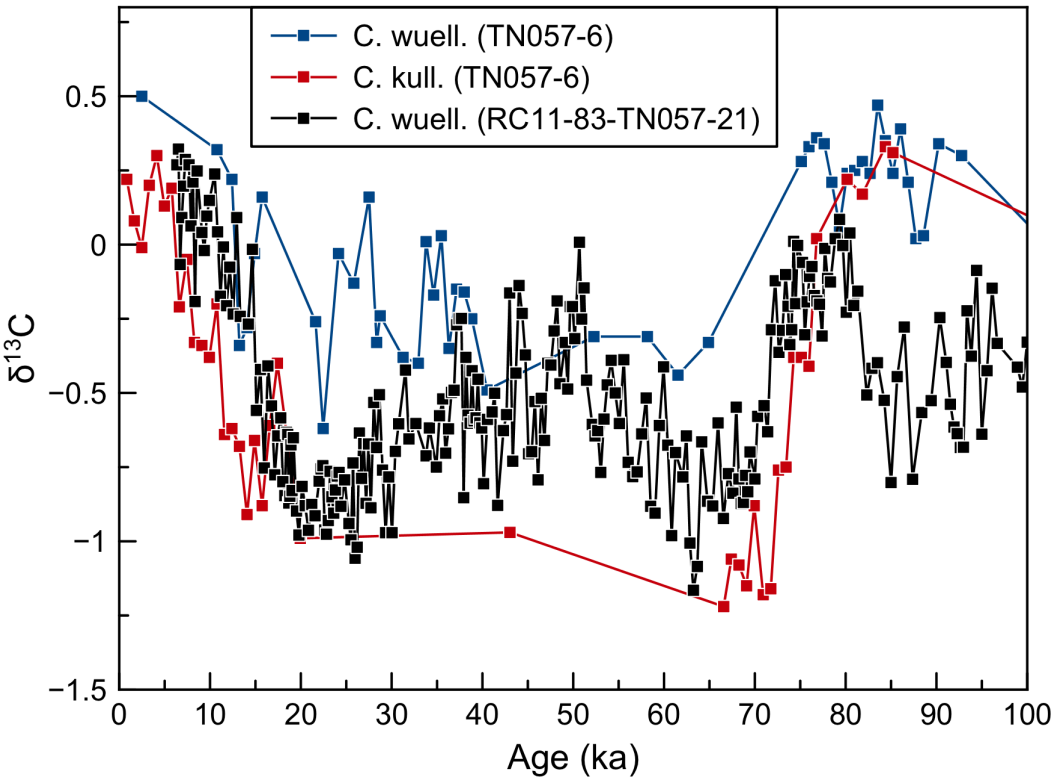

Figure 2.5: South Atlantic ε_{Nd} records

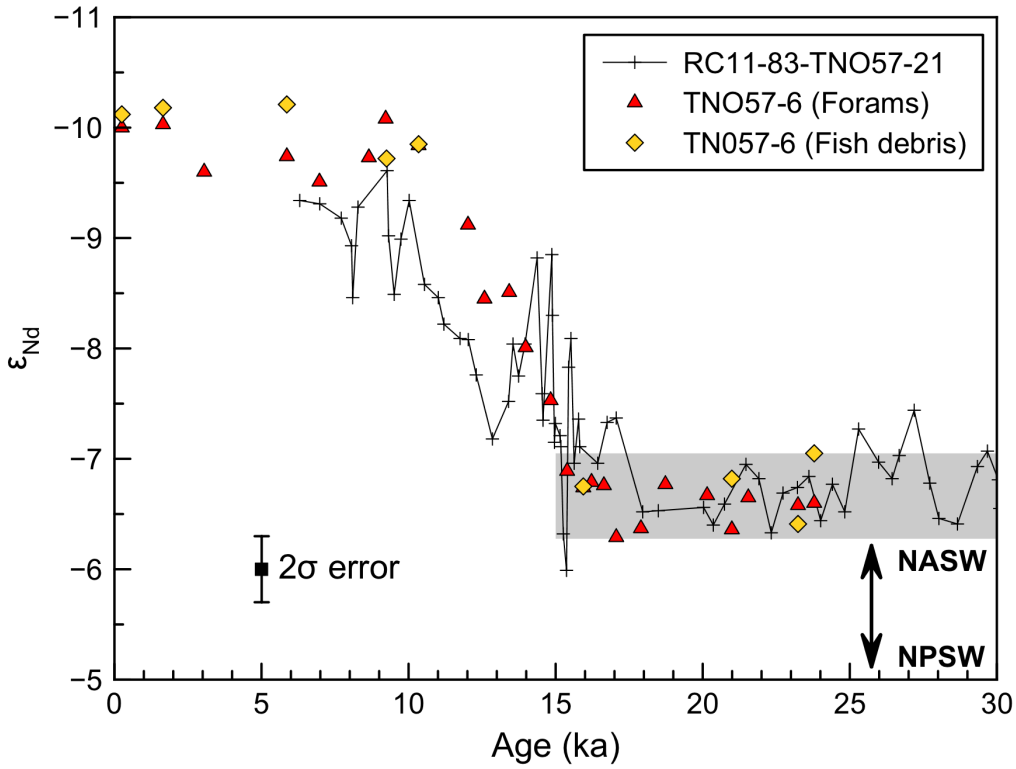

Figure 2.6: $\delta^{13}C$, ε_{Nd} and %NASW of core TNO57-6

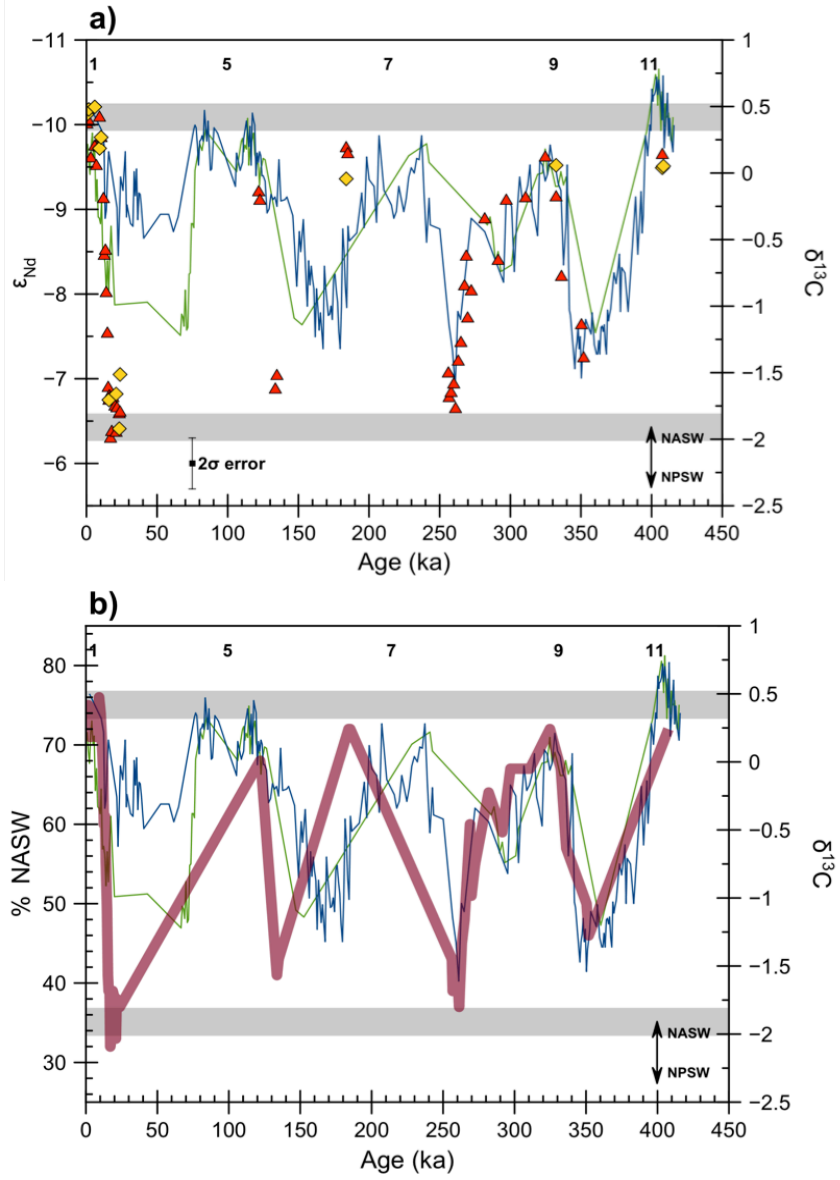

Figure 2.7: TNO57-6 isotope records and globally averaged benthic $\delta^{18}O$

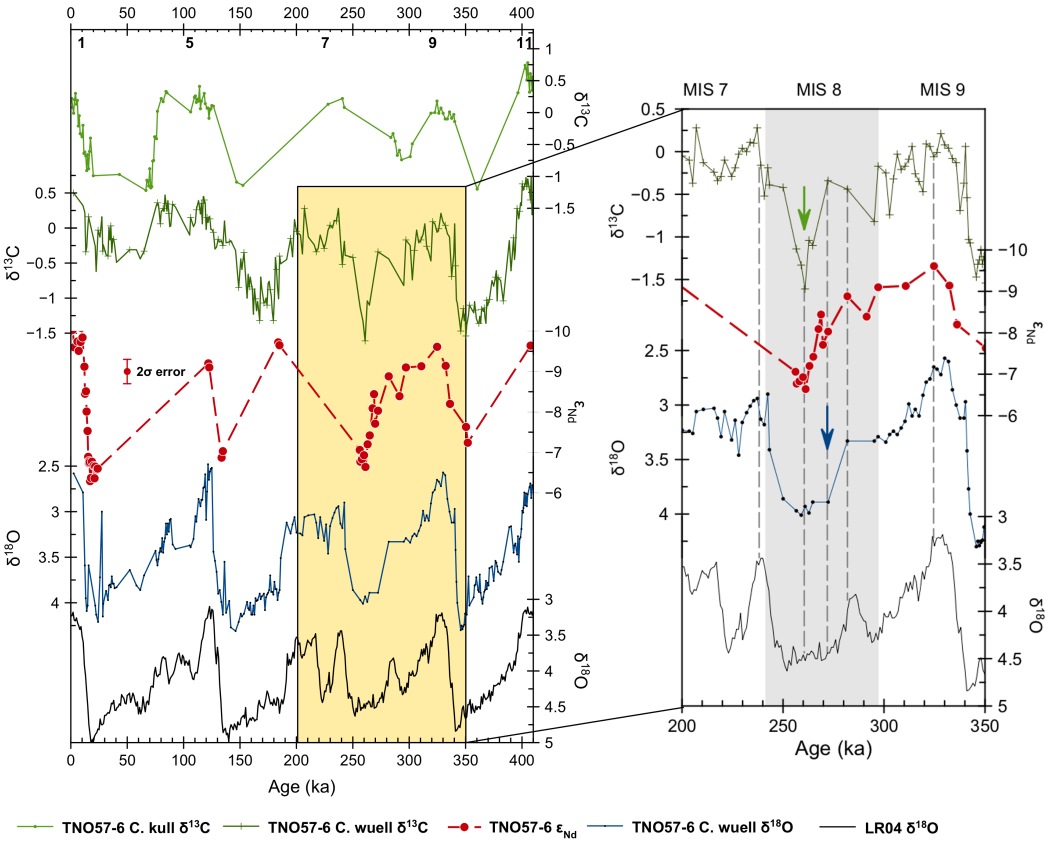

Chapter 3: Introduction to Nd concentrations and isotope compositions in the North Atlantic Ocean

3.1 Introduction

The first works to recognize the variability of neodymium (***Nd***) isotopes within seawater and (***Fe-Mn***) crusts were published over thirty years ago and laid the groundwork for the development of a water mass tracer that is still utilized today (O'Nions et al. 1978, Piepgras et al., 1979; Goldstein and O'Nions et al., 1981). The Nd isotopic composition of bottom waters are preserved in a variety of deep sea archives and can be extracted from sediment cores at high temporal resolution to reveal changes in water mass mixing without the influence of nutrient cycling (e.g. Rutberg et al., 2000; Thomas et al., 2003; Thomas, 2004; Scher and Martin, 2004, 2008; Piotrowski et al., 2004, 2005, 2008, 2012; Gutjahr et al., 2008; 2010; Gourlan et al., 2008; Klevenz et al., 2008; Pahnke et al., 2008; Martin and Scher, 2006; Roberts et al. 2010, 2012; Gutjahr and Lippold, 2011; Wilson et al., 2012, Kraft et al., 2013; Pena et al., 2013; Pena and Goldstein, 2014). Though used extensively for these studies, the input and internal cycling of Nd within the water column is not well understood and it has been suggested that Nd composition of deep waters and therefore the records derived from deep-sea cores are strongly influenced by factors other than changes in water mass mixing such as aeolian input, interaction with shelf sediments, re-suspended sediments at depth and vertical supply (e.g. Lacan and Jeandel, 2005, Chen et al., 2013). In an effort to address the unknowns of Nd cycling there have been continued attempts to increase the global database of seawater Nd concentrations and isotopes. A major mechanism for this increased sampling and analysis has been the GEOTRACES initiative (geotraces.org) wherein Nd has been listed as a key trace element and isotope. ***(TEI)***.

Of particular interest to Nd studies is the advancement and retreat of North Atlantic Deep Water (***NADW***) into the Southern Ocean during glacial-interglacial transitions. This type of work requires that the marine cycle of Nd to the modern North Atlantic and North Pacific be reasonably well constrained. The earliest work on Nd in seawater in the NADW source region showed that waters had Nd isotopic compositions (ε_{Nd}) between -26 in the Labrador Current and about -8.6 the Irminger Sea (east of Greenland). Outside of the northern seas and further along its transport path southward, mature NADW possesses a ε_{Nd}-value of -13.5 (Piepgras and Wasserburg, 1987). ε_{Nd} ($^{143}Nd/^{144}Nd$ normalized to the Chondritic Uniform Reservoir value of $^{143}Nd/^{144}Nd$ value (0.512638) in parts per 10,000; Jacobsen and Wasserburg, 1980) varies in seawater as a result of the "crustal age" of terrigenous material that is weathered into the ocean basins (reviewed in Frank, 2002 and Goldstein and Hemming, 2003), with old continental crust having low values, and young mantle derived crust having high values. As a result, the North Atlantic, surrounded by old continental crust, has some of the lowest seawater ε_{Nd} values. Conversely, the North Pacific ocean basin has the highest average ε_{Nd} values (-4) because of the young, volcanic source of the terrigenous material being weathered from the surrounding continents, and the Southern Ocean has intermediate values of ~ -8.

3.2 Regional Circulation

A summary of the water masses that are discussed in this introduction and their physical properties is presented in Table 3.1. The North Atlantic is dominated by the northward transport of shallow warm waters in the Gulf Stream from the Straits of Florida, and the successive transformation of these waters into cold, deep water in the northern extents of the basin (Figure 3.1; e.g. Schmitz and McCartney, 1993; Schmitz, 1996; van Aken, 2000, and references therein).

These tropical sourced shallow waters sink to combine with intermediate depth waters to form North Atlantic Deep Water (***NADW***), which moves as a deep western boundary current southward along the western edge of the basin. There are three principle cold water masses that contribute to NADW. Labrador Sea Water (***LSW***) originates from the Labrador Sea, is comparatively warm and shallow, very unradiogenic in ε_{Nd} (-13.5), and spreads into the Irminger and South Icelandic basin where it intermingles with overflow waters from intermediate depths sourced through the Demark Strait and east of Iceland. These water masses are known as Denmark Strait Overflow Water (***DSOW***) and Iceland Scotland Overflow Water (***ISOW***) and have more positive ε_{Nd} values of -10.6 and -11.4 respectively. These overflow waters leave the subpolar basins to flow into the Labrador Sea as part of a deep northern boundary current flowing east to west (e.g. Schmitz et al., 1993; Dickson and Brown, 1994). Another North Atlantic cold water source is southern sourced Antarctic Bottom Water (***AABW***) that reaches the North Atlantic and upwells, warms and contributes to the deep northern boundary current in the eastern portion of the basin. Deep water currents in the eastern basin are sluggish and predominantly made up of ISOW and LSW, with minor contributions of Mediterranean Outflow Water (***MOW***) (e.g. Dickson et al., 1985; van Aken, 2000). Additionally, southern sourced AABW is present along the eastern margin and enters the study region through the Vema Fracture Zone at 11°N (Arhan et al., 1994).

Within the Gulf of Cadiz, MOW overflows into the Atlantic at depths between 300 and 500m and has a distinct warm, saline signature. MOW deepens to ~1200m while leaving the Gulf of Cadiz and is partially entrained in northward flowing currents. The remaining MOW turns west and contributes to intermediate waters in the central gyre (Schmitz and McCartney, 1993). Antarctic Intermediate Water (***AAIW***) is the warmest southern sourced water mass and

contributes to thermocline waters by 32°S and crosses the equator in narrow flows along both boundaries, although more strongly contributing to currents in the western section of the basin (Rintoul, 1991). Surface currents in the study region are dominated by the subtropical gyre, which moves in a clockwise motion and interchanges water with subpolar gyres as well as tropical current systems. The subtropical gyre is flanked by the Gulf Stream on the western edge. The Gulf Stream is a major system in the basin and is dominated by recirculation gyres that strengthen the current (Schmitz, 1996).

3.3 Nd in Seawater

The Nd isotope composition of seawater is a result of water mass mixing and terrigenous inputs. These inputs to the ocean basins mirror the Nd isotopic composition of the continental sources of Nd and seawater in the North Atlantic and North Pacific reflects these differences (Table 3.1). As a result of low Sm/Nd in continental rocks compared to the bulk Earth, the ε_{Nd} of continental materials are heterogeneous around the globe and reflect the regional crustal age, such that older continental terrains, such as those surrounding the North Atlantic, have more negative ε_{Nd} values and younger continent has more positive ε_{Nd} values as seen in the volcanic material surrounding the Pacific Ocean. These signatures are preserved in waters of these ocean basins and recorded in seafloor Fe-Mn deposits (Figure 3.2, Figure 3.3; Goldstein and Hemming, 2003). The ocean residence time of Nd is short compared to ocean mixing times, (e.g. Goldstein and O'Nions 1981, Jeandel et al., 1995; Tachikawa et al., 1999; Sidall et al., 2008), which allows for the use of Nd isotopes as a water mass tracer. Nd isotopes behave conservatively in the deep open ocean and covary with salinity, demonstrating its usefulness as a water mass tracer (Figure

3.4, Figure 3.5; von Blanckenburg 1999; Goldstein and Hemming, 2003, Garcia-Solsona et al., 2014).

Unlike the Nd isotope ratios, Nd concentrations ***[Nd]*** throughout the world's ocean do not follow water mass mixing. The best example of this is known as the Nd paradox and refers to an increase in [Nd] with depth independent of water mass mixing, while at the same time ε_{Nd} varies as expected with the water mass mixtures. This pattern of increasing [Nd] with depth is seen throughout all the world's oceans and in addition, higher concentrations of Nd are seen in the North Pacific or effectively, the oldest deep waters (Figure 3.6; Goldstein and Hemming, 2003). The inconsistency of these observations has been the focus of several studies and several hypotheses have been proposed, although the true mechanism for Nd cycling has yet to be determined. It was suggested by Lacan and Jeandel (2005) that Nd is sourced to the oceans by dissolution of atmospheric inputs at the surface and regenerated at depth in a fashion similar to nutrient cycling; this idea is based on similarities between [Nd] and silicate distributions in the global deep ocean. Surface inputs of Nd to deep waters would also cause Nd isotopes in the deep waters to deviate from non-conservative water mass mixing and would have negative impacts on its utility as a water mass tracer. However, data from seawater profiles show that surface ε_{Nd}-values are often different from bottom water ε_{Nd} compositions and thus do not appear to impact the deep water masses at the same location (Figure 3.7; Goldstein and Hemming, 2003). The decoupling between ε_{Nd} and [Nd] can be replicated using a reversible scavenging model as a process for internal Nd cycling, suggesting that surface scavenging of Nd followed by release at deeper depths plays a significant role in the global Nd distribution (e.g. Siddall et al., 2008). The inconsistencies between the quasi-conservative behavior of ε_{Nd} and the similarity of [Nd] to

nutrient cycling highlight the necessity to expand our understanding of Nd cycling within the water column.

Additional unknowns lie in our understanding of how Nd is sourced to and removed from the oceans. Nd is dissolved in ocean waters after interaction with terrigenous material. River waters have high concentrations of Nd that ultimately drain into ocean basins (~300 pmol/kg) although a significant portion of Nd and other particle reactive elements (upwards of 70%) are scavenged and removed in estuaries (Goldstein and Jacobsen, 1988; Sholkovitz and Elderfield, 1988; Elderfield et al., 1990;). Additionally, aeolian input has been suggested to be a significant source for Nd to the oceans but it has been shown that it cannot solely account for the global distributions of ε_{Nd} (e.g. Nakai et al., 1993, Jones et al., 1994, van de Flierdt et al., 2004; Arsouze et al., 2009). Hydrothermal vent fluids at mid-ocean ridges would likely contribute radiogenic Nd to the oceans but high particle loads result in scavenging of the radiogenic Nd (Michard et al., 1983). Additionally, the volume of Nd contributed to the oceans through groundwater discharge is not well constrained but has been suggested to be a significant source (2.9 – 8.1 x 10^7 mol/yr; Johannesson and Burdge, 2007; Johannesson et al., 2011). Another source of Nd to the oceans is called 'Boundary Exchange' and refers to the persistent interaction of water masses with shelf boundaries and resuspended sediments (e.g. Lacan and Jeandel, 2005a,b; Arsouze et al., 2010), which can alter seawater Nd isotope compositions along a water mass transport path. The overall contributions of these mechanisms for Nd cycling are not well constrained but may be of particular importance in North Atlantic seawater studies, with important implications for understanding studies that use Nd isotopes as a paleocirculation tracer.

Within the North Atlantic Ocean basin, it is essential to identify how the main water masses acquire their Nd isotopic compositions and concentrations. A study of Nd in the source

region of NADW shows that its ε_{Nd} mainly reflects water mass mixing plus a small amount of boundary exchange along the Greenland margin (Lacan and Jeandel, 2005). The Nd signature of the deep water masses in the eastern North Atlantic have been shown to reflect NADW and southern ocean water mass mixing (Goldstein and Hemming, 2003; Rickli et al., 2009). However, there is also evidence that boundary exchange may play a role in the ε_{Nd}-value of intermediate and deep water in the Angola Basin (Rickli et al., 2009). Modeling studies relying on boundary exchange as the only source of Nd to the North Atlantic predict ε_{Nd} distributions that reflect seawater measurements at depths greater than 2500m but require a range of exchange rates (a few days to 0.5 years) (Arsouze et al., 2009; 2010). These studies acknowledge the unknowns tied to the required rates of exchange, and that localized sources are likely to influence surface and intermediate depth seawater ε_{Nd}-values. Until now, these localized sources have been difficult to categorize as a result of lack of data and the seasonal or short-lived lifetime of some input events. Despite the evidence put forward that eolian deposition has minimal influence on the ε_{Nd}-values of seawater in the North Pacific (Jones et al., 1994), Jones et al (2008) effectively modeled the interior Atlantic Ocean ε_{Nd} distribution using solely surface derived Nd inputs. This study suggests boundary exchange plays a much smaller role in the Nd ocean distribution than dust deposition.

One of the major sources of lithogenic material to the ocean is the Saharan dust plume, extending from 25°N to 14°N latitude into the eastern North Atlantic ocean basin. Dust is transported across the basin at both high and low altitudes to distances up to 1500km to the west (e.g. Prospero, 1996; Chiapello et al., 1997; Rickli et al., 2010). Nd isotope measurements have been made on aerosol, seawater and fine sediment material from the northwestern coast of Africa in an attempt to categorize the Nd signature and influence of this massive aerosol input (e.g.

Goldstein et al., 1984; Grousset et al., 1988; Cole et al., 2009; Rickli et al., 2010). North African sediments have ε_{Nd}-values in the range of -18 to -14 (Fig. 3.8b), but as a result of mixing with an atmospheric "background dust", the isotopic composition of Saharan dust (ε_{Nd} = -14.5 to -9.1, Grousset et al., 1998; Rickli et al., 2010) is more radiogenic than the source material. Dust ε_{Nd} compositions along the African coast are more radiogenic (ε_{Nd} = -8.5 to -9.8) at the most northern and southern ends of the sampled area. The distribution of atmospheric ε_{Nd} composition resembles the sediment distribution in such a way that the least radiogenic aerosol samples are just offshore from the least radiogenic lithogenic samples albeit not of the same ε_{Nd} composition. Rickli et al (2010) developed a simple steady state model to show that ~3% to 20% of the eolian Nd reaching the surface ocean close to the northwest African arid regions is dissolved and accounts for surface seawater ε_{Nd} values that are similar to those of dust. Additionally, a peak in Nd concentration in surface waters occurs in the region of discharge from the Congo River and highlights the importance of these freshwater inputs to the Nd cycle (Rickli et al., 2010).

3.4 Historical and current approaches to seawater Nd measurements

Earliest seawater Nd studies sought to increase the spatial resolution of the seawater dataset and ultimately categorize the Nd composition of the major water masses (e.g. Piepgras and Wasserburg, 1980, 1982, 1983, 1985, 1987; Stordal and Wasserburg, 1986; Piepgras and Jacobsen, 1988; Spivak and Wasserburg, 1988). These early studies set the framework for a field that has only slowly expanded due to the difficulties of analyzing Nd in seawater. Because of the low concentration of Nd in seawater (~15 - 45 pmol/kg), analyses required samples between 10 and 40 L and time intensive procedures. Early work relied on a co-precipitation method that effectively scavenged rare earth elements during the precipitation of added Fe or Mn oxides. After elemental separation, Nd isotopes are analyzed by thermal ionization mass spectrometry

(TIMS) as either Nd+ or NdO+. The oxide method allows for smaller sample sizes. Recent advances in mass spectrometry and the use of multi-collector inductively coupled plasma mass spectrometers ***(MC-ICPMS)*** have higher sensitivity, which allows for smaller seawater samples of around 3-10L in size, as well as a significant decrease in analysis time (e.g. Vance and Thirlwall, 2002). Additionally, developments in methods to pre-concentrate the Nd have resulted in a reduction in Nd separation time from upwards of a week to a few hours (Shabani et al., 1992). Although utilizing these methods has greatly increased the throughput potential of seawater samples, the Nd isotope database is still limited and large expanses on the world's oceans still remain undefined (Figure 3.9). Despite the limited amount of modern data available, Nd isotopes are increasingly used to study changes in past ocean circulation. Such applications would greatly benefit from a thorough understanding of Nd cycling in the oceans.

The GEOTRACES initiative's mission is to "… identify processes and quantify fluxes that control the distributions of key trace elements and isotopes in the ocean, and to establish the sensitivity of these distributions to changing environmental conditions" (www.geotraces.org). The following chapters of this thesis are undertaken within the framework of GEOTRACES, which promises to significantly expand the Nd seawater database. The effort relies on collaborative and international relationships that will pair such Nd measurements with those of other trace elements and isotopes (***TEIs***) within the water column, yielding an unprecedented database of TEIs.

The goals of the GEOTRACES initiative focus on investigating several key aspects of sources and sinks of TEIs in the water column (Figure 3.10; GEOTRACES Science Plan, 2008). Interfaces with TEI sources include atmospheric deposition, continental run-off, sediment-water boundaries and the ocean crust. As discussed above, most of these features may be important to

Nd cycling in the North Atlantic ocean basin. Additionally, understanding the internal cycling of TEIs is an important GEOTRACES objective. These processes include the uptake and removal in the surface ocean, regeneration and possible uptake in bottom waters, burial at the seafloor and circulation. In order to investigate such a large array of processes, with multiple groups participating, it is important to establish consistency and verify intercalibration.

The intercalibration of REE concentrations and Nd isotopes between several labs involved with GEOTRACES has been completed on a large scale (van de Flierdt et al., 2012, Pahnke et al., 2012). Participating labs processed seawater and particle samples for REE concentrations and Nd isotope ratios, from cuts of the same sample. Fifteen labs reported values for the $^{143}Nd/^{144}Nd$ ratio of seawater from three different locations (BATS 15 m, BATS 2000 m, SAFe 3000 m) and twelve labs reported values for seawater Nd concentration at two BATS' depths. Agreement between labs was within 47 to 50 ppm (2σ standard deviation) for $^{143}Nd/^{144}Nd$ values and within 9% for Nd concentrations (Figure 3.11; van de Flierdt et al., 2012). These agreements are excellent and demonstrate a great potential for comparability of measurements between labs when compiling seawater Nd databases using the described methods. These results were a product of a mix of processing and mass spectometric methods described above and show that there are no significant differences based on which methods are used. Our participation in this study (Lab #3) demonstrates our ability to collect, process and analyze seawater samples for REE concentrations and ε_{Nd} as part of collaborative projects. Particle ε_{Nd} data from five different labs was collected as part of this intercalibration effort but were inconclusive as a result of agreements >60 ppm at two depths in the water column. Shallow water particle samples at BATS were in good agreement with one another despite different processing methods being used. These results may be a result of the heterogeneity of the ε_{Nd} of differing particles on the filters,

dissimilar filter composition on individual pumps or introduced contamination (van de Flierdt et al., 2012). The final state of intercalibration efforts is that these particle tests must be revisited with more labs participating, but they already show that seawater Nd concentrations and isotope compositions can be faithfully reproduced between labs with a variety of processing methods.

With the described intercalibration efforts established and the GEOTRACES program in place, we can expect rapid collection of Nd seawater data. Obtaining superior spatial coverage of the world's ocean at both surface and the depths is a realistic goal for the scientific community (Figure 3.12; www.geotraces.org). One of the contributions toward reaching this goal is reported within this graduate thesis, which presents Nd concentrations and isotopic compositions of North Atlantic waters and specifically, along the cruise track of US GEOTRACES Cruise GA03, which is a zonal cruise across the Atlantic from Lisbon to Mauritania to Woods Hole. The compiled data is a result of a collaboration of three different US labs, that is, LDEO, U of Hawaii, and U of South Carolina. The groups are addressing different subjects with the combined dataset. My focus is on the internal cycling of Nd within the open ocean, to determine the extent that variability reflects water mass mixing versus external inputs. Additional features to be addressed by the other groups include the influence of hydrothermal fluids, dust input and sediment boundary interactions. Due to the large number of TEIs being measured by different labs, eventually there will be an unprecedented integrated dataset for this region of the Atlantic Ocean.

3.5 References

Antonoy, J. I., et al. World Ocean Atlas 2009 Volume 2: Salinity. S. Levitus, Ed., NOAA Atlas NESDIS 69, U.S. Government Printing Office, Washington, D.C., 184 pp. (2010).

Arhan, M., et al. "The eastern boundary of the subtropical North Atlantic." *Journal of Physical Oceanography* 24.6 (1994): 1295-1316.

Arsouze, T., et al. "Reconstructing the Nd oceanic cycle using a coupled dynamical-biogeochemical model." *Biogeosciences* 6.12 (2009): 2829-2846.

Chen, T., et al. "Upper Ocean Vertical Supply: A Neglected Primary Factor Controlling the Distribution of Neodymium Concentrations of Open Ocean Surface Waters?: Surface Seawater Neodymium Concentrations." *Journal of Geophysical Research: Oceans* 118, no. 8 (2013): 3887–94.

Chiapello, I., et al. "Origins of African dust transported over the northeastern tropical Atlantic." *Journal of Geophysical Research: Atmospheres (1984–2012)* 102.D12 (1997): 13701-13709.

Cole, J. M., et al. "Contrasting compositions of Saharan dust in the eastern Atlantic Ocean during the last deglaciation and African Humid Period." *Earth and Planetary Science Letters* 278.3 (2009): 257-266.

Dickson, R. R., et al. "Estimates of the mean circulation in the deep (> 2,000 m) layer of the Eastern North Atlantic." *Progress in Oceanography* 14 (1985): 103-127.

Dickson, R. R., et al. "The Production of North Atlantic Deep Water: Sources, Rates, and Pathways." *Journal of Geophysical Research: Oceans (1978–2012)* 99, no. C6 (1994): 12319–41.

Elderfield, H., R. Upstill-Goddard, and E. R. Sholkovitz. "The rare earth elements in rivers, estuaries, and coastal seas and their significance to the composition of ocean waters." *Geochimica et Cosmochimica Acta* 54.4 (1990): 971-991.

Frank, M. "Radiogenic Isotopes: Tracers of Past Ocean Circulation and Erosional Input." *Reviews of Geophysics* 40, no. 1 (2002).

Garcia-Solsona, E., et al. "Rare Earth Elements and Nd isotopes tracing water mass mixing and particle-seawater interactions in the SE Atlantic." *Geochimica et Cosmochimica Acta* 125 (2014): 351-372.

Goldstein, S. L., and R. K. O'Nions. "Nd and Sr isotopic relationships in pelagic clays and ferromanganese deposits." (1981): 324-327.

Goldstein, S. L., and S. R. Hemming. "6.17. Long-lived isotopic tracers in oceanography, paleoceanography and ice-sheet dynamics." *Treatise on Geochemistry: The Oceans and Marine Geochemistry* 6 (2004): 453.

Goldstein, S. L., R. K. O'nions, and P. J. Hamilton. "A Sm-Nd isotopic study of atmospheric dusts and particulates from major river systems." *Earth and Planetary Science Letters* 70.2 (1984): 221-236.

Goldstein, S.L., and Stein B. Jacobsen. "Rare earth elements in river waters." *Earth and Planetary Science Letters* 89.1 (1988): 35-47.

Gourlan, A. T., Meynadier, L., and Claude J. Allègre. "Tectonically driven changes in the Indian Ocean circulation over the last 25 Ma: Neodymium isotope evidence." *Earth and Planetary Science Letters* 267.1 (2008): 353-364.

Grousset, F. E., et al. "Neodymium isotopes as tracers in marine sediments and aerosols: North Atlantic." *Earth and Planetary Science Letters* 87.4 (1988): 367-378.

Gutjahr, M., and Jörg Lippold. "Early arrival of Southern Source Water in the deep North Atlantic prior to Heinrich event 2." *Paleoceanography* 26.2 (2011).

Gutjahr, M., et al. "Changes in North Atlantic Deep Water strength and bottom water masses during Marine Isotope Stage 3 (45–35kaBP)." *Quaternary Science Reviews* 29.19 (2010): 2451-2461.

Gutjahr, M., et al. "Tracing the Nd isotope evolution of North Atlantic deep and intermediate waters in the Western North Atlantic since the Last Glacial Maximum from Blake Ridge sediments." *Earth and Planetary Science Letters* 266.1 (2008): 61-77.

Jacobsen, S. B., and G. J. Wasserburg. "Sm-Nd isotopic evolution of chondrites." *Earth and Planetary Science Letters* 50.1 (1980): 139-155.

Jeandel, C., et al. "Exchange of neodymium and its isotopes between seawater and small and large particles in the Sargasso Sea." *Geochimica et Cosmochimica Acta* 59.3 (1995): 535-547.

Johannesson, K. H., and David J. Burdige. "Balancing the global oceanic neodymium budget: Evaluating the role of groundwater." *Earth and Planetary Science Letters* 253.1 (2007): 129-142.

Johannesson, K. H., et al. "Submarine groundwater discharge is an important net source of light and middle REEs to coastal waters of the Indian River Lagoon, Florida, USA." *Geochimica et Cosmochimica Acta* 75.3 (2011): 825-843.

Jones, C. E., et al. "Neodymium isotopic variations in North Pacific modern silicate sediment and the insignificance of detrital REE contributions to seawater." *Earth and Planetary Science Letters* 127.1 (1994): 55-66.

Jones, K., et al., "Modeling the Distribution of Nd Isotopes in the Oceans Using an Ocean General Circulation Model." *Earth and Planetary Science Letters* 272.3 (2008): 610-619

Klevenz, V., et al. "Neodymium isotopes in benthic foraminifera: core-top systematics and a down-core record from the Neogene south Atlantic." *Earth and Planetary Science Letters* 265.3 (2008): 571-587.

Kraft, S., et al. "Assessment of seawater Nd isotope signatures extracted from foraminiferal shells and authigenic phases of Gulf of Guinea sediments." *Geochimica et Cosmochimica Acta* 121 (2013): 414-435.

Lacan, F., and C. Jeandel. “Acquisition of the Neodymium Isotopic Composition of the North Atlantic Deep Water: NEODYMIUM ISOTOPIC COMPOSITION.” *Geochemistry, Geophysics, Geosystems* 6, no. 12 (December 2005)

Lacan, F., and C. Jeandel. “Neodymium Isotopes as a New Tool for Quantifying Exchange Fluxes at the Continent–ocean Interface.” *Earth and Planetary Science Letters* 232, no. 3–4 (April 2005): 245–57.

Locarnini, R. A., et al., World Ocean Atlas 2009, Volume 1: Temperature. S. Levitus, Ed., NOAA Atlas NESDIS 68, U.S. Government Printing Office, Washington, D.C., 184 pp. (2010).

Martin, E. E., and H. Scher. “A Nd Isotopic Study of Southern Sourced Waters and Indonesian throughflow at intermediate depths in the Cenozoic Indian Ocean: ND ISOTOPIC STUDY AT ODP SITE 757.” *Geochemistry, Geophysics, Geosystems* 7, no. 9 (2006)

Michard, A., et al. "Rare-earth elements and uranium in high-temperature solutions from East Pacific Rise hydrothermal vent field (13 N)." *Nature* 303.5920 (1983): 795-797.

Nakai, S., Halliday, A., and David K. Rea. "Provenance of dust in the Pacific Ocean." *Earth and Planetary Science Letters* 119.1 (1993): 143-157.

O'Nions, R. K., et al. "Pb, Nd and Sr isotopes in oceanic ferromanganese deposits and ocean floor basalts." *Nature* 273 (1978): 435-438.

Pahnke, K., et al. “GEOTRACES Intercalibration of Neodymium Isotopes and Rare Earth Element Concentrations in Seawater and Suspended Particles. Part 2: Systematic Tests and Baseline Profiles.” *Limnology and Oceanography: Methods* 10 (2012): 252–69.

Pahnke, K., Goldstein, S.L., and Sidney R. Hemming. "Abrupt changes in Antarctic Intermediate Water circulation over the past 25,000 years." *Nature Geoscience* 1.12 (2008): 870-874.

Peucker-Ehrenbrink, B., et al. "Continental bedrock and riverine fluxes of strontium and neodymium isotopes to the oceans." *Geochemistry, Geophysics, Geosystems* 11.3 (2010).

Pena, L. and S. L. Goldstein, “Thermohaline circulation crisis and impacts during the mid-Pleistocene transition.” Science 345 (2014): 318-322.

Pena, L; and S. L. Goldstein, “Thermohaline circulation crisis and impacts during the mid-Pleistocene transition.” *Science* 345 (6194): 318-322.

Piepgras, D. J., and G. J. Wasserburg. "Influence of the Mediterranean outflow on the isotopic composition of neodymium in waters of the North Atlantic." *Journal of Geophysical Research: Oceans (1978–2012)* 88.C10 (1983): 5997-6006.

Piepgras, D. J., and G. J. Wasserburg. "Influence of the Mediterranean outflow on the isotopic composition of neodymium in waters of the North Atlantic." *Journal of Geophysical Research: Oceans (1978–2012)* 88.C10 (1983): 5997-6006.

Piepgras, D. J., and G. J. Wasserburg. "Isotopic composition of neodymium in waters from the Drake Passage." *Science* 217.4556 (1982): 207-214.

Piepgras, D. J., and G. J. Wasserburg. "Strontium and neodymium isotopes in hot springs on the East Pacific Rise and Guaymas Basin." *Earth and planetary science letters* 72.4 (1985): 341-356.

Piepgras, D. J., and G. J. Wasserburg. “Rare Earth Element Transport in the Western North Atlantic Inferred from Nd Isotopic Observations.” *Geochimica et Cosmochimica Acta* 51, no. 5 (1987): 1257–71.

Piepgras, D. J., et al. "The isotopic composition of Nd in different ocean masses." *Earth and Planetary Science Letters* 45.2 (1979): 223-236.

Piepgras, D. J., and G. J. Wasserburg. "Neodymium isotopic variations in seawater." *Earth and Planetary Science Letters* 50.1 (1980): 128-138.

Piepgras, D. J., and Stein B. Jacobsen. "The isotopic composition of neodymium in the North Pacific." *Geochimica et Cosmochimica Acta* 52.6 (1988): 1373-1381.

Piotrowski, A. M., et al. "Reconstructing deglacial North and South Atlantic deep water sourcing using foraminiferal Nd isotopes." *Earth and Planetary Science Letters* 357 (2012): 289-297.

Piotrowski, A. M., et al. “Intensification and Variability of Ocean Thermohaline Circulation through the Last Deglaciation.” *Earth and Planetary Science Letters* 225, no. 1–2 (August 2004): 205–20.

Piotrowski, A. M., et al. “Temporal Relationships of Carbon Cycling and Ocean Circulation at Glacial Boundaries.” *Science* 307, no. 5717 (March 25, 2005): 1933–38. doi:10.1126/science.1104883.

Piotrowski, A. M., et al. "Oscillating glacial northern and southern deep water formation from combined neodymium and carbon isotopes." *Earth and Planetary Science Letters* 272.1 (2008): 394-405.

Prospero, J. M. "Saharan dust transport over the North Atlantic Ocean and Mediterranean: an overview." *The impact of desert dust across the Mediterranean*. Springer Netherlands, 1996. 133-151.

Rickli, J., et al. “Hafnium and Neodymium Isotopes in Surface Waters of the Eastern Atlantic Ocean: Implications for Sources and Inputs of Trace Metals to the Ocean.” *Geochimica et Cosmochimica Acta* 74, no. 2 (January 2010): 540–57.

Rickli, J., Frank, M., and Alex N. Halliday. "The hafnium–neodymium isotopic composition of Atlantic seawater." *Earth and Planetary Science Letters* 280.1 (2009): 118-127.

Rintoul, S. R., and C. Wunsch. "Mass, heat, oxygen and nutrient fluxes and budgets in the North Atlantic Ocean." *Deep Sea Research Part A. Oceanographic Research Papers* 38 (1991): S355-S377.

Roberts, N. L., et al. “Synchronous Deglacial Overturning and Water Mass Source Changes.” *Science* 327, no. 5961 (January 1, 2010): 75–78.

Roberts, Natalie L., et al. "Rare earth element association with foraminifera." *Geochimica et Cosmochimica Acta* 94 (2012): 57-71.

Rutberg, R. L., et al. "Reduced North Atlantic Deep Water flux to the glacial Southern Ocean inferred from neodymium isotope ratios." *Nature* 405.6789 (2000): 935-938.

Scher, H. D., and Ellen E. Martin. "Circulation in the Southern Ocean during the Paleogene inferred from neodymium isotopes." *Earth and Planetary Science Letters* 228.3 (2004): 391-405.

Scher, H. D., and Ellen E. Martin. "Oligocene deep water export from the North Atlantic and the development of the Antarctic Circumpolar Current examined with neodymium isotopes." *Paleoceanography* 23.1 (2008).

Schmitz, W. J. *On the World Ocean Circulation. Volume 1. Some Global Features/North Atlantic Circulation.* DTIC Document, 1996.

Schmitz, W. J., and M. S. McCartney. "On the north Atlantic circulation." *Reviews of Geophysics* 31.1 (1993): 29-49.

Shabani, M. B., et al. "Preconcentration of trace rare-earth elements in seawater by complexation with bis (2-ethylhexyl) hydrogen phosphate and 2-ethylhexyl dihydrogen phosphate adsorbed on a C18 cartridge and determination by inductively coupled plasma mass spectrometry." *Analytical Chemistry* 64.7 (1992): 737-743.

Sholkovitz, E. R., and H. Elderfield. "Cycling of dissolved rare earth elements in Chesapeake Bay." *Global Biogeochemical Cycles* 2.2 (1988): 157-176.

Siddall, M., et al. "Towards explaining the Nd paradox using reversible scavenging in an ocean general circulation model." *Earth and Planetary Science Letters* 274.3 (2008): 448-461.

Spivack, A. J., and G. J. Wasserburg. "Neodymium isotopic composition of the Mediterranean outflow and the eastern North Atlantic." *Geochimica et Cosmochimica Acta* 52.12 (1988): 2767-2773.

Stordal, M. C., and G. J. Wasserburg. "Neodymium isotopic study of Baffin Bay water: sources of REE from very old terranes." *Earth and Planetary Science Letters* 77.3 (1986): 259-272.

Tachikawa, K., et al. "Distribution of rare earth elements and neodymium isotopes in suspended particles of the tropical Atlantic Ocean (EUMELI site)." *Deep Sea Research Part I: Oceanographic Research Papers* 46.5 (1999): 733-755.

Thomas, D. J. "Evidence for deep-water production in the North Pacific Ocean during the early Cenozoic warm interval." *Nature* 430.6995 (2004): 65-68.

Thomas, D. J., Bralower, T.J., and Charles E. Jones. "Neodymium isotopic reconstruction of late Paleocene–early Eocene thermohaline circulation." *Earth and Planetary Science Letters* 209.3 (2003): 309-322.

Van Aken, H. M. “The Hydrography of the Mid-Latitude Northeast Atlantic Ocean: I: The Deep Water Masses.” *Deep Sea Research Part I: Oceanographic Research Papers* 47, no. 5 (2000): 757–88.

Van de Flierdt, T., et al. "New constraints on the sources and behavior of neodymium and hafnium in seawater from Pacific Ocean ferromanganese crusts." *Geochimica et Cosmochimica Acta* 68.19 (2004): 3827-3843.

Van de Flierdt, T., et al. “GEOTRACES Intercalibration of Neodymium Isotopes and Rare Earth Element Concentrations in Seawater and Suspended Particles. Part 1: Reproducibility of Results for the International Intercomparison.” *Limnology and Oceanography: Methods* 10 (2012): 234–51.

Vance, D., and Matthew Thirlwall. "An assessment of mass discrimination in MC-ICPMS using Nd isotopes." *Chemical Geology* 185.3 (2002): 227-240.

von Blanckenburg, F. "Tracing past ocean circulation?." *Science* 286.5446 (1999): 1862-1863.

Wilson, D. J., et al. "A boundary exchange influence on deglacial neodymium isotope records from the deep western Indian Ocean." *Earth and Planetary Science Letters* 341 (2012): 35-47.

3.6 Tables

Table 3.1. Physical properties of water masses sampled and discussed in this study. Potential temperature and salinity measurements are taken from samples where Nd data is available with the exception of MOW, AAIW and AABW which were compiled from WOA09 in their respective source regions (Antonov et al., 2009; Locarnini et al., 2009; detailed in Chapter 4 of this thesis). Nd-compositions are assigned based on data collected by 1. Tachikawa et al., 2004; 2. Lacan and Jeandel, 2005; 3. Jeandel, 1993; 4. Stichel et al., 2012. Water masses are Mediterranean Outflow Water (MOW), North Atlantic Deep Water (NADW), Antarctic Intermediate Water (AAIW), Antarctic Bottom Water (AABW), Denmark Strait Overflow Water (DSOW), Iceland Scotland Overflow Water (ISOW) and Labrador Sea Water (LSW).

Table 3.1: Water masses discussed in this study

Water Mass	T	S	[Nd]	ε_{Nd}	Ref
MOW	13.00	38.30	23.05	-9.05	*1*
NADW	2.25	34.92	21.35	-13.25	*2*
AAIW	3.00	34.20	11.45	-8.00	*3, 4*
AABW	-0.50	34.62	26.00	-8.50	*3, 4*
DSOW	1.36	34.82	18.71	-10.60	*2*
ISOW	2.57	34.96	19.41	-11.40	*2*
LSW	2.87	34.85	17.33	-13.50	*2*

3.7 Figures

Figure 3.1. North Atlantic basin with simplified hydrology modified from Schmitz and McCartney, 1993. Deep, intermediate and shallow water currents are roughly depicted by black, gray and white arrows respectively. Square numbers represent transports in Sverdrups (1Sv = 10^6 m^3/s). Yellow dots represent GEOTRACES cruise track GA03. North Atlantic Deep Water source waters are represented as Denmark Strait Overflow Water (DSOW), Labrador Sea Water (LSW) and Iceland Scotland Overflow Water (ISOW) and labeled in bold text.

Figure 3.2. Global ε_{Nd} composition of seafloor Fe-Mn deposits (source Goldstein and Hemming, 2003). Each ocean basin has a unique ε_{Nd}-value preserved in Fe-Mn deposits. These deposits are representative of bottom water ε_{Nd} composition.

Figure 3.3. Global ε_{Nd} composition of seawater profiles in the Atlantic and Indian Oceans (source Goldstein and Hemming, 2003). Full water profiles of ε_{Nd} demonstrate the variability with depth associated with changes in present water masses especially in the South Atlantic.

Figure 3.4. Plot of ε_{Nd} vs. salinity (source Goldstein and Hemming, 2003). ε_{Nd} covaries with salinity in the ocean and represents nonlinear mixing of two end-members: Southern Component Water (***SCW***) and Northern Component Water (***NCW***).

Figure 3.5. Meridional salinity transect of the Atlantic basin overlaid by ε_{Nd} seawater data (source von Blanckenburg, 1999). Variability in ε_{Nd} at depth in the water column is associated with changes in salinity as a result of changing water mass mixing proportions at each depth.

Figure 3.6. Nd concentrations versus depth for all published Nd seawater data as of 2003 (source Goldstein and Hemming, 2003). The typical 'Nd-paradox' profile exhibits highest [Nd] at depth with greatest [Nd] in oldest, deep Pacific waters similar to seawater nutrient distributions.

Figure 3.7. ε_{Nd} seawater profiles in all ocean basins (source Goldstein and Hemming, 2003). In each ocean basin there is high variability between surface and deep ε_{Nd} suggesting different sources of Nd at surface and deep depths.

Figure 3.8. (A)Hafnium and Neodymium compositions ($\varepsilon_{Hf}/\varepsilon_{Nd}$) of dust samples reported in Rickli et al., 2010. (B) Contour lines represent the Nd isotopic composition of fine sediments of northern Africa and previously reported dust ε_{Nd} (source Rickli et al., 2010).

Figure 3.9. Distribution of all published seawater ε_{Nd} for the Atlantic basin. Only red stations have data at more than seven depths.

Figure 3.10. Diagram representing major influences on the distribution of TEI's in the ocean (source GEOTRACES Science Plan, 2008).

Figure 3.11. Reported dissolved Nd isotopic compositions at two BATS depths for intercalibration (source Pahnke et al., 2012).

Figure 3.12. Completed GEOTRACES cruise tracks in the Atlantic basin (source geotraces.org).

Figure 3.1: Hydrology of the North Atlantic

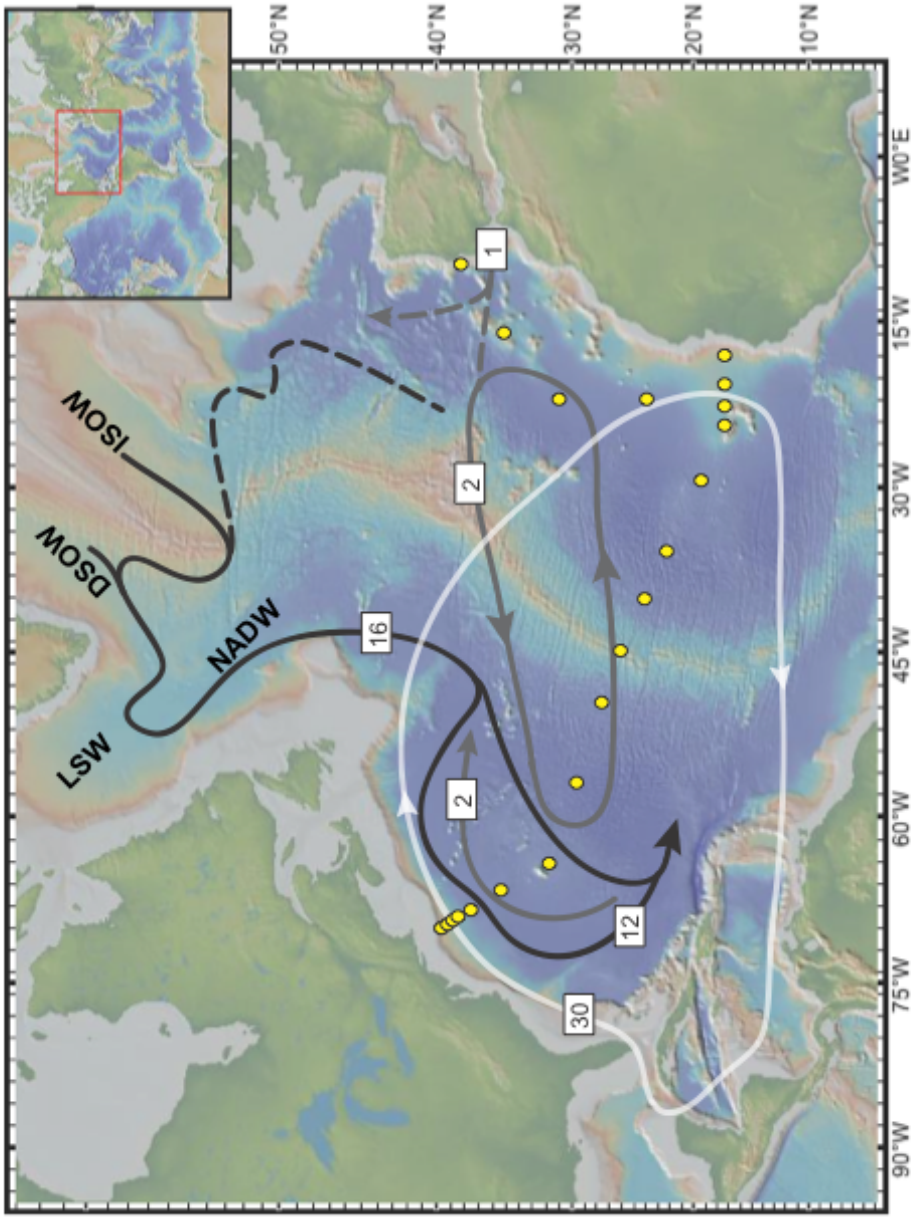

Figure 3.2: ε_{Nd} composition of margin sediments

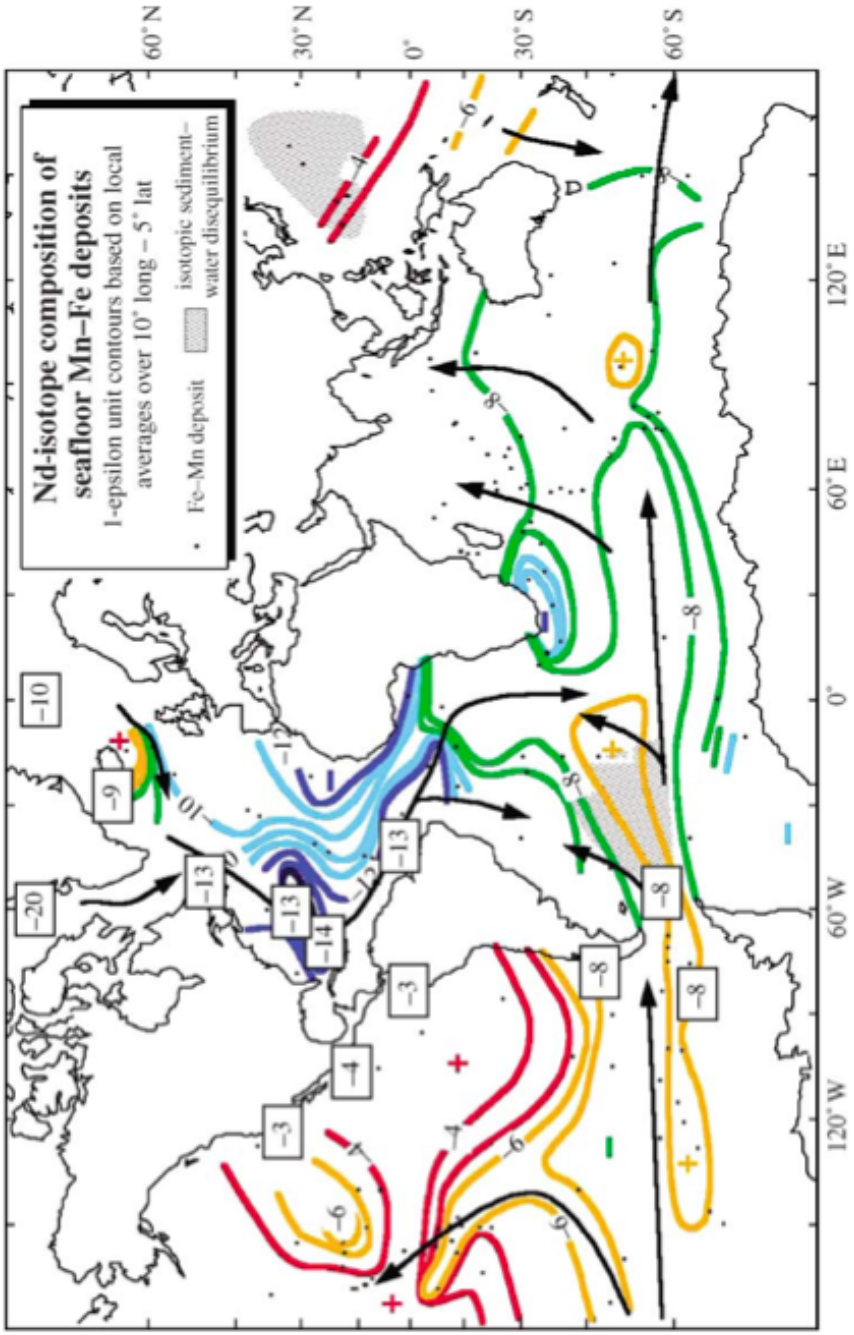

Figure 3.3: ε_{Nd} seawater profiles in the Atlantic and Indian Oceans

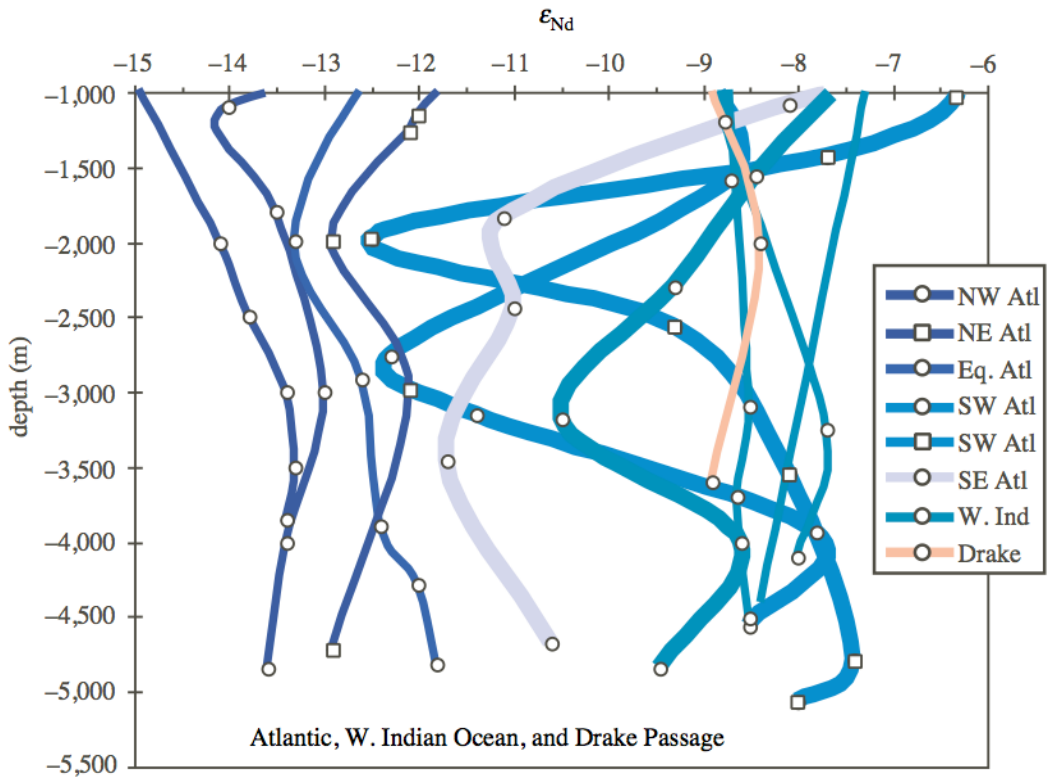

Figure 3.4: ε_{Nd} versus salinity of global seawater measurements

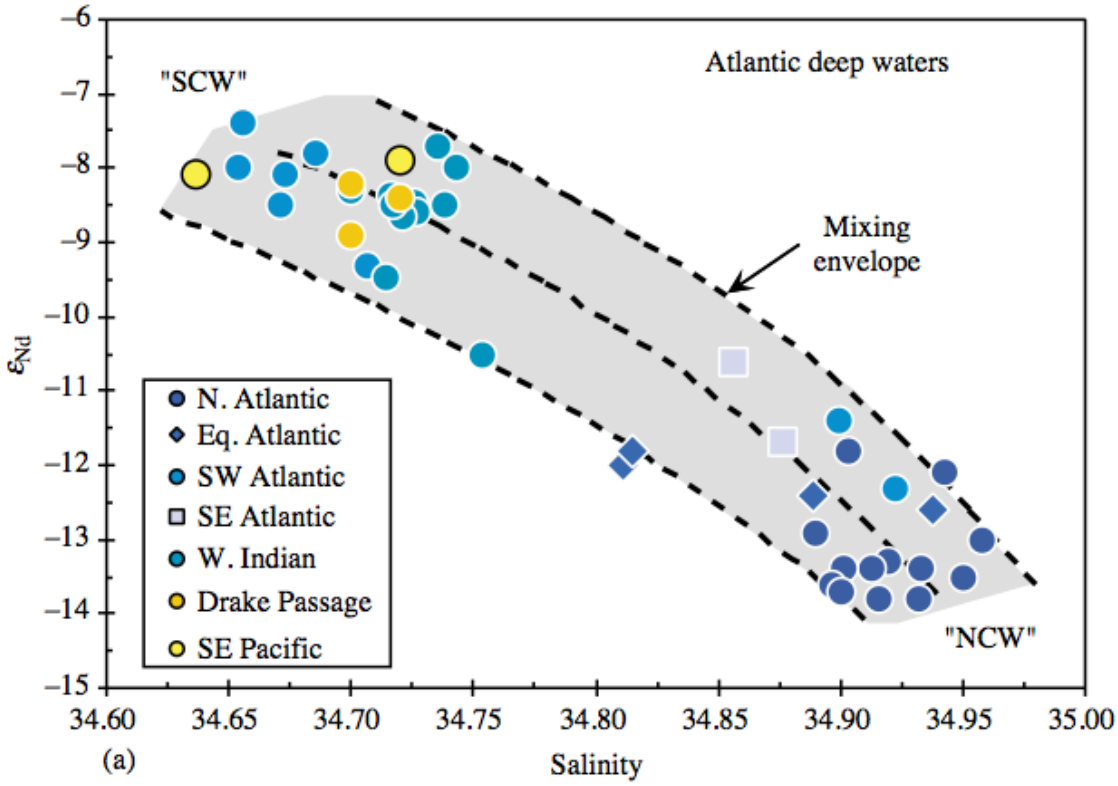

Figure 3.5: Meridional transect of salinity in the Atlantic basin with ε_{Nd} station profiles

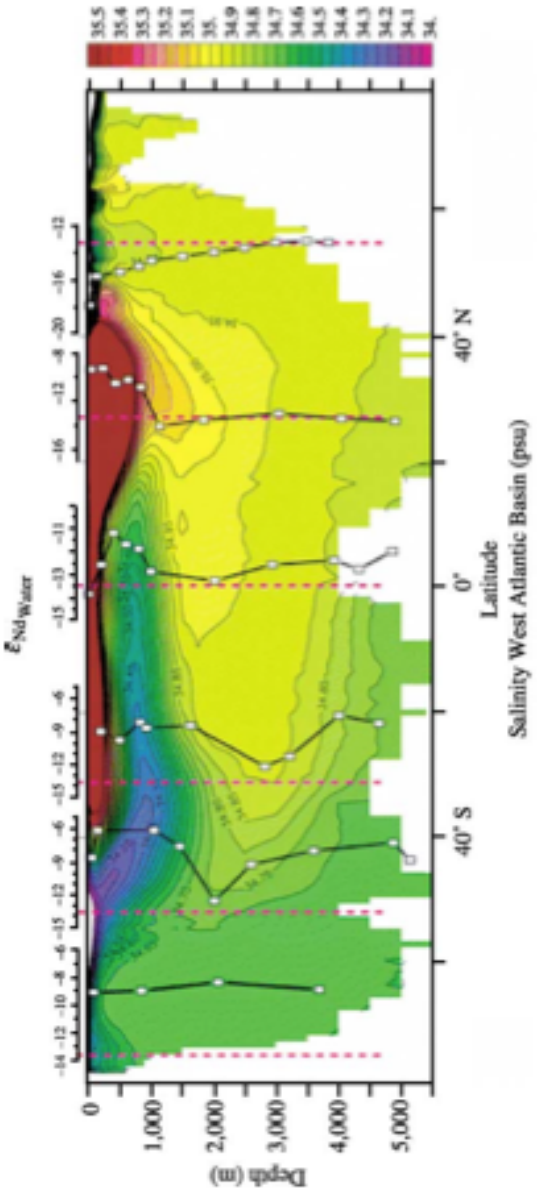

Figure 3.6: Seawater Nd concentration versus depth compiled for all ocean basins

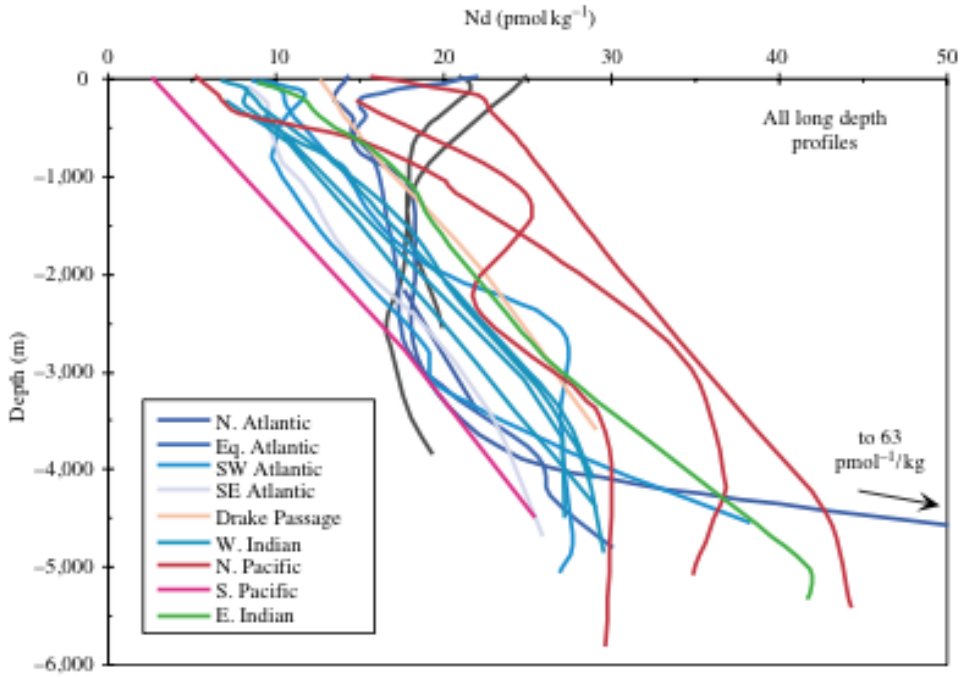

Figure 3.7: ε_{Nd} seawater profiles in the Atlantic, Indian and Pacific Oceans

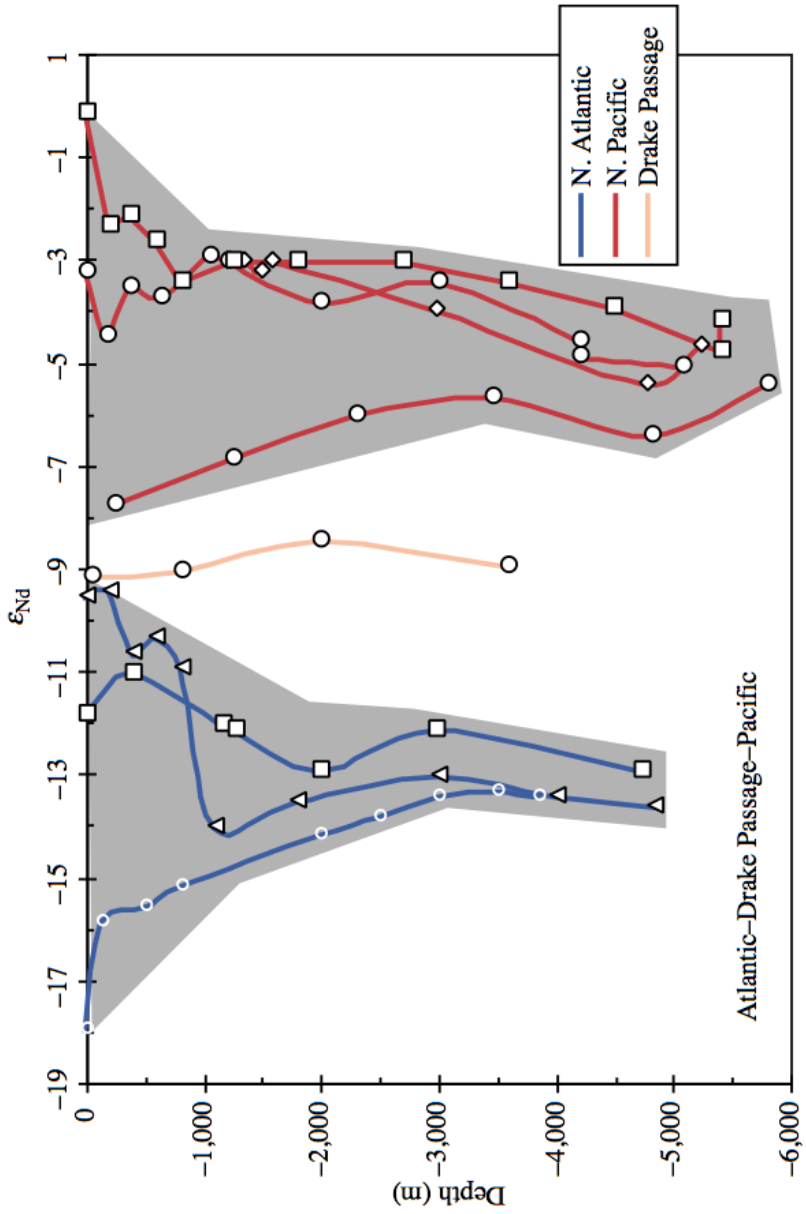

Figure 3.8: ε_{Nd} compositions of dust and fine sediments within the Saharan dust plume

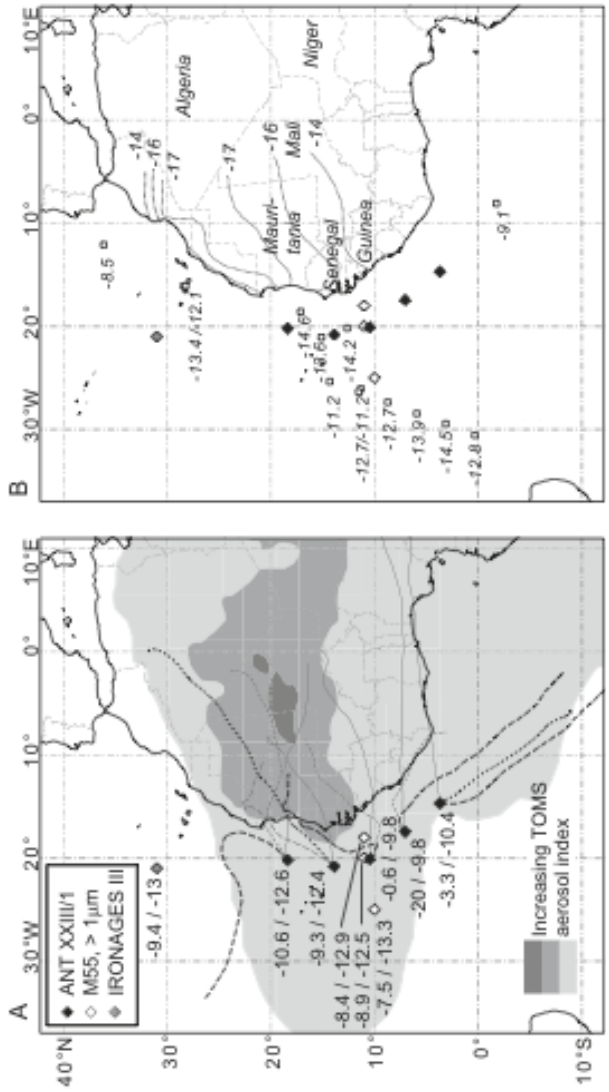

Figure 3.9: Distribution of published seawater ε_{Nd} measurements in the Atlantic basin

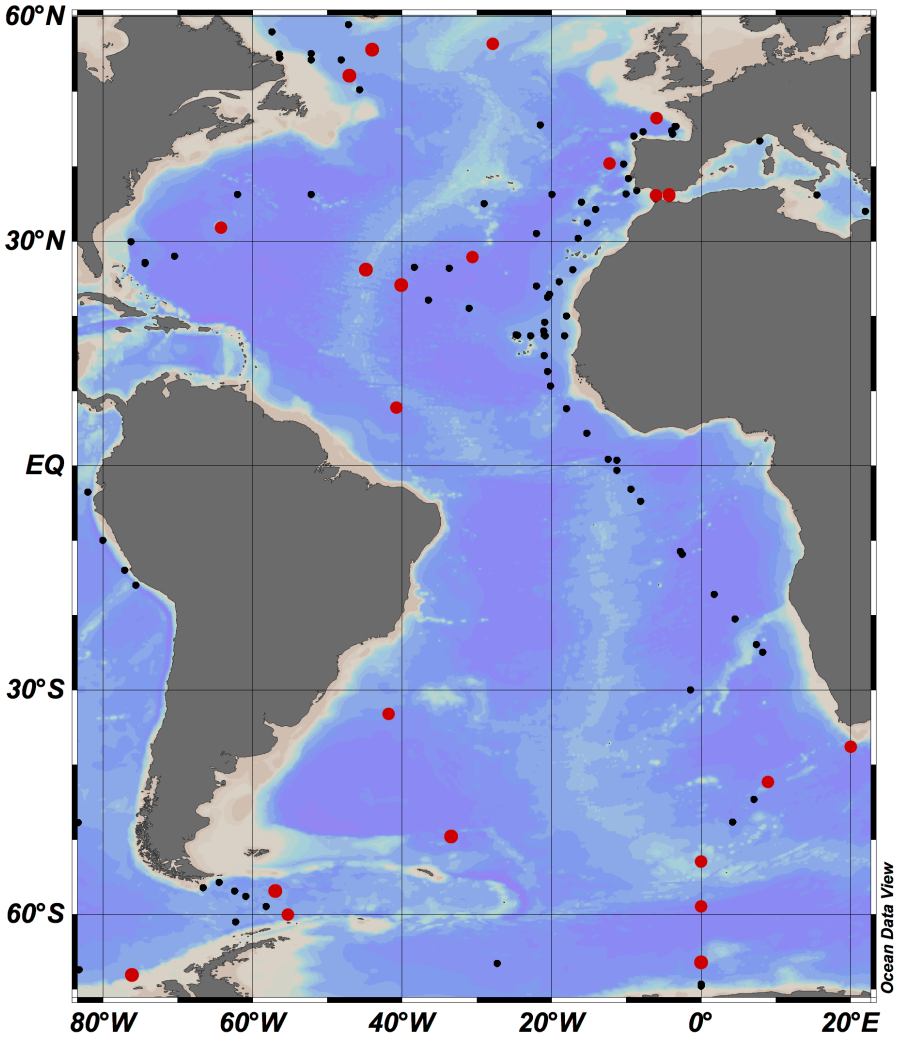

Figure 3.10: Illustration of the important regions for the distribution of TEI'S

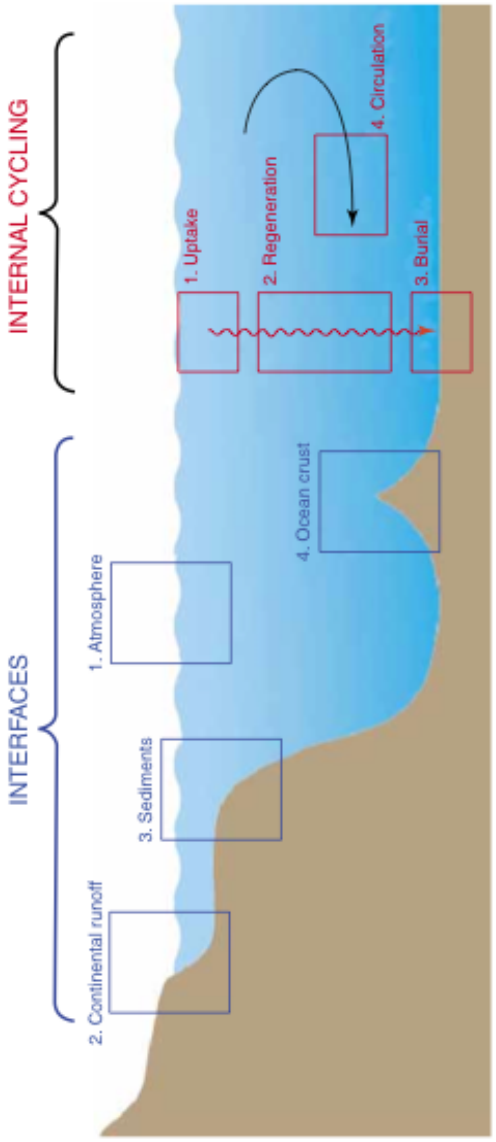

Figure 3.11: Intercalibration results for the measurement of ε_{Nd} within seawater at BATS

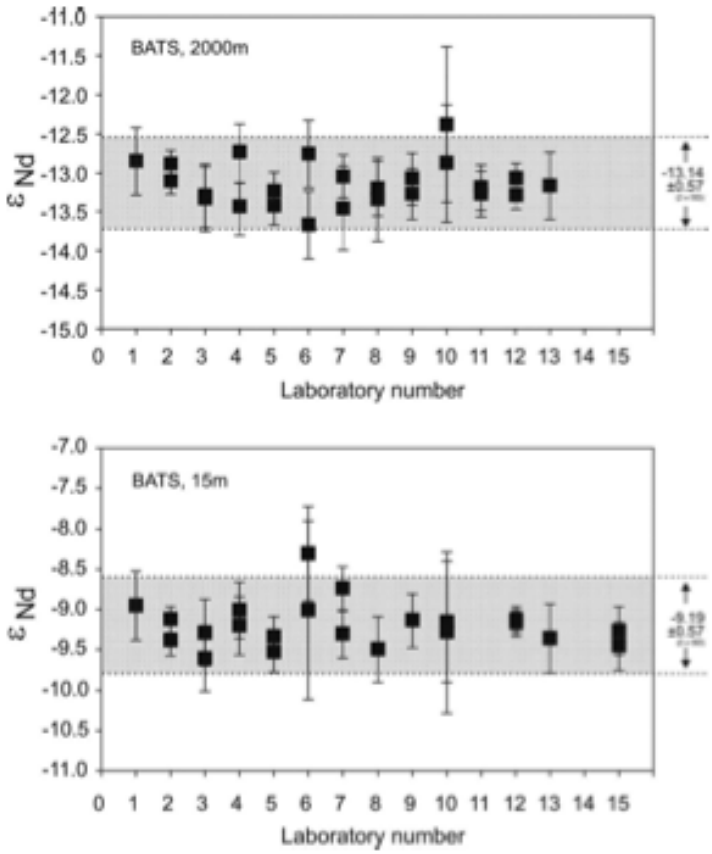

Figure 3.12: Completed GEOTRACES cruise tracks in the Atlantic basin

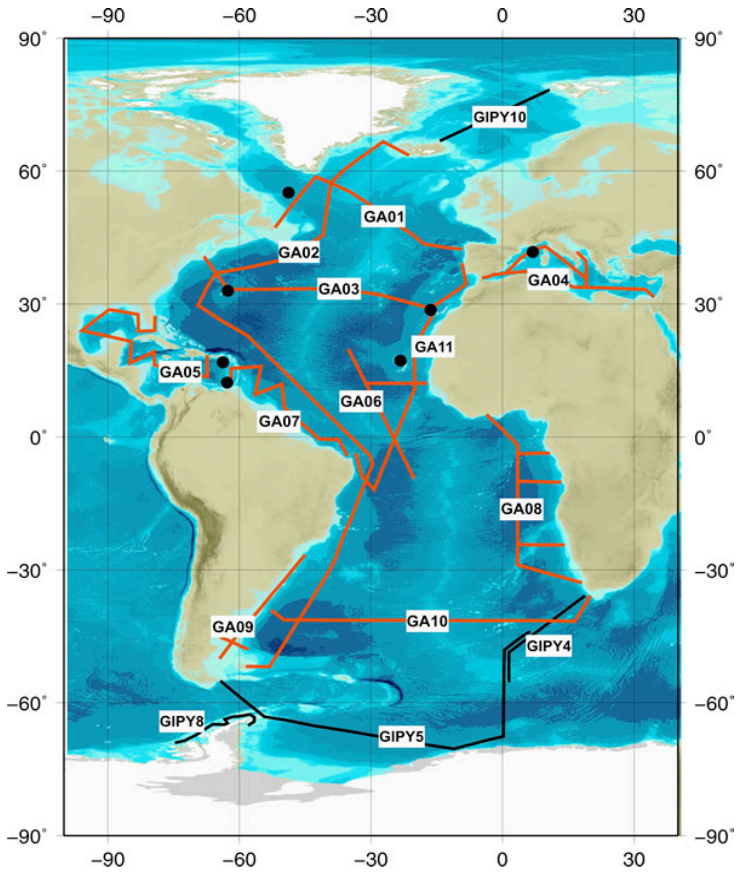

Chapter 4: Seawater neodymium composition in the open ocean North Atlantic: water mass signatures and transport

4.1 Motivation and goals

The North Atlantic Ocean is of particular importance to water mass formation, mixing and transport and is a focus of this thesis. Seawater samples from the GEOTRACES North Atlantic Zonal Cruise GA03 track were collected in two stages during cruises KN199-4 and KN204 in 2010 and 2011 respectively. These samples were analyzed for an array of physical properties, nutrients, trace elements and isotopes. As part of this work, a subset of these samples were processed for neodymium (***Nd***) concentration and isotope composition. Nd isotopes have been shown to be a valuable water mass tracer (e.g. Goldstein and Hemming, 2003) and our goal was to investigate the sources, sinks and cycling of Nd and Nd isotopes in the ocean. Of significant interest to this study, and to paleoceanography, is the application of Nd isotopes to monitor changes in the export of North Atlantic Deep Water (***NADW***) southward to the Southern Ocean through time. As a result of the distinct ε_{Nd} composition of NADW, Nd isotopes are especially useful at tracing these northern-sourced water masses into the Southern Ocean. The ε_{Nd} of bottom waters change in accordance with changes in the mixing contributions of deep water masses and are recorded in the authigenic phases of deep-sea sediments (e.g. Rutberg et al., 2000; Bayon et al., 2002; Thomas et al., 2003; Martin and Scher, 2004; Piotrowski et al., 2004, 2005, 2008, 2012; Gutjahr et al., 2008; 2010; Klevenz et al., 2008; Pahnke et al., 2008; Scher and Martin, 2008; Roberts et al. 2010, 2012; Gutjahr and Lippold, 2011; Kraft et al., 2013; Pena and Goldstein, 2014). Records of these changes show cyclical patterns correlated with glacial-interglacial as well as millennial-scale shifts. Until now the absence of a comprehensive understanding of the sources and sinks of Nd, and even the distribution of ε_{Nd} in the oceans, has

limited its effectiveness as a water mass and as a paleo-ocean circulation tracer. An important question is how much the ε_{Nd} of NADW becomes modified within the North Atlantic system following initial formation by addition of Nd along the transport path. GEOTRACES cruise track GA03 samples NADW and additional major water masses (Mediterranean Outflow Water, Antarctic Intermediate Water and Antarctic Bottom Water), which can be examined for conservative ε_{Nd} behavior (Figure 4.1a). The study region is also host to a suite of biogeochemical processes that may influence the conservative behavior of Nd and is being investigated by other cruise members. The goal of my work is to calculate fractions of different water masses at the sample sites to predict the ε_{Nd}-values based on water mass mixing and to compare these predictions with the measured [Nd] and ε_{Nd}, defined as the ***"Nd-composition"***. Deviation between the predicted and measured Nd-composition can shed light on where processes are impacting the sources and sinks of Nd and causing it to deviate from conservative behavior.

4.2 Approach for determining end-member compositions

One of the initial steps for this process is to be able to identify the water masses sampled in the study area. Every sampled depth along the cruise track represents a mixture of Atlantic basin water masses. By using the conservative water mass properties potential temperature (***T***) and salinity (***S***), we can identify what water masses are contributing to the T and S characteristics at any site and in what proportion. This simplified approach (hereafter called the *"**T-S approach**")* to water mass mixing is dependent on defined end-members that could contribute to mixing based on parameters such as location, depth and T-S compositions. For example, when considering which high *S* water mass may be contributing to the compositions of shallow depths

in the North Atlantic, obviously Pacific Equatorial Water should not be considered as a possible end-member. In addition to such considerations, the characteristics of our water samples compared to water mass end-members on a T-S diagram are instrumental to estimating the mixing components for a set of data.

Although we consider the characteristics of each parcel to be derived from the mixing of major water masses, often these water masses have been modified compared to their original compositions when they approach the study area. Sometimes they are mixtures themselves, or possibly their compositions may have been modified by external Nd. These considerations are important in the North Atlantic in particular when considering the contributions of Antarctic Intermediate Water (***AAIW***) and Antarctic Bottom Water (***AABW***). The source regions for these water masses are in the Southern Ocean and far from the study region, so that along their flow path, T and S and other properties such as ε_{Nd} are modified from their 'pure' compositions. We therefore have to re-define the 'quasi' or 'modified' end-members closer to where our samples are collected. This chapter addresses how the compositions of each end-member were defined (values are in Table 4.1). For our first estimate, we have relied on T-S to define mixing of up to three end-members (illustrated by Equation 1). Due to the complicated mixing often seen at shallow depths, and the influence of sea surface conditions such as evaporation and precipitation, the mixing calculations are only completed for depths >900m.

$$S_1 + S_2 + S_3 = S_{mix}$$

$$\theta_1 + \theta_2 + \theta_3 = \theta_{mix}$$

$$f_1 + f_2 + f_3 = 1$$

Equation 1.

As a more sophisticated alternative to determine the percent contributions of end-members along the GA03 cruise track, Jenkins et al. (2014) used an approach known as Optimum Multi-Paramater Analysis (OMPA). They consider the contributions of up to five water masses at each site using five water mass tracers, and consider mixing at all depths including thermocline waters. The results from the OMPA (end-member values are in Table 4.2) are used in addition to the *T-S approach* calculation to predict ε_{Nd}-values and [Nd] for each sample of water along the cruise track.

In order to use the unique mixture of water mass end-members calculated for each depth to predict an 'expected' Nd-composition at a depth, we must assign each end-member with a [Nd] and ε_{Nd}-value representative of that water mass. Some end-members used represent 'modified' waters, and when direct measurements of ε_{Nd} and [Nd] are not available in the source regions for these end-members, the Nd-composition of a water mass is calculated based on mixing of 'pure' end-members according to Equation 2.

$$\varepsilon Nd_{mix} = \frac{\sum_{i \neq j} \varepsilon Nd_{i \to j} \times [Nd]_{i \to j} \times f_{i \to j}}{\sum_{i \neq j} [Nd]_{i \to j} \times f_{i \to j}}$$

Equation 2.

The mixing equation (Equation 2) is also used to predict the Nd-composition of each sample according to the fraction of each water mass. The Nd-compositions for each sample calculated using results from both the *T-S approach* and OMPA and are listed in Table 4.3.

4.3 Water mass end-members

4.3.1 Major water masses

The end-members used for water mass mixing calculations are discussed in the following paragraphs and summarized in Tables 4.1 and 4.2. Select properties of the end-members (T, S, and ε_{Nd}) are plotted in Figure 4.2. Additionally, Figure 4.1b shows the sample locations of published data used to assign Nd-compositions to end-members.

In the eastern basin of the North Atlantic Ocean, Mediterranean Outflow Water (***MOW***) overflows from the Mediterranean Basin into the Gulf of Cadiz at 400m depth and deepens further from the sill to depths up to 1500m (Baringer and Price, 1997). This warm, saline water has ε_{Nd} -9.4 to -10.1 on the eastern side of the Strait of Gibraltar *("pure"* MOW, Table 4.1; Piepgras and Wasserburg, 1983; Spivack and Wasserburg, 1988; Tachikawa et al., 2004). However, the properties of MOW are changed downstream from the outflow sill and therefore we use a modified MOW end-member. This modified end-member is derived from the CTD measurements made during our cruise KN199-4, and represents the salinity maximum at intermediate depths at the station closest to the source region for MOW. Station USGT10-01 at 1186 m depth (Figure 4.1b) is used to represent MOW (θ = 12.15°C, S = 36.50) and has a measured ε_{Nd} = -10.3 and [Nd] of 18.77 pmol/kg. The OMPA MOW end-member (***MOW$_{OMPA}$***) is based on the most eastern station of WOCE cruise track A03 (Jenkins et al., 2014) and has similar T-S properties to the modified MOW end-member used in the *T-S approach* (θ = 12.65°C, S = 36.63). Because the T-S properties are comparable, the Nd-composition used for the ***MOW$_{OMPA}$*** end-member is the same as the composition used for MOW in the 'simplified approach'.

NADW is sourced from the northern seas of the Atlantic Ocean and is formed in the deep western basin. The T-S properties of NADW warm slightly along the western basin and become slightly more saline (Figure 4.3c). The Nd-composition of NADW has been extensively investigated and is well constrained to be within the range of ε_{Nd} = -14 to -12 and [Nd] = 20-30 pmol/kg (e.g. Piepgras and Wasserburg, 1987; Lacan and Jeandel, 2005). The NADW end-member is used within the western and central basin but eastern basin waters at NADW depths exhibit a higher salinity than what can be accounted for by the NADW source waters. NADW enters the eastern basin through the Romance Fracture Zone at the Equator and enters the study region from the south. As a result of mixing with MOW and the sluggish circulation in the eastern basin, this 'eastern NADW' acquires a warmer and more saline signature. To define this water mass for our calculations, we designate a deep open ocean sample collected during cruise KN199-4 to represent Eastern North Atlantic Deep Water (***ENADW***). Station USGT10-07 (Figure 4.1b), depth 2222m is used as the ENADW end-member for mixing calculations in the eastern basin and has a measured ε_{Nd} = –11.62 and [Nd] = 18.60 pmol/kg (θ = 3.39°C, S = 35.02). The OMPA calculations are comprised of several deep northern sourced water masses as a result of taking into account the minor water masses that contribute to NADW. Additionally, northern sourced waters that may contribute to intermediate waters are considered in OMPA calculations. The water masses are Denmark Straight Outflow Water (***DSOW***), Iceland Scotland Outflow Water (***ISOW***), Classic Labrador Sea Water (***CLSW***), Upper Labrador Sea Water (***ULSW***) and Irminger Sea Water (***ISW***) (Table 4.2). The Nd-compositions of these waters are predominantly defined by the work of Lacan and Jeandel (2005) and are chosen based on similarities in T-S characteristics of the samples they collected. Their Station 15 at depth 1000m most closely represents the end-member T-S properties used by Jenkins et al. (2014) in OMPA

of DSOW (θ = 1.36°C, S = 34.82) and has a measured ε_{Nd} = -10.6 and [Nd] = 18.71 pmol/kg. ISOW (θ = 2.57°C, S = 34.96) is defined by Lacan and Jeandel (2005), Station 12 between 2500m and 2800m with ε_{Nd} = -11.4 and [Nd] = 19.41 pmol/kg. CLSW (θ = 2.87°C, S = 34.85) is defined by their Station 2 at depth 1600m with ε_{Nd} = -13.5 and [Nd] = 17.33 pmol/kg. ULSW (θ = 3.89°C, S = 34.88) is defined by their Station 3 depths 400-1000m and has ε_{Nd} = -15 and [Nd] = 21.5 pmol/kg. ISW (θ = 4.1°C, S = 34.9) is defined by their Station 9 depth 601m and has ε_{Nd} = -13.3 and [Nd] = 18.72 pmol/kg.

Antarctic Intermediate Water (***AAIW***) is a southern sourced, low-salinity water mass that crosses the equator along the western edge of the North Atlantic basin. It contributes to intermediate depths in both the eastern and western basins and has T-S properties that are defined by its source region off the coast of Antarctica (Figure 4.4). The Nd-composition of this water mass is estimated based on the closest published Nd data that has the same T-S properties of the water masses in the source region (Jeandel, 1993; Stichel, et al. 2012). AAIW has an average $\varepsilon_{Nd} \sim$ -8 and [Nd] = 11.45 pmol/kg. As AAIW progresses to the North Atlantic, the T-S properties are modified. Modified T-S properties are chosen from the WOA09 dataset (Antonoy et al., 2009; Locarnini et al., 2009) at intermediate depths at 0-10 degrees N (Figure 4.5). The Nd-composition of modified AAIW (ε_{Nd} = -8.45, [Nd] = 12.40 pmol/kg) is calculated based on these T-S properties and binary mixing of pure AAIW and MOW. The OMPA AAIW end-member (***AAIW$_{OMPA}$***) also represents a modified water mass near the equator but is assigned a Nd-composition based on the nearest seawater measurements (7°44'N, 40°42'W, TT0/TAS Sta. 63 - 790 m depth; θ = 5.23°C, S = 34.61) and has a ε_{Nd} = -11.90 and [Nd] = 15.90 pmol/kg (Piepgras and Wasserburg, 1987).

Antarctic Bottom Water (***AABW***) is a silicate rich water mass that obtains its T-S properties as it forms in the Ross and Weddell Seas off the coast of Antarctica (Figure 4.4). The Nd-composition of pure AABW has ε_{Nd} = -8.5 and [Nd] = 26 pmol/kg and is based on the available Nd seawater data in the Atlantic sector of the Southern Ocean (Jeandel, 1993; Stichel et al., 2012). AABW is found at depth in the North Atlantic but is modified from its pure composition as it moves north towards the equator, becoming slightly warmer and saltier. Modified AABW T-S properties are determined from the waters reaching 0-10 deg N within the western basin and the Nd-composition is calculated based on binary mixing between pure AABW and NADW (ε_{Nd} = -10.24; [Nd] 24.30 pmol/kg). An additional AABW end-member was used in water mass mixing calculations within the eastern basin due to the saltier deep waters found in this region (herein referred to as Eastern Antarctic Bottom Water). The Nd-composition of this water mass was calculated based on mixing between saltier ENADW and AABW but was found to poorly predict measured ε_{Nd} in this region (Figure 4.6). Figure 4.7 demonstrates that the deep silicate rich waters in this region have measured ε_{Nd} values ~ -11.9 and therefore represent the ε_{Nd} of the southern sourced waters at bottom depths. Modified AABW in the eastern basin (***EAABW***) has ε_{Nd} = -11.9 and [Nd] = 23.72. $AABW_{OMPA}$ is based on modified southern sourced waters near the equator and has ε_{Nd} = -11.6 and [Nd] = 30.1 pmol/kg based on the closest measured Nd data (7°44'N, 40°42'W, TT0/TAS Sta. 63 - 4810 m depth; θ = 1.23°C, S = 34.81; Piepgras and Wasserburg, 1987). Additionally, OMPA takes into account contributions from Upper Circumpolar Deep Water (***UCPDW***) as another southern sourced water mass. It is hard to distinguish the Nd-composition of this water mass from overlying waters in the Southern Ocean (Stichel et al., 2012). An Nd-composition of ε_{Nd} = -12.6 and [Nd] = 16.2 pmol/kg is assigned to

UCPDW based on the closest measured data available with similar T-S properties (7°44'N, 40°42'W, TT0/TAS Sta. 63 - 980 m; θ = 4.81°C, S = 34.70; Piepgras and Wasserburg, 1987).

4.3.2 Additional water masses

The above defined water mass end-members were used to calculate predicted water mass contributions and Nd compositions for each sample (Table 4.3.). For intermediate waters (900m - 3000m), the calculated ε_{Nd} were poor at predicting the observed ε_{Nd} in the western basin (Figure 4.8b). The offset is the result of relying on MOW to represent the warmest and most saline component of the mixing triangle used to explain intermediate depths (Figure 4.8a). MOW has high ε_{Nd} (as discussed above, we use ~ -10.3) and predicted ε_{Nd}-values in intermediate waters have higher ε_{Nd} than their measured value. In addition, MOW is not the most suitable water mass to define high T and S features in the western basin but instead a warm, saline water mass with a lower ε_{Nd} such as ISW would be more appropriate as shown by the corresponding T-S diagram (Figure 4.8c). ISW is defined as having ε_{Nd} = -13.3 and [Nd] = 18.75 pmol/kg in both the *T-S* and OMPA approaches (Lacan and Jeandel, 2005).

Intermediate depths at eastern basin stations (GT10-05, -07, -09, -10, -11, -12 and GT11-16, -18, -20, -22, 24) show an offset between calculated and measured ε_{Nd} (Figure 4.6). Additionally, unlike other western basin stations, T-S at intermediate depths at central Atlantic stations (GT11-12, -14) cannot be explained by mixing with ISW (Figure 4.8c). In order to predict ε_{Nd} at intermediate depths at the above mentioned stations, we consider North Atlantic Central Water (***NACW***) in our water mass calculations, which is a warm and less saline water mass that has a ε_{Nd} = -12 and [Nd] =13.87 pmol/kg (Figure 4.2; Figure 4.9; Copard et al., 2011; Piepgras and Wasserburg, 1983). Within the OMPA analysis, central waters are NACW,

Southwest Atlantic Central Water (***SWACW***) and Atlantic Equatorial Water (***AEW***). These end-members are defined as an array for OMPA calculations (Figure 4.9; Jenkins et al., 2014) but are assigned distinct Nd-compositions based on the closest measured data available from our study or the literature. For example, Station GT10-05 at depth 250m best represents the T-S properties defined by the NACW array and has a measured ε_{Nd} = -10.6 and [Nd] = 15.02 pmol/kg (Figure 4.9; this study). The SWACW assigned Nd-composition is defined by station GT11-16/420m and has ε_{Nd} = -11.61 and [Nd] = 17 pmol/kg (Figure 4.9; this study). AEW has a ε_{Nd} = -12.6 and [Nd] = 15.3 based on the closest data available in the equatorial Atlantic (7°44'N, 40°42'W, TT0/TAS Sta. 63 - 200 m; θ = 10.33°C, S = 35.01; Piepgras and Wasserburg, 1987).

4.4 Assigning water mass mixing end-members in the *T-S approach*

With the end-members well defined, we can use the T-S properties measured for each sample to calculate a ε_{Nd} and [Nd] based on simple water mass mixing. In order to do this the data from the study area are broken up into different regional and depth dependent subsets that can be defined by three-member mixing triangles. The western basin is made up of stations USGT11-01, -02, -03, -04, -06, -08, -10, -12, and -14. Samples at depths >3000 m are defined by mixing between NADW and AABW with minimal contributions from AAIW (Figure 4.10c). Samples collected at depths between 900 and 3000m are defined by mixing between NADW, AAIW and ISW or NACW (Figure 4.10a,b). Within the eastern basin, stations USGT10-01, -03, and -05 are considered to have the biggest MOW influence. At intermediate depths (900 m - 2300 m), samples at stations USGT10-01, -03, -05 and -07 reflect a mixing of MOW, AAIW and ENADW (Figure 4.11a). Deep waters at GT10-01 and -03 (>2300m) and one sample at GT10-05 (~2400 m) are defined by mixing between MOW, ENADW and EAABW (Figure 4.12a). The

more southern stations in the eastern basin (USGT10-09, -10, -11, -12 and USGT11-24, -22, -20, -18 and -16) are influenced by NACW, AAIW and ENADW at depths between 900 and 2000 m (Figure 4.11b). At these stations, samples at depths > 2000 m, are influenced by ENADW, AAIW and EAABW (Figure 4.12b). This mixing triangle is also used to describe the T-S properties at samples >2900 m at Sta. GT10-05.

The results of these calculations are used to determine a predicted ε_{Nd} and [Nd] for each sample for comparison to measured data. In addition, the results of the OMPA are used for comparison with our first order approach and to calculate Nd-compositions of the water column. The results of this work are summarized in Table 4.3.

4.5 Variability in water mass end-member Nd-compositions

As a result of the limited amount of seawater Nd data available in the oceans, the ε_{Nd} and [Nd] data assigned to any particular end-member may be based on Nd measurements from parcels of waters at different depths or with T-S properties that are not precisely those defined for the end-members. We must rely on the limited data available to infer the Nd-compositions of such end-members, but in some instances there is a collection of Nd measurements available in end-member source regions that we can use. In these cases, we can consider a range of ε_{Nd} and [Nd] for the end-member and decide the best value. In order to determine the best value, we determine how the different potential Nd-compositions for the end-member influence calculated ε_{Nd} and [Nd] by applying a sensitivity test in both the T-S calculations and OMPA derived calculations.

In the simplified *T-S approach* we apply the sensitivity test to the Nd-composition of NADW in the western basin (Stations GT11-01, -02, -03, -04, -06, -08, -10, -12, -14) in order to

investigate the impacts on a radiogenic anomaly seen at St. GT11-12 and -14. Available data from seawater profiles in the literature and this study suggest a range in ε_{Nd} from -13.6 to -12.0 between 2500m and 4000m depth along the western boundary (Figure 4.13). With this information, we apply a range of ε_{Nd} from -13.5 to -12.0 to the NADW end-member as a sensitivity test (-13.5, -13.25, -13.0 and -12.0). The final *T-S approach* calculations are made using an ε_{Nd} value of -13.5 for NADW. In the OMPA-derived calculations, we investigated a range of ε_{Nd} values for the composition of ULSW in an attempt to address the sensitivity of calculated Nd-compositions to this water mass. This water mass is assigned an unradiogenic value (ε_{Nd} = -15.0) based on the closest available Nd data (Station 3 depths 400-1000m; θ = 3.89°C, S = 34.88; Lacan and Jeandel, 2005). This results in an unradiogenic excursion across the basin in calculated ε_{Nd}. Taking a closer look at the available data in the ULSW source region suggests a range of the ε_{Nd} composition of this end-member (Figure 4.14). Based on this information, we run repeat calculations with the OMPA results and vary the ULSW ε_{Nd} from -15.0 to -14.0 (-15.0, -14.75, -14.5, -14.25 and -14.0).

4.6 Tables

Table 4.1. Water mass end-member compositions used in the *T-S approach* water mass mixing calculations. Water masses include: 'pure' Mediterranean and modified Mediterranean Outflow Water (MOW), North Atlantic Deep Water (NADW), Eastern North Atlantic Deep Water (ENADW), 'pure' Antarctic Intermediate Water and modified Antarctic Intermediate water (AAIW), 'pure' Antarctic Bottom Water and modified Antarctic Bottom Water (AABW), Eastern Antarctic Bottom Water (EAABW), Irminger Sea Water (ISW) and North Atlantic Central Water (NACW). Nd-compositions are taken from the following references: 1. Tachikawa et al., 2004; 2. Lacan and Jeandel, 2005; 3. Jeandel, 1993; 4. Stichel et al., 2012; 5. Piepgras and Wasserburg, 1983; 6. Copard et al., 2011; 7. This study (the Nd-composition of these modified end-members was either measured as part of this study (mod MOW, ENADW, EAABW) or calculated based on the water mass mixing of pure end-members(mod AAIW, mod AABW).

Table 4.2. Water mass end-member compositions used in OMPA to determine water mass fractions for each sample (Jenkins et al., 2014). We note that central waters are defined as an array of properties and are plotted in Figure 5.9. Additionally, Nd-compositions of these end-members are shown and were assigned based on the closest measured Nd data available in the literature or compiled by this study. References are: 1. Piepgras and Wasserburg, 1987; 2. Lacan and Jeandel, 2005; 3. This study. Water masses include: Antarctic Bottom Water (AABW), Denmark Strait Overflow Water (DSOW), Iceland-Scotland Overflow Water (ISOW), Classic Labrador Sea Water (CLSW), Mediterranean Outflow Water (MOW), Upper Labrador Sea Water (ULSW), Upper Circumpolar Deep Water (UCPDW), Antarctic Intermediate Water (AAIW), Irminger Sea Water (ISW), North Atlantic Central Water (NACW), Southwest Atlantic Central Water (SWACW) and Atlantic Equatorial Water (AEW).

Table 4.3. Selected water mass properties for each processed sample in this study including Nd-composition, calculated fractions of each water mass by the *T-S approach* and predicted ε_{Nd} and [Nd] based on water mass mixing of these end-members. Additionally, this table presents calculated ε_{Nd} and [Nd] based on water mass mixing contributions derived by OMPA where available (Jenkins et al., 2014).

Table 4.1. End-member water mass compositions used in T-S approach

	θ	S	SiO_2	[Nd]	ε_{Nd}	Ref.
***'pure'* MOW**	13.00	38.30	11.1	23.05	-9.05	*1*
***mod* MOW**	12.15	36.50	2.5	18.77	-10.30	*7*
NADW	2.25	34.92	14.5	21.35	-13.25	*2*
ENADW	3.39	35.01	29.1	18.60	-11.62	*7*
***'pure'* AAIW**	3.00	34.20	44.6	11.45	-8.00	*3, 4*
***mod* AAIW**	4.75	34.50	39.1	12.40	-8.45	*7*
***'pure'* AABW**	-0.50	34.62	123.0	26.00	-8.50	*3, 4*
***mod* AABW**	0.75	34.73	83.2	24.30	-10.24	*7*
EAABW	1.75	34.88	50.0	23.27	-11.85	*7*
NACW	11.50	35.60	2.5	13.87	-12.00	*5, 6*
ISW	7.11	35.12	6.7	18.72	-13.30	*2*

Table 4.2. End-member water mass compositions used in OMPA calculations

	θ	S	SiO_2	[Nd]	ε_{Nd}	Ref.
AABW	0.18	34.702	116.50	30.10	-11.60	*1*
DSOW	1.29	34.870	7.50	18.71	-10.60	*2*
ISOW	2.55	34.965	11.00	19.41	-11.40	*2*
CLSW	2.95	34.864	9.20	17.33	-13.50	*2*
MOW	12.65	36.629	7.46	18.77	-10.30	*3*
ULSW	3.50	34.800	8.35	21.50	-15.00	*2*
UCPDW	4.28	34.662	31.64	16.20	-12.60	*1*
AAIW	4.37	34.399	30.99	15.90	-11.90	*1*
ISW	7.11	35.118	6.70	18.72	-13.30	*2*
NACW				15.02	-10.60	*3*
SWACW	Array shown in Figure 4.9			17.00	-11.61	*3*
AEW				15.30	-12.60	*1*

Table 4.3. Sample properties with measured and calculated Nd-compositions

Station Info	Samp No	Depth (m)	Sal (psu)	Pot T	Silicate (µmol/kg)	εNd	error	[Nd] (pmol/kg)	MOW	NADW	ENADW	AAIW	AABW	EAABW	ISW	NACW	Calculated [Nd]	Calculated εNd	OMPA derived [Nd]	OMPA derived εNd
USGT10-01	5086	17.8	36.32	20.23	0.49	-10.22	0.36	15.56												
Lat: 38.33	5084	67.5	36.34	17.26	0.58	-10.69	0.31	13.64											18.06	-10.83
Long: -9.66	5080	185.9	36.01	14.30	2.54	-11.43	0.31	16.98											18.43	-10.62
UH	5136	235	35.90	13.59	3.32	-11.38	0.22	16.23											17.42	-10.6
	5078	416.7	35.77	12.33	4.78	-11.78	0.24	17.81											17.98	-10.6
	5077	656.5	36.28	12.69	5.65	-10.78	0.27	17.77											21.3	-10.73
	5523	796.3	36.35	12.69	5.85	-10.69	0.71	18											21.03	-10.68
	5522	953.5	36.41	12.31	6.82	-10.67	0.45	18.46											19.59	-10.64
	5520	1186	36.50	12.15	7.51	-10.28	0.24	18.77	1.00	0	0	0	0	0	0	0	18.77	-10.30	18.84	-10.57
	5518	1481.6	36.27	10.53	10.04	-10.69	0.24	18.55	0.85	0	0.15	0	0	0	0	0	18.74	-10.50	19.01	-11.24
	5516	1776.3	35.42	5.94	16.39	-11.86	0.27	18.44	0.29	0	0.69	0.03	0	0	0	0	18.48	-11.18	19.30	-13.15
	5514	2367.3	35.06	3.53	26.44	-11.59	0.27	18.18	0.05	0	0.74	0	0	0.20	0	0	19.56	-11.61	20.16	-12.10
	5513	2662.3	34.98	2.81	32.59	-11.45	0.22	19.25	0.01	0	0.56	0	0	0.42	0	0	20.58	-11.71	20.96	-11.99
	5512	2809.5	34.95	2.62	35.42	-11.43	0.24	19.92	0.01	0	0.48	0	0	0.51	0	0	20.98	-11.74	21.27	-11.94
USGT10-03	5210	21.7	36.64	22.16	0.29	-10.89	0.34	12.97												
Lat: 35.20	5204	297.9	35.82	13.31	3.71	-11.73	0.36	16.59											17.03	-10.64
Long: -15.99	5202	485.4	35.64	11.90	5.36	-12.38	0.26	17.91											16.79	-10.63
LDEO	5201	603.7	35.61	11.01	7.41	-12.37	0.32	19.14											20.96	-11.35
	5200	766.1	35.73	10.48	9.36	-11.85	0.24	19.32											19.71	-11.31
	5199	865.4	35.81	10.29	9.85	-11.83	0.32	18.97											19.13	-11.31
	5291	986.4	35.92	10.13	10.63	-12.18	0.23	19.55											18.45	-11.25
	5290	1040.7	35.94	9.98	10.82	-11.73	0.36	17.89	0.71	0	0.03	0.26	0	0	0	0	17.12	-10.00	18.37	-11.37
	5288	1337.6	35.75	8.29	12.29	-11.42	0.24	18.95	0.54	0	0.34	0.12	0	0	0	0	17.92	-10.60	19.17	-12.27
	5286	1683.8	35.31	5.47	14.73	-12.15	0.26	18.77	0.23	0	0.71	0.07	0	0	0	0	18.22	-11.17	19.75	-13.54
	5284	2079.3	35.10	3.97	21.08	-12.07	0.36	18.06	0.06	0	0.93	0.01	0	0	0	0	18.57	-11.52	19.16	-12.52
	5282	2474.2	35.00	3.09	28.01	-12.11	0.48	18.94	0.02	0	0.70	0	0	0.28	0	0	19.91	-11.67	20.18	-12.20
	5281	2572.9	34.99	2.94	30.06	-12.53	0.28	23.15	0.01	0	0.64	0	0	0.35	0	0	20.23	-11.69	20.59	-12.05
	5280	2803.3	34.96	2.70	33.37	-11.92	0.23	19.36	0.01	0	0.53	0	0	0.46	0	0	20.77	-11.73	20.90	-12.02
USGT10-05	5317	31.8	37.24	24.33	0.49	-9.91	0.45	12.45												
Lat: 31.00	5319	81.5	36.64	19.84	0.49	-10.08	0.22	12.31												
Long: -22.00	5323	249.7	36.32	16.56	2.05	-10.52	0.22	15.02											15.7	-10.61
UH	5325	546.3	35.67	12.27	5.85	-11.35	0.22	17											15.07	-10.61
	5326	843.2	35.45	9.34	12.97	-11.44	0.31	17.42											19.15	-11.46
	5328	1188.9	35.56	8.07	14.14	-11.52	0.22	17.2	0.48	0	0.19	0.33	0	0	0	0	16.65	-10.13	18.45	-12.17
	5385	1482.6	35.44	6.57	14.93	-11.54	0.22	17.04	0.34	0	0.51	0.16	0	0	0	0	17.70	-10.80	19.84	-13.76
	5386	1778.9	35.22	4.99	15.12	-12.1	0.4	17.02	0.17	0	0.75	0.08	0	0	0	0	18.12	-11.21	18.90	-12.61
	5387	2074.9	35.09	3.99	19.32	-12.1	0.22	17.12	0.06	0	0.91	0.02	0	0	0	0	18.46	-11.48	19.68	-12.36
	5388	2370.5	35.02	3.33	23.91	-11.87	0.22	17.19	0.02	0	0.86	0	0	0.13	0	0	19.19	-11.63	20.93	-11.98
	5390	2961.9	34.95	2.56	33.86	-11.79	0.22	18.8	0	0	0.51	0	0	0.49	0	0	20.89	-11.75	22.01	-11.81
	5393	3848.6	34.91	2.12	43.14	-11.44	0.22	22.28	0	0	0.22	0.01	0	0.78	0	0	22.19	-11.80	22.21	-11.78
	5394	4242.4	34.90	2.03	45.18	-11.58	0.22	26.81	0	0	0.15	0.01	0	0.84	0	0	22.46	-11.80	22.41	-11.76
	5395	4685.9	34.89	1.98	46.65	-11.32	0.22	27.55	0	0	0.12	0.01	0	0.87	0	0	22.59	-11.81	22.51	-11.74
	5396	5029.9	34.89	1.97	46.84	-11.53	0.22	28.5	0	0	0.11	0.01	0	0.88	0	0	22.62	-11.81		
USGT10-07	5490	33.2	36.72	25.65	0.39	-11.59	0.26	20.88												
Lat: 24.00	5492	72.9	36.92	22.80	0.58	-11.67	0.28	16.81												
Long: -22.00	5498	497.4	35.62	12.01	8.29	-11.39	0.26	20.48											18.12	-11.06
LDEO	5499	744.3	35.19	8.65	17.17	-11.48	0.26	20.23											18.93	-11.35

Table 4.3 continued

Station Info	Samp No	Depth (m)	Sal (psu)	Pot T	Silicate (µmol/kg)	εNd	error	[Nd] (pmol/kg)	MOW	NADW	ENADW	AAIW	AABW	EAABW	ISW	NACW	Calculated [Nd]	Calculated εNd	OMPA derived [Nd]	OMPA derived εNd
	5500	991.9	35.18	7.29	19.32	-11.32	0.24	18.56	0.34	0	0	0.66	0	0	0	0	14.55	-9.26	17.31	-11.71
	5501	1189.7	35.27	6.83	18.93	-11.22	0.26	17.73	0.32	0	0.23	0.44	0	0	0	0	15.90	-10.02	18.07	-12.29
	5567	1483.1	35.18	5.31	20.88	-11.93	0.24	17.98	0.19	0	0.60	0.21	0	0	0	0	17.31	-10.87	18.44	-13.08
	5568	1729.7	35.12	4.51	24.3	-11.65	0.32	17.54	0.11	0	0.78	0.11	0	0	0	0	17.95	-11.23	18.14	-13.19
	5569	1975.6	35.05	3.81	26.93	-11.5	0.36	18.14	0.04	0	0.92	0.04	0	0	0	0	18.38	-11.48	19.71	-12.60
	5570	2222.3	35.01	3.39	29.08	-11.62	0.32	18.6	0	0	1.00	0	0	0	0	0	18.60	-11.62	20.06	-12.45
	5570	2222.3	35.01	3.39	29.08	-11.62	0.32	18.6	0	0	0.99	0	0	0	0	0.01	18.56	-11.62		
	5570	2222.3	35.01	3.39	29.08	-11.62	0.32	18.6	0	0	1.00	0	0	0	0	0	18.60	-11.62		
	5572	2715.3	34.96	2.76	34.84	-11.48	0.36	19.78	0	0	0.62	0	0	0.38	0	0	20.39	-11.72	20.94	-12.14
	5574	3207.6	34.93	2.35	40.5	-11.36	0.36	21.65	0	0	0.36	0	0	0.63	0	0	21.55	-11.77	21.68	-11.92
	5576	3779.4	34.90	2.09	45.48	-11.84	0.32	25.5	0	0	0.19	0.01	0	0.80	0	0	22.30	-11.80	22.24	-11.81
	5577	4104.3	34.89	2.00	46.65	-11.95	0.38		0	0	0.13	0.01	0	0.86	0	0	22.54	-11.80	22.40	-11.77
	5578	4586.2	34.89	1.97	47.72	-12.2	0.32	27.63	0	0	0.11	0.01	0	0.88	0	0	22.61	-11.80	22.51	-11.77
USGT10-09	5763	5	35.81	27.97		-12.06	0.36	36.65												
Lat: 17.35	5671	22.4	35.77	27.87	0.59	-12	0.63													
Long: -18.25	5670	52.1	36.09	18.96	3.41	-10.56	1.47													
USC	5669	91.2	35.79	15.50	6.83	-10.86	0.29												16.93	-12.05
	5667	150.3	35.53	13.69	8.49	-11.8	0.25	21.87											17.16	-12.17
	5664	457	35.24	10.36	14.63	-11.23	0.57	24.22											19.85	-11.88
	5663	560.6	35.12	9.24	17.17	-10.78	0.16												18.71	-11.91
	5662	659.5	35.05	8.45	18.74	-11.14	0.53	22.56											19.09	-11.29
	5661	792.5	34.94	7.29	21.66	-11.75	0.61	23.92											17.96	-11.49
	5704	1087.2	34.95	5.82	23.91	-11.74	0.38	22.1	0	0	0.38	0.39	0	0	0	0.23	15.08	-10.69	16.94	-12.38
	5703	1235.5	34.97	5.17	23.91	-11.56	0.23	21	0	0	0.55	0.28	0	0	0	0.17	16.07	-11.00	17.65	-12.88
	5702	1383.6	34.99	4.72	23.62	-11.37	0.32	27.93	0	0	0.67	0.20	0	0	0	0.13	16.77	-11.20	18.00	-13.16
	5701	1531.6	34.99	4.25	23.42	-11.7	0.35	21.32	0	0	0.78	0.14	0	0	0	0.08	17.34	-11.33	18.29	-13.43
	5700	1679.6	34.98	3.93	23.91	-11.8	0.47	20.21	0	0	0.84	0.11	0	0	0	0.05	17.71	-11.40	18.38	-13.56
	5699	1877.1	34.98	3.61	25.08	-12.1	0.26	20.82	0	0	0.91	0.08	0	0	0	0.01	18.04	-11.45	19.50	-12.72
	5698	2074.6	34.97	3.33	27.13	-11.63	0.27	21.29	0	0	0.86	0.06	0	0.08	0	0	18.63	-11.52	19.65	-12.74
	5697	2271.9	34.96	3.08	29.57	-12.26	0.26	22.12	0	0	0.73	0.04	0	0.22	0	0	19.38	-11.60	20.01	-12.60
	5696	2469.2	34.95	2.88	32.11	-12.12	0.44		0	0	0.63	0.03	0	0.34	0	0	19.99	-11.65	20.55	-12.33
	5695	2666.4	34.94	2.72	34.45	-11.77	0.44		0	0	0.55	0.02	0	0.43	0	0	20.46	-11.69	20.85	-12.25
	5744	2928.8	34.93	2.49	40.3	-12.65	0.57	23.08	0	0	0.42	0.02	0	0.56	0	0	21.12	-11.73	21.81	-11.91
	5743	2958	34.93	2.46	40.21	-12.11	0.69		0	0	0.41	0.02	0	0.58	0	0	21.20	-11.74	21.89	-11.88
	5742	2983	34.93	2.45	42.84	-12.52	0.63	24.78	0	0	0.39	0.02	0	0.59	0	0	21.25	-11.74	22.20	-11.82
	5741	2997.3	34.93	2.44	43.62	-13.37	0.71	25.41	0	0	0.39	0.02	0	0.59	0	0	21.26	-11.74	22.30	-11.80
	5740	3011.7	34.93	2.44	43.23	-12.36	0.32	25.18	0	0	0.39	0.02	0	0.59	0	0	21.26	-11.74	22.27	-11.80
	5693	3019.3	34.93	2.45	41.77	-12.38	0.41		0	0	0.40	0.02	0	0.59	0	0	21.25	-11.74	21.89	-11.99
USGT10-10	5802	5.1	36.22	27.35		-12.36	0.22	28.39												
Lat: 17.36	5777	27.2	36.28	26.15	0.58	-12.03	0.22	25.42												
Long: -20.83	5776	51.8	35.83	17.93	3.8	-12.84	0.22	17.07												
UH	5775	86.6	35.67	15.21	6.93	-11.92	0.22	17.99											15.79	-12.29
	5774	101	35.58	14.49	7.41	-11.62	0.22	18.23											15.43	-12.31
	5773	140.7	35.58	13.84	8.29	-11.73	0.22	18.93											17.43	-12.08
	5772	185	35.41	12.91	9.17	-11.43	0.22	18.55											16.45	-12.23
	5771	234.5	35.44	12.66	9.46	-11.16	0.27	19.62											17.07	-11.98
	5770	288.4	35.38	12.04	10.54	-11.15	0.22	21.24											17.61	-11.94
	5769	416.6	35.28	10.78	13.27	-11.09	0.22	22.31											18.8	-11.87

Table 4.3 continued

Station Info	Samp No	Depth (m)	Sal (psu)	Pot T	Silicate (µmol/kg)	εNd	error	[Nd] (pmol/kg)	MOW	NADW	ENADW	AAIW	AABW	EAABW	ISW	NACW	*Calculated* [Nd]	*Calculated* εNd	*OMPA derived* [Nd]	*OMPA derived* εNd
	5768	495.9	35.18	9.89	15.61	-11.5	0.94	22.73											18.94	-11.92
	5767	659.2	35.02	8.24	19.32	-11.57	0.22	22.07											18.94	-11.32
	5766	792.2	34.92	7.12	22.35	-11.52	0.4	21.31											17.77	-11.49
	5859	1089.5	34.95	5.78	23.13	-11.27	0.22	18.86	0	0	0.39	0.38	0	0	0	0.23	15.17	-10.73	17.40	-12.34
	5858	1237.9	34.99	5.35	22.83	-11.43	0.22	18.82	0	0	0.53	0.27	0	0	0	0.20	16.00	-11.02	17.77	-12.89
	5856	1731	35.00	3.92	24.01	-11.2	0.53	18.37	0	0	0.86	0.09	0	0	0	0.05	17.83	-11.44	18.38	-13.55
	5855	1977.9	34.98	3.50	25.86	-11.58	0.22	18.83	0	0	0.93	0.06	0	0	0	0.00	18.20	-11.49	19.56	-12.73
	5854	2224.5	34.97	3.18	28.4	-11.55	0.22	19.01	0	0	0.80	0.04	0	0.16	0	0	19.09	-11.58	19.94	-12.55
	5852	2717.5	34.94	2.69	34.25	-11.56	0.22	20.25	0	0	0.54	0.02	0	0.44	0	0	20.54	-11.70	20.92	-12.19
	5851	2964.8	34.93	2.50	37.57	-11.39	0.36	23	0	0	0.43	0.01	0	0.55	0	0	21.10	-11.73	21.30	-12.06
	5850	3260.7	34.92	2.30	42.74	-11.8	0.22	23.51	0	0	0.31	0.01	0	0.68	0	0	21.69	-11.76	21.97	-11.94
	5849	3324.3	34.91	2.22	45.48	-11.79	0.31	24.47	0	0	0.26	0.01	0	0.73	0	0	21.91	-11.77	22.22	-11.92
USGT10-11	5871	5	36.22	27.35	0.58	-12.09	0.32	24.42												
Lat: 17.35	5907	31.5	36.20	27.10	0.39	-12.71	0.3	25.6												
Long: -22.78	5906	65	36.74	21.43	1.07	-11.25	0.36	15.95												
LDEO	5905	86.7	36.44	18.79	2.83	-10.99	0.36	18.35												
	5904	136	36.12	16.11	5.07	-10.63	0.46	19.33											17.89	-11.33
	5903	180.3	35.93	14.86	6.05	-11.23	0.36	21.12											17.98	-11.33
	5902	200.3	35.88	14.59	6.44	-11.55	0.36	21.04											18.09	-11.35
	5901	249.5	35.70	13.40	8.1	-11.25	0.36	21.89											18.61	-11.47
	5900	298.6	35.58	12.64	9.36	-11.58	0.36	22.94											18.95	-11.53
	5899	347.7	35.50	11.93	10.34	-11.25	0.24	22.51											18.79	-11.56
	5898	446.9	35.31	10.53	13.27	-11.27	0.36	23.36											18.7	-11.66
	5897	594.8	35.11	8.78	17.27	-11.67	0.24	21.9											19.39	-11.3
	5896	791.8	34.94	7.01	21.66	-11.18	0.23	21.14											17.66	-11.62
	5919	891.1	34.93	6.48	22.93	-11.67	0.32	20											16.99	-11.73
	5918	1088.4	34.97	5.72	23.23	-11.31	0.22	20.02	0	0	0.42	0.35	0	0	0	0.23	15.34	-10.80	17.14	-12.58
	5917	1286.3	35.03	5.22	22.64	-11.62	0.32	18.56	0	0	0.62	0.18	0	0	0	0.19	16.54	-11.25	17.94	-12.98
	5916	1482.6	35.02	4.51	23.03	-11.48	0.28	19.75	0	0	0.77	0.11	0	0	0	0.12	17.35	-11.40	18.26	-13.33
	5915	1729.8	35.00	3.92	23.81	-11.65	0.32	19.15	0	0	0.87	0.08	0	0	0	0.05	17.86	-11.46	18.42	-13.57
	5914	1976.5	34.98	3.47	26.45	-11.66	0.36	19.1	0	0	0.94	0.06	0	0	0	0.00	18.26	-11.50	19.59	-12.72
	5913	2223.7	34.96	3.13	28.3	-11.99	0.32	19.52	0	0	0.77	0.04	0	0.19	0	0	19.24	-11.59	19.85	-12.63
	5912	2470	34.95	2.90	31.23	-12.46	0.36	20.36	0	0	0.65	0.03	0	0.32	0	0	19.93	-11.65	20.36	-12.40
	5911	2715.8	34.94	2.69	33.57	-12.04	0.32	21.19	0	0	0.54	0.02	0	0.44	0	0	20.55	-11.70	20.76	-12.20
	5910	2962.8	34.93	2.51	36.11	-11.62	0.36	22.01	0	0	0.44	0.01	0	0.55	0	0	21.08	-11.74	21.11	-12.06
	5909	3160.3	34.92	2.37	39.52	-11.65	0.24	23.44	0	0	0.36	0.01	0	0.63	0	0	21.47	-11.76	21.48	-11.99
	5908	3336.5	34.92	2.28	41.67	-11.15	0.3	23.85	0	0	0.31	0.01	0	0.68	0	0	21.73	-11.77	21.74	-11.94
USGT10-12	6000	5.1	36.93	26.79		-11.36	0.36	22.45												
Lat: 17.40	6012	31.8	36.92	26.66	0.39	-10.94	0.3	17.6												
Long: -24.50	6011	50.4	36.90	23.99	0.49	-9.82	0.36	14.4												
USC	6010	71.9	36.81	21.97	0.88	-9.88	0.27	14.65												
	6009	91.6	36.73	20.58	1.46	-10.2	0.34	15.01												
	6008	136.5	36.64	18.63	1.95	-9.51	0.28	18.42											16.61	-10.66
	6007	185.4	36.15	16.04	4.88	-10.34	0.2	20.28											18.1	-11.21
	6006	235	35.86	14.45	6.83	-11.11	0.1	20.8											18.53	-11.39
	6005	284.7	35.66	13.20	8.68	-11.36	0.13	22.32											19.13	-11.54
	6004	348.7	35.48	11.98	10.63	-11.44	0.16	22.35											19.2	-11.65
	6003	447.3	35.29	10.51	13.66	-11.5	0.2	22.87											19.06	-11.74

Table 4.3 continued

Station Info	Samp No	Depth (m)	Sal (psu)	Pot T	Silicate (µmol/kg)	εNd	error	[Nd] (pmol/kg)	MOW	NADW	ENADW	AAIW	AABW	EAABW	ISW	NACW	*Calculated* [Nd]	*Calculated* εNd	*OMPA derived* [Nd]	*OMPA derived* εNd
	6002	595.2	35.05	8.53	18.25	-11.45	0.1	21.21											19.24	-11.32
	6001	792.6	34.93	6.98	22.54	-11.15	0.42	21.01											17.56	-11.53
	6069	891.2	34.92	6.38	22.64	-13.01	0.23	30.02											16.96	-11.82
	6068	1068.7	34.96	5.83	22.74	-12.16	0.28	23.15	0	0	0.39	0.37	0	0	0	0.24	15.19	-10.75	17.30	-12.43
	6067	1266.1	35.01	5.18	22.25	-11	0.23	18.82	0	0	0.61	0.21	0	0	0	0.19	16.43	-11.18	18.02	-13.04
	6066	1483.3	35.02	4.56	22.35	-10.49	0.2	18.11	0	0	0.75	0.13	0	0	0	0.12	17.22	-11.37	18.36	-13.36
	6065	1729.5	35.00	3.94	23.52	-10.38	0.23	19.84	0	0	0.86	0.08	0	0	0	0.05	17.84	-11.46	18.48	-13.59
	6064	1976.1	34.98	3.51	25.37	-11.41	0.3	20.92	0	0	0.93	0.07	0	0	0	0	18.18	-11.48	19.50	-12.74
	6063	2222.8	34.97	3.20	27.42	-11.35	0.3	19.61	0	0	0.80	0.05	0	0.15	0	0	19.03	-11.57	19.79	-12.62
	6062	2469.5	34.96	2.95	29.57	-12.51	0.14	19.94	0	0	0.68	0.03	0	0.29	0	0	19.77	-11.64	20.21	-12.41
	6061	2715.8	34.95	2.73	32.5	-11.33	0.23	20.13	0	0	0.56	0.02	0	0.42	0	0	20.44	-11.69	20.69	-12.21
	6060	2962.8	34.94	2.55	35.52	-10.71	0.2	21.6	0	0	0.46	0.01	0	0.52	0	0	20.97	-11.73	21.13	-12.05
	6059	3209.4	34.92	2.37	38.84	-10.58	0.4	21.77	0	0	0.36	0.01	0	0.63	0	0	21.48	-11.76	21.50	-11.95
	6058	3531.3	34.91	2.25	42.16	-10.53	0.36	22.52	0	0	0.29	0.01	0	0.70	0	0	21.84	-11.78	21.88	-11.89
USGT11-01	6192	1.5	35.05	19.56		-11.03	0.24	19.31												
Lat: 39.70	6237	30.2	34.98	19.38	0.88	-11.25	0.22	19.26												
Long: -69.83	6235	89.2	36.04	15.80	5.18	-10.53	0.24	16.77											17.07	-11.41
UH	6234	109.9	35.86	14.38	6.15	-10.66	0.24	16.72											17.11	-11.27
	6233	135.4	35.73	13.51	6.84	-10.84	0.27	17.04											16.79	-11.25
	6230	285.9	35.29	10.00	12.51	-11.01	0.24	17.16											16.32	-11.34
	6229	324.8	35.18	8.95	14.27	-11.23	0.24	16.99											19.63	-11.55
	6228	419.5	35.12	7.65	14.07	-12.12	0.24	17.55											18.48	-12.19
	6227	474.7	35.09	6.84	13.68	-12.64	0.22	17.91											18.08	-12.68
	6226	523.9	35.05	6.11	13.09	-13.26	0.24	18.51											18.9	-13.2
	6147	599.7	35.01	5.29	12.02	-14.02	0.24	19.24											19.67	-13.87
	6146	663.7	34.98	4.91	11.34	-14.86	0.36	19.84											20.11	-14.12
	6144	964	34.96	4.35	10.85	-14.43	0.22	19.19	0	0.53	0	0.09	0	0	0.39	0	19.55	-13.00	20.73	-14.43
	6142	1196.8	34.98	4.22	11.53	-13.82	0.24	18.73	0	0.58	0	0.04	0	0	0.39	0	19.99	-13.15	20.69	-14.43
	6140	1500.7	34.95	3.82	11.92	-13.93	0.24	18.32	0	0.65	0	0.06	0	0	0.29	0	20.07	-13.09	20.82	-14.59
	6139	1649.7	34.95	3.76	12.12	-13.78	0.24	18.29	0	0.66	0	0.05	0	0	0.28	0	20.12	-13.10	20.79	-14.60
	6137	1999	34.95	3.50	13.19	-13.78	0.24	17.98	0	0.72	0	0.05	0	0	0.23	0	20.33	-13.13	21.30	-14.58
	6161	2029.9	34.94	3.22	14.66	-13.35	0.24	17.78	0	0.78	0	0.04	0	0	0.18	0	20.56	-13.16	18.19	-13.03
	6160	2044.2	34.94	3.20	14.76	-13.47	0.45	17.89	0	0.79	0	0.03	0	0	0.18	0	20.57	-13.16	18.29	-12.95
	6136	2048.4	34.95	3.45	13.58	-13.87	0.27	17.97	0	0.73	0	0.04	0	0	0.22	0	20.38	-13.14	21.70	-14.54
	6159	2058.9	34.94	3.19	14.85	-13.37	0.24	17.74	0	0.79	0	0.03	0	0	0.18	0	20.58	-13.16	18.25	-12.99
	6158	2068.4	34.94	3.19	14.76	-13.33	0.22	17.57	0	0.79	0	0.03	0	0	0.17	0	20.59	-13.16	18.17	-13.01
	6156	2077.2	34.94	3.18	15.15	-13.33	0.31	17.74	0	0.79	0	0.03	0	0	0.17	0	20.59	-13.16	18.45	-12.81
USGT11-02	6330	35.6	35.42	20.72	0.78	-10.23	0.18													
Lat: 39.35	6328	69.6	36.10	17.24	3.8	-9.95	0.18												15.25	-11.51
Long: -69.55	6327	99.3	35.91	14.88	5.75	-10.37	0.18													
LDEO	6324	235.2	35.31	10.49	12.68	-10.2	0.18												17.52	-11.58
	6322	323.9	35.13	8.01	14.34	-11.62	0.18												18.79	-11.98
	6321	420.2	35.06	6.35	13.17	-13.17	0.18												18.4	-13.17
	6344	524	35.04	5.46	12.3	-13.44	0.18												19.72	-13.67
	6285	657.8	35.02	4.92	11.51	-13.71	0.18												20.29	-14.09
	6284	824	35.00	4.46	11.22	-13.64	0.18												20.63	-14.35
	6283	962.8	34.97	4.16	11.03	-13.81	0.18		0	0.58	0	0.05	0	0	0.37	0	19.94	-13.12	20.82	-14.50
	6281	1347.8	34.96	3.76	12.1	-13.71	0.18		0	0.67	0	0.04	0	0	0.29	0	20.22	-13.14	20.82	-14.60

Table 4.3 continued

Station Info	Samp No	Depth (m)	Sal (psu)	Pot T	Silicate (µmol/kg)	εNd	error	[Nd] (pmol/kg)	MOW	NADW	ENADW	AAIW	AABW	EAABW	ISW	NACW	*Calculated* [Nd]	*Calculated* εNd	*OMPA derived* [Nd]	*OMPA derived* εNd
	6280	1497.3	34.96	3.60	12.78	-13.52	0.18		0	0.70	0	0.04	0	0	0.26	0	20.34	-13.15	20.76	-14.62
	6279	1645.9	34.95	3.45	13.17	-13.44	0.18		0	0.73	0	0.04	0	0	0.23	0	20.41	-13.15	17.93	-13.16
	6277	1993.4	34.95	3.18	15.42	-13.08	0.18		0	0.80	0	0.02	0	0	0.18	0	20.70	-13.20	18.45	-12.83
	6276	2196.3	34.94	2.99	16.69	-12.67	0.18		0	0.84	0	0.02	0	0	0.14	0	20.82	-13.21	18.75	-12.61
	6275	2452.2	34.93	2.74	17.08	-12.77	0.18		0	0.89	0	0.02	0	0	0.09	0	20.92	-13.19	18.95	-12.33
USGT11-03	6389	28.4	36.17	24.51	0.68	-8.91	0.33	18.98												
Lat: 38.67	6388	61.2	36.34	24.14	0.19	-9.37	0.14	15.34											17.51	-10.65
Long: -69.11	6387	86.4	36.68	23.57	0.68	-9.44	0.18	15.82											16.99	-10.65
USC	6386	108.8	36.75	21.64	1.07	-9.84	0.11	15.26											15.14	-10.72
	6385	135.6	36.76	20.26	0.78	-9.93	0.32	14.76											18.4	-12.38
	6384	186.5	36.64	18.91	0.29	-9.72	0.25	14.42												
	6383	234.7	36.56	18.18	0.68	-10.06	0.15	13.14												
	6381	417.8	36.02	15.07	3.51	-10.83	0.21	13.14												
	6379	668.5	35.11	7.45	13.27	-12.54	0.29	17.33												
	6436	962.8	35.00	4.71	11.71	-13.56	0.8	18.54	0	0.48	0	0.03	0	0	0.49	0	19.76	-13.17	20.39	-14.20
	6435	1077.1	34.99	4.43	11.51	-11.14	0.94	16.02	0	0.54	0	0.03	0	0	0.43	0	19.92	-13.17	20.59	-14.34
	6434	1201	34.98	4.18	11.42	-13.15	0.96	18.17	0	0.58	0	0.04	0	0	0.37	0	19.97	-13.14	20.72	-14.46
	6432	1500	34.97	3.83	12.2	-12.46	1.34	18.13	0	0.66	0	0.04	0	0	0.31	0	20.22	-13.16	20.76	-14.56
	6430	2096.9	34.95	3.23	14.74	-12.73	0.14	17.45	0	0.78	0	0.03	0	0	0.19	0	20.60	-13.18	18.30	-12.91
	6429	2402.1	34.94	2.91	17.47	-12.37	0.45	15.56	0	0.86	0	0.01	0	0	0.13	0	20.90	-13.22	18.93	-12.47
	6427	2898.2	34.92	2.38	19.71	-12.79	0.2	17.97	0	0.96	0	0.02	0	0	0.02	0	21.15	-13.20	19.57	-11.87
	6426	3109.2	34.91	2.15	20.79	-13.4	0.24	21.6	0	0.93	0	0	0.07	0	0	0	21.53	-13.00	19.91	-11.62
	6425	3265.3	34.89	1.95	20.3	-13.1	0.24	19.56	0	0.86	0	0	0.14	0	0	0	21.76	-12.78	19.86	-11.45
USGT11-04	6480	39.4	36.13	23.53	0.39	-9.7	0.23													
Lat: 38.33	6478	90.8	36.14	23.55	0.29	-9.7	0.48													
Long: -68.86	6474	236.7	36.62	18.75	0.58	-9.75	0.24	14.49											16.94	-10.65
UH	6470	621.7	35.72	13.13	6.14	-10.88	0.27	17.52											15.29	-10.94
	6469	797.4	35.22	9.15	13.37	-10.89	0.24	20.93											19.79	-11.56
	6500	960.5	35.07	6.13	12.98	-13.1	0.26		0	0.19	0	0.02	0	0	0.79	0	19.09	-13.22	18.71	-13.33
	6498	1191.7	34.99	4.64	11.71	-14	0.23		0	0.48	0	0.05	0	0	0.46	0	19.65	-13.11	20.42	-14.23
	6497	1488.5	34.97	4.16	11.81	-13.8	0.23		0	0.59	0	0.04	0	0	0.37	0	19.98	-13.13	20.67	-14.45
	6496	1790.6	34.97	3.84	12.49	-14.1	0.23		0	0.66	0	0.03	0	0	0.31	0	20.23	-13.16	20.71	-14.54
	6494	2394.3	34.94	3.23	14.83	-13.5	0.23		0	0.78	0	0.03	0	0	0.18	0	20.58	-13.17	18.21	-13.02
	6493	2697.6	34.94	2.98	17.08	-13	0.23		0	0.84	0	0.02	0	0	0.14	0	20.82	-13.21	18.70	-12.63
	6491	3290.7	34.92	2.48	18.83	-12.5	0.23		0	0.94	0	0.02	0	0	0.04	0	21.09	-13.20	19.25	-12.02
	6490	3672.3	34.89	1.87	31.52	-13	0.32		0	0.83	0	0	0.17	0	0	0	21.86	-12.67	21.56	-11.35
	6489	3770.6	34.88	1.85	33.86	-12.8	0.23		0	0.81	0	0	0.19	0	0	0	21.90	-12.63	22.01	-11.38
USGT11-06	6663	39.6	36.00	23.39	0.59	-9.45	0.18													
Lat: 37.59	6662	64.6	36.03	23.40	0.59	-9.39	0.18													
Long: -68.46	6661	89.6	36.07	23.44	0.59	-9.61	0.24													
LDEO	6660	111.1	36.08	23.43	0.59	-9.42	0.18													
	6659	139.6	36.16	20.48	1.75	-10.48	0.24													
	6658	160	36.37	19.79	1.95	-10.13	0.18													
	6657	232.9	36.05	16.04	4.1	-10.49	0.24												15.15	-11.32
	6655	474.2	35.30	10.16	12.59	-10.99	0.24												16.88	-11.44
	6654	664.2	35.08	6.62	13.27	-13.71	0.24												18.1	-12.99
	6653	960.9	35.02	4.83	11.51	-12.77	0.24		0	0.46	0	0.01	0	0	0.53	0	19.88	-13.25	20.37	-14.15

Table 4.3 continued

Station Info	Samp No	Depth (m)	Sal (psu)	Pot T	Silicate (µmol/kg)	εNd	error	[Nd] (pmol/kg)	MOW	NADW	ENADW	AAIW	AABW	EAABW	ISW	NACW	*Calculated* [Nd]	*Calculated* εNd	*OMPA derived* [Nd]	*OMPA derived* εNd
	6652	1191.8	34.99	4.29	11.61	-13.75	0.18		0	0.56	0	0.03	0	0	0.40	0	20.00	-13.17	20.63	-14.40
	6595	1503.4	34.97	3.80	12.39	-13.49	0.18		0	0.67	0	0.02	0	0	0.31	0	20.33	-13.19	20.74	-14.56
	6594	1797.9	34.96	3.50	13.47	-13.28	0.18		0	0.73	0	0.03	0	0	0.24	0	20.48	-13.19	17.97	-13.14
	6593	2092.1	34.95	3.27	15.32	-13.14	0.24		0	0.78	0	0.01	0	0	0.20	0	20.69	-13.22	18.37	-12.91
	6592	2385.6	34.95	2.99	17.66	-12.82	0.18		0	0.84	0	0.01	0	0	0.15	0	20.90	-13.24	18.86	-12.56
	6590	2989.4	34.92	2.44	21.76	-12.35	0.18		0	0.96	0	0.01	0	0	0.04	0	21.18	-13.23	19.77	-11.91
	6588	3590.3	34.90	2.00	26.74	-11.95	0.24		0	0.88	0	0	0.12	0	0	0	21.69	-12.86	20.51	-11.54
	6586	4191.1	34.88	1.84	34.06	-12.58	0.18		0	0.82	0	0	0.18	0	0	0	21.89	-12.63	21.30	-11.51
	6585	4423.1	34.88	1.81	36.21	-12.77	0.18		0	0.80	0	0	0.20	0	0	0	21.95	-12.57	21.65	-11.48
	6584	4517.1	34.88	1.79	37.48	-12.83	0.24		0	0.79	0	0	0.21	0	0	0	21.98	-12.54	21.91	-11.46
USGT11-08	6722	31.3	36.35	23.07	0.39	-8.8	0.28	13.68												
Lat: 35.42	6721	68	36.35	23.06	0.39	-9.29	0.33	14.32												
Long: -66.52	6718	186.3	36.62	18.65	0.88	-10.06	0.24	13.48											16.49	-10.60
USC	6716	291.5	36.59	18.08	0.97	-9.73	0.38	13.51											16.31	-10.63
	6714	550.0	36.17	15.90	2.83	-10.29	0.46	17.17											15.09	-10.67
	6713	800.2	35.34	10.33	11.22	-11.47	0.19	16.6											15.77	-11.24
	6712	1001.4	35.06	6.12	12.88	-13.45	0.16	16.89	0	0.19	0	0.03	0	0	0.78	0	19.02	-13.19	18.76	-13.34
	6711	1198.8	35.01	4.83	11.71	-13.61	0.19	16.38	0	0.46	0	0.02	0	0	0.52	0	19.80	-13.21	20.33	-14.12
	6779	1495.7	34.98	4.20	11.32	-13.39	0.26	17.03	0	0.59	0	0.03	0	0	0.39	0	20.08	-13.18	20.74	-14.46
	6778	1793.1	34.97	3.82	12.2	-13.27	0.21	17.94	0	0.66	0	0.03	0	0	0.31	0	20.30	-13.19	20.78	-14.57
	6777	2091.9	34.96	3.48	13.95	-13.14	0.23	18.14	0	0.74	0	0.02	0	0	0.24	0	20.53	-13.20	18.05	-13.13
	6776	2391.1	34.95	3.09	16.79	-12.8	0.1		0	0.82	0	0.01	0	0	0.17	0	20.81	-13.23	18.50	-12.77
	6775	2688.2	34.95	2.87	19.42	-12.36	0.22	16.63	0	0.87	0	0	0	0	0.13	0	21.01	-13.25	19.04	-12.42
	6772	3592.3	34.90	2.09	25.67	-12.35	0.18	20.88	0	0.92	0	0	0.08	0	0	0	21.59	-12.97	20.42	-11.59
	6770	4232.5	34.89	1.90	31.13	-12.5	0.17	24.91	0	0.84	0	0	0.16	0	0	0	21.81	-12.73	21.04	-11.49
	6769	4556.1	34.88	1.84	34.55	-12.8	0.29	25.63	0	0.81	0	0	0.19	0	0	0	21.90	-12.62	21.46	-11.48
	6768	4880.2	34.88	1.76	11.71	-13.13	0.44	21.94	0	0.77	0	0	0.23	0	0	0	22.04	-12.48		
USGT11-10	6825	41.8	36.55	24.13	0.19	-9.53	0.22													
Lat: 31.75	6824	75.7	36.60	24.17	0.1	-9.39	0.22													
Long: -64.17	6823	89.1	36.66	22.10	0	-9.64	0.22													
LDEO	6822	109.7	36.72	20.53	0.49	-9.98	0.38	13.71												
	6821	182.4	36.59	18.45	0.49	-10.03	0.38												17.33	-10.67
	6820	233.3	36.59	18.20	0.78	-9.8	0.24												16.69	-10.62
	6819	281.4	36.58	18.02	0.88	-10.11	0.24												16.57	-10.61
	6817	497.1	36.32	16.65	2.05	-10.63	0.24												15.5	-10.63
	6816	796.9	35.36	10.43	11.32	-11.32	0.38	17.21											16.34	-11.28
	6815	969	35.08	6.67	13.47	-13.03	0.22	18.07	0	0.07	0	0.03	0	0	0.89	0	18.69	-13.18	18.04	-12.95
	6814	1197.3	35.03	4.98	11.81	-13.55	0.22	18.33	0	0.43	0	0	0	0	0.57	0	19.85	-13.28	20.18	-14.06
	6845	1492.8	34.98	4.11	12	-13.63	0.22	17.77	0	0.61	0	0.02	0	0	0.37	0	20.18	-13.20	20.66	-14.45
	6844	1794	34.98	3.70	13.47	-13.5	0.22	17.08	0	0.70	0	0.01	0	0	0.30	0	20.52	-13.25	20.59	-14.52
	6843	2094	34.98	3.44	16.49	-13.03	0.22	16.8	0	0.70	0	0	0	0	0.30	0	20.56	-13.26	18.40	-12.98
	6842	2289.4	34.97	3.22	18.93	-12.75	0.38	16.94	0	0.74	0	0	0	0	0.26	0	20.66	-13.26		
	6840	2990.2	34.92	2.38	23.13	-12.81	0.38	20.29	0	0.97	0	0.01	0	0	0.02	0	21.23	-13.23	19.86	-11.87
	6838	3584	34.90	1.97	29.18	-12.52	0.22	25.18	0	0.87	0	0	0.13	0	0	0	21.72	-12.82	20.70	-11.56
	6836	4178.9	34.88	1.83	35.33	-12.72	0.22	28.73	0	0.81	0	0	0.19	0	0	0	21.92	-12.61	21.46	-11.51
	6835	4419.3	34.88	1.81	36.89	-12.65	0.38	28.87	0	0.80	0	0	0.20	0	0	0	21.95	-12.57	21.62	-11.51
	6920	4431.4	34.88	1.81	36.69	-12.84	0.38		0	0.80	0	0	0.20	0	0	0	21.95	-12.57	21.64	-11.50
	6919	4461.6	34.88	1.81	36.4	-12.48	0.24		0	0.79	0	0	0.21	0	0	0	21.95	-12.57	21.66	-11.49

Table 4.3 continued

Station Info	Samp No	Depth (m)	Sal (psu)	Pot T	Silicate (µmol/kg)	εNd	error	[Nd] (pmol/kg)	MOW	NADW	ENADW	AAIW	AABW	EAABW	ISW	NACW	Calculated [Nd]	Calculated εNd	OMPA derived [Nd]	OMPA derived εNd
	6918	4493	34.88	1.81	36.79	-12.35	0.24		0	0.79	0	0	0.21	0	0	0	21.96	-12.56	21.62	-11.51
	6917	4511	34.88	1.81	36.89	-12.76	0.24	29.5	0	0.79	0	0	0.21	0	0	0	21.96	-12.56	21.68	-11.49
	6834	4522.5	34.88	1.81	37.18	-12.58	0.22	28.97	0	0.79	0	0	0.21	0	0	0	21.96	-12.56	21.75	-11.49
	6916	4530.9	34.88	1.81	36.99	-12.94	0.24		0	0.79	0	0	0.21	0	0	0	21.96	-12.56	21.78	-11.48
	6915	4550.4	34.88	1.81	37.18	-12.79	0.24		0	0.79	0	0	0.21	0	0	0	21.96	-12.56	21.63	-11.52
USGT11-12	7119	1.1	36.75	24.74		-9.7	0.16													
Lat: 29.7	7040	40	36.98	24.84	0.19	-9.9	0.3													
Long: -56.82	7039	101.2	36.71	19.82	0.19	-9.7	0.26													
UH	7037	233.7	36.55	18.00	0.88	-9.4	0.26												16.6	-10.64
	7035	421.3	36.37	16.86	1.66	-10	0.26												16.08	-10.64
	7033	995	35.12	6.76	14.25	-12.3	0.26		0	0.36	0	0.21	0	0	0	0.43	16.24	-12.02	18.00	-12.83
	7032	1196.1	35.11	5.61	13.17	-12.6	0.26		0	0.57	0	0.09	0	0	0	0.34	18.03	-12.64	19.70	-13.54
	7031	1496.6	35.05	4.50	12.59	-13.1	0.23		0	0.72	0	0.06	0	0	0	0.23	19.14	-12.87	20.40	-14.22
	7030	1794	35.04	4.01	15.32	-12.5	0.26		0	0.80	0	0.02	0	0	0	0.19	19.79	-13.03	20.13	-14.23
	7061	2090.5	35.01	3.58	19.03	-12.3	0.25		0	0.85	0	0.01	0	0	0	0.14	20.22	-13.10	18.74	-12.81
	7060	2390.7	34.98	3.17	22.93	-12	0.14		0	0.90	0	0.01	0	0	0	0.10	20.56	-13.15	19.38	-12.50
	7059	2691.2	34.96	2.90	26.64	-11.9	0.15		0	0.93	0	0.01	0	0	0	0.07	20.79	-13.18	20.01	-12.26
	7058	2988.1	34.95	2.65	28.01	-12.1	0.14		0	0.95	0	0.01	0	0	0	0.04	20.98	-13.20	20.37	-12.05
	7056	3582.4	34.91	2.19	29.37	-12	0.14		0	0.96	0	0	0.04	0	0	0	21.46	-13.12	20.76	-11.68
	7054	4280.4	34.89	1.87	39.43	-12.2	0.14		0	0.82	0	0	0.18	0	0	0	21.88	-12.64	21.98	-11.55
	7052	5073	34.86	1.61	51.53	-12.1	0.31		0	0.66	0	0	0.34	0	0	0	22.35	-12.14	23.22	-11.56
	7051	5436.2	34.85	1.59	52.6	-11.9	0.23		0	0.65	0	0	0.35	0	0	0	22.39	-12.10	23.41	-11.55
	7050	5588.1	34.85	1.59	53.19	-11.8	0.23		0	0.65	0	0	0.35	0	0	0	22.39	-12.10	23.47	-11.56
USGT11-14	7315	1	36.99	25.50		-8.37	1.58													
Lat: 27.58	7244	40.1	36.91	25.35	0.39	-10.51	0.24												16.81	-10.6
Long: -49.63	7243	69.4	37.02	23.42	0.19	-10.15	0.42												16.77	-10.63
USC	7242	99	37.04	21.86	0.1	-10.42	0.14												16.42	-10.66
	7241	113.8	36.95	21.14	0.1	-10.46	0.45												15.31	-10.88
	7240	133.7	36.83	20.28	0.1	-10.12	0.26												19.85	-11.64
	7239	183.8	36.68	18.88	0.58	-9.9	0.24												16.81	-10.6
	7238	233.6	36.57	18.10	0.78	-10.09	0.19												16.77	-10.63
	7236	428.6	36.21	15.99	2.14	-10.77	0.32												16.42	-10.66
	7235	646.9	35.59	12.00	7.22	-11.53	0.16												15.31	-10.88
	7234	773	35.28	9.27	12.1	-11.22	0.24												19.85	-11.64
	7305	965.2	35.12	6.93	15.61	-11.77	0.29		0	0.32	0	0.24	0	0	0	0.44	15.93	-11.89	17.79	-12.48
	7233	1196.1	35.13	5.79	14.44	-12.2	0.22		0	0.56	0	0.08	0	0	0	0.36	17.93	-12.63	19.38	-13.33
	7304	1447.9	35.14	5.10	14.34	-12.56	0.2		0	0.68	0	0	0	0	0	0.32	18.94	-12.96	19.81	-13.78
	7303	1793.8	35.05	3.92	17.95	-12.01	0.26		0	0.81	0	0	0	0	0	0.19	19.93	-13.08	18.62	-12.84
	7301	2394.4	34.97	3.02	25.57	-12.01	0.3		0	0.91	0	0.01	0	0	0	0.08	20.69	-13.17	19.73	-12.39
	7300	2696.1	34.95	2.77	29.08	-11.88	0.6		0	0.94	0	0.01	0	0	0	0.05	20.87	-13.18	20.25	-12.21
	7298	3394.6	34.91	2.24	36.3	-11.74	0.62		0	0.97	0	0.01	0.02	0	0	0	21.34	-13.16		
	7296	3990.3	34.89	1.91	40.99	-12.16	0.2		0	0.82	0	0	0.18	0	0	0	21.87	-12.66		
	7295	4094.1	34.89	1.90	41.48	-12.1	0.44		0	0.82	0	0	0.18	0	0	0	21.89	-12.64		
	7294	4217.6	34.88	1.86	42.16	-12.2	0.22		0	0.80	0	0	0.20	0	0	0	21.94	-12.58		
USGT11-16	7508	1.1	37.39	25.16		-11.3	0.22	15.63												
Lat: 26.14	7459	39.7	37.39	25.13	0.19	-11.24	0.31	15.69												
Long: -44.83	7457	89.9	37.23	23.14	0	-10.51	0.36	14.38												

Table 4.3 continued

Station Info	Samp No	Depth (m)	Sal (psu)	Pot T	Silicate (µmol/kg)	εNd	error	[Nd] (pmol/kg)	MOW	NADW	ENADW	AAIW	AABW	EAABW	ISW	NACW	Calculated [Nd]	Calculated εNd	OMPA derived [Nd]	OMPA derived εNd
UH	7456	110.7	37.11	21.97	0	-11.28	0.53	13.69											17.6	-10.6
	7454	185.7	36.72	18.95	0.39	-10.28	0.4	13.96											16.46	-10.61
	7453	234.8	36.55	17.91	0.97	-10.48	0.24	14.71											16.62	-10.67
	7450	420.3	36.09	15.27	2.63	-11.61	0.58	17											19.41	-11.65
	7448	801.4	35.22	8.84	13.76	-11.7	0.24	17.55												
	7381	962.2	35.04	6.84	17.86	-11.95	0.58	17.75	0	0	0.28	0.36	0	0	0	0.37	14.65	-10.79	17.50	-12.15
	7380	1194.3	35.03	5.56	16.69	-11.85	0.22	17.45	0	0	0.55	0.22	0	0	0	0.23	16.14	-11.16	18.93	-13.21
	7379	1492.8	35.09	4.86	14.05	-12.85	0.31	17.27	0	0	0.79	0.04	0	0	0	0.17	17.55	-11.59	19.97	-13.93
	7377	2092.5	35.00	3.42	20.69	-12.17	0.31	17.14	0	0	0.98	0.02	0	0.00	0	0	18.51	-11.59	19.11	-12.61
	7375	2986.6	34.94	2.63	31.33	-12.09	0.36	19.59	0	0	0.51	0.01	0	0.48	0	0	20.73	-11.72	20.66	-12.10
	7374	3183.8	34.93	2.43	35.91	-11.43	0.24	18.48	0	0	0.39	0.01	0	0.60	0	0	21.30	-11.74	21.12	-12.01
	7373	3283.9	34.92	2.41	36.11	-11.71	0.24	18.84	0	0	0.38	0.01	0	0.61	0	0	21.37	-11.75	21.23	-11.97
	7372	3383.8	34.92	2.40	35.82	-11.71	0.24	19.52	0	0	0.37	0.01	0	0.61	0	0	21.38	-11.75	21.19	-11.96
	7371	3487.4	34.92	2.37	35.52	-11.9	0.24	21.36	0	0	0.36	0.01	0	0.63	0	0	21.46	-11.75	21.32	-11.90
	7370	3605.3	34.92	2.36	35.72	-11.96	0.24	21.56	0	0	0.35	0.01	0	0.64	0	0	21.51	-11.76	21.26	-11.92
USGT11-18	7586	38.9	37.63	25.23	0.1	-9.19	0.24													
Lat: 24.15	7583	113.9	37.30	22.21	0	-10.96	0.38												16.79	-10.6
Long: -40.22	7580	233	36.60	18.09	0.78	-10.11	0.38												16.4	-10.62
LDEO	7578	348.9	36.26	16.16	2.05	-9.38	0.24												15.91	-10.64
	7577	422.3	35.96	14.34	3.61	-9.81	0.24												15.23	-10.69
	7576	598.1	35.59	11.60	7.12	-10.15	0.24												19.25	-11.63
	7575	795.9	35.31	8.98	13.17	-11.61	0.32												17.60	-12.12
	7607	958.7	35.15	7.17	16.88	-10.67	0.24		0	0	0.36	0.22	0	0	0	0.43	15.23	-11.21	18.49	-13.09
	7606	1145.3	35.10	5.94	17.08	-10.5	0.24		0	0	0.56	0.15	0	0	0	0.29	16.29	-11.35	19.37	-13.64
	7605	1493.2	35.13	4.92	17.08	-12.06	0.24		0	0	0.79	0	0	0	0	0.21	17.62	-11.68	19.52	-12.54
	7603	2088.5	35.00	3.38	24.1	-11.86	0.38		0	0	0.96	0.02	0	0.02	0	0	18.60	-11.59	21.19	-11.99
	7601	2988.1	34.94	2.54	35.42	-10.7	0.24		0	0	0.47	0	0	0.52	0	0	21.01	-11.75	22.15	-11.78
	7599	3777.3	34.90	2.10	43.04	-11.54	0.38		0	0	0.20	0.01	0	0.79	0	0	22.24	-11.79	22.31	-11.77
	7598	4175	34.89	2.02	44.79	-11.56	0.24		0	0	0.14	0.01	0	0.85	0	0	22.47	-11.80	22.35	-11.76
	7597	4277.4	34.89	2.01	44.99	-11.79	0.32		0	0	0.13	0.01	0	0.86	0	0	22.51	-11.80	22.51	-11.72
	7596	4386.1	34.89	2.00	45.18	-10.76	0.24		0	0	0.13	0.01	0	0.86	0	0	22.52	-11.80		
USGT11-20	7732	74.3	37.42		0.00	-10.76	0.21													
Lat: 22.33	7731	99.7	37.30	22.42	0.00	-10.77	0.16													
Long: -35.87	7729	183.8	36.59	18.16	1.36	-10.02	0.21												15.91	-10.62
USC	7727	300.8	36.23	16.01	2.34	-10.55	0.17												15.53	-10.63
	7726	374.3	36.03	14.79	3.41	-10.13	0.35												19.34	-11.57
	7724	736.3	35.26	8.93	14.05	-11.01	0.15												17.39	-12.16
	7723	920.8	35.04	6.72	18.83	-11.16	0.31													
	7722	1055.2	35.01	6.04	19.52	-10.83	0.21		0	0	0.40	0.33	0	0	0	0.27	15.27	-10.86	17.50	-12.75
	7753	1195	35.04	5.48	18.64	-11.37	0.13		0	0	0.57	0.21	0	0	0	0.22	16.27	-11.19	18.53	-13.21
	7751	1888.6	35.02	3.79	21.57	-11.41	0.35		0	0	0.92	0.03	0	0	0	0.04	18.20	-11.56	19.08	-12.77
	7750	2288.6	34.99	3.18	26.74	-11.77	0.21		0	0	0.85	0.01	0	0.14	0	0	19.17	-11.63	19.77	-12.51
	7749	2685.6	34.96	2.76	31.81	-11.46	0.11		0	0	0.61	0.00	0	0.39	0	0	20.38	-11.71	20.61	-12.16
	7747	3482.5	34.91	2.22	40.79	-11.46	0.10		0	0	0.27	0.01	0	0.72	0	0	21.92	-11.78	21.59	-11.89
	7746	4281.7	34.89	2.00	45.67	-11.46	0.14		0	0	0.13	0.01	0	0.86	0	0	22.53	-11.80	22.19	-11.80
	7742	5815.3	34.88	1.88	48.50	-11.40	0.27		0	0	0.04	0.02	0	0.94	0	0	22.89	-11.81	22.68	-11.72

Table 4.3 continued

Station Info	Samp No	Depth (m)	Sal (psu)	Pot T	Silicate (µmol/kg)	εNd	error	[Nd] (pmol/kg)	MOW	NADW	ENADW	AAIW	AABW	EAABW	ISW	NACW	Calculated [Nd]	Calculated εNd	OMPA derived [Nd]	OMPA derived εNd
USGT11-22	7861	1	37.17	24.81	0.1	-11.6	0.22	20.79												
Lat: 19.43	7937	50	37.17	24.80	0.29	-12.05	0.25	20.9												
Long: -29.38	7936	74.5	37.17	24.79	0.29	-11.91	0.25	20.22												
UH	7935	84	37.09	23.22	0.39	-11.8	0.22	16.76												
	7934	123.8	36.66	19.49	2.05	-11.04	0.3	15.76												
	7933	183.9	36.14	15.93	4.29	-10.9	0.25	17.46											16.87	-11.08
	7932	233.1	36.03	15.14	5.27	-10.83	0.25	18											17.84	-11.1
	7931	283.3	35.91	14.32	5.56	-11.09	0.22	18.83											17.08	-11.03
	7929	568.2	35.36	10.19	12.68	-11.34	0.25	19.33											17.93	-11.33
	7928	662.8	35.21	8.87	15.42	-11.11	0.25	18.78											19.31	-11.45
	7927	897.7	34.92	6.24	22.15	-11.23	0.24	18.59											17.03	-11.97
	7926	1195.2	35.03	5.49	20.39	-11.51	0.22	17.26	0	0	0.56	0.22	0	0	0	0.22	16.19	-11.16	18.23	-13.01
	7957	1793.1	35.01	3.80	21.76	-12.16	0.25	17.06	0	0	0.91	0.05	0	0	0	0.04	18.09	-11.52	19.14	-13.80
	7956	2091.6	34.99	3.38	24.4	-12.15	0.24	17.49	0	0	0.94	0.03	0	0.03	0	0	18.56	-11.57	19.58	-12.53
	7955	2389.8	34.97	3.05	27.91	-11.92	0.45	18.37	0	0	0.76	0.02	0	0.22	0	0	19.53	-11.65	20.21	-12.25
	7953	2988	34.93	2.46	36.69	-11.64	0.24	20.68	0	0	0.43	0	0	0.57	0	0	21.23	-11.76	21.45	-11.92
	7951	3586.2	34.90	2.11	43.43	-11.7	0.24	24.86	0	0	0.20	0.01	0	0.79	0	0	22.22	-11.79	22.23	-11.77
	7949	4183.5	34.89	1.98	46.55	-11.7	0.2	27.15	0	0	0.11	0.01	0	0.87	0	0	22.60	-11.80	22.67	-11.71
	7948	4580.7	34.89	1.96	46.94	-11.99	0.24	27.94	0	0	0.10	0.02	0	0.89	0	0	22.65	-11.80	22.71	-11.71
	7947	4969.7	34.89	1.95	47.43	-11.72	0.25	27.16	0	0	0.09	0.02	0	0.89	0	0	22.66	-11.80	22.90	-11.66
USGT11-24	8140	38	36.81		0	-10.56	0.21													
Lat: 17.40	8138	71.6	36.48		1.75	-10.78	0.21													
Long: -24.5	8134	234.5	35.61		7.71	-11.21	0.21												16.55	-11.66
LDEO	8131	430.1	35.27		12.29	-10.83	0.32												16.82	-11.74
	8130	594.9	35.08		16.49	-11.66	0.32												19.6	-11.39
	8103	1076.1	34.96	5.88	21.96	-11.13	0.38		0	0	0.38	0.38	0	0	0	0.24	15.09	-10.71	17.19	-12.57
	8102	1263.3	35.00	5.27	21.57	-11.7	0.32		0	0	0.57	0.24	0	0	0	0.19	16.22	-11.11	18.10	-13.06
	8099	1973.3	34.98	3.55	24.4	-11.4	0.38		0	0	0.93	0.06	0	0	0	0.01	18.18	-11.49	19.37	-12.76
	8095	2957.1	34.93	2.53	34.94	-12.18	0.32		0	0	0.45	0.01	0	0.53	0	0	21.01	-11.73	20.82	-12.11
	8094	3202.1	34.92	2.37	38.06	-10.29	0.24		0	0	0.36	0.01	0	0.63	0	0	21.49	-11.76	21.22	-11.99

4.7 Figures

Figure 4.1. a) Cruise track of GA03 (blue dots) in the North Atlantic completed during KN199-4 (bold, GT10) and KN204 (GT11) in December 2010 and 2011. Sampled stations are labeled and highlighted in red. b) Cruise track (red) with locations of Nd data used to assign end-member Nd-compositions (black). The following water masses are defined by stations sampled by Lacan and Jeandel, 2005: A) Upper Labrador Sea Water; B) Classic Labrador Sea Water; C) Irminger Sea Water; D) Denmark Strait Outflow Water; E) Iceland-Scotland Outflow Water. The following water masses are defined by stations sampled as part of this study: F) Southwest Atlantic Central Water; G) Eastern North Atlantic Deep Water; H) North Atlantic Central Water; I) Mediterranean Outflow Water. Station J was sampled by Piepgras and Wasserburg, 1987 and used to define the Nd-composition of Atlantic Equatorial Water, Antarctic Intermediate Water, Upper Circumpolar Deep Water and Antarctic Bottom Water in OMPA calculations.

Figure 4.2. End-member properties plotted as both T vs S and ε_{Nd} vs S. a) T vs S of end-members used in *T-S approach* including 'pure' Antarctic Intermediate Water and Antarctic Bottom Water. b) ε_{Nd} vs S of end-members used in the *T-S approach* including 'pure' Antarctic Intermediate Water and Antarctic Bottom Water. c) T vs S of end-members used in OMPA calculations with the exception of central waters (see Figure 4.9). d) ε_{Nd} vs S of end-members used in OMPA calculations with the exception of central waters (plotted as an array in Figure 4.9).

Figure 4.3. North Atlantic Deep Water temperature and salinity properties in the northern and western Atlantic based on WOA09 (Antonoy et al., 2009; Locarnini et al., 2009). a) T vs S plot for waters in the NADW source region (see map for area used). b) T vs S plot for waters along the western boundary in the North Atlantic (see map for area used). c) T vs S plot for waters in both the source region and along western boundary. At a reference depth of 3500m, T-S properties of NADW along the western basin are slightly more saline and warmer than in the northern seas or source regions of NADW. The composition of the NADW end-member used for the T-S calculations is $\theta = 2.25°C$ and S = 34.92 (red circle).

Figure 4.4. Antarctic Intermediate and Bottom Water temperature and salinity properties in the Southern Ocean based on WOA09 (Antonoy et al., 2009; Locarnini et al., 2009). a) Depth profile of potential temperature. Colors represent silicate concentrations. b) Depth profile of salinity. Colors represent silicate concentrations. c) T vs S plot of waters in the southern ocean. Colors represent potential temperature. AAIW is defined as a salinity minimum at intermediate depths and AABW is the coldest, silicate rich water. 'Pure' AAIW and 'pure' AABW are marked by red circles (Table 4.1).

Figure 4.5. Modified Antarctic Intermediate and Bottom Water temperature and salinity properties near the equator in the Atlantic Ocean based on WOA09 (Antonoy et al., 2009; Locarnini et al., 2009). Unmodified or 'pure' T-S compositions of AAIW and AABW (gray squares) as defined in Figure 4.4 are plotted with the T-S data available near the equator. In both cases, the modified waters are warmer and more saline in the Equatorial Atlantic ocean.

Figure 4.6. *T-S approach* water mass mixing calculated and measured ε_{Nd} in the northeastern Atlantic. When the modified AABW end-member (or the AABW value used in the western

basin) is used there is poor agreement between predicted and measured ε_{Nd}. The calculated ε_{Nd} for deep waters (green line) is more radiogenic than measured values. Additionally, these profiles show the offset between measured and calculated (red line) ε_{Nd} for intermediate samples in the eastern basin. This offset reflects the radiogenic influence of the MOW end-member on the calculated values.

Figure 4.7. Silicate vs. ε_{Nd} in the northeastern Atlantic. These data show that the southern-sourced, high silicate end-member in this region (or Eastern Antarctic Bottom Water) possesses a less radiogenic ε_{Nd} composition than the one calculated based on water mass mixing between AABW and ENADW. The ε_{Nd} of EAABW is adjusted in following calculations to reflect this less radiogenic ε_{Nd} composition.

Figure 4.8. Comparison of T, S, calculated and measured ε_{Nd} in the northwestern Atlantic (Sta. GT11-01, -02, -03, -04, -06, -08, -10). a) T vs S plot of CTD data in the western basin with end-members (MOW, NADW and AAIW). b) ε_{Nd} vs S with both calculated and measured ε_{Nd} and same end-members. There is a noticeable offset between calculated and measured ε_{Nd} demonstrating the influence of the radiogenic MOW end-member on the calculated value. c) T vs S showing mixing triangle with ISW instead of MOW to define water mass mixing in this area. Stations GT11-12 and -14 are not influenced by ISW.

Figure 4.9. Array of T-S properties for central waters used to define water mass mixing in OMPA calculations (Jenkins et al., 2014). The central waters shown are Southwest Atlantic Central Waters (SWACW), Atlantic Equatorial Waters (AEW) and North Atlantic Central Water (NACW). The T-S data is overlain by the discreet T-S values of samples used to define the Nd-composition of each respective water mass. Note that the discreet T-S value used to define the Nd-composition of SWACW does not sit on the array used to define this water mass in OMPA. Although this sample is the closest available Nd measurement, the T-S properties are quite different. SWACW plays a minimal role in water mass mixing (~ 10%) so any offset because of this difference in not apparent. SWACW and AEW are only used in the OMPA calculations whereas NACW is defined by different Nd data in the T-S approach and OMPA calculations. References for the Nd-composition for each water mass are summarized in the text and Table 4.1 and 4.2.

Figure 4.10. Mixing triangles used for water mass mixing calculations in the western Atlantic Basin. a) Mixing at intermediate depths (900 – 3000 m) at Sta. GT11-03, -04, -06, -08, -10. The end-members used here are Irminger Sea Water (ISW), Antarctic Intermediate Water (AAIW) and North Atlantic Deep Water (NADW). b) Mixing at intermediate depths (900 - 3000 m) at Sta. GT11-12 and -14. The end-members used here are North Atlantic Central Water (NACW), Antarctic Intermediate Water (AAIW) and North Atlantic Deep Water (NADW). c) Mixing of deep samples (>3000 m) at Sta. GT11-01, -03, -04, -06, -08, -10, -12, -14. ε_{Nd}-members used here are Antarctic Intermediate Water (AAIW), North Atlantic Deep Water (NADW) and Antarctic Bottom Water (AABW).

Figure 4.11. Mixing triangles used for water mass mixing calculations at intermediate depths of the eastern Atlantic basin. a) Mixing at intermediate depths (1000 – 2300 m) at Sta. GT10-01, -03, -05, -07 (north-south transect). The end-members used here are Mediterranean Outflow

Water (MOW), Antarctic Intermediate Water (AAIW) and eastern North Atlantic Deep Water (ENADW). b) Mixing at intermediate depths (900 – 2000 m) at Sta. GT10-07, -10, -11, -12 and GT11-16, -18, -20, -22 and -24 (east-west transect). End-members used here are North Atlantic Central Water (NACW), Antarctic Intermediate Water (AAIW) and eastern North Atlantic Deep Water (ENADW).

Figure 4.12. Mixing triangles used for water mass mixing calculations at deep depths in the eastern Atlantic basin. a) Mixing at deep depths (>2300 m) at Sta. GT10-01 and -03 and at ~2400 m at Sta. GT10-05. The end members used here at Mediterranean Outflow Water (MOW), eastern North Atlantic Deep Water (ENADW) and eastern Antarctic Bottom Water (EAABW). b) Mixing at deep depths at Sta. GT10-05 (>2900 m) and at depths greater than 2000 m at Sta. GT10-07, -09, -10, -11, -12 and GT11-16, -18, -20, -22 and -24. The end-members used here are Antarctic Intermediate Water (AAIW), eastern North Atlantic Deep Water (ENADW) and eastern Antarctic Bottom Water (EAABW).

Figure 4.13. Available ε_{Nd} data in the western North Atlantic. a) Station profiles for selected stations, which are compiled from the following studies: Piepgras and Wasserburg, 1987 (green, red, maroon); Pahnke et al., 2012 (light pink); this study (dark pink, black). b) T vs S for selected samples between 2500 and 4000 m depth as a reference for possible ε_{Nd}-compositions of NADW in the study region. c) ε_{Nd} vs S demonstrating the range of ε_{Nd} in the area of interest. The potential ε_{Nd} composition for NADW in this region ranges between -13.5 and -12.0. This range is used to define the NADW end-member in the *T-S approach* water mass calculations. NADW was assigned an ε_{Nd} value of -13.25 (yellow circle).

Figure 4.14. Available ε_{Nd} data in the Labrador Sea. a) Station profiles for selected stations, which are compiled from the following studies: Piepgras and Wasserburg, 1987 (yellow, purple); Lacan and Jeandel, 2005 (red, black, green, blue). b) T vs S for selected samples between 600 and 1700 m depth as a reference for possible ULSW ε_{Nd}-compositions. c) ε_{Nd} vs S for selected samples demonstrating the range of ε_{Nd} between -13.5 and -15.25. A range of -14.0 to -15.0 was used to define the ULSW end-member in water mass calculations using OMPA results. ULSW was assigned an ε_{Nd} value of -15.0 (yellow circle).

Figure 4.1: GA03 Cruise Map

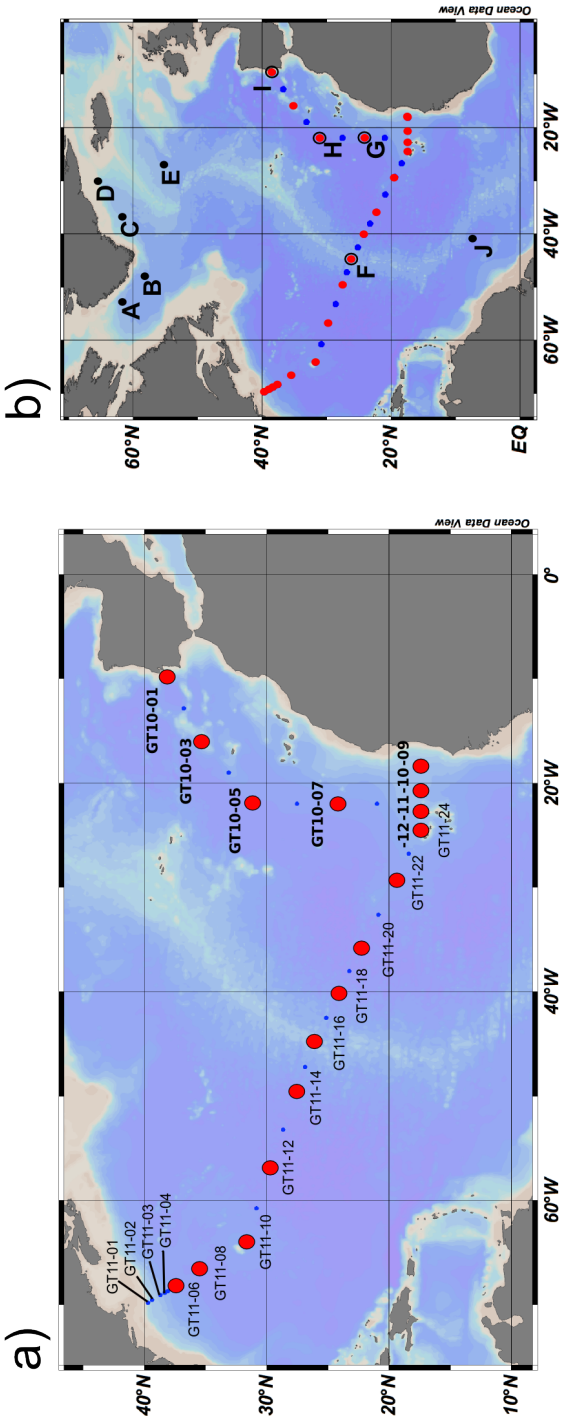

Figure 4.2: T vs S and ε_{Nd} vs S for both sets of end-members used in water mass mixing calculations

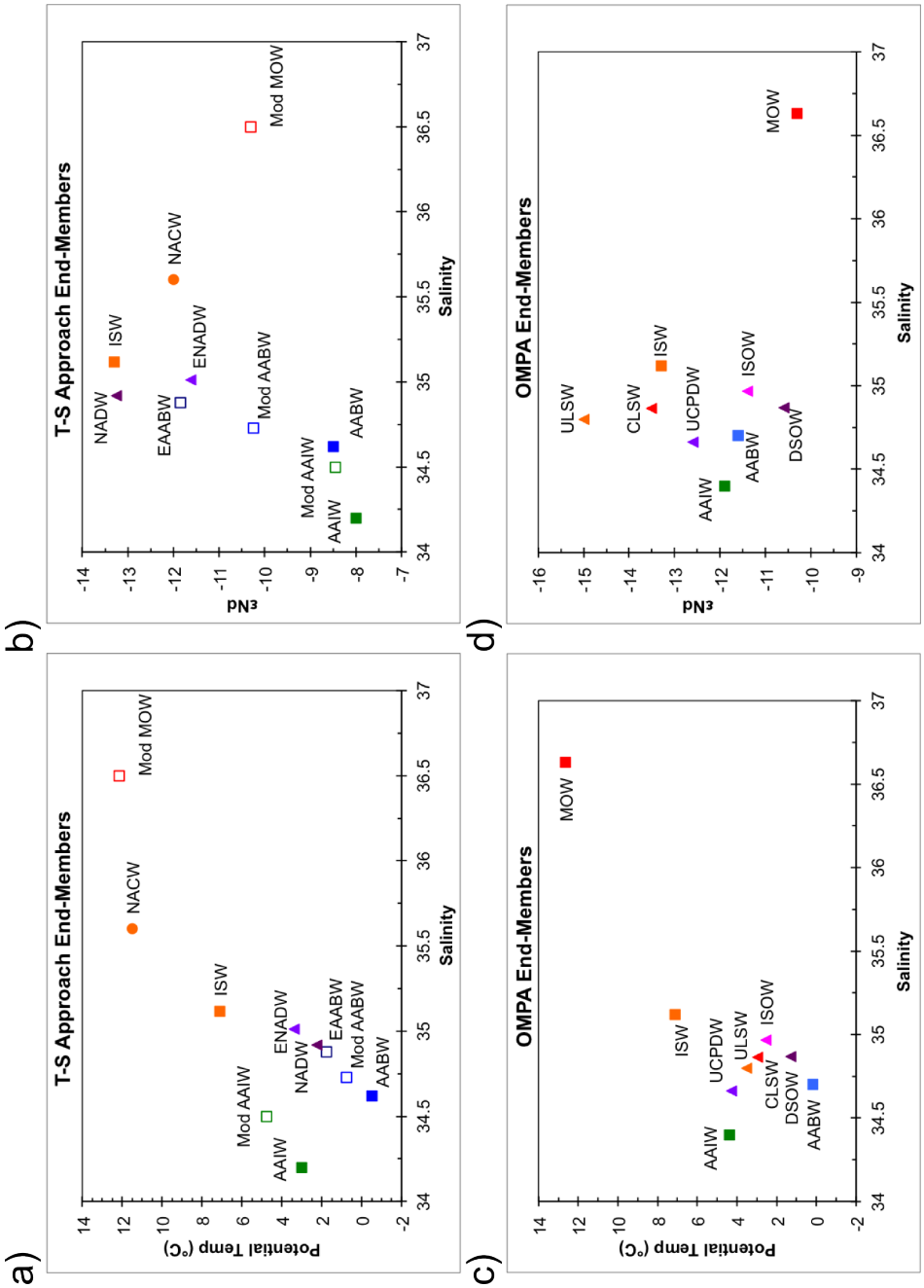

Figure 4.3: North Atlantic Deep Water T-S properties

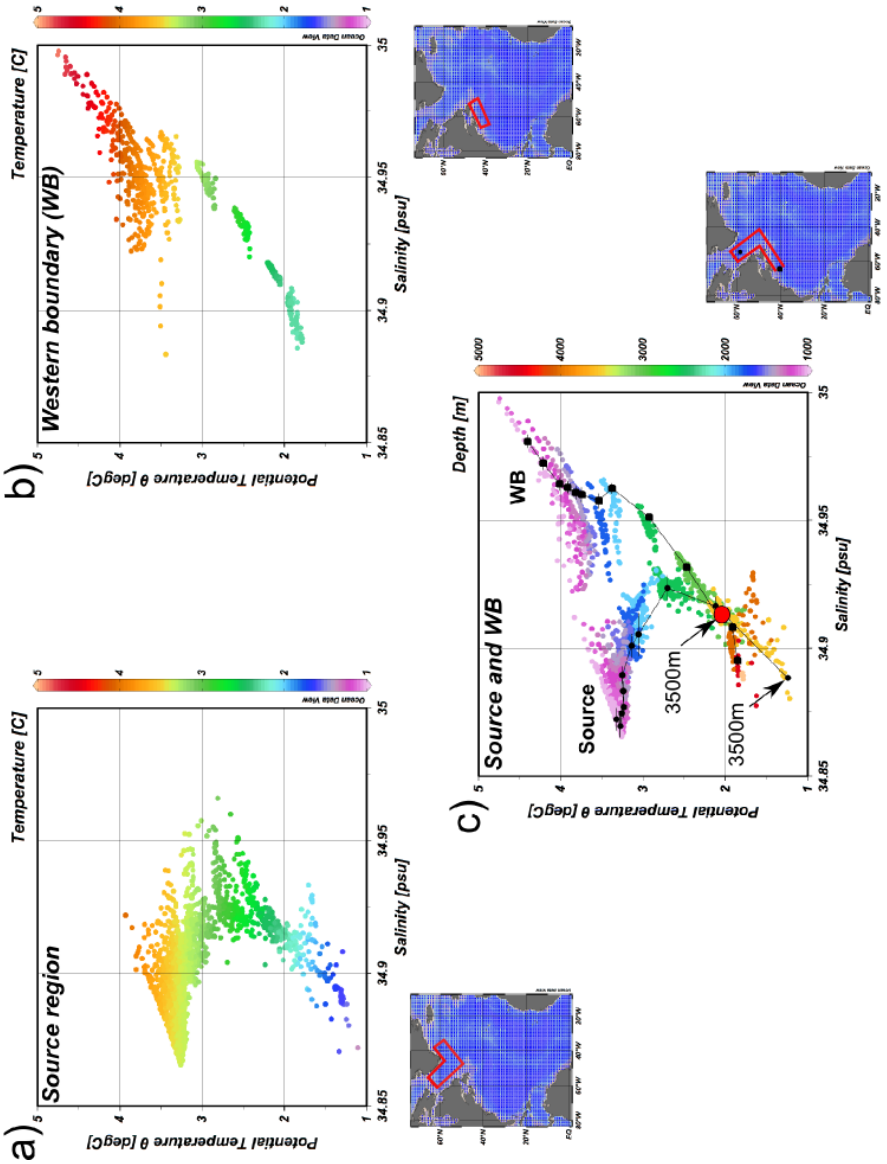

Figure 4.4: Antarctic Intermediate and Bottom Water T-S properties

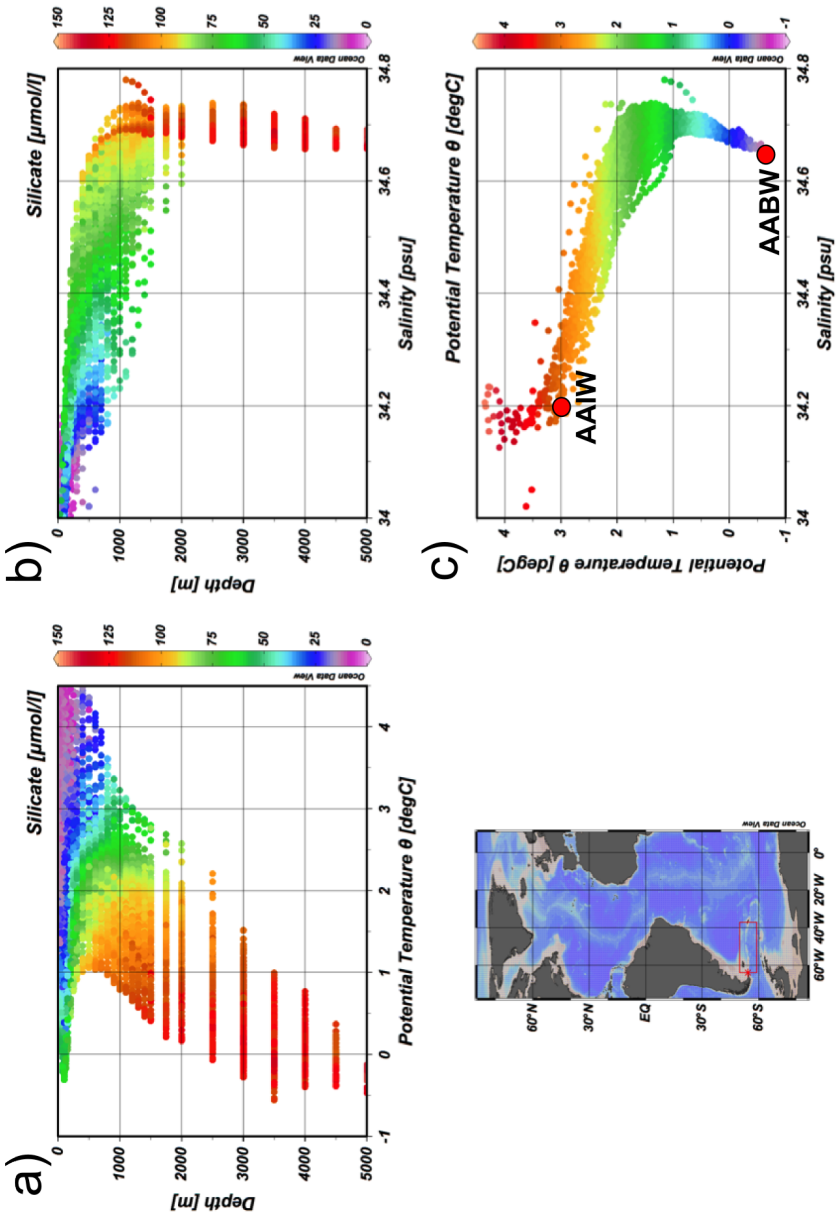

Figure 4.5: Modified Antarctic Intermediate and Bottom Water T-S properties

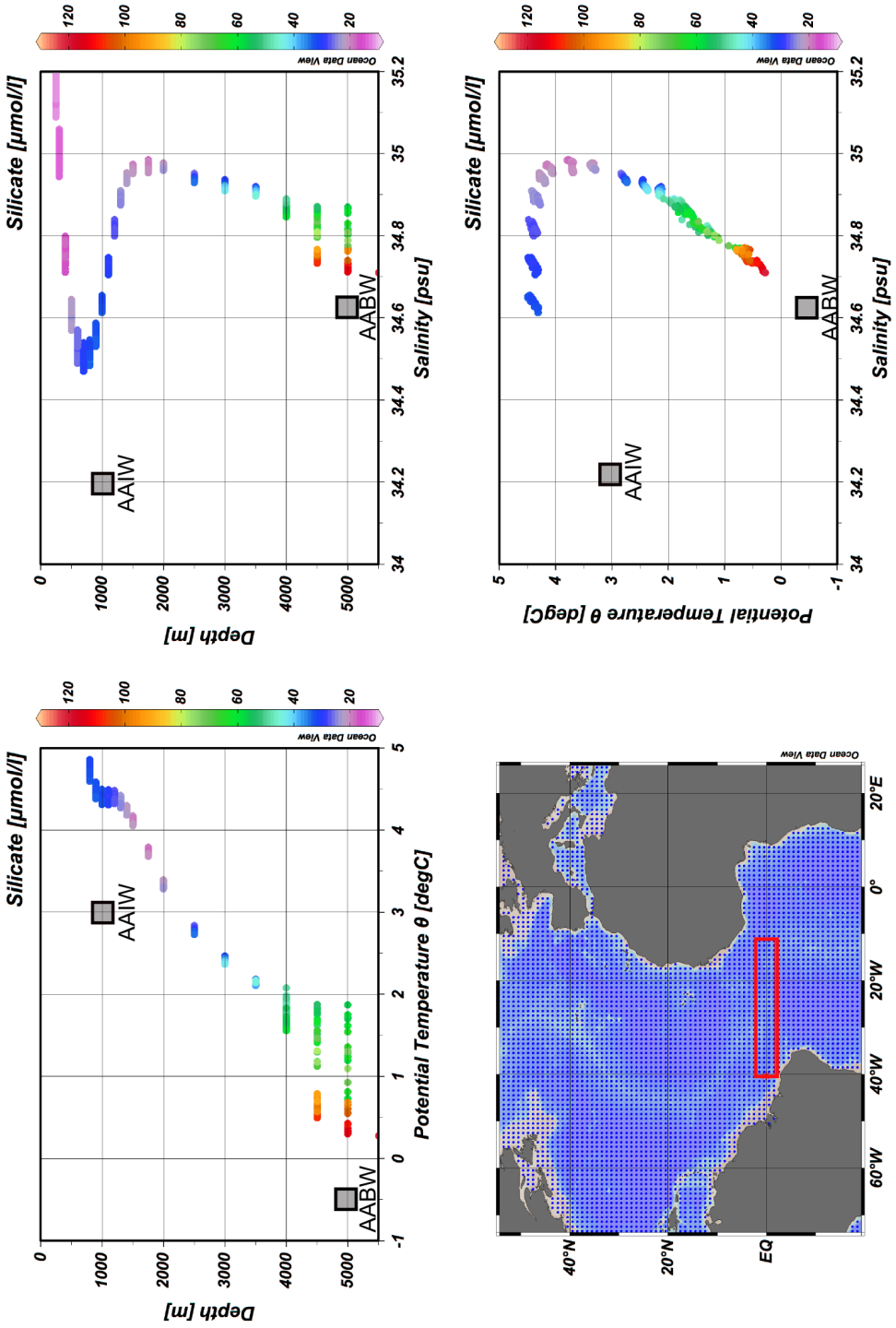

Figure 4.6: Measured and calculated ε_{Nd} in the northeastern Atlantic Ocean

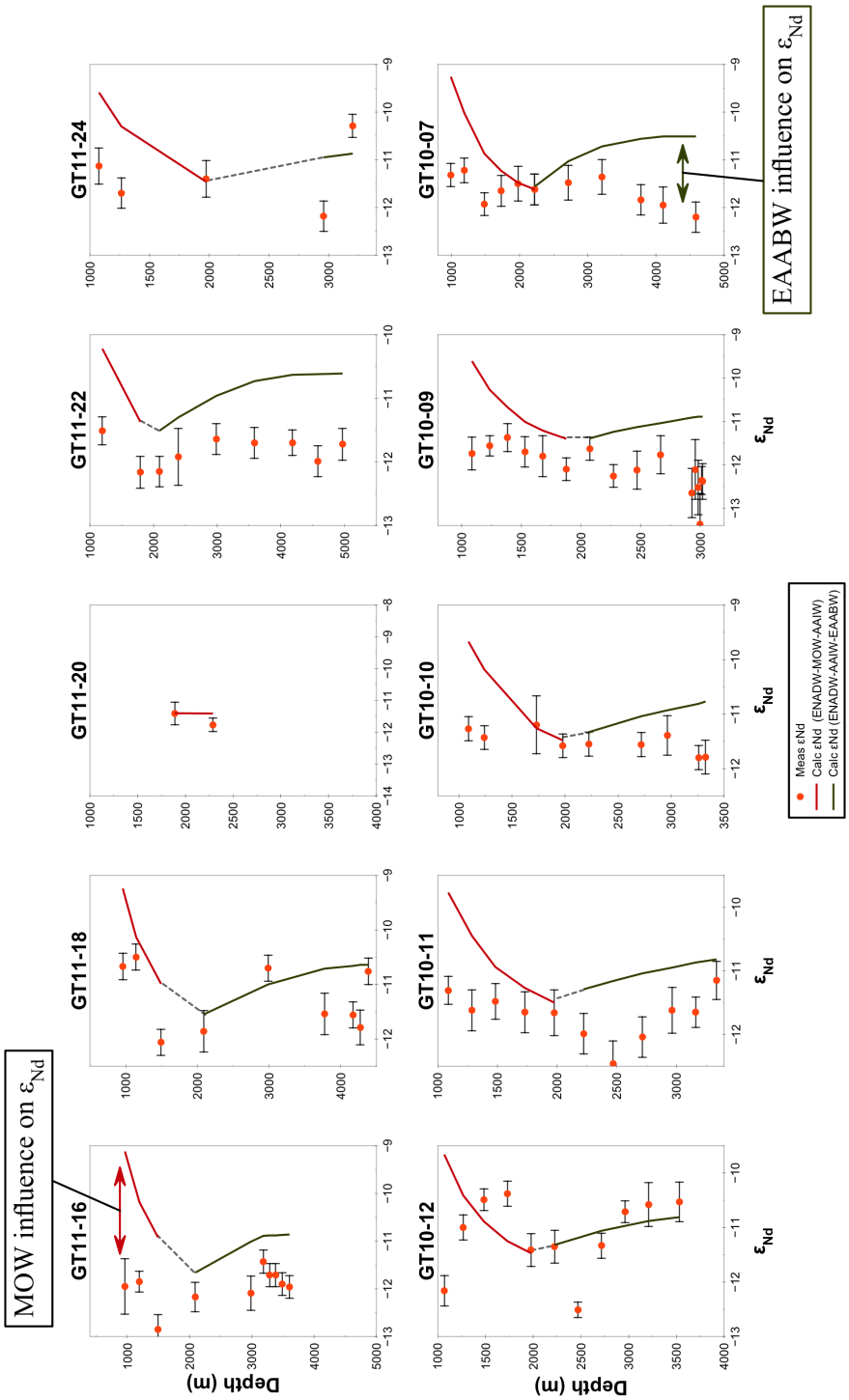

Figure 4.7: Silicate vs. ε_{Nd} in the northeastern Atlantic Ocean

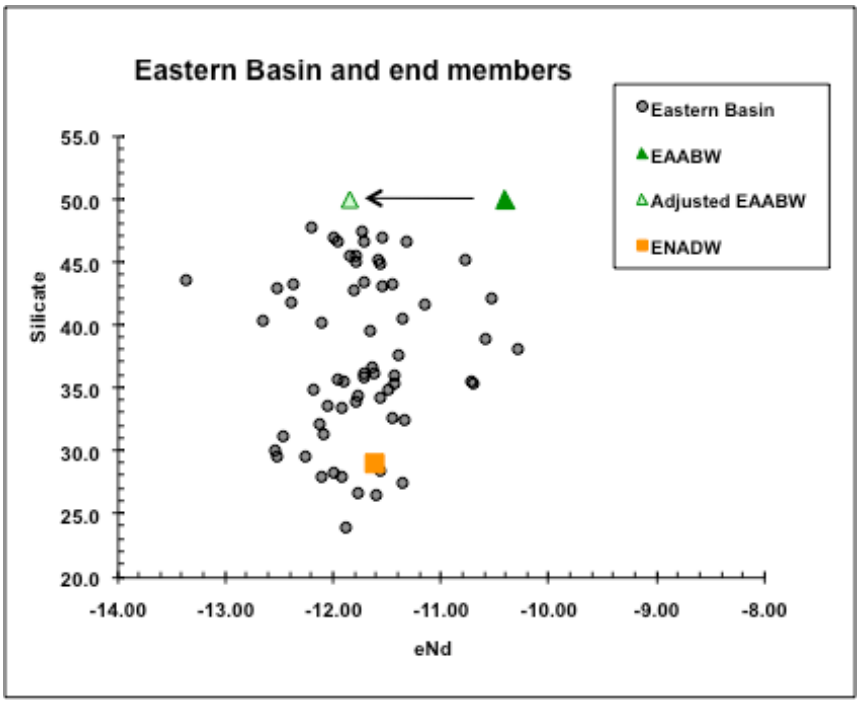

Figure 4.8: Compiled data from the northwestern Atlantic Ocean

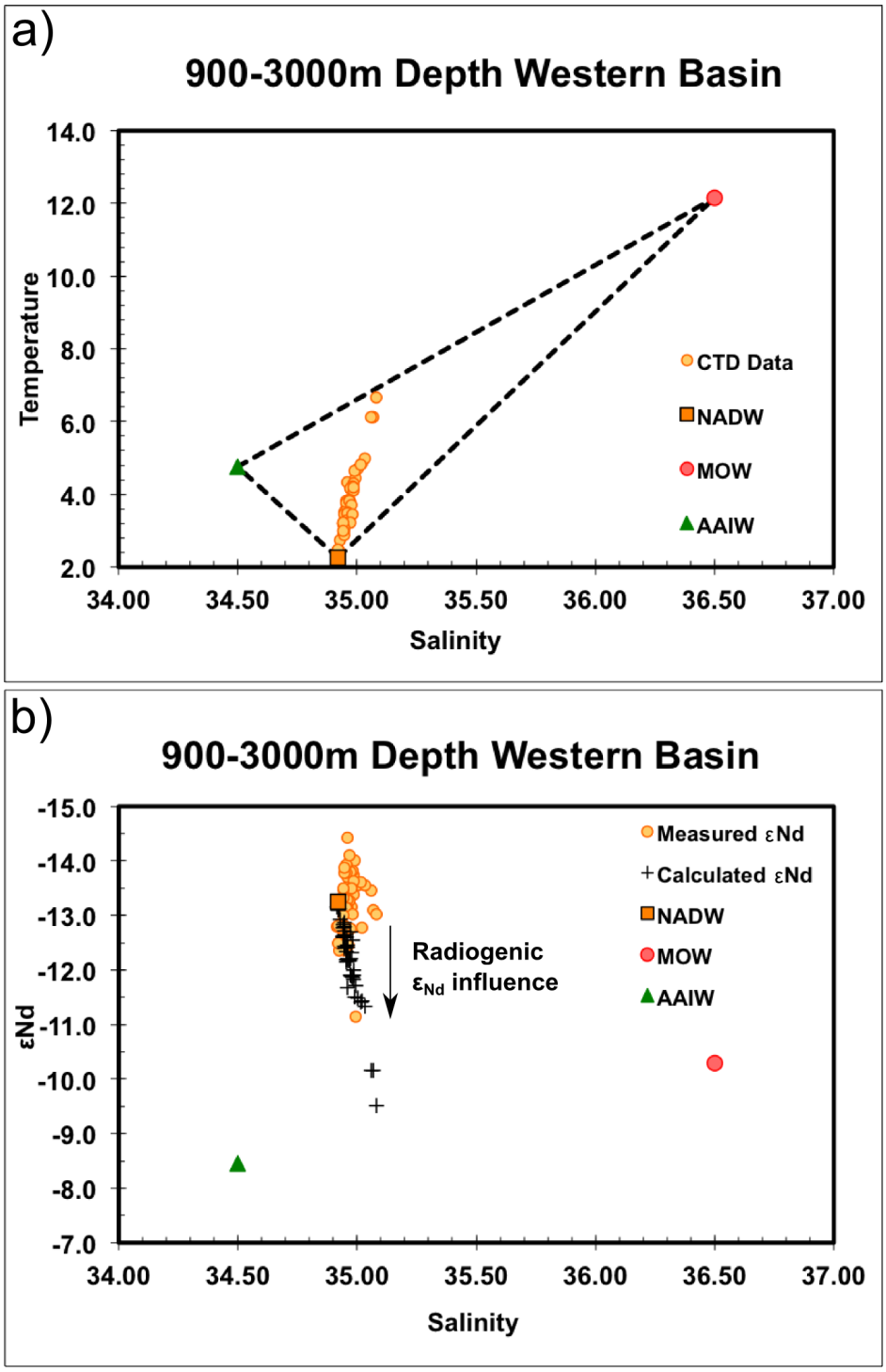

Figure 4.8 continued

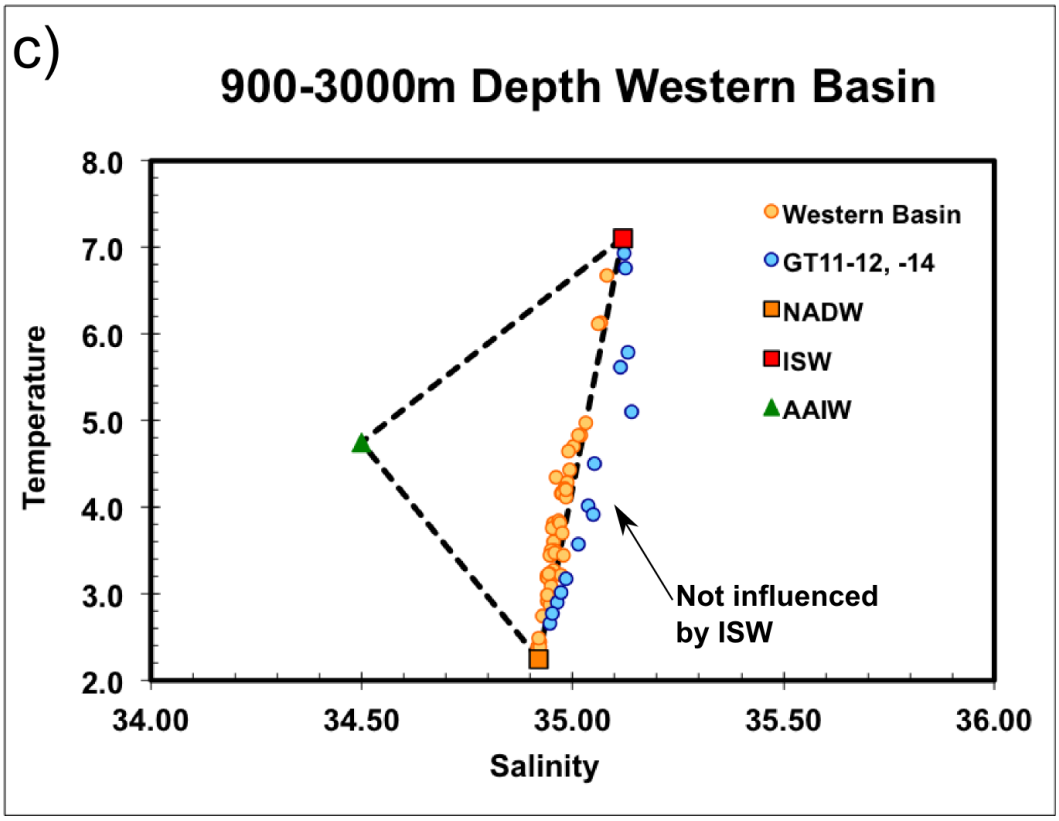

Figure 4.9: Central water T-S array used in OMPA calculations and T-S of samples used to define Nd-compositions

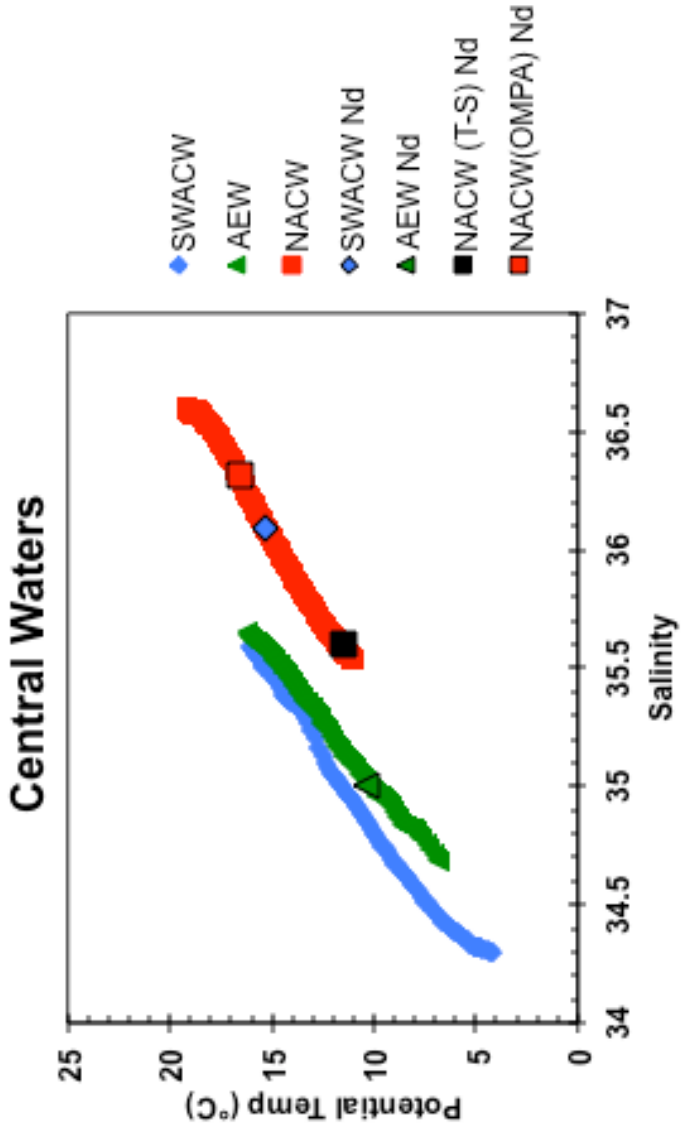

Figure 4.10: Mixing triangles for samples in the western Atlantic basin

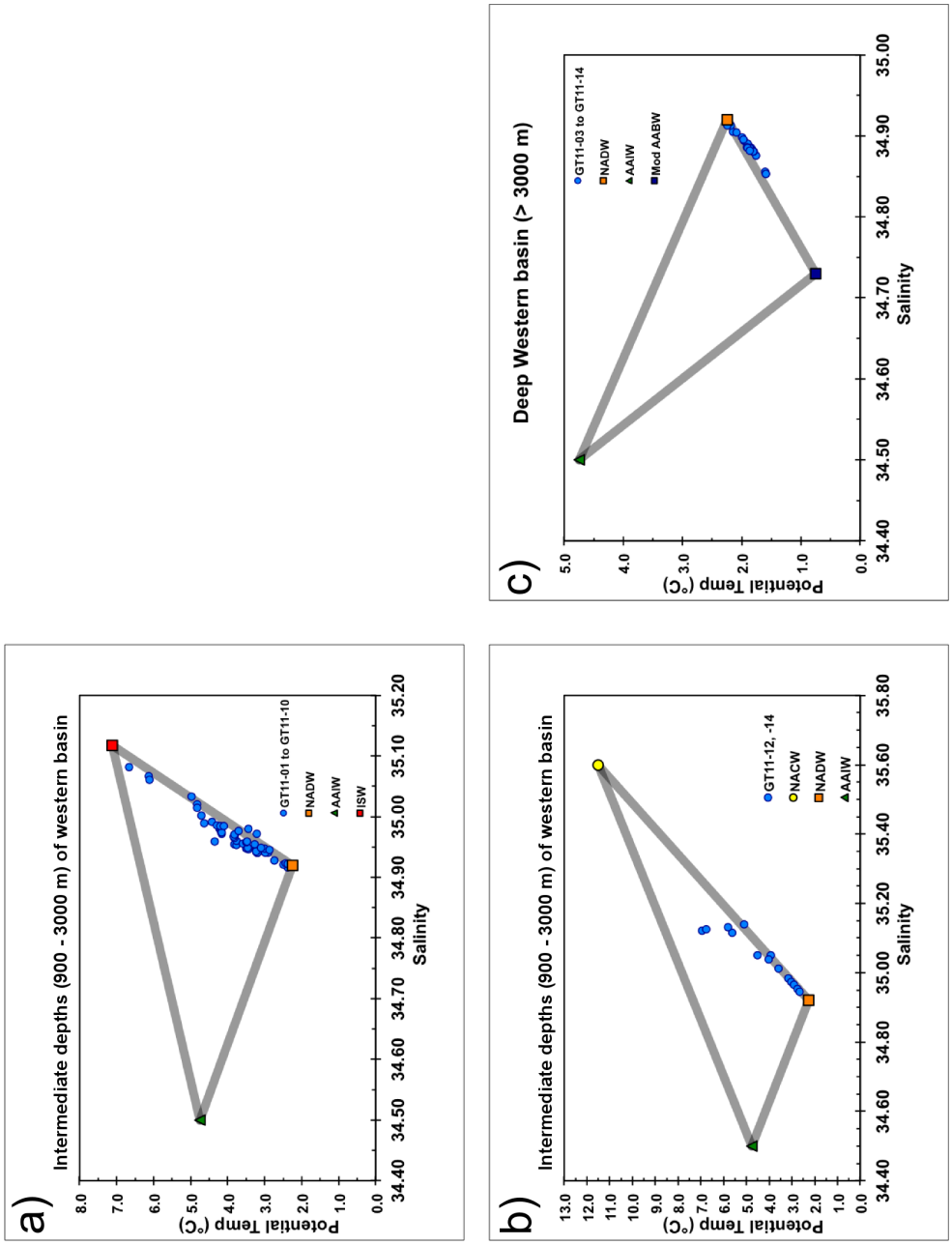

Figure 4.11: Mixing triangles for intermediate waters in the eastern Atlantic basin

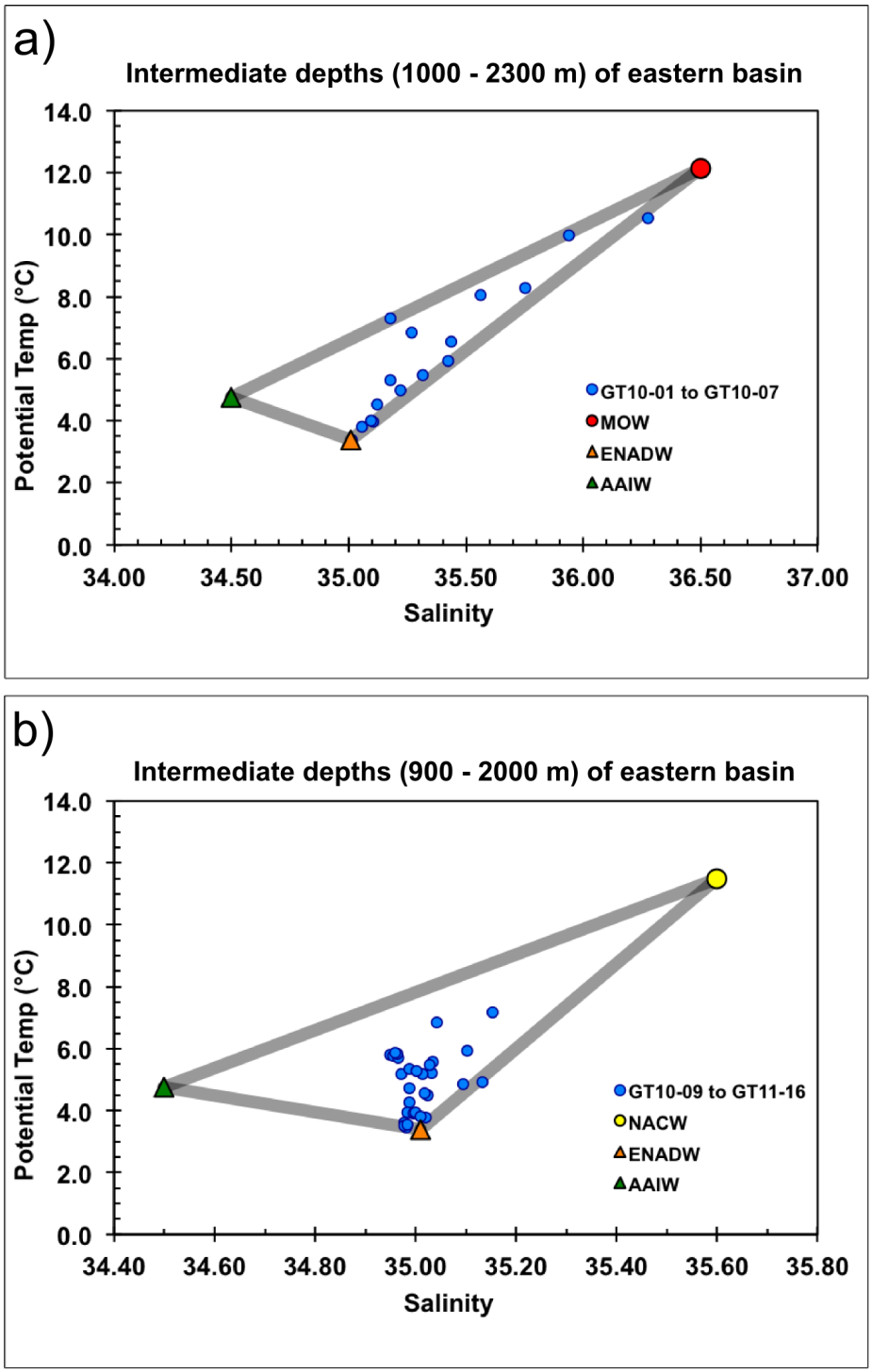

Figure 4.12: Mixing triangles for deep water in the eastern Atlantic Basin

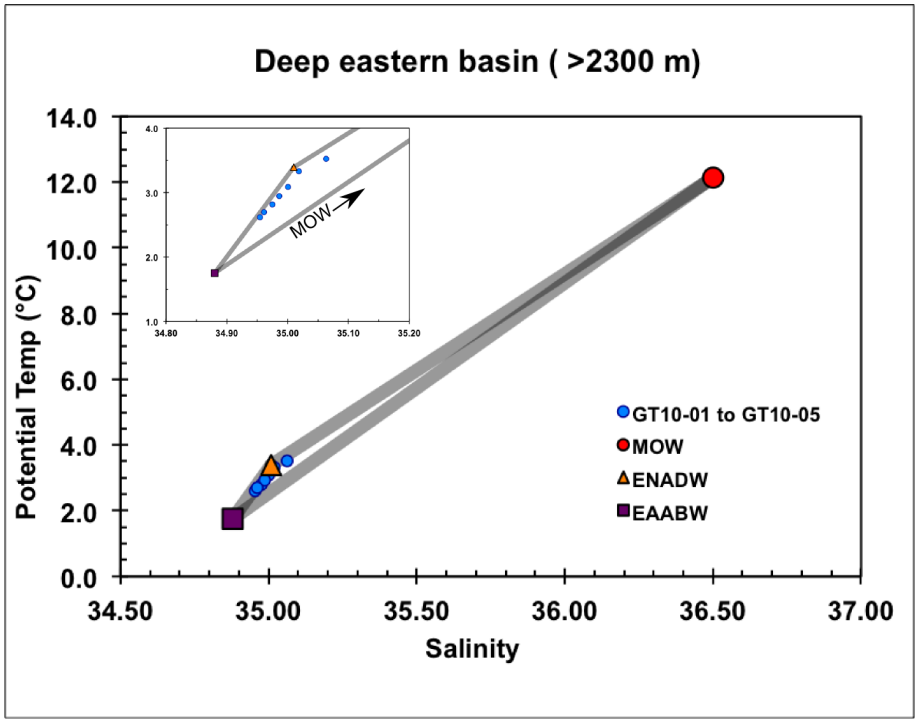

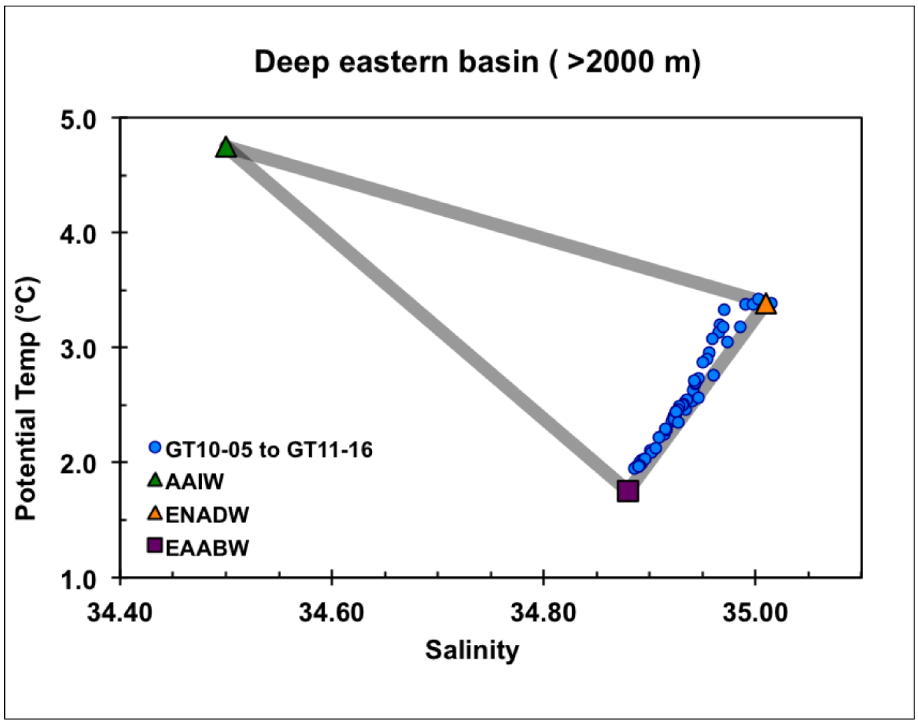

Figure 4.13: Available ε_{Nd} in the western Atlantic Basin to define NADW Nd-composition

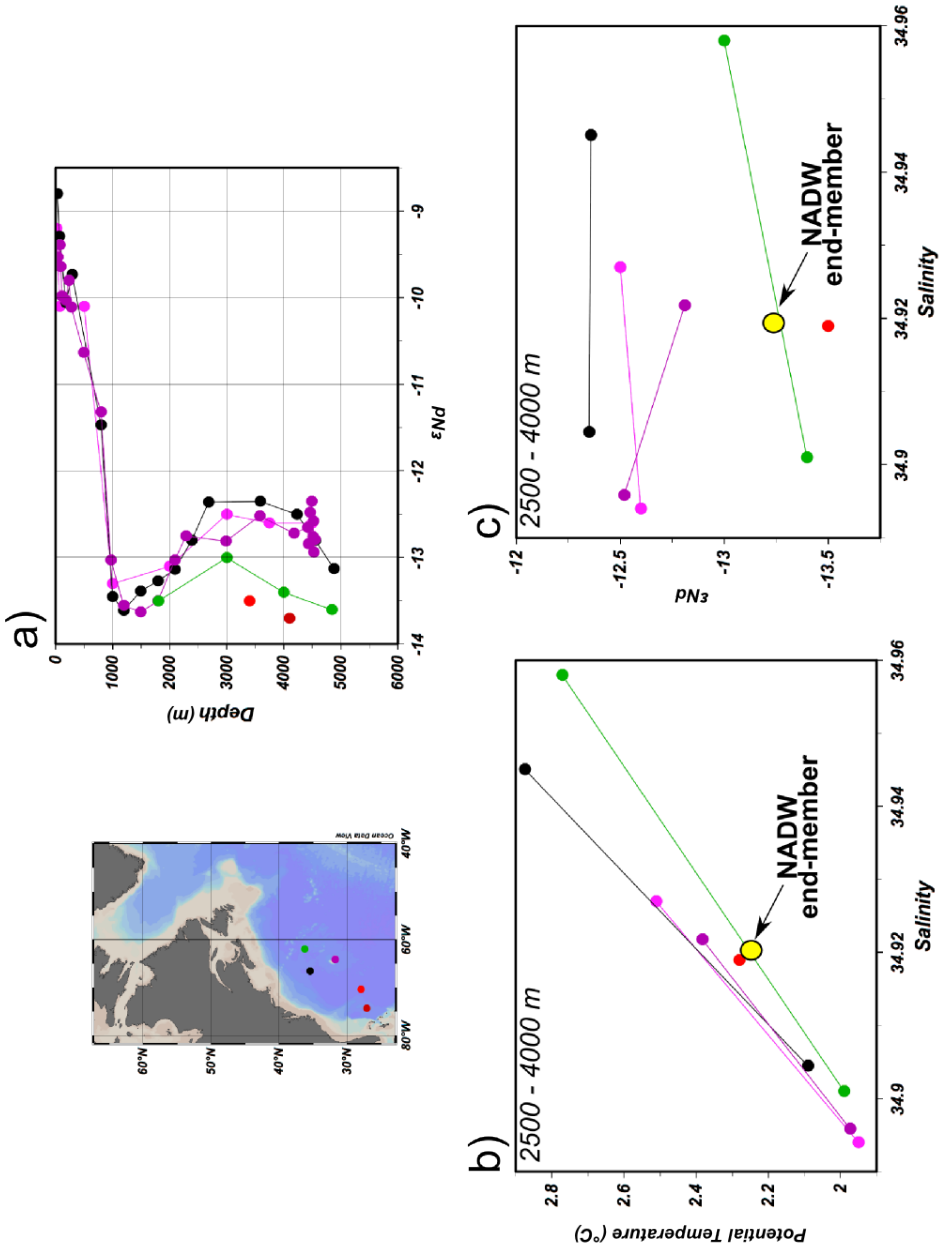

Figure 4.14: Available ε_{Nd} data in the Labrador Sea to define ULSW Nd-composition

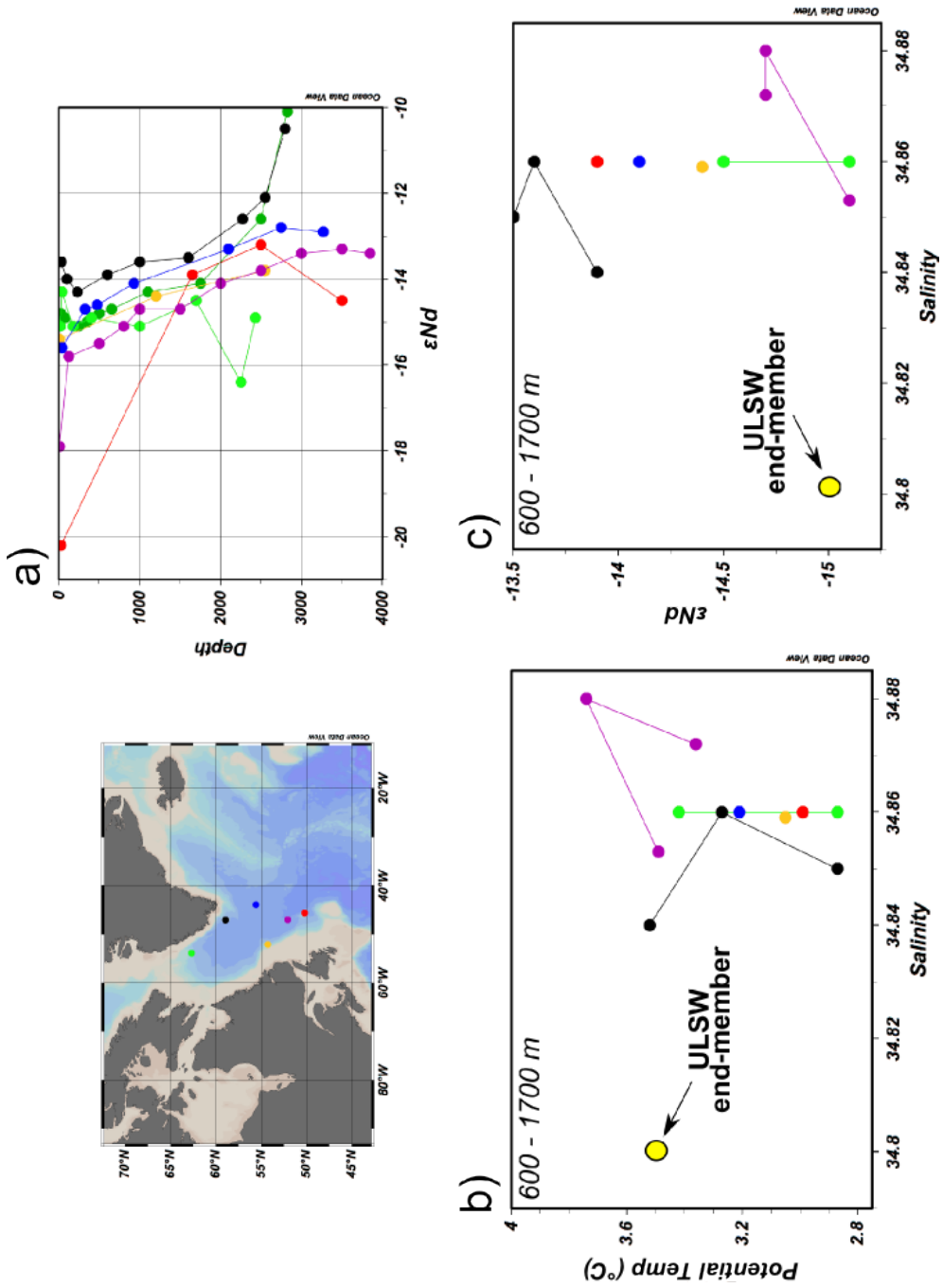

Chapter 5: Seawater neodymium composition in the open ocean North Atlantic: water mass signatures and transport

Abstract

Neodymium (Nd) isotope ratios in seawater fingerprint water masses over long transport distances and they are increasingly applied to trace modern and paleo-water ocean circulation. Persistent unknowns on the controls of its global distribution in seawater include the extent to which processes such as eolian deposition, boundary exchange and hydrothermal systems influence the Nd cycle. As part of the GEOTRACES program, extensive efforts are underway to determine the distribution of Nd in the North Atlantic basin in different environments. Here we focus on the observed distribution of Nd compared to predictions based on water mass mixing, using samples collected on the US Atlantic transects from Lisbon via Mauritania to Woods Hole. Observed offsets between calculated and measured Nd isotope ratios (ε_{Nd}) and concentrations [Nd] suggest unaccounted for isotope exchange along margins or with particles, and sources and sinks of Nd within the water column. The offset between measured and calculated ε_{Nd} is small in depths greater than ~1000m, indicating persistent 'conservative' behavior of ε_{Nd} across the study region, although the sensitivity to variations in the ε_{Nd} of end-members highlight the importance of constraining the Nd composition of these water masses. Above the mid-Atlantic hydrothermal plume there is a high particle load with low observed [Nd] compared to predictions from water mass mixing, highlighting the importance of Nd scavenging. At deep sites (>4000m), anomalously high [Nd] is seen across the basin, exceeding concentrations predicted from water mass mixing. Additionally, the large nepheloid layers at these depths in the western basin

contribute [Nd] to deep waters without influencing the ε_{Nd} of water mass mixing in the region, indicating the added Nd is mainly derived from re-dissolution of authigenic precipitates.

5.1 Introduction

5.1.1 Neodymium isotopes as a water mass tracer

Studies utilizing neodymium (Nd) isotopes as a water mass tracer are becoming prevalent in both modern and paleo-ocean circulation studies. At the core of this approach is an assumption of 'quasi-conservative' behavior of Nd isotopes for tracing of water mass transport and mixing within the oceans (Goldstein and Hemming, 2003). Although the Nd isotope ratios of water masses have been shown to persist over long transport paths within the oceans, sources and sinks are poorly constrained, leaving an unbalanced Nd budget for the ocean. For example, while Nd isotopic compositions in the deep oceans generally trace water mass mixing, Nd concentrations appear to be decoupled and this is known as the 'Nd Paradox'. The US GEOTRACES North Atlantic transects from Lisbon, Portugal via Mauritania and the Cape Verde Islands to Woods Hole, MA, USA (Figure 5.1) affords an excellent opportunity to study the Nd cycle because of the prevalence of multiple water masses in combination with different processes and environments that affect the sources and sinks of REEs, such as a pervasive oxygen minimum zone ***(OMZ)*** near Mauritania, major eolian deposition associated with the Saharan dust plume, continental margins, nepheloid layers and hydrothermal activities at the Mid Atlantic Ridge. Constraining the Nd cycle in the deep North Atlantic is of great importance because of the role of North Atlantic Deep Water (***NADW***) in contributing to deep waters to the world's ocean. Additionally, Southern Ocean-sourced waters (Antarctic Intermediate and Bottom Water) enter the North Atlantic, and transport their Nd isotopic signals into this basin. Finally, paleo-

circulation studies investigating the mixing of northern and southern-sourced water masses through time rely on understanding the behavior of Nd isotopes in the water column. This study aims to constrain the sources and sinks of Nd within the oceans by investigating the dissolved 'Nd composition' (which refers to its isotopic composition and concentration) of seawater along the US GEOTRACES zonal cruise track.

5.1.2 Nd isotopes in the global ocean

Nd isotope ratios vary in seawater as a reflection of the "crustal age" of terrigenous material that is weathered into the ocean basins (reviewed in Frank, 2002 and Goldstein and Hemming, 2003), whereby old continental crust has low values, and young mantle derived crust has high values (denoted by ε_{Nd}, which is the fractional deviation of the $^{143}Nd/^{144}Nd$ from the Chondritic Uniform Reservoir value of 0.512638 in parts per 10,000; Jacobsen and Wasserburg, 1980). Early work on Nd in seawater in the North Atlantic showed that waters have ε_{Nd} as low as -26.0 ± 0.4 in the Labrador Current and as high as -9.4 ± 0.4 in shallow (300 m) waters of the western basin, but concluded that NADW has an ε_{Nd} close to -13.5 (Piepgras and Wasserburg, 1980, 1987). Conversely, the North Pacific has the highest average ε_{Nd} values (-4 to 0, e.g. Piepgras and Wasserburg, 1980; Piepgras and Jacobsen, 1988; Shimizu et al., 1994), reflecting input of Nd from young mantle derived volcanic rocks surrounding the basin, and the Southern Ocean has intermediate values ($\varepsilon_{Nd} \approx -8$; e.g. Piepgras and Wasserburg 1982; Jeandel 1993, Stichel et al., 2012). The heterogeneous distribution of ε_{Nd} in the oceans reflects the estimated residence time of Nd (500-1500 years), on the same order as the ocean mixing time (e.g. Goldstein and O'Nions, 1981; Jeandel, 1993; 1995; Jeandel et al., 1998; Tachikawa et al., 1999; 2003; Bayon et al., 2004). ε_{Nd} can be used to effectively trace water masses within ocean basins

and has been shown to co-vary with other water mass tracers like salinity and silicate (e.g. Piepgras and Wasserburg, 1987; Jeandel, 1993; Blanckenburg, 1999). However, sources and sinks can influence the Nd concentration ***([Nd]***). That is, measured ε_{Nd} at any particular location could be a result of factors other than changes in water mass mixing such as dust input, submarine ground water discharge, interaction with shelf sediments and re-suspended sediments at depth (e.g. Lacan and Jeandel, 2005a,b; Johannesson and Burdige, 2007; Siddall et al., 2008; Arsouze et al., 2010; Chen et al., 2013). Finally, ε_{Nd} may be used as a paleoceanographic circulation tracer because bottom water ε_{Nd} is faithfully recorded in deep-sea iron-manganese oxides, first recognized in Fe-Mn nodules and crusts (O'Nions et al., 1978, Piepgras et al., 1979; Goldstein and O'Nions, 1981; Albarède and Goldstein, 1992). These studies paved the way for high temporal resolution studies of global thermohaline circulation on glacial-interglacial to sub-millennial time scales, based on deep sea sediment coatings, foraminifera and fish debris (e.g. Vance and Burton, 1999; Rutberg et al., 2000; Thomas et al., 2003; Thomas, 2004; Scher and Martin, 2004, 2008; Piotrowski et al., 2004, 2005, 2008, 2012; Vance et al., 2004; Gutjahr et al., 2008; 2010; Gourlan et al., 2008; Klevenz et al., 2008; Pahnke et al., 2008; Martin and Scher, 2006; Roberts et al. 2010, 2012; Gutjahr and Lippold, 2011; Wilson et al. 2012, Kraft et al., 2013; Pena et al., 2013; Pena and Goldstein, 2014).

5.1.3 North Atlantic Regional Circulation

The oceanographic circulation in the North Atlantic has been extensively reviewed and is only briefly introduced here (Figure 5.2; e.g. Schmitz and McCartney, 1993; Schmitz, 1996; Talley, 1996; van Aken, 2000, 2001). A summary of the temperature, salinity and neodymium properties of relevant water masses discussed in this study can be found in Table 5.1. The

shallow waters of the western North Atlantic are dominated by northward transport via the Gulf Stream from the Straits of Florida, which are successively transformed into cold, negatively buoyant water in the northern extents of the basin. These tropical sourced shallow waters sink and combine with intermediate depth waters to form North Atlantic Deep Water (***NADW***), which moves southward as a deep western boundary current transporting 17-18 Sv along the western edge of the basin and crosses the equator (Schmitz and McCartney, 1993). There are three principle cold-water masses that contribute to NADW (Figure 5.2). Labrador Sea Water (***LSW***) originates from the Labrador Sea and is comparatively warm and shallow, and spreads eastward into the Irminger and South Iceland basins where it intermingles with Iceland-Scotland Overflow Water (***ISOW***) and Denmark Strait Overflow Water (***DSOW***) from intermediate depths in the Greenland Sea. These overflow waters leave the subpolar basins to flow into the Labrador Sea as part of a deep northern boundary current flowing east to west (e.g. Schmitz and McCartney, 1993; Dickson and Brown, 1994). Another cold-water source in the North Atlantic is southern sourced Antarctic Bottom Water (***AABW***) of which 4-5 Sv crosses the equator, reaches the North Atlantic and upwells, contributing to the deep northern boundary current in the eastern portion of the basin (e.g. Schmitz and McCartney, 1993). Deep-water currents in the eastern basin are sluggish and predominantly made up of ISOW and LSW, and Mediterranean Outflow Water (***MOW***) (e.g. Dickson et al., 1985; van Aken, 2000). Additionally, southern sourced AABW is present along the eastern margin after entering the northeast Atlantic through the Vema Fracture Zone at 11°N (Arhan et al., 1994).

At intermediate depths in the Gulf of Cadiz, MOW overflows the Gibraltar Sill into the Atlantic at depths between 300 and 500m and has a distinct warm, saline signature. MOW deepens to ~1200m following the sill slope and is entrained in northward flowing currents. Some

MOW continues traveling north into polar seas while another portion flows westward between 25°N and 45°N and contributes to intermediate water masses there (Price et al., 1993; Reid 1994; Schmitz, 1996; Jenkins et al., 2014). Roughly 13 Sv of Antarctic Intermediate Water (***AAIW***) crosses the equator with 8 Sv converted to thermocline waters at 32°S and the remaining AAIW acting as "upper" intermediate water (Rintoul, 1991; Schmitz and McCartney, 1993). AAIW crosses the equator along both the western and eastern basins with modeling studies suggesting at least 3-4 Sv entering the eastern basin (Machín and Pelegrí, 2009). Surface currents in the study region are dominated by the subtropical gyre, which moves in a clockwise motion and may interchange water with subpolar gyres as well as tropical current systems. The subtropical gyre is flanked by the Gulf Stream on the western edge. The Gulf Stream is a dominant feature in the western basin and is composed of strong northward transport with multiple recirculating gyres (Schmitz, 1996).

5.1.4 Materials and Methods

Samples were collected aboard the R/V Knorr first during Leg 1 (KN199-4), completed November 2010, and during a second leg completed in December 2011 (KN204). Leg 1 spanned Portugal to the Cape Verde Islands and Leg 2 operated from Woods Hole, MA, to the Cape Verde Islands (Figure 1). From hereon, the prefix USGT10 and 11 indicate stations from Leg 1 and Leg 2, respectively. Both onboard and laboratory procedures were completed following quality control procedures consistent with the GEOTRACES intercalibration studies for Nd and REE (Pahnke et al., 2012; van de Flierdt et al., 2012). Twenty-two full water stations were sampled using a polyurethane powder-coated stainless steel rosette frame to minimize metallic contamination. The rosette is fitted with temperature and conductivity sensors, an SBE43 oxygen

sensor and a Seapoint STM turbidity sensor. Twenty-four 10L General Oceanics Niskin bottles with 0.25 mm think nylon-coated stainless steel springs and Viton O-rings at the end caps were attached to the rosette. Five liter-sized samples were collected from these bottles after being filtered through acid cleaned AcroPak500 (0.8/0.45μm) filter cartridges and collected into acid cleaned LDPE cubitainers. Three 5L samples were collected at each depth and reserved for Nd/REE analysis, thorium and protactinium analysis and archives. In preparation of storage, samples were acidified to pH <2 using ultra-clean 6N HCl and double-bagged.

The analyses of the collected seawater samples have been collaborative between three different laboratories. The samples were divided between Lamont-Doherty Earth Observatory ***(LDEO)***, University of Hawaii ***(UH)*** and University of South Carolina ***(USC)***. However, UH's USGT11 stations 4 (except samples 6469, 6470 and 6474) and 12 had to be purified and analyzed at University of Oldenburg (UO), using GEOTRACES protocols. At LDEO and USC an aliquot (200-500mL) was removed from the 5L samples for REE concentration analysis. Preconcentration of Nd and other REEs for KN199-4 (Leg 1) samples used the following procedure. A ^{150}Nd (at LDEO) or ^{146}Nd (at UH) spike was added, and the spiked samples were allowed to equilibrate for at least 24 hours. About 20mg of cleaned Fe was added, and the pH was then raised above 8.5 using ultra-clean NH_4OH, caused to co-precipitate Nd with FeOOH. The precipitate was left to settle for at least 4 days. The supernatant was siphoned away and the remaining precipitate was rinsed three times with Millipore water buffered to pH ~8. Samples were then transferred to a 15mL Teflon vial, dried and either 1mL 8N HNO_3 (LDEO) or 400μL aqua regia (UH) were added. Vials were capped and left on the hotplate at ~110 °C to break down organic compounds. At UH, samples were dried down and converted to Cl^- form after evaporation in lmL 6N HCl. At LDEO Fe(III) was reduced to Fe(II) with L-ascorbic acid and

then was immediately loaded onto 150µL Re-Spec resin for the separation of REEs from other major cations. At UH this separation was completed using a 1.5mL AG50W-8X Biorad resin bed (200-400µm).

Preconcentration of Nd and other REEs for all samples at USC, and KN204 (Leg 2) samples at LDEO, and Leg 2 stations 1, 4 and 12 at UH, used C-18 cartridges (Waters Inc.). They were loaded with the REE complexing agent bis (2-ethylexyl) hydrogen phosphate ***(HDEHP)*** modified after the procedure of Shabani et al. (1992). Using a peristaltic pump, seawater was pumped through rinsed cartridges at a flow rate of 20mL/min. Following the pumping of the 5L sample, the cartridges were washed with 5mL of 0.01N HCl to remove Ba. 35mL of 6N ultraclean HCl was then pumped through the cartridges at a flow rate of 10mL/min to elute REEs. At LDEO, the samples were loaded onto 150µL Re-Spec resin for the separation of REEs from remaining organics.

The isolation of Nd from REEs at UH for all samples from both Legs, and for all KN199-4 (Leg 1) samples at LDEO, as well as for KN204 samples with <10 ng Nd at LDEO, used 0.2 alpha-hydroxyisobuteric acid ***(alpha-hiba)*** adjusted to a pH of 4.5, on ~700µL of AG50W-X8 (200-400µm) resin. This separation is essential for analysis on the thermal ionization mass spectrometer ***(TIMS)***, because it allows effective isolation of Nd from interfering Pr ($^{141}Pr^{18}O^{+}$ interferes with $^{143}Nd^{16}O^{+}$). At USC, for all samples from both Legs, and at LDEO for Leg 2 KN204 samples with > 10ng Nd, and samples from stations 4 and 12 (Leg 2) from UH, the Nd was isolated using Eichrom LN-Spec resin, which elutes lighter REE first, in preparation for analysis by inductively coupled plasma mass spectrometry ***(ICPMS)***. A 2mL column of 50-100 µm resin was used at USC and pre-packed ~700uL columns of 100-150 µm resin were used at LDEO.

Each lab had its own measurement protocol, as explained below. All labs corrected for internal mass fractionation using $^{146}Nd/^{144}Nd$ =0.7219 and an exponential mass fractionation law. All corrected their final results using the value of $^{143}Nd/^{144}Nd$ = 0.512115 for the JNdi-1 Nd standard (Tanaka et al., 2000).

At UH (all samples) and LDEO (samples from both Legs KN199-4 and KN204 if they had Nd <10 ng) Nd was analyzed using a VG-Sector and VG-Sector54 TIMS, respectively. The samples were loaded with 1 µl 2N HCl on 1 µl silica gel as an activator on a Re filament and measured as NdO^+. At UH, the samples were run at 400 to 600 mV on $^{142}Nd^{16}O^+$ for 18 blocks with 21 ratios each in dynamic mode (3 cycles per ratio). Repeated measurements of both spiked and unspiked Nd standard JNdi-1 yielded $^{143}Nd/^{144}Nd$ = 0.512095±0.000012 (2σ, n = 29). The $^{143}Nd/^{144}Nd$ was corrected offline for oxygen isotopes and spike contributions. At LDEO, the samples were measured for 12 blocks (20 ratios each) with a controlled oxygen bleed into the source and a target intensity of ~300 mV on $^{144}Nd^{16}O^+$. The measurements were made during three intervals during which repeat measurements of the Nd standard JNdi-1 were $^{143}Nd/^{144}Nd$ = 0.512083±0.000015 (2σ, n = 31), $^{143}Nd/^{144}Nd$ = 0.512096±0.000015 (2σ, n = 29) and $^{143}Nd/^{144}Nd$ = 0.512083±0.000016 (2σ, n = 30).

Unspiked Nd isotope composition at USC, LDEO (Leg 2 KN204 >10 ng) and UO were measured on a ThermoScientific Neptune Plus multi-collector ICPMS. At USC, a JNdi-1 Nd standard was measured every four samples with an aiming intensity of 2.5 V on ^{145}Nd. The resulting average external error of $^{143}Nd/^{144}Nd$ was ±0.000022 (2σ, n = 53). At LDEO, a JNdi-1 standard was measured before and after every sample and for two analysis periods yielded $^{143}Nd/^{144}Nd$ = 0.512017±0.000013 (2σ, n = 36) and $^{143}Nd/^{144}Nd$ = 0.512036±0.000009 (2σ,

n = 47). UH's samples analyzed at UO yielded an average variation of JNdi-1 on $^{143}Nd/^{144}Nd$ of ±0.000012 (n = 33).

At UH and LDEO, Nd concentrations were determined by isotope dilution on the same samples measured for isotope ratios. At UH, spiking of 5 aliquots from one seawater sample (surface water near Oahu, HI) yielded an error of <2% (2σ) for [Nd]. Uncertainties in [Nd] at LDEO for seawater measurements are less than 3% (Pahnke et al. 2012). At USC, Nd concentration samples were processed according to the method developed by Antle (2013). To the samples, a precisely known amount of ^{145}Nd spike was added. Nd was pre-concentrated with 100 µl of cleaned Toyopearl AF Chelate 650 resin. After 24 hours the resin was washed with 1-2 ml of Millipore water, followed by 1 ml of single distilled 1M HNO_3 to elute and collect Nd. Once removed from the resin, this aliquot was directly analyzed using a ThermoScientific Element-2 ICP-MS. These samples were corrected for instrumental blanks, which accounted to up 0.8% of the overall intensities. Accuracy of the analysis was checked with a seawater sample from the North Pacific (SAFe), which yielded an average [Nd] of 47.55 pmol/kg ±3% (n=6) (within error equal to the published average value of two laboratories of 44.37 pmol/kg; Pahnke et al., 2012).

5.2 Results

5.2.1 Seawater measurements

The results of ε_{Nd} and [Nd] measurements on seawater samples collected in this chapter are summarized in Table 4.3 (pg. 125), and locations of stations are shown in Figure 5.1. Nd isotope compositions range from ε_{Nd} = -14.86 to -8.37. The highest ε_{Nd} values are recorded at stations USGT11-08 and 11-14 with ε_{Nd} = -8.8 and -8.37 respectively. These measurements are

surface samples from two open ocean sites in the western basin. The lowest ε_{Nd} values are measured at the westernmost station (USGT11-01) at depths of 663m and 964m with ε_{Nd} = -14.86 and -14.43 respectively. [Nd] measurements range from 12.3 pmol/kg to 36.7 pmol/kg. The lowest [Nd] values are 12.3 pmol/kg and 12.5 pmol/kg and are reported at station USGT10-05, an open ocean station in the eastern part of the basin, at depths 81 m and 31 m, respectively. The highest [Nd] values are recorded at stations closest to the north African coast and have values of 30.0 pmol/kg and 36.7 pmol/kg and USGT10-12 (890 m) and USGT10-09 (5 m), respectively. The next highest [Nd] values at stations for which data is reported, are for the open ocean site USGT11-10 near Bermuda where depths 4511 m and 4522 m have concentrations of 29.5 pmol/kg and 29.0 pmol/kg respectively.

The western basin stations are USGT11-01, -02, -03, -04, -06, -08, -10, -12 and -14 (Figure 5.1) and are fairly similar in their ε_{Nd} profiles (Figure 5.3a). The highest ε_{Nd} values for each profile in the western basin is seen at the surface and range between -10.5 and -8.4 with the exception of near shore Sta. USGT11-01, which has a surface value of -11.3. This station is at the very western extent of the section and very close to the North American coast in addition, these depths are also associated with water mass properties indicating a unique northern sourced water mass to be discussed further below. The lowest ε_{Nd} values at an open ocean site in the western basin are at station USGT11-04, depths 1790 m and 1191m where $\varepsilon_{Nd} \approx$ -14.0. Below ~2000 m, ε_{Nd} in the western basin is fairly homogenous with values ranging from ~ -13.6 to -12 (Figure 5.3a). [Nd] data in the western basin are limited to Sta. USGT11-01, -03, -08, -10 and -12. At Sta. USGT11-01 and 11-10, [Nd] reaches a maximum at depths below the water column oxygen minimum zone and is followed by a slight decrease. At USGT11-01 (near shore) [Nd] ranges from 19.8 pmol/kg at 660 m to 17.7 pmol/kg at 2077 m. USGT11-10 near Bermuda

(Bermuda Atlantic time-series (***BATS***)), on the other hand, shows a steady increase below 2500 m from ~17 pmol/kg to 29.5 pmol/kg (Figure 5.3b). In the western basin, nepheloid layers are detected as decreased transmittance at depth at Sta. USGT11-04, 11-08 and 11-10.

The eastern basin zonal transect is composed of the five open ocean stations USGT11-16, -18, -20, -22 and -24 and four Mauritania transect stations USGT10-09, -10, -11, -12. Station USGT11-24 is a crossover station with USGT10-12 at the Cape Verde Islands, located at the Tropical Eastern Atlantic Time-Series Observatory (TENATSO). Station GT10-09 is considered a near shore station because of due to its close proximity to the Mauritanian coast. The remaining stations discussed in this study follow a meridional transect between Mauritania and Lisbon, Portugal. These stations are three open ocean stations, USGT10-07, -05 and -03 and one near shore station GT10-01 off the coast of Portugal (Figure 5.1). The USGT10 eastern boundary stations are extensively addressed by Stichel et al. (2014) and only briefly reviewed here. The Mauritania transect stations between Mauritania and the Cape Verde Islands (USGT10-09, -10, -11, -12) are unique within the dataset and exhibit the lowest ε_{Nd} values at the surface, they show a shift to highest ε_{Nd} values in the chlorophyll max and a return to intermediate values at depths around 400 m. These features are associated with elevated [Nd] at the surface, a quick reduction in [Nd] within the chlorophyll max and elevated [Nd] at depths of ~400 m at the OMZ. ε_{Nd} is fairly uniform below ~ 400 m at GT10-10 and G10-11 with a ~4 pmol/kg increase of [Nd] to bottom depth (Figure 5.3e,f). ε_{Nd} is more variable in the water column at USGT10-12 and at near bottom depths at USGT10-09 (Figure 5.3e). The ε_{Nd} variability at depth at Sta. USGT10-09 is accompanied by a decrease in transmittance indicating increased particle load in the water column.

The remaining eastern basin stations (USGT10-01, -03, -07 and USGT11-16, -18, -20, -22, -24) exhibit high ε_{Nd} values in the surface waters and have less than 2 ε_{Nd} unit variability at depths >800 m, with the exception of GT10-01 (Figure 5.3c). At 500 m depth at USGT10-01 (near the coast of Portugal), ε_{Nd} deviates to a higher ε_{Nd} value of -10 before decreasing abruptly to -12 at 1800 m. This excursion coincides with a salinity maximum reflecting the presence of MOW. Surface waters at these stations show elevated [Nd] in comparison to a subsurface [Nd] minimum with the exception of stations USGT10-03, -05. At these open ocean sites between Portugal and Mauritania, a [Nd] minimum occurs at the surface. At depths below the [Nd] minimum, [Nd] increases to a local maximum at depths closely correlated with an oxygen minimum zone within the water column. At all stations east of USGT11-16 [Nd] increases between 1 and 11 pmol/kg between 1000 m and bottom depth (Figure 5.3d). This increase is generally more pronounced at intermediate depths and leads to slightly more uniform values several hundred meters from the seafloor. Sta. USGT11-16 is located at the Mid-Atlantic Ridge (***MAR***) and exhibits a decrease in [Nd] of ~3 pmol/kg between 2986 m and 3283m with a subsequent increase in to 21.6 pmol/kg at 3605m. The decrease in [Nd] at this site occurs along with a decrease in a transmittance reading as a result of the presence of a hydrothermal plume at the MAR.

5.2.2 Water mass mixing calculations

Nd compositions for each sample were calculated based on water mass mixing and are listed in Table 4.3. In order to evaluate the degree that Nd isotope ratios in the North Atlantic are (or are not) behaving conservatively with respect to mixing of source water masses, we have calculated the expected Nd isotopic compositions and Nd abundances of each sampled depth

based on the compositions of the contributing end-member water masses in two ways as reviewed in Chapter 4. The simplified calculation scheme, herein referred to as the ***T-S approach***, is applied to samples >1000 m only and uses the T-S compositions of samples to predict the fraction of different water mass end-members contributing to them. For each sample a different combination of three end-members are used to describe the mixture. The end-members are chosen based on the sample's T-S characteristics and their position in end-member mixing triangles using appropriate ε_{Nd} and [Nd] end-member values from the source regions. The fractions of each end-member in the samples are then used to calculate a predicted ε_{Nd} and [Nd] for each sample. The end-members used for this approach are North Atlantic Deep Water, 'Eastern' North Atlantic Deep Water, Antarctic Intermediate Water, Mediterranean Outflow Water, Irminger Sea Water, North Atlantic Central Water, Antarctic Bottom Water or 'Eastern' Antarctic Bottom Water as detailed in the supplement. The compositions of the end-members are summarized in Table 5.1. Our second calculation scheme uses the end-member water mass fractions calculated for each sample by Jenkins et al. (2014) using an Optimal MultiParameter Analysis ***(OMPA)*** study in order to calculate the predicted ε_{Nd} and [Nd] values for each sample. The compositions of the end-members used in this approach are summarized in Table 5.2.

In samples representing the maximum and minimum predicted ε_{Nd} values by the two approaches, there are significant differences between the approaches, sometimes of more than 1 ε_{Nd}-unit. However, the average calculated ε_{Nd} value for the *T-S approach* and OMPA are very similar with -12.1 ± 0.85 and -12.6 ± 1.0, respectively. The maximum ε_{Nd} value predicted by the *T-S approach* is -9.3, at open ocean Sta. GT10-07 (992 m depth) in the eastern basin, where OMPA predicts ε_{Nd} of -11.7 (Figure 5.4 and Figure 5.5). The minimum ε_{Nd} predicted by the *T-S approach* is -13.3 at Sta. GT11-10 (1197 m) near Bermuda, where OMPA predicts ε_{Nd} = -14.1.

The highest ε_{Nd} predicted by OMPA is -10.6, offshore of Portugal at Sta. GT10-01 (1186 m), where the *T-S approach* predicts a similar ε_{Nd} of -10.3. OMPA predicts a minimum ε_{Nd} value of -14.6 at western basin Sta. GT11-02 (1497 m) where the T-S approach predicts ε_{Nd} = -13.2. For both approaches, calculated ε_{Nd} is highest at shallow depths (~1000 m), decreases slightly with depth and is then fairly uniform at depths >2000 m with the exception of Sta. USGT11-08, -12 and -14, where deep samples show larger increases (up to 1.5 ε_{Nd} unit) from ~3000 m to bottom depth. The most distinct feature in calculated ε_{Nd} using the OMPA results is the predicted low ε_{Nd} water at intermediate depths (Figure 5.5). That is, at nearly every station, there is an excursion to less radiogenic values centered at ~1750 m depth, which it turns out, is associated with OMPA predicted presence of Upper Labrador Sea Water (***ULSW***) at these depths. Below depths of ~3000 m calculated ε_{Nd} is fairly uniform based on the OMPA results.

The calculated ε_{Nd} values for the *T-S approach* are offset between the western and eastern basin by ~ 1 ε_{Nd} unit with the eastern basin predicted to be more radiogenic as a result of the more radiogenic ENADW end-member used at these sites (Figure 5.4). A similar pattern is seen in the calculated ε_{Nd} values using OMPA although it is more constrains to the top 2000 m (Figure 5.5). Below 2000 m, OMPA predicts similar ε_{Nd} values in both the west and east. The average difference between the two calculations or $\Delta\varepsilon_{Nd}$-*calcs* ($\Delta\varepsilon_{Nd}$-*calcs* = $\varepsilon_{Nd\text{-}(T\text{-}S)} - \varepsilon_{Nd\text{-}(OMPA)}$) is ~ 1 ε_{Nd} unit (Figure 5.6). For this comparison we consider a difference >0.75 ε_{Nd} units to be of significance because it is higher than our analytical error (~ ±0.35 ε_{Nd} units). In the western basin, there is a positive 1 ε_{Nd} unit offset at depths between 1000 and 2000 m indicating that the *T-S approach* predicts a more radiogenic ε_{Nd} than OMPA at these depths (Figure 5.6). Also in the western basin, there is a negative offset between the two predictions at depths 3000 – 4500 m indicating that the *T-S approach* predicts a less radiogenic value than OMPA calculations

(Figure 5.6). In the eastern basin, the largest $\Delta\varepsilon_{Nd}$-*calcs* is at depths between 1000 and 2000 m. This offset is positive like in the western basin though larger (~2 ε_{Nd} units) and means that the *T-S approach* predicts a more radiogenic value than OMPA. At depths >2000 m there is no significant ε_{Nd} offset between the *T-S approach* and OMPA in the eastern basin.

For each approach, the predicted [Nd] values are similar and show no significant offset for any particular sample. The average calculated [Nd] for the *T-S approach* and OMPA results are comparable, 19.9 pmol/kg and 20.1 pmol/kg respectively. The highest [Nd] predicted by the *T-S approach* is 22.9 pmol/kg at Sta. USGT11-20 (5815 m). OMPA predicts a maximum [Nd] of 22.9pmol/kg at Sta. USGT11-22 (4969 m). The lowest predicted [Nd] for the *T-S approach* is 14.6 pmol/kg at Sta. USGT10-07 (992 m) in the eastern basin, where OMPA predicts [Nd] = 17.3 pmol/kg. OMPA predicts the lowest [Nd] along the Mauritania transect at Sta. USGT10-11 (1088 m) where [Nd] = 17.1 pmol/kg and the *T-S approach* predicts [Nd] = 15.3 pmol/kg. The lowest predicted [Nd] for each station is at the shallowest depth (~1000 m) and increases by ~1 pmol/kg for every increase in 250 m. The highest [Nd] is predicted for the deepest sample at every station using both water mass mixing approaches. The OMPA calculations have been applied to even shallow depths, and they show much more variability at depths < 900 m. The average offset between calculated [Nd] for both approaches is ~0.9 pmol/kg (Δ[Nd]-*calcs* = $[Nd]_{T\text{-}S\ approach} - [Nd]_{OMPA}$). For this study we consider Δ[Nd] > 3 pmol/kg to be significant, as this is nearly 15% of the average measured [Nd]. The highest Δ[Nd]-*calcs* is at 1000 m depth in the central Atlantic stations (~2.5 pmol/kg) and at 2000 m in the western basin (~2 pmol/kg) though neither of these offsets are significant (Figure 5.6).

We compare the measured and the predicted values and report them in a fashion similar to the comparison between two approaches for the calculated Nd-compositions. For each

predicted value, a $\Delta\varepsilon_{Nd}$ ($\Delta\varepsilon_{Nd} = \varepsilon_{Nd}$-*meas* – ε_{Nd}-*calc*) and Δ[Nd] (Δ[Nd] = [Nd]-*meas* – [Nd]-*calc*) was calculated (Figures 5.7, 5.8, 5.9, 5.10). The average $\Delta\varepsilon_{Nd}$ of the *T-S approach* and *OMPA* are -0.06 ε_{Nd} units and +0.32 ε_{Nd} units respectively. The average Δ[Nd] for the *T-S approach* and OMPA calculations are +0.84 pmol/kg and +1.0 pmol/kg respectively. We consider $\Delta\varepsilon_{Nd}$ of more than 0.75 ε_{Nd} units to be significant as in the above comparisons and to represent regions where Nd-isotopes are not behaving conservatively. Δ[Nd] greater than 3 pmol/kg is considered to be significant and represents regions where Nd concentrations do not behave conservatively.

5.3 Discussion

5.3.1 Using Nd isotopes to trace water masses in the North Atlantic Ocean

In order to evaluate the degree that Nd behaves conservatively in the North Atlantic, we compare measured and calculated ε_{Nd} and [Nd] within the water column, and we consider that the smaller the difference between the two values, the closer the system approaches conservative behavior, keeping in mind the uncertainties resulting from choosing the hydrographic end-members for OMPA (Jenkins et al., 2014) and the ε_{Nd} and [Nd] end-members for the calculation of predicted Nd compositions. The difference between predicted and measured ε_{Nd} and [Nd] are denoted as $\Delta\varepsilon_{Nd}$ and Δ[Nd] respectively where Δ = measured value – calculated value. Across the study region, the $\Delta\varepsilon_{Nd}$ of the *T-S approach* at the open ocean sites at depths >1000m ranges between -0.9 and +0.9, with the exception of stations GT11-12 and -14 at 2000-3500m water depth in the western Atlantic where the measured ε_{Nd} value is around ~1.5 ε_{Nd} units more positive than the predicted value (Figure 5.7). The general absence of a significant offset (>0.75 ε_{Nd} unit) between these predicted and observed values at depths > 1000m in the North Atlantic

suggests that the ε_{Nd} distribution can be predicted based on "simple mixing" alone and the water masses are effectively traced by ε_{Nd} (Figure 5.7).

Calculated ε_{Nd} based on OMPA results exhibit higher $\Delta\varepsilon_{Nd}$ than the offset predicted by the *T-S approach* in some cases (Figure 5.8). At intermediate depths (1000 and 2000 m) in the central North Atlantic, OMPA yields ε_{Nd} of about 1.5 units lower. At some near bottom samples, and intermediate depths in the eastern basin most strongly influenced by MOW, the measured ε_{Nd} is more negative than the predicted values. Additionally, measured values are lower than those predicted by ~2 ε_{Nd} units within the eastern basin OMZ (Figure 5.8).

In comparing measured and calculated [Nd] (Figures 5.9, 5.10), agreement is best at intermediate depths at open basin stations. There is a positive offset in the deepest samples, indicating an excess in [Nd] compared to the water mass mixing predictions. This feature is known as the 'Nd-Paradox' and is seen in all of the world's oceans (e.g. Goldstein and Hemming, 2003). This feature resembles nutrient like distributions and has been suggested to be a result of reversible scavenging within the water column (e.g. Siddall et al., 2008; Arsouze et al., 2010; Chen et al., 2013). Observed [Nd] is lower than predicted for surface samples using OMPA results, where scavenging of REEs by lithogenic and biogenic particles likely contributes to the observed deficit compared to the predictions. This depletion of [Nd] at the surface has been previously seen in the North Atlantic and in other parts of the oceans (e.g. Jeandel et al., 1995; Rickli et al., 2010; Stichel, et al., 2014) and is discussed further below. Additionally, observed [Nd] is higher than predicted by both the *T-S approach* and OMPA calculations at USGT11-08 and -10 in the western basin below 4000 m depth and is likely to be higher at other stations though limited [Nd] is available.

At Sta. USGT11-01, increased observed [Nd] between 600 and 950 m (Figure 5.3b) is associated with the presence of the northern sourced water mass ULSW, which has [Nd] of 21.5 pmol/kg. Based on OMPA results, this parcel of water is defined as 80% ULSW (Jenkins et al., 2014). Predicted [Nd] based on both approaches (T-S and OMPA) are consistent with the observed Nd concentrations (Figs. 5.9, 5.10). The measured ε_{Nd} values of waters are low at Sta. USGT11-01 to USGT11-10 (BATS) between ~1000m and 2000m depth, ranging from -14.1 to -13.7, and are likely a result of the contributions from ULSW (Figure 5.11). The ε_{Nd} of ULSW is unradiogenic (-15.0) and OMPA predicts ULSW is responsible for up to 90% of the water samples' composition at USGT11-01, consistent with the low measured ε_{Nd} value. As you move east across the section, ULSW continues to contribute to mixing, with increasing influence of other northern sourced, unradiogenic end-members, ISW (-13.3) and Central Labrador Sea Water (***CLSW***) (-13.5). At Sta. USGT11-10, water at ~1000 m depth is nearly 60% ISW. Pahnke et al., (2012) described the low ε_{Nd} waters at this depth at Sta. USGT11-10 as Upper NADW (ε_{Nd} = -13.5) and it is comparable to the CLSW defined here. This negative ε_{Nd} excursion in the western basin is also associated with a CFC-11 concentration maximum, indicating recently ventilated waters (Figure 5.11; Smethie, unpublished data). In this study, the ε_{Nd} signature of ULSW in the source region is defined as -15.0 whereas CLSW is defined as -13.5 (Table 5.2; Lacan and Jeandel, 2005a). There is no evidence in T-S data for pure ULSW reaching this region and accordingly, no ε_{Nd} signature is as negative as -15.0. At the greatest contributions of ULSW (80-82%) in this region, calculated ε_{Nd} based on OMPA contributions are between -14.6 and -14.4. Measured ε_{Nd} values at Sta. USGT11-01 (closest to the margin) at 600-900m depth are the lowest values measured in this study and are ~ -14.3, showing good agreement with predicted ε_{Nd}. This agreement suggests that closest to the western boundary, Nd is behaving as a

conservative tracer in this region and northern component waters preserve their ε_{Nd} while traveling southward. At open ocean sites in the western basin between 1000 and 2000 m (GT11-08, -10, -12, -14), the contribution of ULSW predicts a low ε_{Nd} value resulting in a positive $\Delta\varepsilon_{Nd\text{-}OMPA}$ and our *T-S approach* calculations more accurately predict the measured ε_{Nd} value at these intermediate depths (Figure 5.7). The Nd isotopic composition of these sites can thus be predicted based on the "simple water mass mixing" alone. However, these are cases where OMPA concludes there are several end-member water masses, such as ISW, ULSW and CLSW, which cannot be resolved in *T-S approach* predictions.

Southern sourced water masses have modified T and S properties by the time they enter the North Atlantic and the *T-S approach* uses "modified" end-member values compared to their "pristine" T-S-Nd values in the high latitude Southern Hemisphere source regions. The modified end-member values we use for the T-S approach are those observed near the equator as these water masses approach the North Atlantic (Table 5.1). Regions with good agreement between measured and calculated Nd properties indicate minimal influence of external sources or sinks besides water mass mixing. The OMPA results indicate that the areas strongly influenced by southern sourced AABW are deep waters >3500m across the region, and those strongly influenced by AAIW are between 800-1500m depth from the central North Atlantic (Sta. USGT11-14) to the Mauritania coast, and as far north as Sta. USGT10-05 in the northwestern basin (Jenkins et al., 2014). The offset between measured and calculated ε_{Nd} for the OMPA approach is near zero in these regions, indicating that ε_{Nd} effectively traces mixing of AAIW and AABW with the North Atlantic waters (Figure 5.8). The exception for the *T-S approach* is in the Iberia-Mauritania transect in the eastern basin where waters at ~1000 m depth at Sta. USGT10-01, 10-03 and 10-05 have a $\Delta\varepsilon_{Nd}$ value close to -2 ε_{Nd} units, thus measured values are more

negative than those predicted from water mass mixing (Figure 5.7). This offset might reflect an overestimate of the influence of MOW on ε_{Nd}, or addition of some external Nd in this region. Comparing measured ε_{Nd} and values predicted by OMPA also indicates conservative behavior of ε_{Nd} in the deep basin, with the largest deviation of $\Delta\varepsilon_{Nd} = -1$ occurring in the far western portion of the section, thus indicating that the OMPA model accounts well for mixing of AABW with the North Atlantic waters. At intermediate depths, the offset between measured and OMPA-derived ε_{Nd} is ~ +1.5 ε_{Nd} units between 1000 and 2000m across the entire section. It is unclear whether or not this signal is a result of some nonconservative behavior of Nd-isotopes or a result of incorrect assignment of ε_{Nd} in end-member water masses; as previously discussed, the OMPA-derived water mass mixture includes a large component of ULSW at these depths, which would contribute a very strong unradiogenic ε_{Nd} signal that could be the cause of this offset.

5.3.2 Sensitivity of water mass mixing calculations to end-member compositions

The end-member ε_{Nd} compositions used in the water mass mixing calculations are averages of available data within the water mass source regions; they are listed in Tables 5.1 and 5.2 and the assignment of compositions is discussed in Chapter 4 of this dissertation. Because some of these compositions are based on limited data, in some cases the ε_{Nd}-values are not tightly constrained. It is therefore important to test the sensitivity of our calculated ε_{Nd} to small changes in end-member ε_{Nd} compositions, in order to evaluate the significance of the calculated ε_{Nd} compositions and consequently significance of any offsets between measured and calculated ε_{Nd}. For this study we apply this test to two northern-sourced end-members in order to explain two anomalies in the $\Delta\varepsilon_{Nd}$ dataset identified in the previous section; we adjust the ε_{Nd} of the NADW end-member in the western basin in order to explain the anomaly observed between

2000 and 4000m at Sta. USGT11-12 and -14 (Figure 5.7), and the ULSW ε_{Nd} in the OMPA results to investigate the positive $\Delta\varepsilon_{Nd}$ anomaly at ~1750m across the section (Figure 5.8).

In the *T-S Approach*, there is a positive anomaly of >1 ε_{Nd} units at Sta. USGT11-12 and USGT11-14 between depths 2000 and 4000m. For these depths, two different three-component mixtures are used to predict the ε_{Nd} of these waters. NADW is used in both of these calculations (with the value of ε_{Nd} = -13.25). Because this anomaly is not evident in the $\Delta\varepsilon_{Nd}$ dataset derived from OMPA, we suspect that our use of only one northern-sourced water mass (i.e. NADW) fails to correctly characterize the water masses contributing to mixing in this area. In contrast, OMPA uses four northern sourced water masses to predict mixing in this area and in particular uses DSOW and ISOW. These two water masses are defined by ε_{Nd} of -10.6 and -11.4 for DSOW and ISOW respectively, (Table 5.2) which are more radiogenic than the NADW end-member and would appropriately explain the more positive measured ε_{Nd} of the seawater. In order to test whether our ε_{Nd}-value for NADW here should be more positive, we adjusted it in the western basin to values between -13.5 and -12.0 for repeat calculations (Figure 5.12). This range for the ε_{Nd} of NADW is reasonable based on the available data (-13.6 to -12.0; see also Chapter 4). A value of ε_{Nd} = -13.25 represents the original calculation and predicts a >1 ε_{Nd} unit offset between measured and calculated ε_{Nd} within the region. By decreasing NADW ε_{Nd} to -13.5, as expected the anomaly is intensified within this region and there is an additional positive offset in $\Delta\varepsilon_{Nd}$ seen at ~3000m at Sta. USGT11-08 near the western part of the basin. By increasing the NADW ε_{Nd} to -13.0, the anomaly is reduced to <1 ε_{Nd} unit at GT11-12 and is only slightly higher than 1 ε_{Nd} unit at two sample depths at Sta. USGT11-14. Throughout the rest of the western basin, $\Delta\varepsilon_{Nd}$ equals nearly zero and suggests no significant offset between measured and calculated ε_{Nd}, and therefore conservative behavior of Nd. Increasing the NADW ε_{Nd} to -12.0 reduces $\Delta\varepsilon_{Nd}$ to ~ 0 at

the depths of the anomaly at Sta. USGT-11-12 and -14 but introduces negative offsets at shallower and deeper depths of Sta. USGT11-12 and -14 and at the more western stations in the basin (Figure 5.12). Using a NADW ε_{Nd} composition of -12.0 poorly defines mixing in the western basin and at deep and intermediate depths in the central Atlantic.

Between 1000m and 2000m near the western boundary and between 1800 and 2000m in the eastern basin measured values are significantly higher than predicted values ($\Delta\varepsilon_{Nd} = 2$) using OMPA water mass fractions and our end-members (Figure 5.8). This feature coincides with the highest mixing fractions of ULSW and may be a reflection of the unradiogenic value assigned to this end-member ($\varepsilon_{Nd} = -15.0$). Our sensitivity test here varies the ε_{Nd} of ULSW at 0.25 increments between -15.0 and -14.0 (Figure 5.13; see also Chapter 4). By adjusting the ε_{Nd} of ULSW to -14.75, the $\Delta\varepsilon_{Nd}$ within the western basin (Sta. USGT11-01 to -10) is reduced to < 0.75, suggesting conservative behavior at intermediate depths in this region. This is a minor shift in end-member composition but has a considerable influence on calculated ε_{Nd}. Adjusting the end-member composition to -14.5 further reduces the $\Delta\varepsilon_{Nd}$ within the western basin such that USGT11-12 and -14 show no offset between measured and calculated ε_{Nd} with the exception of a few outliers (USGT11-12, ~500 m and ~2000m). The trend continues when ULSW is assigned $\varepsilon_{Nd} = -14.25$, and additionally, the positive anomaly is reduced at stations in the eastern portion of the basin as well. When ULSW is assigned $\varepsilon_{Nd} = -14$, the $\Delta\varepsilon_{Nd}$ positive anomaly is limited to the OMZ off the Mauritania coast (Figure 5.13). Moreover, these increases in the ε_{Nd} of ULSW produce no additional offsets elsewhere in the water column. These tests show that offsets between measured and calculated ε_{Nd} may be a result of poorly constrained end-member compositions, and do not necessarily imply additional sources or sinks of Nd, leading to non-conservative behavior in the oceans.

5.3.3 Modeling the eastern basin Nd distribution

The dataset comprised of Sta. USGT10-01, -03, -05, -07, -09, -10, -11, and -12, from Iberia to Mauritania to the Cape Verde Islands (Figure 5.1) is discussed in detail in a study that focuses on processes influencing Nd distribution in the eastern basin (Stichel et al., 2014). We can further investigate the eastern basin features by comparing measured [Nd] and ε_{Nd} values with those predicted from the water mass mixing calculations in this study. A distinct water mass in this region is MOW and is traced as salinity maximum as far south as USGT10-05. As discussed in Stichel et al. (2014), evidence for this water mass in the Nd data may be compromised due to scavenging of Nd during the outflow of MOW into the Atlantic. Our calculations support these findings, predicting more radiogenic ε_{Nd} than the measured values at intermediate depths, as a result of the influence of MOW, at USGT10-01, 10-03 and 10-05 (Figure 5.7). In both water mass mixing approaches, the entire water column is shown to be influenced by MOW at these stations, but the largest ε_{Nd} offset is seen at intermediate depths (~1000 m; Figure 5.7 and 5.8). There is good agreement at depths > 2500 m for ε_{Nd} but greater offset in [Nd] at depths >4000 m (Figures 5.9 and 5.10).

At Sta. USGT10-07 just north of the Mauritanian transect, and for stations along the Mauritanian transect (USGT10-09, -10, -11, and -12), the *T-S approach* predicted ε_{Nd} values within 0.75 ε_{Nd} unit of measured ε_{Nd} values. The predicted ε_{Nd} derived from OMPA, however, show a larger offset at intermediate depths and measured values are more radiogenic than predicted. This feature, centered around 1750m, is a result of the influence of the ULSW end-member in OMPA calculations, which has an unradiogenic signature as already discussed. The *T-S approach* calculations do not take into account this water mass in the Eastern Basin and

show better agreement with measured data. Based on this agreement, we expect Nd to behave conservatively in this region and predict that ULSW is either not the dominant water mass contributing to the T-S composition of this region as suggested by OMPA results or has a poorly defined Nd composition. An exception to the general agreement seen with the *T-S approach* mixing calculations is at Sta. USGT10-12, near the Cape Verde Islands, which shows higher measured ε_{Nd} of as much as 1.5 ε_{Nd} units. We conclude that this offset is a regional feature and a result of the influence of the volcanic Cape Verde Islands. Crossover Sta. USGT11-24 (same location as USGT10-12) shows a similar result in the deepest depth sample but smaller $\Delta\varepsilon_{Nd}$ in the rest of water column.

Along this same Iberia to Cape Verde transect, [Nd] is predicted well by both approaches at depths < 4000 m, with the exception of Sta. USGT10-09. At this site, the closest to the African margin, measured [Nd] is higher than predicted values at depths > 1500 m. Δ[Nd] derived from the *T-S approach* is greater than 5 pmol/kg and ~ 3 pmol/kg in OMPA derived predictions. In this profile, it is likely that the proximity to shelf sediments has contributed to [Nd] within the water column while only slightly influencing ε_{Nd}, which is predicted well by the *T-S approach* ($\Delta\varepsilon_{Nd}$ < 1). These observations support the conclusion (Stichel et al., 2014) that [Nd] at USGT10-09 is influenced by interaction with lithogenic-sourced material in this region (Figure 5.9 and Figure 5.10).

Intermediate depths have elevated measured [Nd] within the OMZ in the eastern portion of the basin compared to both *T-S approach* and OMPA derived water mass mixing calculations, suggesting that the [Nd] maximum reflects addition of external Nd. The reducing conditions at these depths are likely contributing to the remobilization of Nd that was scavenged in the surface waters (Stichel et al., 2014). The OMPA derived calculated ε_{Nd} shows a positive (2 ε_{Nd} unit)

anomaly within the OMZ. While increasing our end-member ε_{Nd} value for ULSW reduced this anomaly within the OMZ, it did not eliminate it. Thus, the multicomponent OMPA calculation indicates that there is addition of external Nd with higher ε_{Nd} in this region. On the other hand, based on the *T-S approach* calculation, $\Delta\varepsilon_{Nd}$ is near zero despite the release of Nd at these depths, suggesting that the OMZ feature does not significantly impact the ε_{Nd} of water masses in this region (for a detailed discussion of the OMZ see Stichel et al., 2014).

5.3.4 Near surface waters

The lowest measured [Nd] is seen in the surface waters (0-500 m) throughout the cruise section, with the exception of the Mauritania transect below the Saharan dust plume, which shows elevated surface [Nd] as a result of dust input (Rickli et al., 2010; Stichel et al., 2014). Low surface [Nd] at stations away from Mauritania is accompanied by high ε_{Nd} values between -9.0 and -10.0 at these same depths. These characteristics are consistent with the composition of central and gyre waters that are low in [Nd] and have a more radiogenic value than NADW, ISW, ULSW and CLSW (e.g. Piepgras and Wasserburg, 1982; Lacan and Jeandel 2005a,b; Pahnke et al., 2012; Stichel et al., 2014). Our *T-S approach* calculations exclude surface waters, but the OMPA results consider the water mass mixing compositions at all depths and therefore can be used here to assess the conservative behavior of Nd near the surface. Figures 5.8 and 5.10 show the offset of the measured values of ε_{Nd} and [Nd] in comparison to the predicted values using OMPA results. Measured ε_{Nd} is within 0.75 ε_{Nd} unit of the predicted values in the western basin but is slightly higher than predicted. Measured [Nd] is lower than predicted in these surface waters, indicating scavenging. It has been suggested that Nd cycling in the western basin, like the eastern basin, is strongly influenced by the deposition and dissolution of eolian particles from the

Saharan dust plume (Jeandel et al., 1995). However, in our dataset, there is no clear evidence for large supply of Nd from Saharan dust in the western and northeastern basin, rather the data suggest scavenging of Nd.

5.3.5 Nepheloid layers

Along the cruise track, there are several key regions for the study of Nd particle-seawater exchange that could influence this tracer's conservative behavior in seawater. Benthic nepheloid layers (***BNL***) are near bottom regions of increased suspended particle load where REEs potentially exchange with surrounding seawater (e.g. Pahnke et al., 2012; Grenier et al., 2013). Within the study area, nepheloid layers were detected at several stations using transmissometer data. As already noted, the station closest to Mauritania, Sta. USGT10-09, has a nepheloid layer at ~2800 m that locally influences the deep ε_{Nd} signature (Stichel et al., 2014), such that lithogenic material from the shelf sinks and is resuspended at depth, with exchange resulting in an excursion to less radiogenic ε_{Nd} of seawater within the nepheloid layer. The deep [Nd] max at Sta. USGT10-09 is comparable to nearby stations where no nepheloid layer is present and thus suggests limited influence on [Nd]. Water mass mixing calculations in this region can reveal whether or not the behavior of ε_{Nd} and [Nd] within the nepheloid layer represents local inputs or sinks. As discussed above, both the *T-S approach* and OMPA derived [Nd] show good agreement (<15% offset) with measured values. Although there is an unradiogenic influence on measured ε_{Nd} within the nepheloid layer, the offset between measured and calculated ε_{Nd} is still less than 0.75 ε_{Nd} unit (Figure 5.7 and Figure 5.8). This agreement indicates that any change in ε_{Nd} from interactions with nepheloid layers cannot be distinguished from water mass mixing.

The deep western basin has BNL along the continental margin at Sta. USGT11-04, 11-08 and 11-10. Previous studies have concluded that the influence of this nepheloid layer on the deep ocean Nd cycle has only small regional influence (Piepgras and Wasserburg, 1987, Jones, 2010). Results indicate near zero change in measured ε_{Nd} between intermediate depths and depths associated with nepheloid layers at Sta. USGT11-04 (3290 m to 3770 m), Sta. USGT11-08 (4550 m and 4880 m) and Sta. USGT11-10 (4170 m to 4550 m). In order to distinguish any influence of the nepheloid layer on the Nd compositions, we again compare our calculations with our measurements. In contrast to the eastern basin nepheloid layer, there is a larger offset between measured and calculated [Nd] at depths >4000 m at Sta. USGT11-08 and -10 (Figure 5.9 and 5.10). At this location measured [Nd] is higher than the calculated [Nd] by nearly 30% using both the *T-S approach* and OMPA. This excess is nearly twice the offset in the rest of the deep basin, and indicates that there is an additional source of Nd to this region. The transmittance data of the nepheloid layer in this region suggests the particle load is large in comparison to the Sta. USGT10-09 feature in the eastern basin and could be an explanation as to why it is a source of Nd. Additionally, the particles within the western basin nepheloid layers show much less excess Fe in comparison with the USGT10-09 BNL, which could shed light on to the differing behavior of Nd at these two sites (Ohnemus, 2014). Within the eastern BNL, there is evidence for precipitation of Fe and Mn oxides near the sediment-water interface that could be a sink for dissolved Nd in these deep waters. This is in direct contrast to the western boundary where there is no evidence for authigenic oxide formation. Nevertheless, despite the influx of Nd in the deep western boundary, measured ε_{Nd} agrees well with calculated ε_{Nd}, with the offset slightly larger (~1 ε_{Nd} unit) using OMPA results (Figure 5.8). The offset between measured and calculated [Nd], while at the same time there is little offset in ε_{Nd}, may be a reflection of two features: (1)

the Nd sourced from the deep sediments have ε_{Nd} signatures similar to the deep-water masses in this region, or (2) the extra Nd is not coming from the nepheloid layers, although the coincidence of the high [Nd] samples with the nepheloid layers strongly indicate a relationship. While the ε_{Nd}-values of bulk terrigenous material in this region are too negative to be the source for the extra dissolved Nd in this region, the sediment phase available for exchange with seawater has yet to be constrained (Jones, 2010), and it is possible that the extra Nd is redissolved from authigenic phases that previously precipitated from the deep water and thus has the same ε_{Nd} as the deep water..

5.3.6 Nd cycling at the mid-ocean ridge

Sta. USGT11-16 is the Trans-Atlantic Geotraverse (***TAG***) hydrothermal location on the Mid-Atlantic Ridge, where a decrease in optical transmittance, representing increased suspended particle load, was detected between ~3200-3400m. Previous studies have been inconclusive on the influence of hydrothermal input to the Nd cycle in the ocean. Most have concluded that it has negligible impact, and that increased particle load makes hydrothermal sites a Nd sink (e.g. Michard et al., 1983; Piepgras and Wasserburg, 1985; German et al., 1990; Jeandel et al., 2013). Additionally, it has been difficult to determine whether hydrothermal processes influence the ε_{Nd} of nearby waters. A recently proposed mechanism, referred to as 'Ridge exchange', has been described as a means to influence the ε_{Nd} of water masses, with the addition of very positive ε_{Nd} from ocean ridges, despite rapid scavenging during the precipitation of Fe and Mn oxides (Jeandel et al., 2013). The role of hydrothermal sites in the Nd cycle can be further investigated using the mid-ocean ridge data collected as part of this study (Figure 5.14).

Directly above the TAG plume at Sta. USGT11-16 at 2986m, where there is no decrease of optical transmittance and thus no sign of the hydrothermal plume, the Nd is defined by ε_{Nd} = -12.09 ± 0.36 and [Nd] = 19.6 pmol/kg. At the top of the plume and the first sign of decreased optical transmittance, at 3183m depth, there is a shift in ε_{Nd} to -11.43 ±0.24 and [Nd] = 18.5 pmol/kg. Within the plume, to 3383m depth, ε_{Nd} stays constant at -11.71 ±0.24 and [Nd] = 18.8 pmol/kg. Below the plume, ε_{Nd} remains constant at -11.9 ±0.24 and [Nd] increases to 21.36 pmol/kg (Figure 5.14). At this site, both ε_{Nd} and [Nd] appear to be responding to the presence of hydrothermal fluids, because the positive shift in ε_{Nd} is consistent with some contribution from hydrothermal fluids that have come into contact with ocean ridge basalt and the decrease of [Nd] is consistent with scavenging of Nd by precipitating Fe-Mn oxides. It remains to be seen if exchange in these environments is significant enough to influence basin wide water mass compositions.

In order to gauge the influence of the TAG plume, we can use the calculated ε_{Nd} and [Nd] derived from water mass mixing calculations. At the depth range of the decrease in [Nd], there is a deficit on the order of ~13% and 12% compared to predictions of the *T-S approach* and OMPA, respectively, and this deficit in [Nd] likely represents scavenging of Nd within the TAG plume. In terms of the ε_{Nd}, the offset within the plume is <0.5 ε_{Nd} units, indicating only a small impact (if any) of the hydrothermal plume. We conclude therefore that although there is a radiogenic excursion of ε_{Nd} within and below the TAG plume, the $\Delta\varepsilon_{Nd}$ is small and this feature is not significant enough to influence the Nd signature of waters moving through this area.

5.4 Conclusions

The GEOTRACES North Atlantic Zonal transect presents an optimal study area for investigating Nd cycling within the oceans. Multiple water masses are sampled along the cruise track and provide an opportunity to evaluate the ε_{Nd} and [Nd] of North Atlantic water masses as they interact with additional sources and sinks of Nd. For surface and mixed layer samples where water mass mixing and biological and particle effects are complex, predicting the ε_{Nd} and [Nd] can shed light on how these processes impact the Nd cycle. The study also shows that small changes in the ε_{Nd} used to define end-member water masses can have a significant influence on the predicted ε_{Nd} composition based on water mass mixing. The data show that generally the ε_{Nd} and [Nd] compositions of intermediate and deep open ocean sites can be faithfully predicted based on water mass mixing calculations alone. Exceptions to these observations occur at deep ocean sites where calculated [Nd] is much higher than measured and in the presence of nepheloid layers in the western basin where ε_{Nd} is more positive than expected from deep water masses at these depths.

5.5 References

Albarède, F., and S. L. Goldstein. "World map of Nd isotopes in sea-floor ferromanganese deposits." *Geology* 20.8 (1992): 761-763.

Antle, R. "Tidal Flux of Transition Metals and Rare Earth Elements From A Barrier Island Salt Marsh." (2013).

Arhan, M., et al. "The eastern boundary of the subtropical North Atlantic." *Journal of Physical Oceanography* 24.6 (1994): 1295-1316.

Arsouze, T., et al. "Modeling the Nd isotopic composition in the North Atlantic basin using an eddy-permitting model." *Ocean Science* 6.3 (2010): 789-797.

Bayon, G., et al. "Sedimentary Fe–Mn oxyhydroxides as paleoceanographic archives and the role of aeolian flux in regulating oceanic dissolved REE." *Earth and Planetary Science Letters* 224.3 (2004): 477-492.

Bertram, C. J., and H. Elderfield. "The geochemical balance of the rare earth elements and neodymium isotopes in the oceans." *Geochimica et Cosmochimica Acta* 57.9 (1993): 1957-1986.

Chen, T., et al. "Upper Ocean Vertical Supply: A Neglected Primary Factor Controlling the Distribution of Neodymium Concentrations of Open Ocean Surface Waters?: Surface Seawater Neodymium Concentrations." *Journal of Geophysical Research: Oceans* 118, no. 8 (August 2013): 3887–94.

Dickson, R. R., et al. "Estimates of the mean circulation in the deep (> 2,000 m) layer of the Eastern North Atlantic." *Progress in Oceanography* 14 (1985): 103-127.

Dickson, R. R., et al. "The Production of North Atlantic Deep Water: Sources, Rates, and Pathways." *Journal of Geophysical Research: Oceans (1978–2012)* 99, no. C6 (1994): 12319–41.

Frank, M. "Radiogenic Isotopes: Tracers of Past Ocean Circulation and Erosional Input." *Reviews of Geophysics* 40, no. 1 (2002).

German, C. R., et al. "Hydrothermal scavenging of rare-earth elements in the ocean." *Nature* 345.6275 (1990): 516-518.

Goldstein, S. L., and R. K. O'Nions. "Nd and Sr isotopic relationships in pelagic clays and ferromanganese deposits." (1981): 324-327.

Goldstein, S. L., and S. R. Hemming. "6.17. Long-lived isotopic tracers in oceanography, paleoceanography and ice-sheet dynamics." *Treatise on Geochemistry: The Oceans and Marine Geochemistry* 6 (2004): 453.

Gourlan, A. T., et al. "Tectonically driven changes in the Indian Ocean circulation over the last 25 Ma: Neodymium isotope evidence." *Earth and Planetary Science Letters* 267.1 (2008): 353-364.

Grenier, M., et al. "From the subtropics to the central equatorial Pacific Ocean: Neodymium isotopic composition and rare earth element concentration variations." *Journal of Geophysical Research: Oceans* 118.2 (2013): 592-618.

Gutjahr, M., and Jörg Lippold. "Early arrival of Southern Source Water in the deep North Atlantic prior to Heinrich event 2." *Paleoceanography* 26.2 (2011).

Gutjahr, M., et al. "Changes in North Atlantic Deep Water strength and bottom water masses during Marine Isotope Stage 3 (45–35kaBP)." *Quaternary Science Reviews* 29.19 (2010): 2451-2461.

Gutjahr, M., et al. "Tracing the Nd isotope evolution of North Atlantic deep and intermediate waters in the Western North Atlantic since the Last Glacial Maximum from Blake Ridge sediments." *Earth and Planetary Science Letters* 266.1 (2008): 61-77.

Jacobsen, S. B., and G. J. Wasserburg. "Sm-Nd isotopic evolution of chondrites." *Earth and Planetary Science Letters* 50.1 (1980): 139-155.

Jeandel, C. "Concentration and isotopic composition of Nd in the South Atlantic Ocean." *Earth and Planetary Science Letters* 117.3 (1993): 581-591.

Jeandel, C., et al. "Exchange of neodymium and its isotopes between seawater and small and large particles in the Sargasso Sea." *Geochimica et Cosmochimica Acta* 59.3 (1995): 535-547.

Jeandel, C., et al. "Rare Earth Element Concentrations and Nd Isotopes in the Southeast Pacific Ocean: REE and Nd isotopes in the southeast Pacific." *Geochemistry, Geophysics, Geosystems* 14, no. 2 (February 2013): 328–41.

Jenkins, W. J., et al. "Water mass analysis for the US GEOTRACES (GA03) North Atlantic sections." *Deep Sea Research Part II: Topical Studies in Oceanography* (2014).

Johannesson, K. H., and D. J. Burdige. "Balancing the global oceanic neodymium budget: Evaluating the role of groundwater." *Earth and Planetary Science Letters* 253.1 (2007): 129-142.

Jones, K. M. *An Evaluation of Radiogenic Isotopes as Tracers of Ocean Circulation and Sediment Transport: Modeling, Seawater, and Sediment Studies*. Columbia University, 2010. http://gradworks.umi.com/34/20/3420820.html.

Klevenz, V., et al. "Neodymium isotopes in benthic foraminifera: core-top systematics and a down-core record from the Neogene south Atlantic." *Earth and Planetary Science Letters* 265.3 (2008): 571-587.

Kraft, S., et al. "Assessment of seawater Nd isotope signatures extracted from foraminiferal shells and authigenic phases of Gulf of Guinea sediments." *Geochimica et Cosmochimica Acta* 121 (2013): 414-435.

Lacan, F., and C. Jeandel. “Acquisition of the Neodymium Isotopic Composition of the North Atlantic Deep Water: NEODYMIUM ISOTOPIC COMPOSITION.” *Geochemistry, Geophysics, Geosystems* 6, no. 12 (December 2005)

Lacan, F., and C. Jeandel. “Neodymium Isotopes as a New Tool for Quantifying Exchange Fluxes at the Continent–ocean Interface.” *Earth and Planetary Science Letters* 232, no. 3–4 (April 2005): 245–57.

Machín, F., and J. L. Pelegrí. "Northward penetration of Antarctic intermediate water off Northwest Africa." *Journal of Physical Oceanography* 39.3 (2009): 512-535.

Martin, E. E., and H. Scher. “A Nd Isotopic Study of Southern Sourced Waters and Indonesian throughflow at intermediate depths in the Cenozoic Indian Ocean: Nd isotopic study at ODP site 757.” *Geochemistry, Geophysics, Geosystems* 7, no. 9 (September 2006)

Michard, A., et al. "Rare-earth elements and uranium in high-temperature solutions from East Pacific Rise hydrothermal vent field (13 N)." *Nature* 303.5920 (1983): 795-797.

O'Nions, R. K., et al. "Pb, Nd and Sr isotopes in oceanic ferromanganese deposits and ocean floor basalts." *Nature* 273 (1978): 435-438.

Ohnemus, D. C. *The biogeochemistry of marine particulate trace metals*. Diss. Massachusetts Institute of Technology, 2014.

Pahnke, K., et al. “GEOTRACES Intercalibration of Neodymium Isotopes and Rare Earth Element Concentrations in Seawater and Suspended Particles. Part 2: Systematic Tests and Baseline Profiles.” *Limnology and Oceanography: Methods* 10 (2012): 252–69.

Pahnke, K., Goldstein, S.L., and Sidney R. Hemming. "Abrupt changes in Antarctic Intermediate Water circulation over the past 25,000 years." *Nature Geoscience* 1.12 (2008): 870-874.

Pena, L; and S. L. Goldstein, “Thermohaline circulation crisis and impacts during the mid-Pleistocene transition.” *Science* 345 (6194): 318-322.

Pena, L. D., et al. "Rapid changes in meridional advection of Southern Ocean intermediate waters to the tropical Pacific during the last 30kyr." *Earth and Planetary Science Letters* 368 (2013): 20-32.

Piepgras, D. J., and G. J. Wasserburg. "Isotopic composition of neodymium in waters from the Drake Passage." *Science* 217.4556 (1982): 207-214.

Piepgras, D. J., and G. J. Wasserburg. "Neodymium isotopic variations in seawater." *Earth and Planetary Science Letters* 50.1 (1980): 128-138.

Piepgras, D. J., and G. J. Wasserburg. "Strontium and neodymium isotopes in hot springs on the East Pacific Rise and Guaymas Basin." *Earth and planetary science letters* 72.4 (1985): 341-356.

Piepgras, D. J., and G. J. Wasserburg. “Rare Earth Element Transport in the Western North Atlantic Inferred from Nd Isotopic Observations.” *Geochimica et Cosmochimica Acta* 51, no. 5 (1987): 1257–71.

Piepgras, D. J., et al. "The isotopic composition of Nd in different ocean masses." *Earth and Planetary Science Letters* 45.2 (1979): 223-236.

Piepgras, D. J., and S. B. Jacobsen. "The isotopic composition of neodymium in the North Pacific." *Geochimica et Cosmochimica Acta* 52.6 (1988): 1373-1381.

Piotrowski, A. M., et al. "Oscillating glacial northern and southern deep water formation from combined neodymium and carbon isotopes." *Earth and Planetary Science Letters* 272.1 (2008): 394-405.

Piotrowski, A. M., et al. "Reconstructing deglacial North and South Atlantic deep water sourcing using foraminiferal Nd isotopes." *Earth and Planetary Science Letters* 357 (2012): 289-297.

Piotrowski, A. M., et al. "Intensification and Variability of Ocean Thermohaline Circulation through the Last Deglaciation." *Earth and Planetary Science Letters* 225, no. 1–2 (August 2004): 205–20.

Piotrowski, A. M., et al. "Temporal Relationships of Carbon Cycling and Ocean Circulation at Glacial Boundaries." *Science* 307, no. 5717 (March 25, 2005): 1933–38. doi:10.1126/science.1104883.

Price, J. F., et al. "Mediterranean Outflow Mixing and Dynamics." *Science* 259.5099 (1993): 1277-1282.

Reid, J. L. "On the total geostrophic circulation of the North Atlantic Ocean: Flow patterns, tracers, and transports." *Progress in Oceanography* 33.1 (1994): 1-92.

Rickli, J., et al. "Hafnium and Neodymium Isotopes in Surface Waters of the Eastern Atlantic Ocean: Implications for Sources and Inputs of Trace Metals to the Ocean." *Geochimica et Cosmochimica Acta* 74, no. 2 (January 2010): 540–57.

Rintoul, S. R., and C. Wunsch. "Mass, heat, oxygen and nutrient fluxes and budgets in the North Atlantic Ocean." *Deep Sea Research Part A. Oceanographic Research Papers* 38 (1991): S355-S377.

Roberts, N. L., et al. "Synchronous Deglacial Overturning and Water Mass Source Changes." *Science* 327, no. 5961 (January 1, 2010): 75–78.

Roberts, N. L., et al. "Rare earth element association with foraminifera." *Geochimica et Cosmochimica Acta* 94 (2012): 57-71.

Rutberg, R. L., et al. "Reduced North Atlantic Deep Water flux to the glacial Southern Ocean inferred from neodymium isotope ratios." *Nature* 405.6789 (2000): 935-938.

Scher, H. D., and Ellen E. Martin. "Circulation in the Southern Ocean during the Paleogene inferred from neodymium isotopes." *Earth and Planetary Science Letters* 228.3 (2004): 391-405.

Scher, H. D., and Ellen E. Martin. "Oligocene deep water export from the North Atlantic and the development of the Antarctic Circumpolar Current examined with neodymium isotopes." *Paleoceanography* 23.1 (2008).

Schmitz Jr, W. J. *On the World Ocean Circulation. Volume 1. Some Global Features/North Atlantic Circulation.* DTIC Document, 1996.

Schmitz, W. J., and M. S. McCartney. "On the north Atlantic circulation." *Reviews of Geophysics* 31.1 (1993): 29-49.

Shabani, M. B., et al. "Preconcentration of trace rare-earth elements in seawater by complexation with bis (2-ethylhexyl) hydrogen phosphate and 2-ethylhexyl dihydrogen phosphate adsorbed on a C18 cartridge and determination by inductively coupled plasma mass spectrometry." *Analytical Chemistry* 64.7 (1992): 737-743.

Shimizu, H., et al. "Cerium and neodymium isotope ratios and REE patterns in seawater from the North Pacific Ocean." *Geochimica et cosmochimica acta* 58.1 (1994): 323-333.

Siddall, M., et al. "Towards explaining the Nd paradox using reversible scavenging in an ocean general circulation model." *Earth and Planetary Science Letters* 274.3 (2008): 448-461.

Stichel, T., et al. "Biogeochemical cycling of Nd at the Eastern Margin of the North Atlantic" (*submitted*)

Tachikawa, K., et al. "Distribution of rare earth elements and neodymium isotopes in suspended particles of the tropical Atlantic Ocean (EUMELI site)." *Deep Sea Research Part I: Oceanographic Research Papers* 46.5 (1999): 733-755.

Tachikawa, K., et al. "Neodymium budget in the modern ocean and paleo‐oceanographic implications." *Journal of Geophysical Research: Oceans (1978–2012)* 108.C8 (2003).

Talley, L. D. "Antarctic intermediate water in the South Atlantic." *The South Atlantic*. Springer Berlin Heidelberg, 1996. 219-238.

Tanaka, T., et al. "JNdi-1: a neodymium isotopic reference in consistency with LaJolla neodymium." *Chemical Geology* 168.3 (2000): 279-281.

Thomas, D. J. "Evidence for deep-water production in the North Pacific Ocean during the early Cenozoic warm interval." *Nature* 430.6995 (2004): 65-68.

Thomas, D. J., Bralower, T.J., and Charles E. Jones. "Neodymium isotopic reconstruction of late Paleocene–early Eocene thermohaline circulation." *Earth and Planetary Science Letters* 209.3 (2003): 309-322.

Van Aken, H. M. "The Hydrography of the Mid-Latitude Northeast Atlantic Ocean: I: The Deep Water Masses." *Deep Sea Research Part I: Oceanographic Research Papers* 47, no. 5 (2000): 757–88.

Van de Flierdt, T., et al. "GEOTRACES Intercalibration of Neodymium Isotopes and Rare Earth Element Concentrations in Seawater and Suspended Particles. Part 1: Reproducibility of Results for the International Intercomparison." *Limnology and Oceanography: Methods* 10 (2012): 234–51.

Vance, De., et al. "The use of foraminifera as a record of the past neodymium isotope composition of seawater." *Paleoceanography* 19.2 (2004).

von Blanckenburg, F. "Tracing past ocean circulation?." *Science* 286.5446 (1999): 1862-1863.

Wilson, D. J., et al. "A boundary exchange influence on deglacial neodymium isotope records from the deep western Indian Ocean." *Earth and Planetary Science Letters* 341 (2012): 35-47.

5.6 Tables

Table 5.1. Water mass end-member compositions used in the *T-S approach*. Water masses include: 'pure' Mediterranean Outflow Water and Mediterranean Outflow Water (MOW), North Atlantic Deep Water (NADW), Eastern North Atlantic Deep Water (ENADW), 'pure' Antarctic Intermediate Water and Antarctica Intermediate water (AAIW), 'pure' Antarctic Bottom Water and Antarctic Bottom Water (AABW), Eastern Antarctic Bottom Water (EAABW), Irminger Sea Water (ISW) and North Atlantic Central Water (NACW). ε_{Nd} and [Nd] are from the following references: 1. Tachikawa et al., 2004; 2. Lacan and Jeandel, 2005; 3. Jeandel, 1993; 4. Stichel et al., 2012; 5. Piepgras and Wasserburg, 1983; 6. Copard et al., 2011; 7. The ε_{Nd} and [Nd] of these end-members were measured as part of this study or calculated based on the water mass mixing of modified end-members.

Table 5.2. Water mass end-member ε_{Nd} and [Nd] used in Optimal MultiParameter Analysis ***(OMPA)*** calculations (Jenkins et al., 2014). The compositions of these end-members are assigned based on the closest measured Nd data available in the literature or compiled by this study. 1. Piepgras and Wasserburg, 1987; 2. Lacan and Jeandel, 2005; 3. This study. Water masses include: Antarctic Bottom Water (AABW), Denmark Strait Overflow Water (DSOW), Iceland-Scotland Overflow Water (ISOW), Classic Labrador Sea Water (CLSW), Mediterranean Outflow Water (MOW), Upper Labrador Sea Water (ULSW), Upper Circumpolar Deep Water (UCPDW), Antarctic Intermediate Water (AAIW), Irminger Sea Water (ISW), North Atlantic Central Water (NACW), Southwest Atlantic Central Water (SWACW) and Atlantic Equatorial Water (AEW). Jenkins et al. (2014) gives more information on the characteristics of each end-member.

Table 5.1: Water mass end-member compositions used in mixing calculations

	θ	S	SiO_2	[Nd]	ε_{Nd}	Ref.
***'pure'* MOW**	13.00	38.30	11.1	23.05	-9.05	*1*
MOW	12.15	36.50	2.5	18.77	-10.30	*7*
NADW	2.25	34.92	14.5	21.35	-13.25	*2*
ENADW	3.39	35.01	29.1	18.60	-11.62	*7*
***'pure'* AAIW**	3.00	34.20	44.6	11.45	-8.00	*3, 4*
AAIW	4.75	34.50	39.1	12.40	-8.45	*7*
***'pure'* AABW**	-0.50	34.62	123.0	26.00	-8.50	*3, 4*
AABW	0.75	34.73	83.2	24.30	-10.24	*7*
EAABW	1.75	34.88	50.0	23.27	-11.85	*7*
NACW	11.50	35.60	2.5	13.87	-12.00	*5, 6*
ISW	7.11	35.12	6.7	18.72	-13.30	*2*

Table 5.2: ε_{Nd} end-member compositions used in OMPA

	[Nd]	ε_{Nd}	Ref.
AABW	30.10	-11.60	*1*
DSOW	18.71	-10.60	*2*
ISOW	19.41	-11.40	*2*
CLSW	17.33	-13.50	*2*
MOW	18.77	-10.30	*3*
ULSW	21.50	-15.00	*2*
UCPDW	16.20	-12.60	*1*
AAIW	15.90	-11.90	*1*
ISW	18.72	-13.30	*2*
NACW	15.02	-10.60	*3*
SWACW	17.00	-11.61	*3*
AEW	15.30	-12.60	*1*

5.7 Figures

Figure 5.1. Cruise track for GA03 completed in two sections. KN199-4 (USGT10-; bold) was completed between October and November 2010 and KN204 (USGT11-) was completed during November and December 2011. Sampled stations are highlighted in red.

Figure 5.2. North Atlantic basin with simplified hydrology modified from Schmitz and McCartney, 1993. Deep, intermediate and shallow water currents are roughly depicted by black, gray and white arrows respectively. Square numbers represent transports in Sverdrups (1Sv = 10^6 m^3/s). Yellow dots represent sampled station locations along GEOTRACES cruise track GA03.

Figure 5.3. Measured ε_{Nd} and [Nd] along cruise track GA03. a) ε_{Nd} data from western basin Sta. USGT11-01, -02, -03, -04, -06, -08, -10, -12 and -14. b) [Nd] data from western basin Sta. USGT11-01, -03, -08, -10, -12. c) ε_{Nd} data from eastern basin open ocean Sta. USGT11-16, -18, -20, -22 and GT10-03, -05, -07. d) [Nd] data from eastern basin open ocean Sta. USGT11-16, -22, and USGT10-03, -05, -07. e) ε_{Nd} data from eastern basin near shore Sta. USGT10-01, -09, -10, -11, -12 and USGT11-24. f) [Nd] data from eastern basin near shore Sta. USGT10-01, -09, -10, -11, -12 and USGT11-24.

Figure 5.4. Predicted ε_{Nd} and [Nd] derived from the *T-S approach* are shown for the section. Station profiles in the western basin are similar and are shown in blue-black. Eastern basin stations are similar to one another and shown in red-pink colors. The calculated [Nd] is similar in both basins at depths > 3000 m with the western basin showing more variability at intermediate depths. There is a distinct offset between calculated ε_{Nd} in the western and eastern basins as a result of the different NADW end-member used in each basin. This offset is nearly 1 ε_{Nd} unit at depths between 1000 and 3000 m with the eastern basin being more positive. In the eastern basin the predicted ε_{Nd} at depths > 3000 m is uniform and deep samples in the western basin become slightly more radiogenic at depth. Both the western and eastern basins show ε_{Nd} variability at intermediate depths.

Figure 5.5. Predicted ε_{Nd} and [Nd] derived from OMPA calculations are shown for the study region. Because of the increased variability of these profiles in comparison to the *T-S approach* (Figure 5.4), the data is presented by region. a) Predicted ε_{Nd} for the western Atlantic basin demonstrates the unradiogenic feature at ~1750 m depth and uniform ε_{Nd} in the basin at depths > 3000 m. b) Predicted [Nd] for the region shows greater [Nd] at ~ 1750 m and increasing concentration with depth. c) ε_{Nd} in the open ocean eastern basin also shows an unradiogenic feature at ~ 1750 m with more uniform values at depth though Sta. USGT10-03 and -07 (far eastern basin) are more positive. d) Predicted [Nd] concentrations for the open ocean eastern basin show a nearly linear increase in [Nd] with depth of similar magnitude at all stations. e) Predicted ε_{Nd} for the eastern basin near margin stations show good agreement between Sta. USGT10-09, -10, -11 and -12 (Mauritania transect). There is less agreement in the predicted ε_{Nd} records between the crossover stations USGT11-24 and USGT10-12. Sta. USGT10-01 off shore of Portugal shows more radiogenic values. f) Predicted [Nd] for the Mauritania transect shows good agreement and a reduced [Nd] feature at ~ 1000 m though the feature is slightly shallower at USGT11-24. Profiles are fairly uniform at depths > 2000 m with the exception of USGT11-24.

Figure 5.6. The calculated offset between the *T-S approach* and OMPA for predicted ε_{Nd} and [Nd] values where $\Delta\varepsilon_{Nd\text{-}calcs} = \varepsilon_{Nd}$-*T-S approach* $-\varepsilon_{Nd}$-OMPA and Δ[Nd] = [Nd]-*T-S approach* – [Nd]-OMPA. Western basin stations are shown in blue-black colors and eastern basin stations are shown in red-pink. The largest (~ +2) offset between the two calculations in the western basin occurs between 2000 and 3000 m depth. In the eastern basin, the largest offset (~ -2) is between 1000 and 2000 m depth. There is no significant offset between the two calculations in the eastern basin at depths > 2000 m whereas in the western basin there is an offset of ~ -1 ε_{Nd} unit. At depths < 2000 m, there is positive offset between the two calculations in both basins with a 1 ε_{Nd} unit offset in the eastern basin and a 2 ε_{Nd} unit offset in the western basin.

Figure 5.7. Section profile showing offset between measured and calculated ε_{Nd} based on the *T-S approach* (three-component water mass mixing). Colors represent $\Delta\varepsilon_{Nd}$ where $\Delta\varepsilon_{Nd} = meas\text{-}\varepsilon_{Nd} - calc\text{-}\varepsilon_{Nd}$. Positive values represent areas where measured ε_{Nd} are more positive (radiogenic) in comparison to the ε_{Nd} predicted from water mass mixing. Values between -0.75 and +0.75 are shown as pale green and represent an offset of < 0.75 ε_{Nd} unit. These regions are interpreted to show conservative behavior of Nd isotopes.

Figure 5.8. Section profile of offset between calculated and measured ε_{Nd} based on OMPA water mass fraction results (Jenkins et al., 2014). Colors represent $\Delta\varepsilon_{Nd}$ where $\Delta\varepsilon_{Nd} = meas\text{-}\varepsilon_{Nd} - calc\text{-}\varepsilon_{Nd}$. Positive values represent areas where measured ε_{Nd} is more positive (radiogenic) in comparison to the ε_{Nd} predicted from water mass mixing. Values between -0.75 and +0.75 are shown as pale green and represent an offset of < 0.75 ε_{Nd} unit. These regions are interpreted to show conservative behavior of Nd isotopes.

Figure 5.9. Section profile of offset between calculated and measured [Nd] based on the *T-S approach*. Colors represent Δ[Nd] where Δ[Nd] = *meas*-[Nd] – *calc*-[Nd]. Positive values represent areas where measured [Nd] exceeds calculated [Nd] based on water mass mixing alone. Values between -3.0 and +3.0 pmol/kg are considered to be insignificant offsets and regions where [Nd] behaves conservatively. Contours are ± 3 and ± 6.

Figure 5.10. Section profile of offset between calculated and measured [Nd] based on OMPA derived water mass fractions (Jenkins et al., 2014). Colors represent Δ[Nd] where Δ[Nd] = *meas*-[Nd] – *calc*-[Nd]. Positive values represent areas where measured [Nd] exceeds calculated [Nd] based on water mass mixing alone. Values between -3.0 and +3.0 pmol/kg are considered to be insignificant offsets and regions where [Nd] behaves conservatively. Contours are ± 3 and ± 6.

Figure 5.11. Section profile of measured ε_{Nd} in the Western Atlantic with contours representing the CFC-11 concentration (Smethie, *unpub*). There is agreement between evidence for northern-sourced, unradiogenic water masses as measured by ε_{Nd} and northern-sourced, recently ventilated waters as measured by CFC-11.

Figure 5.12. Four section plots in the Western Atlantic demonstrating the sensitivity of $\Delta\varepsilon_{Nd}$ to shifting end-member ε_{Nd} compositions for NADW in the *T-S approach*. This range in end-member compositions is within uncertainty of the constraints based on available data. In this test, we focus on the positive anomaly in the western basin and demonstrate that a more positive end-member ε_{Nd} value can reduce the positive anomaly seen in the $\Delta\varepsilon_{Nd}$ profile.

Figure 5.13. Five section plots for the North Atlantic basin that demonstrate the sensitivity of calculated $\Delta\varepsilon_{Nd}$ to shifting end-member ε_{Nd} composition for ULSW in the OMPA derived water mass mixing calculations. This range in ULSW ε_{Nd} composition is within uncertainty of the constraints based on available data. In this test we focus on the positive anomaly seen at ~1750m depth across the section where ULSW dominates. By shifting the ULSW ε_{Nd} composition to more positive values, the positive anomaly is reduced in the far western basin and is limited to the area just off shore Mauritania.

Figure 5.14. Section profile at USGT11-16 or the TAG hydrothermal plume. Transmittance data, ε_{Nd} data and [Nd] illustrate the influence of hydrothermal activity on dissolved seawater Nd. The gray bar represents reduced transmittance and increased suspended particle load. At site of greatest hydrothermal sourced suspended particles, [Nd] is reduced by 3 pmol/kg and demonstrates unusually low deep water [Nd]. Additionally, ε_{Nd} shows a slight positive (radiogenic) excursion consistent with the influences of hydrothermal fluids interacting with ocean ridge basalt. However, calculated ε_{Nd} and [Nd] based on *T-S approach* show that these features are not significantly different from those predicted by water mass mixing alone.

Figure 5.1: GA03 Cruise Track

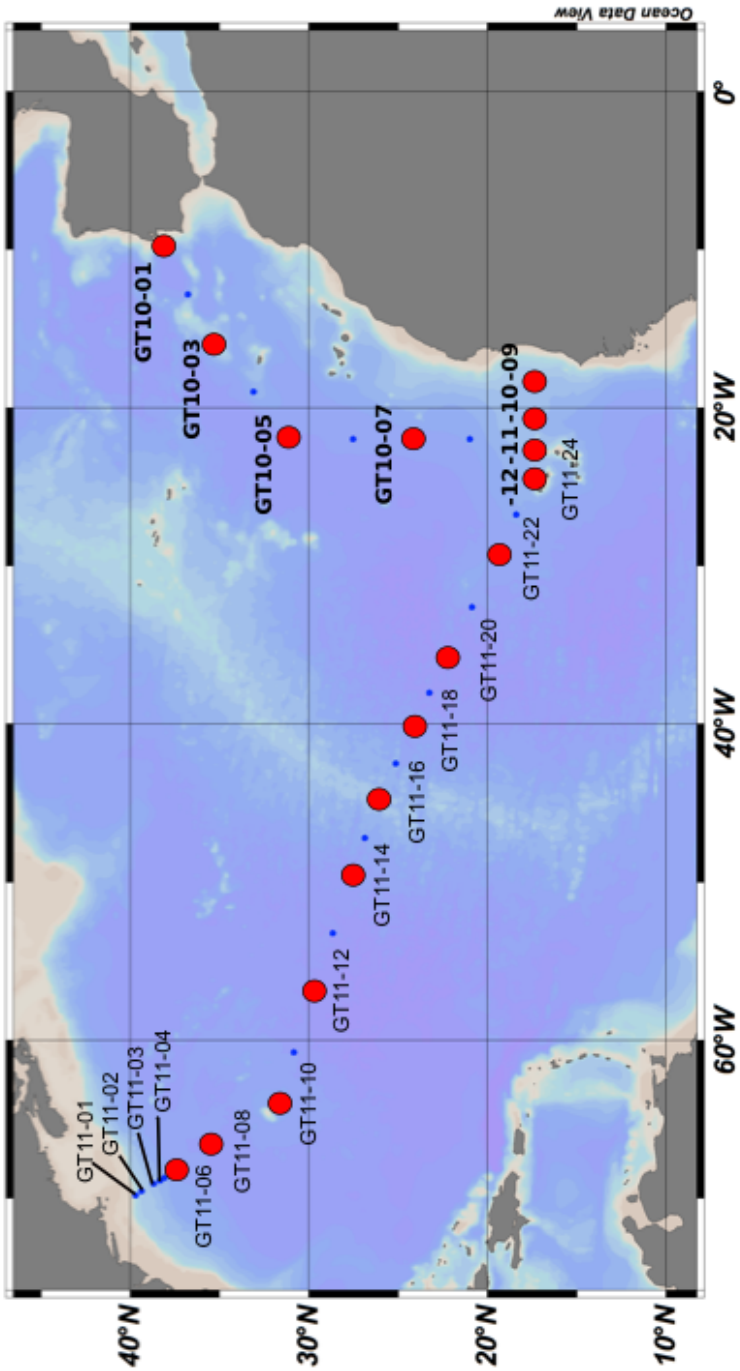

Figure 5.2: Hydrology of the North Atlantic

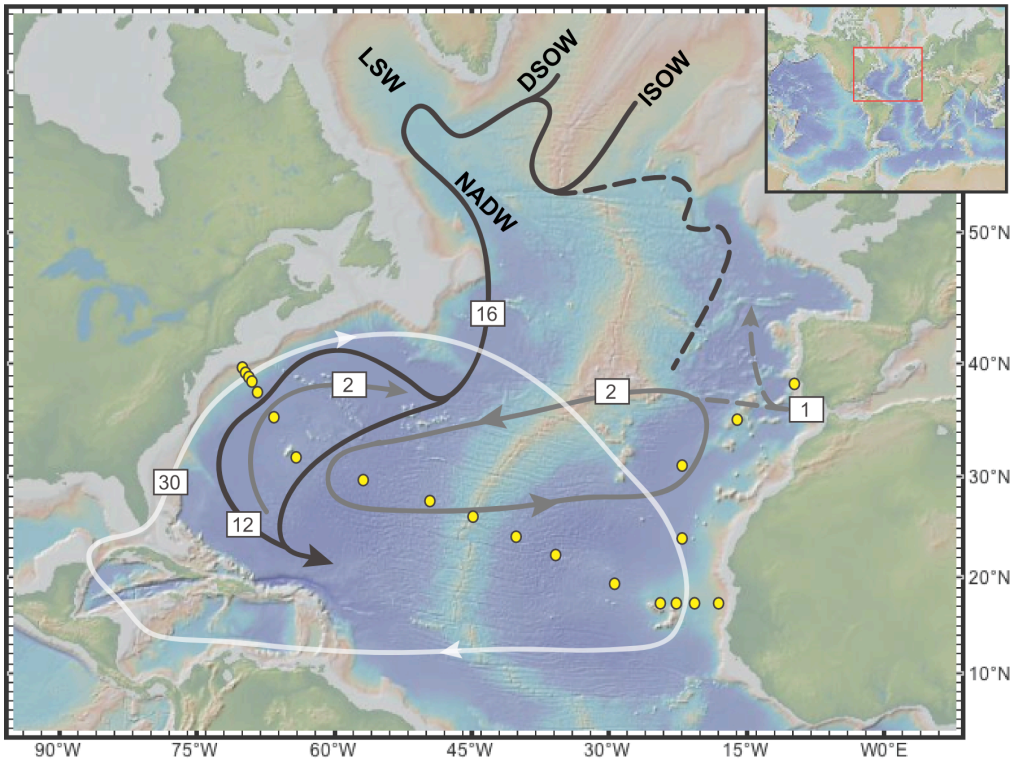

Figure 5.3: Measured ε_{Nd} and [Nd] for seawater profiles in the North Atlantic

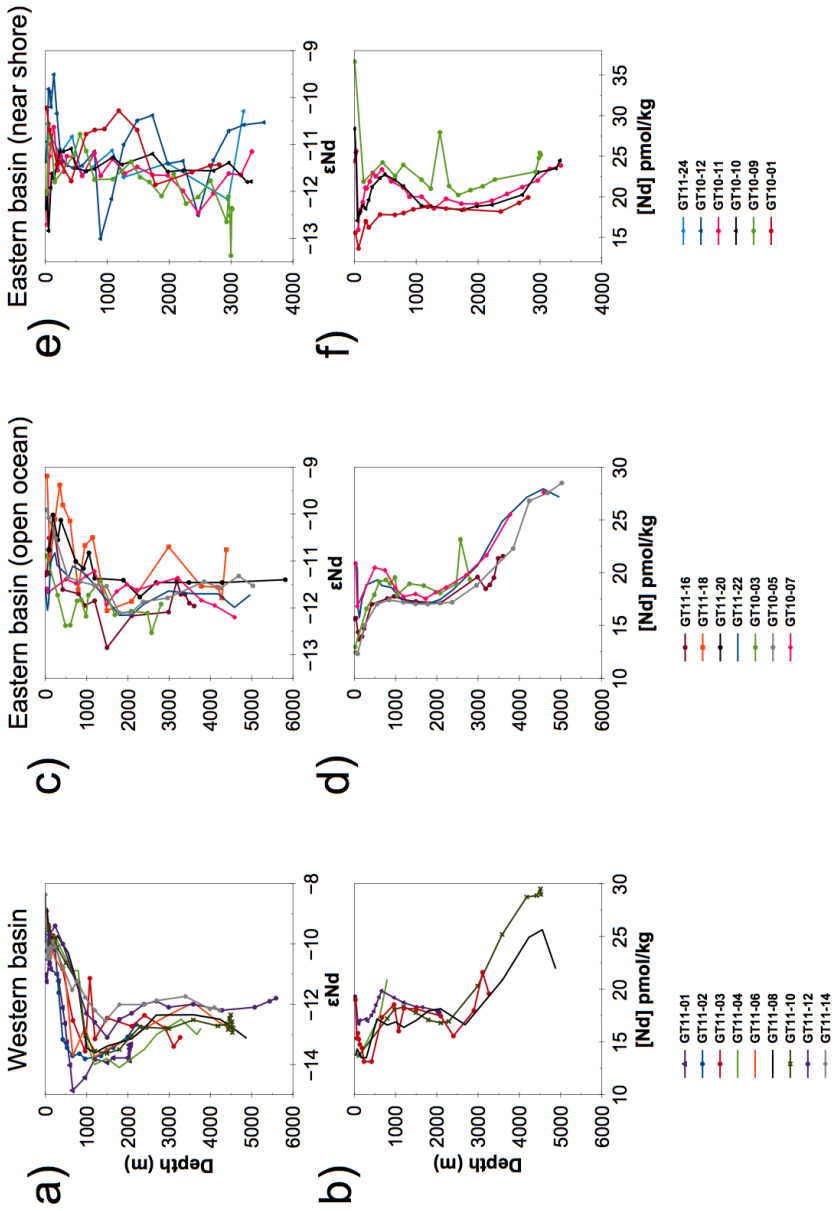

Figure 5.4: Calculated [Nd] and ε_{Nd} based on the *T-S approach*

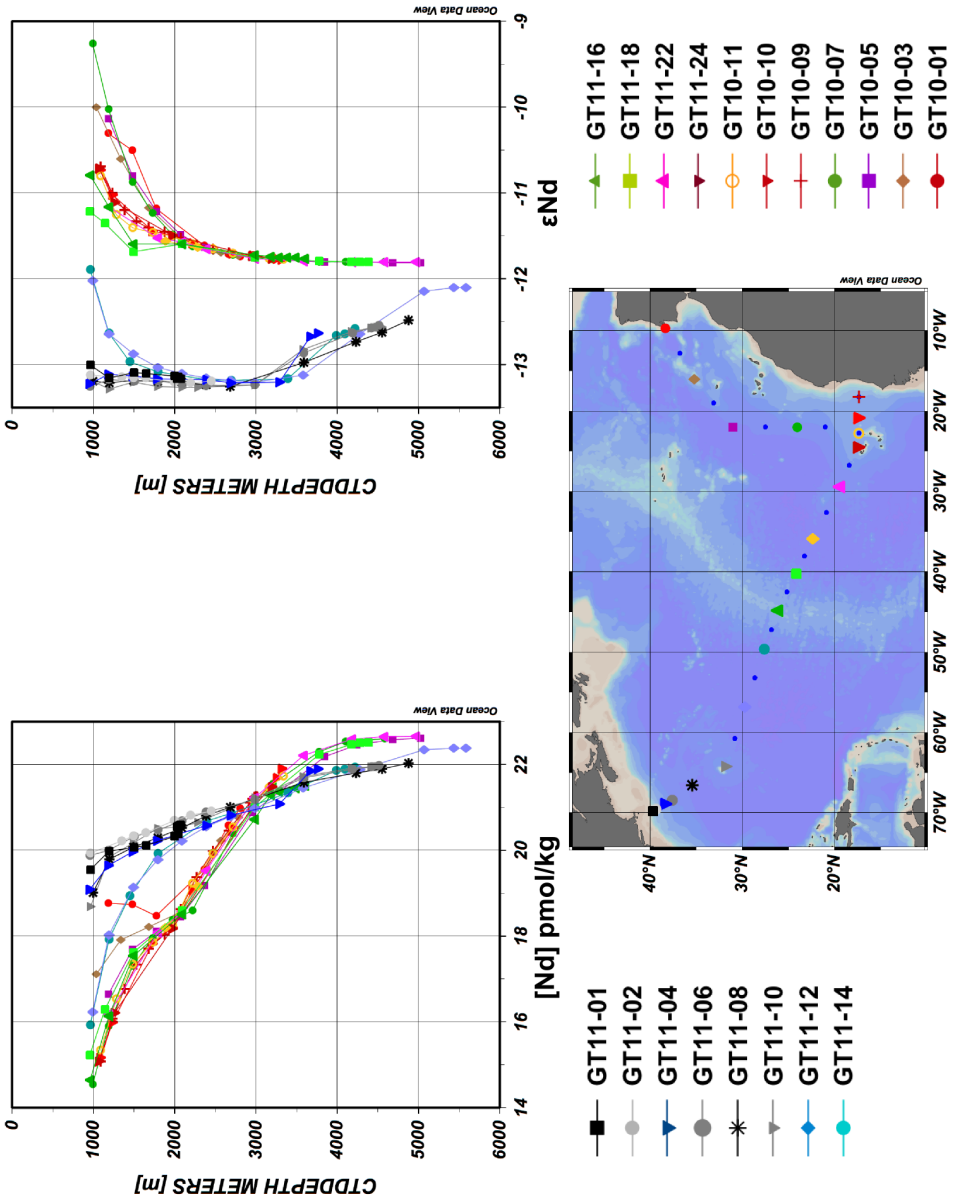

Figure 5.5: Calculated [Nd] and ε_{Nd} based on OMPA calculations

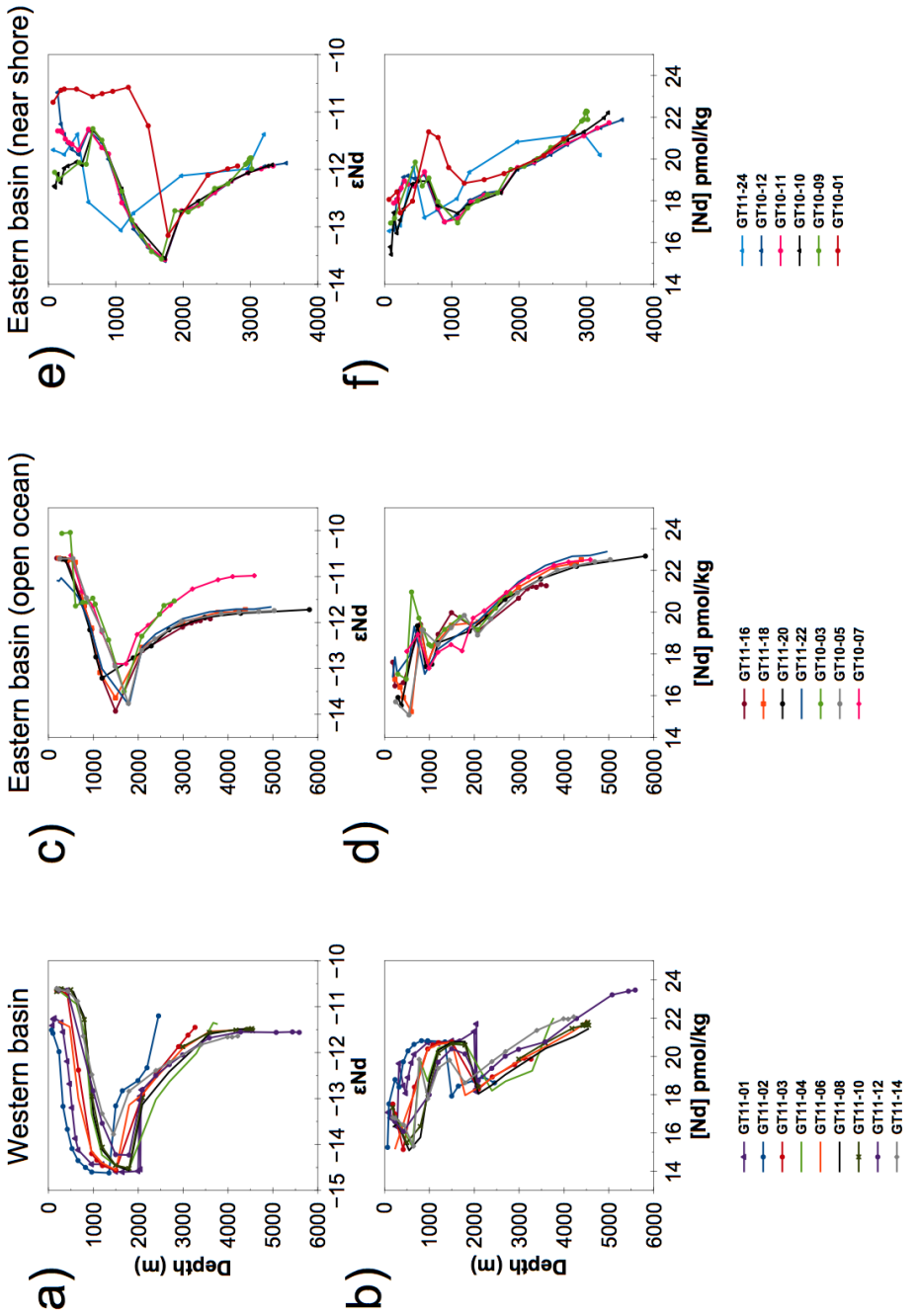

Figure 5.6: Offsets between predicted [Nd] and ε_{Nd} from *T-S approach* and OMPA

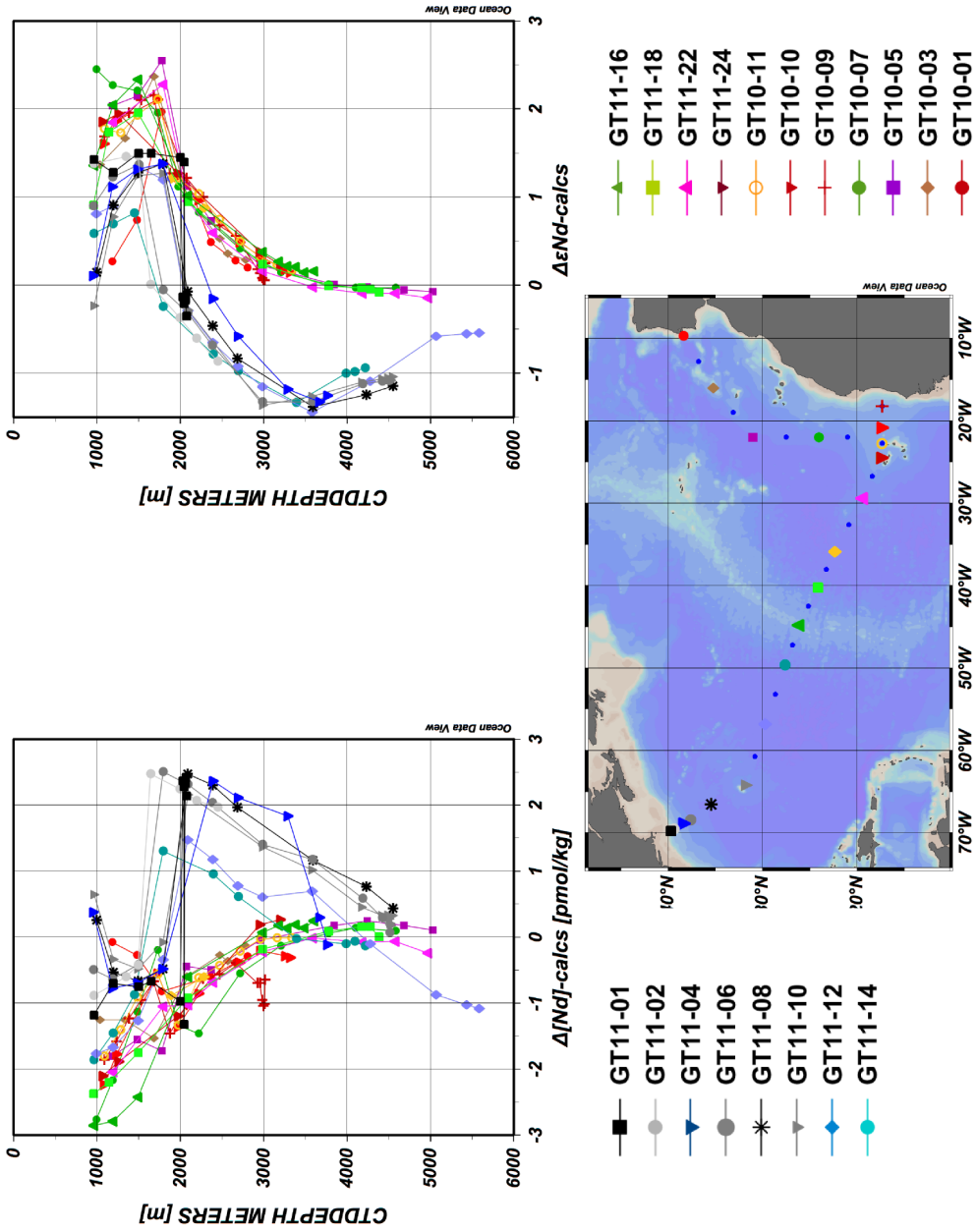

Figure 5.7: $\Delta\varepsilon_{Nd}$ derived from *T-S approach* results

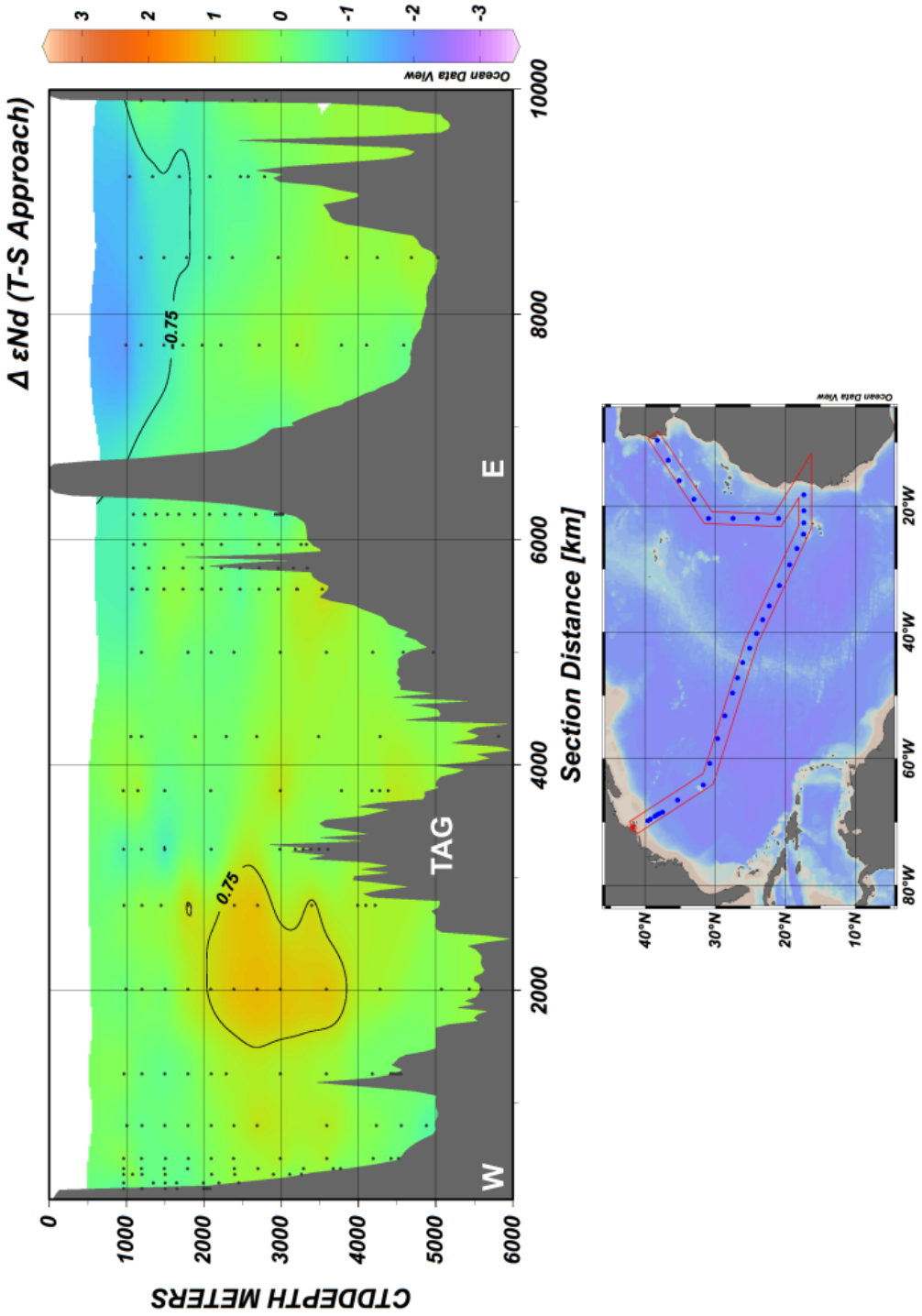

Figure 5.8: $\Delta\varepsilon_{Nd}$ derived from OMPA results

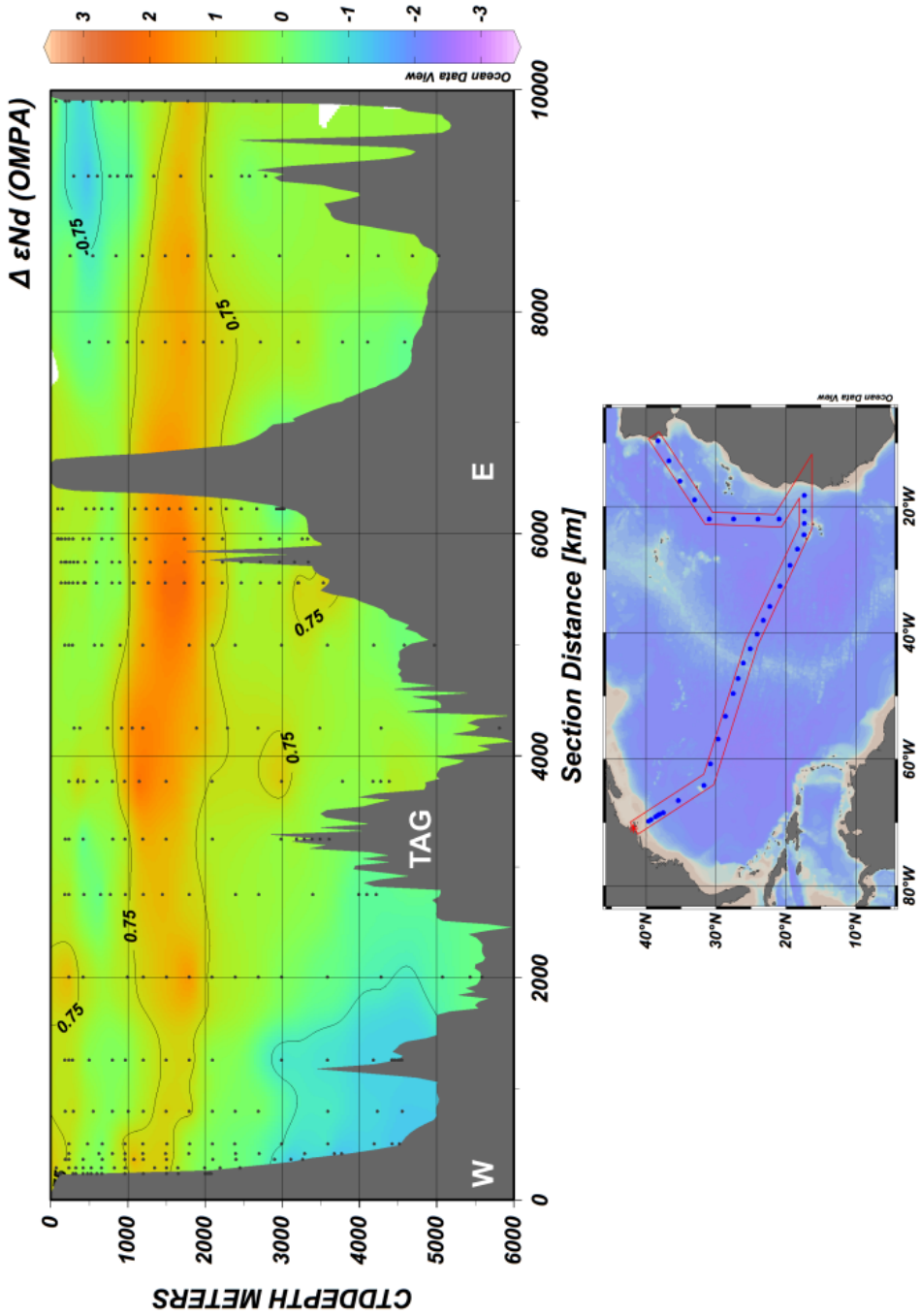

Figure 5.9: Δ[Nd] derived from *T-S approach*

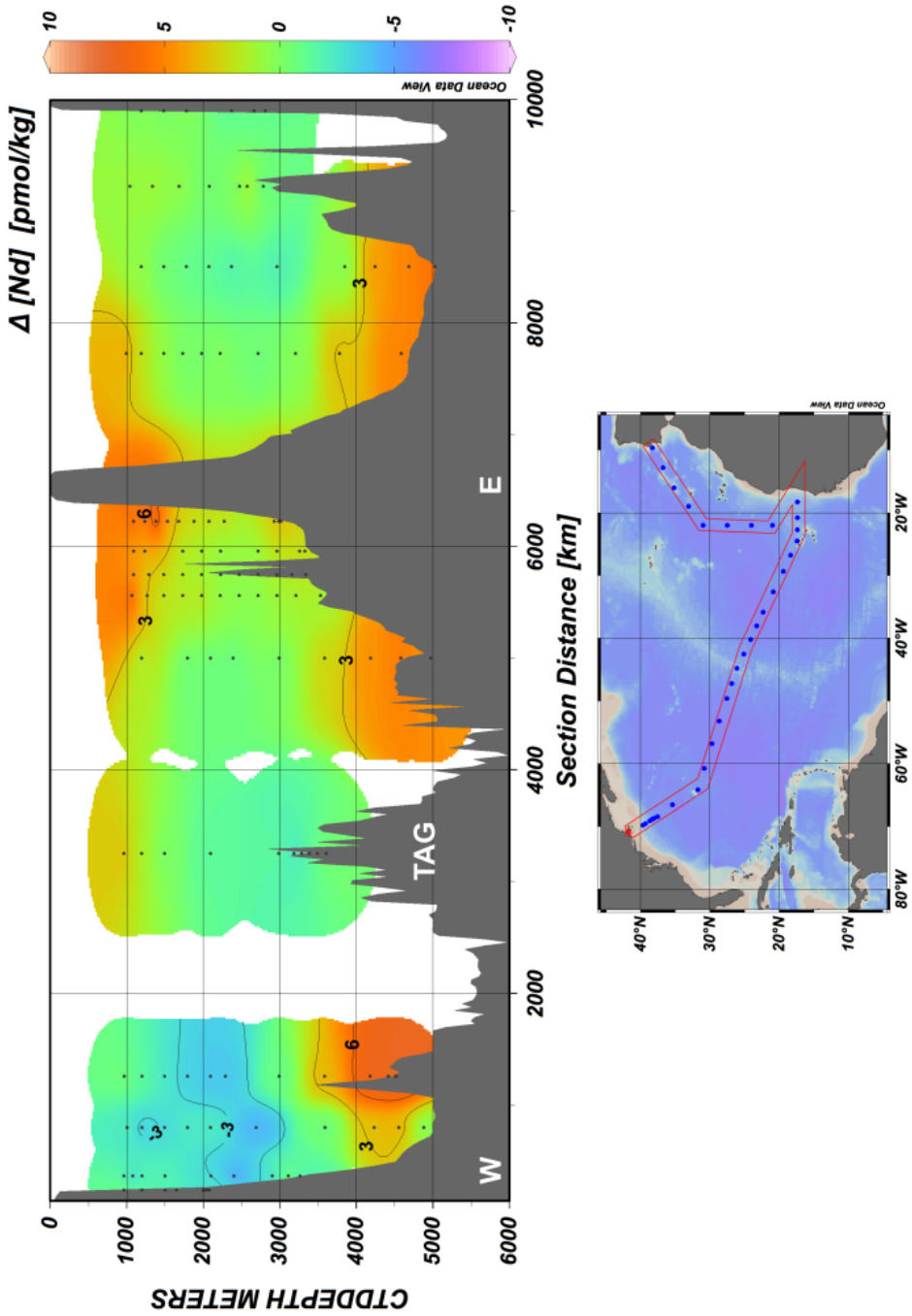

Figure 5.10: Δ[Nd] derived from OMPA results

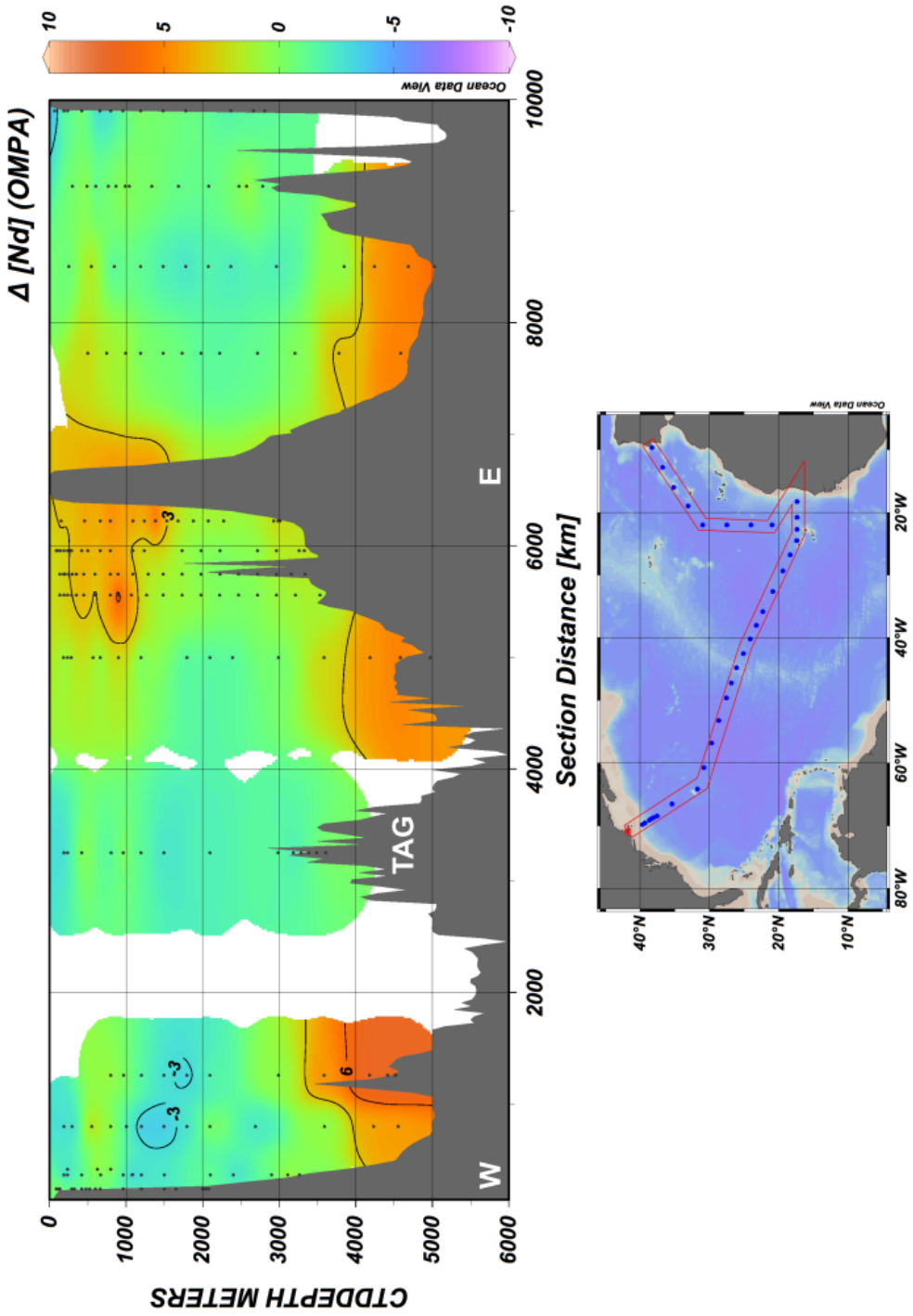

Figure 5.11: Western basin measured ε_{Nd} and CFC-11 concentrations

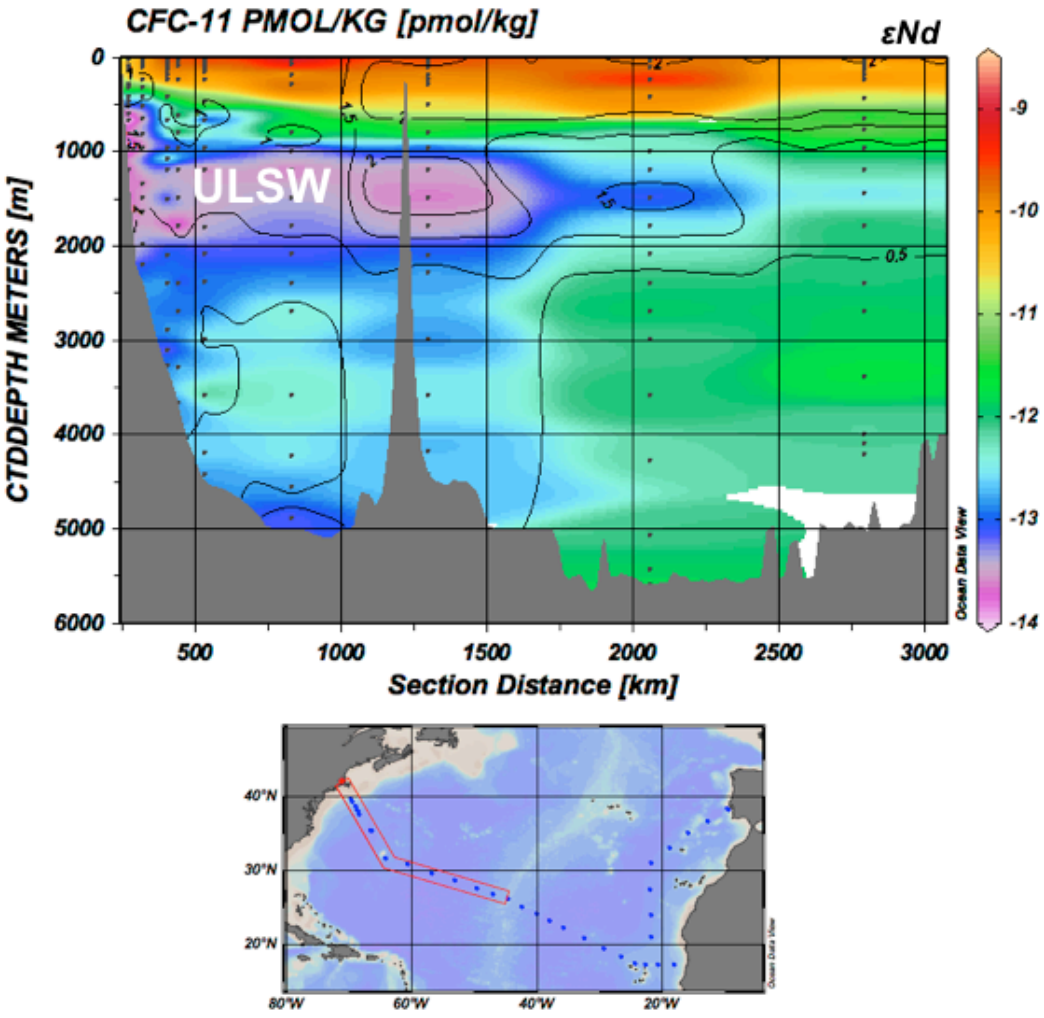

Figure 5.12: Western basin $\Delta\varepsilon_{Nd}$ sections for varying NADW ε_{Nd} compositions

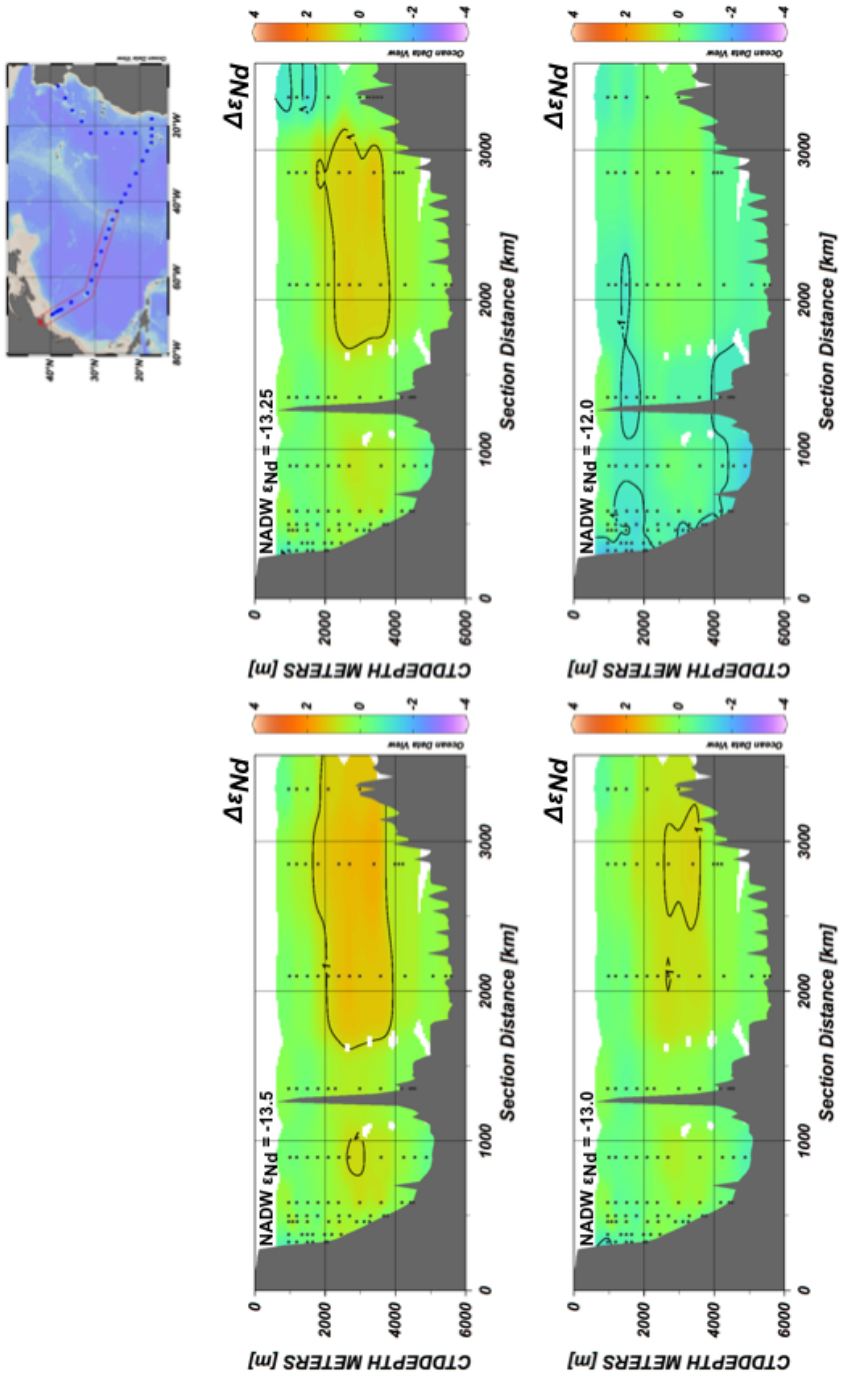

Figure 5.13: North Atlantic $\Delta\varepsilon_{Nd}$ sections for varying ULSW ε_{Nd} compositions

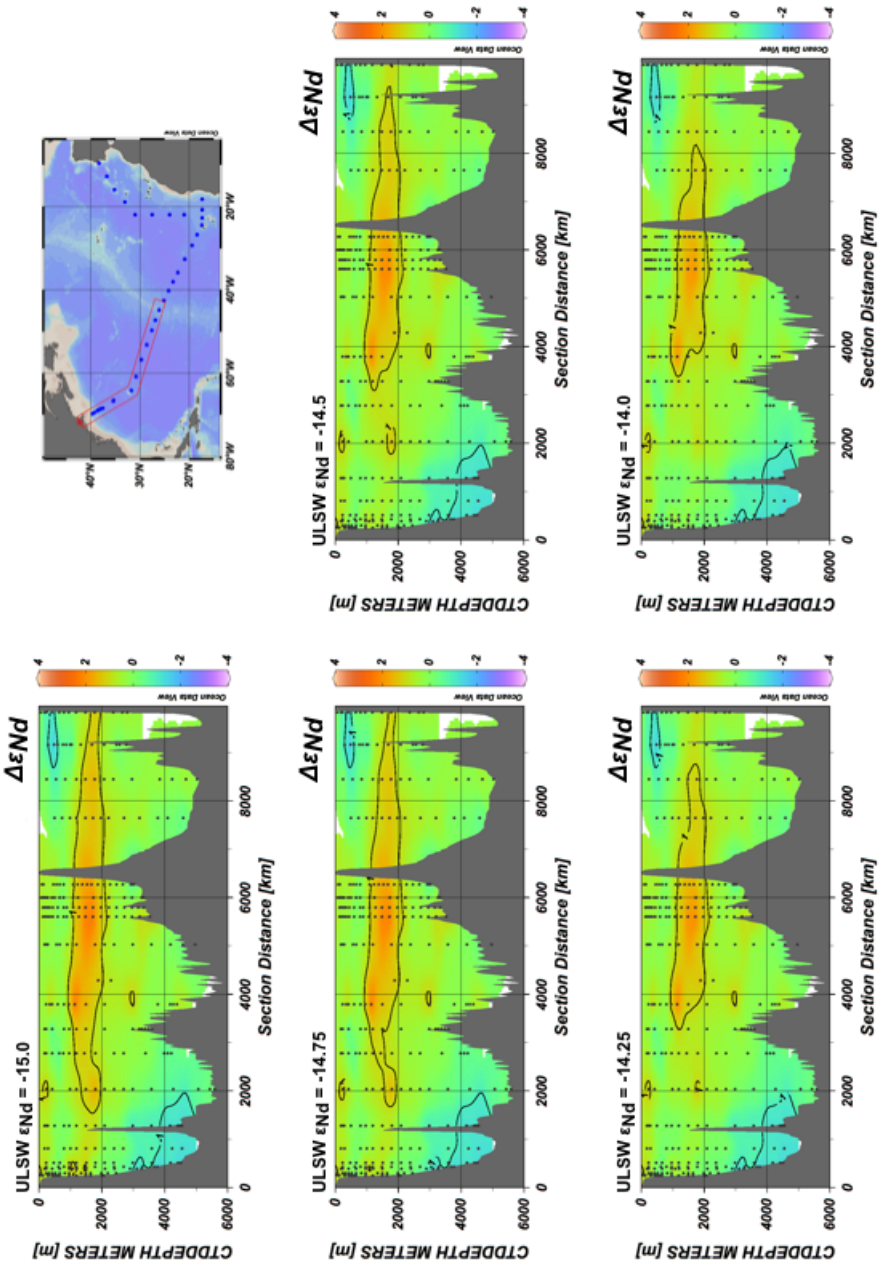

Figure 5.14: Details of data measured at TAG hydrothermal site (USGT11-16)

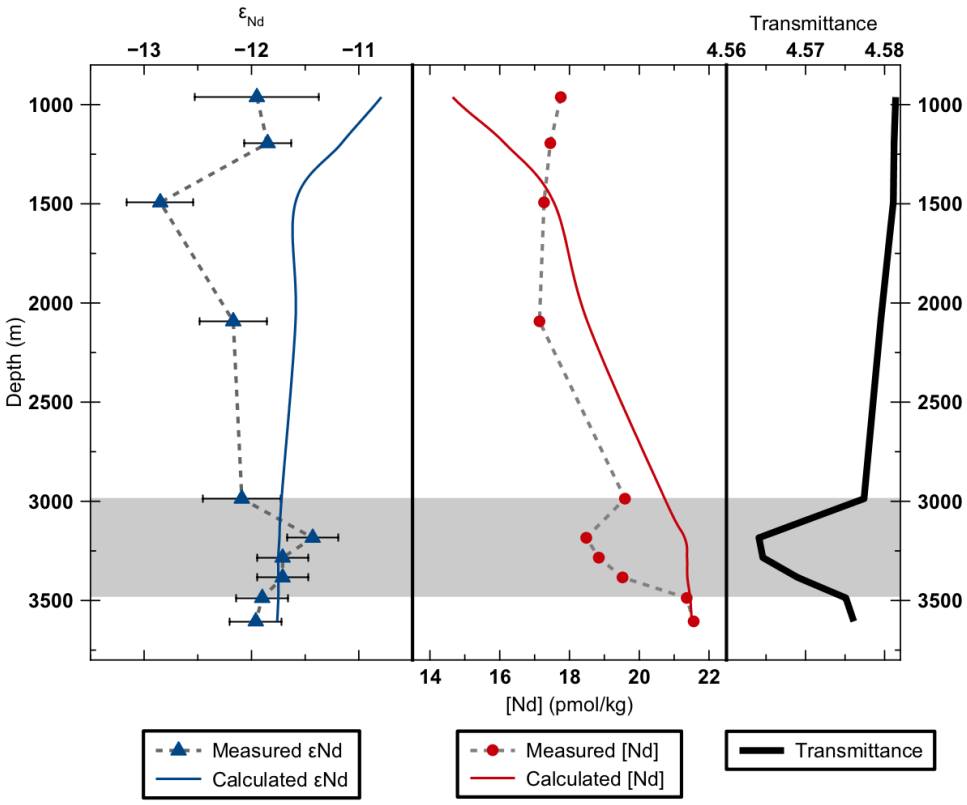

Appendix: Relevant analytical procedures

A-1 Sediment leachates

The following procedure is adapted from Chester and Hughes, 1967; Rutberg et al., 2000; Piotrowski et al., 2004 and Gutjahr et al., 2007 and is used to obtain the authigenic Nd signal from fine and bulk sediment leachates.

Supplies:

1M Acetic acid buffer solution

1M $MgCl_2$

0.05M Hydroxylamine hydrochloride- 15% acetic acid

3M Nitric acid

1. Weigh ~300 mg dry bulk or fine fraction sediment sample to acid cleaned 50mL centrifuge tube
2. Add 10mL acetic acid buffer solution, disaggregate thoroughly and leave tube on rocking table. Vent tube frequently to release pressure from the build up of CO_2. Leave sample in solution on rocking table until no more gas is produced (likely overnight).
3. Remove from rocking table and centrifuge at ~3600 RPM for 15 minutes.
4. Decant acetic acid solution.
5. Add an additional 10mL acetic acid buffer solution to centrifuge tube, disaggregate and return to rocking table.
6. When no more gas is produced during decarbonation, repeat centrifuge and decant solution.

7. Add 10mL 1M $MgCl_2$ to centrifuge tube, disaggregate and centrifuge at ~3600 RPM for 15 minutes.
8. Decant $MgCl_2$ solution and add ~20mL Milli-Q or double distilled H_2O.
9. Disaggregate sample thoroughly, centrifuge and decant H_2O. Repeat two more times.
10. Add 10mL of 0.05M Hydroxylamine hydrochloride- 15% acetic acid to the tube and shake thoroughly to disaggregate sample.
11. Leave sample on rocking table for no more than 1 hour. Centrifuge and decant solution into acid cleaned 15mL centrifuge tube being sure to avoid transferring any solids.
12. Centrifuge 15mL tubes at >3600 RPM for 15 minutes.
13. Transfer supernatant to cleaned 15mL tube and dry on hotplate until barely dry.
14. Add 1mL of 3M nitric acid and dry down until barely dry. Repeat.
15. The sample to ready for column chemistry.

A-2. Nd preconcentration of seawater

A-2.1 Fe co-precipitation

Supplies:

LaMES spike

REE free Fe solution

Optima grade NH_4OH

3M HNO_3

1. The acidified seawater sample should be weighed in a tared cubitainer and an appropriate amount of the Lamont multi-element spike (LaMES) should be obtained.

2. The spike should be diluted in at least ~2mL of weak acid and added to the sample, the sample shaken and allowed to equilibrate for at least 24 hours.
3. Following spike equilibration, add ~4mg of Fe from a REE clean Fe solution and allow to homogenize for several hours.
4. Adjust the pH of the sample to 8.5-9.0 using NH_4OH to allow for the precipitation of Fe.
5. Precipitation of Fe will take at least ~ 7days and will settle in the cubitainer as a fluffy orange layer. Take care to not agitate the cubitainer to disperse the Fe.
6. Without moving the cubitainer excessively, siphon off the seawater from the top of the cubitainer until only the fluffy layer is left.
7. Transfer the residues to a 250mL centrifuge tube, centrifuge and decant supernatant. It may require several cycles to transfer all material to the centrifuge tube.
8. When all the Fe is in one centrifuge tube, add ~4mL 3M HNO_3 and swirl to dissolve all Fe.
9. Transfer solution to a cleaned Teflon vial and dry down.
10. Add 1mL of 3M HNO_3 and dry down. Sample is ready for chemistry.

A-2.2 C18 cartridges

The following procedure is adapted from Shabani et al., 1992; Jeandel et al., 1998 and Lacan and Jeandel, 2005.

Supplies:

Optima grade NH_4OH

SepPAK SPE C18 cartridges (Waters Inc; #WAT051910)

2-ethylhexyldihydrogen-phosphate (H2MEHP)

0.01M HCl

6M HCl

1. Rinse the C18 cartridge with at least 100mL 1M HCl.
2. Load the cartridge with 300ul H2MEHP and connect to acid resistant tubing.
3. Adjust the pH of the acidified seawater sample to pH = 2.5-3.5 using NH_4OH.
4. Pump seawater sample through acid resistant tubing into the cartridges using a peripump. With more than one pump head, several samples can be done in tandem.
5. Nd adheres to the cartridge and the pumped through water can go to waste. Remove the cartridge from the tubing and pipette 5mL of 0.01M HCl through the cartridge to remove Barium.
6. Replace the cartridge to the tubing and using the peripump, pump 35mL of 6N HCl through the cartridge. Collect the eluted solution in a cleaned 60mL Teflon vial.
7. Dry down the solution in the vial at 100ºC for several hours. When the volume has reduced by half, increase the temperature for quicker evaporation.
8. Before the solution has completely dried, transfer to a 15mL beaker and dry completely.
9. Add 1mL of 1N HNO_3 and dry. Repeat.
10. The sample is now ready for chemistry.

References

Chester, R., and M. J. Hughes. "A chemical technique for the separation of ferro-manganese minerals, carbonate minerals and adsorbed trace elements from pelagic sediments." *Chemical geology* 2 (1967): 249-262.

Gutjahr, M., et al. "Reliable extraction of a deepwater trace metal isotope signal from Fe–Mn oxyhydroxide coatings of marine sediments." *Chemical Geology* 242.3 (2007): 351-370.

Jeandel C., et al. Concentrations and isotopic compositions of neodymium in the eastern Indian Ocean and Indonesian Straits. *Geochim. Cosmochim. Acta*, 62 (1998): 2597-2607.

Lacan F. and C. Jeandel. Neodymium isotopes as a new tool for quantifying exchange fluxes at the continent-ocean interface. *Earth Planet. Sci. Lett*. 232 (2005): 245-257.

Piotrowski, A. M; et al. "Intensification and variability of ocean thermohaline circulation through the last deglaciation." *Earth and Planetary Science Letters* 225 (2004): 205-220.

Rutberg, R. H., et al. "Reduced North Atlantic Deep Water flux to the glacial Southern Ocean inferred from neodymium isotope ratios." *Nature* 405. (2000)

Shabani M.B., et al. Preconcentration of Trace Rare Earth Elements in Seawater by Complexation with Bis(2-ethylexyl) hydrogen phosphate and 2- Ethylexyl Dihydrogen Phosphate Adsorbed on a C18 Cartridge and Determination Inductively Coupled Plasma Mass Spectrometry. Anal Chem. 64 (1992): 737-743.